Differential contributions of RhoA, -B and -C to cellular processes and host pathogen interactions

Von der Fakultät für Lebenswissenschaften

der Technischen Universität Carolo-Wilhelmina zu Braunschweig

zur Erlangung des Grades

einer Doktorin der Naturwissenschaften (Dr. rer. nat.)

genehmigte

D i s s e r t a t i o n

von Jessica Halfen
aus Koblenz

1. Referentin: Prof. Dr. Theresia Stradal
2. Referentin: Prof. Dr. Susanne Engelmann
eingereicht am: 17.09.2018
mündliche Prüfung (Disputation) am: 03.12.2018
Druckjahr 2018

Vorveröffentlichungen der Dissertation

Teilergebnisse aus dieser Arbeit wurden mit Genehmigung der Fakultät für Lebenswissenschaften, vertreten durch die Mentorin der Arbeit, in folgenden Beiträgen vorab veröffentlicht:

Publikationen

Halfen J, Kollasser J, Gröbe L, Hagendorff P, Geffers R, Steffen A, Brakebusch CH, Rottner K, Stradal TE. Dissecting the role of RhoA, -B and -C during host pathogen interaction. (2016) Mol. Biol. Cell 27, 3947 [Abstracts #P93 (Poster) and #E127 (Oral)]

Tagungsbeiträge

Halfen J, Kollasser J, Gröbe L, Steffen A, Brakebusch CH, Rottner K, Stradal TE. Evil bacteria vs. holy immune system - Welcome to the arena. Vortrag. 17th Annual Retreat HZI GS-FIRE, Goslar-Hahnenklee (2016).

Halfen J, Kollasser J, Gröbe L, Hagendorff P, Geffers R, Steffen A, Brakebusch CH, Rottner K, Stradal TE. Dissecting the role of RhoA, -B and -C during host pathogen interaction. Vortrag E127. Annual Meeting of the American Society for Cell Biology, San Francisco (2016).

Halfen J, Kollasser J, Gröbe L, Hagendorff P, Geffers R, Steffen A, Brakebusch CH, Rottner K, Stradal TE. Analysis of bacterial virulence factors that interfere with RhoA signaling. Vortrag. 8th Annual Retreat HZI GS-FIRE, Goslar-Hahnenklee (2017).

Posterbeiträge

Halfen J, Kollasser J, Gröbe L, Steffen A, Brakebusch CH, Rottner K, Stradal TE. Analysis of bacterial virulence factors that interfere with RhoA signaling. Poster P17. 6th Annual Retreat HZI GS-FIRE, Goslar-Hahnenklee (2015).

Halfen J, Kollasser J, Gröbe L, Steffen A, Brakebusch CH, Rottner K, Stradal TE. Analysis of bacterial virulence factors that interfere with RhoA signaling. Poster P31. 8th Annual PhD Symposium HZI GS-FIRE, Braunschweig (2015).

Halfen J, Kollasser J, Gröbe L, Steffen A, Brakebusch CH, Rottner K, Stradal TE. Analysis of bacterial virulence factors that interfere with RhoA signaling. Poster P2-04. International Meeting of the German Society for Cell Biology, Martinsried (2016).

Halfen J, Kollasser J, Gröbe L, Hagendorff P, Geffers R, Steffen A, Brakebusch CH, Rottner K, Stradal TE. Dissecting the role of RhoA, -B and -C during host pathogen interaction. Poster P93. Annual Meeting of the American Society for Cell Biology, San Francisco (2016).

Halfen J, Kollasser J, Gröbe L, Hagendorff P, Geffers R, Steffen A, Brakebusch CH, Rottner K, Stradal TE. Dissecting the role of RhoA, -B and -C during host pathogen interaction. Poster P18. Conférences Jacques Monod: Actin and microtubule cytoskeleton - bridging scales from single molecules to tissues, Roscoff (2017).

Halfen J, Kollasser J, Gröbe L, Hagendorff P, Geffers R, Steffen A, Brakebusch CH, Rottner K, Stradal TE. Dissecting the role of RhoA, -B and -C during host pathogen interaction. Poster P27. 10^{th} Annual PhD Symposium HZI GS-FIRE, Braunschweig (2017).

Contents

List of Figures

List of Tables

Abbreviations

A	adenine
ADF	actin depolymerizing factor
ADP	adenosine diphosphate
AIP	actin interacting protein
Amp	ampicillin
ATP	adenosine triphosphate
a.u.	arbitrary unit
bp	base pair
BSA	bovine serum albumin
C	cytosine
°C	degree Celsius
Cas	CRISPR associated proteins
CK1	casein kinase 1
Cm	chloramphenicol
CNF	cytotoxic necrotizing factor
CRISPR	clustered regularly interspaced palindromic repeats
DMEM	Dulbecco's modified eagle medium
DNA	deoxyribonucleic acid
ECM	extracellular matrix
ELISA	enzyme linked immunosorbent assay
ER	endoplasmic reticulum
FACS	fluorescence associated cell sorting
FBS	fetal bovine serum
g	gram
x g	standard gravity
G	guanine

GAP GTPase activating protein

GDI GDP dissociation inhibitor

GDP guanosine diphosphate

GEF guanine nucleotide exchange factor

GFP green fluorescent protein

GTP guanosine triphosphate

Kan kanamycin

KO knockout

L liter

LB lysogeny broth

LIMK LIM kinase

LPA lysophosphatidic acid

M molar

mg milligram

ml milliliter

MLC myosin light chain

mM millimolar

MOI multiplicity of infection

MRCK myotonic dystrophy kinase related Cdc42 binding kinase

µg microgram

µl microliter

µM micromolar

ng nanogram

nm nanometer

nM nanomolar

NPF nucleation promoting factor

OD optical density

PAM protospacer adjacent motif

PBS phosphate buffered saline

PCR polymerase chain reaction

PFA paraformaldehyde

p.i. post infection

PKA protein kinase A

PKC protein kinase C

PKN protein kinase N

PLD phospholipase D

PRL phosphatase of regenerating liver

PVDF polyvinylidene difluoride

PVP polyvinylpyrrolidon

RISC RNA induced silencing complex

qPCR quantitative polymerase chain reaction

Rho Ras homology gene family

RNA ribonucleic acid

ROCK Rho associated protein kinase

rpm rounds per minute

RSV respiratory syncytial virus

SCV *Salmonella* containing vacuole

SDS-PAGE sodium dodecyl sulfate polyacrylamide gel electrophoresis

SEM standard error of the mean

SNX sorting nexin

Spec spectinomycin

SPI *Salmonella* pathogenicity island

SRF serum response factor

Strep streptomycin

T thymine

T3SS type three secretion system

TAE Tris acetate EDTA

TBST Tris buffered saline with Tween 20

TIAM T-cell lymphoma invasion and metastasis inducing protein

TSB tryptic soy broth

UV ultraviolet

WDR WD repeat containing protein

WT wildtype

1 Introduction

Eukaryotic cells contain three different types of cytoskeleton: actin, microtubules and intermediate filaments. Microtubules are formed by α- and β-tubulin dimers and are very dynamic. Two important processes mediated by these filaments are cell division and intracellular trafficking [1]. Motor proteins such as kinesins or dyneins are involved in the transport of cellular structures along microtubules [2]. Intermediate filaments are less well defined than actin filaments or microtubules, since they consist of a variety of proteins and are accordingly classified into different types. The filaments are linked to each other as well as different cellular components and are hypothesized to influence cell mechanics [3]. The actin cytoskeleton will be explained in more detail in the following paragraphs.

1.1 The actin cytoskeleton

Actin exists as globular G-actin monomers and filamentous F-actin. Thermodynamically, the barbed-end of F-actin filaments, also called plus-end, has a higher probability for polymerization, while the pointed-end, also called minus-end, preferentially depolymerizes. Both filament ends have the capability to grow and depolymerize, which renders the actin cytoskeleton highly dynamic. Hydrolysis of actin-bound adenosine triphosphate (ATP) to adenosine diphosphate (ADP) plays an important role in this process. ATP-bound G-actin monomers are added at the growing barbed end while nucleotide hydrolysis is associated with the treadmilling of the filament leading to ADP-actin dissociation from the pointed end [4]. Involvement of the actin cytoskeleton in essential cellular processes such as cell division or cell migration has been studied extensively [5].

1.1.1 Actin nucleation

Actin nucleation is the initial step which induces formation and polymerization of F-actin filaments and is tightly regulated. Spontaneous nucleation of actin, which is initiated by formation of a G-actin trimer, is a rare event. Furthermore, sequestering proteins, such as profilin, bind G-actin and inhibit nucleation [6] [7]. However, many actin nucleation factors are known, which can be divided into three groups: the Arp2/3 complex, formins and a rather diverse class including proteins such as Spire. The following paragraphs only describe mammalian actin nucleation factors, while it has to be considered that specific bacterial effector proteins, such as VopL from *Vibrio parahaemolyticus*, can also induce actin nucleation [8].

The Arp2/3 complex is the only actin nucleation factor not inducing linear actin polymerization but instead generating branches developing from the side of an already existing filament. This occurs by direct binding of Arp2/3 to the filament [9]. Arp stands for actin-related-protein and the complex consists of seven

protein subunits. The subunits Arp2 and Arp3 are structurally similar to actin monomers and thereby form a new nucleation complex by binding to the F-actin filament [10]. Nevertheless, the Arp2/3 complex can not induce nucleation without the help of a nucleation promoting factor (NPF). NPFs contain a VCA domain which enables binding to the Arp2/3 complex and actin monomers at the same time, inducing actin polymerization at the new developing branch [11]. So far identified NPFs are WASH, WHAMM, WAVE and WASP proteins [7].

Formins induce linear actin polymerization by binding to the fast growing barbed end of actin filaments. They consist of several domains with specific functions. The DID and DAD domain bind each other and thereby induce autoinhibition of the protein. This inhibition is released by binding of a specific Ras homology gene family (Rho) GTPase. Then, the formin FH1 domain binds profilin-bound actin, providing the actin filament bound by the FH2 domain with new monomers for polymerization [12]. There are four formin families in mammalian cells: Dia, Daam, FMNL and FHOD. The different family members have been shown to interact with various Rho GTPases and thereby induce different actin structures [13]. mDia1 induces stress fibers [14], while mDia2 leads to filopodia formation [15]. Daam proteins induce filopodia [16], while FMNL formins have been implicated in the formation of lamellipodia as well as filopodia [17] [18]. FHOD proteins are implicated in stress fiber formation [19], but are thought to rather stabilize existing stress fibers instead of forming new filaments [20].

The third protein family, including Spire, Cordon-bleu and JMY, clusters G-actin monomers. With their WH2 domain, these proteins bind multiple actin monomers to form a nucleus, thereby initiating actin polymerization [21].

1.1.2 F-actin structures

F-actin forms different structures, which perform specific functions and are shown schematically in Figure 1.1. The most prominent and best-studied cellular structures are lamellipodia, filopodia and stress fibers.

Lamellipodia are flat cellular protrusions, containing branched actin networks. Actin nucleation in lamellipodia is mediated by the Arp2/3 complex. The Arp2/3 complex has been implicated in cell migration, yet controversial studies exist considering its role during directed migration and chemotaxis [22] [23]. In addition to Arp2/3, actin polymerization in the lamellipodium is controlled by capping protein, which can bind to barbed ends, thereby stopping actin polymerization in a regulatory fashion [24].

Filopodia are finger-like protrusions containing linear F-actin filaments, which extend from the cell body. This linear organization implies barbed ends all pointing towards the plasma membrane. Myosin-X transports many proteins, including transmembrane receptors, along the parallel filaments towards the filopodial tip [25]. Transport of adhesion factors along filopodia aids in cell

migration and adhesion. This was for instance shown for epithelial cells, where filopodia induce contact with neighboring cells to generate confluent epithelial layers [26]. Stress fibers will be described in more detail in the next chapter.

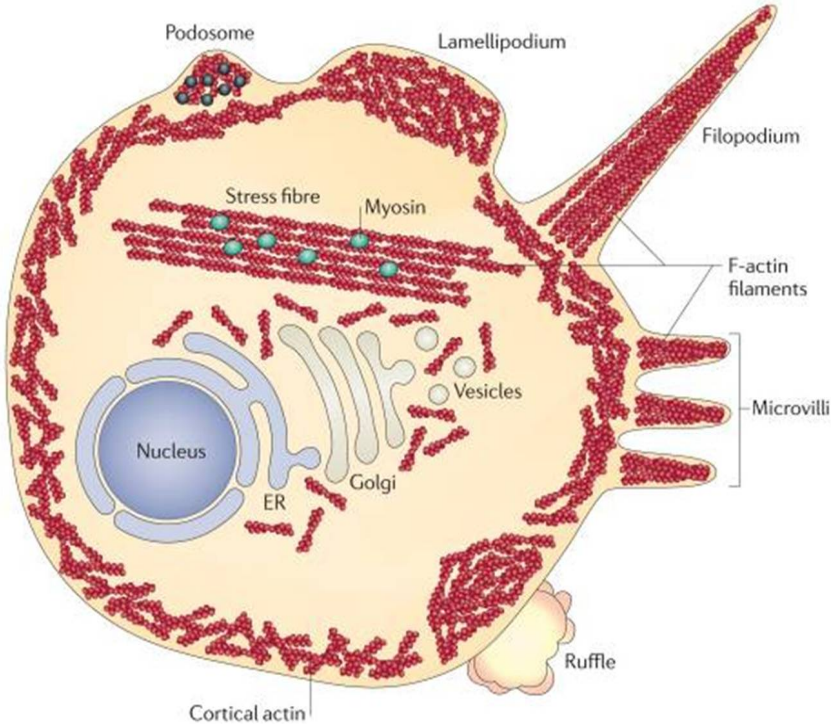

Figure 1.1: F-actin structures in the cell. F-actin, in red, forms various structures in the cell, including lamellipodia, filopodia and stress fibers, the latter of which are decorated with myosin shown in green [27].

1.1.3 Stress fibers

Stress fibers are composed of actin bundles decorated with α-actinin and non-muscle myosin II and mediate contraction [28] [29] [30]. The overall structure is shown in Figure 1.1, while the localization pattern of α-actinin and myosin II in stress fibers is displayed in Figure 1.2. The main function of stress fibers is to induce contraction, which is mediated via phosphorylation of myosin light chain [31].

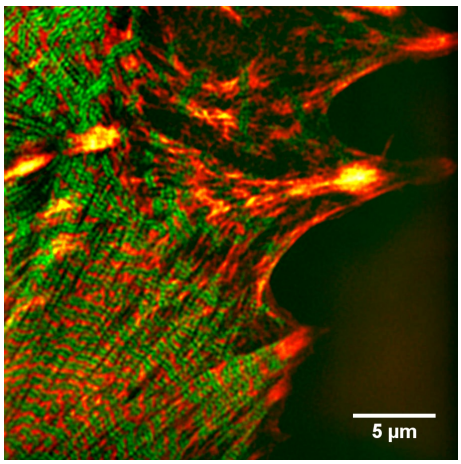

Figure 1.2: Localization of α-actinin and myosin light chain in stress fibers. Image shows how α-actinin in in red and myosin light chain in green are distributed along stress fibers (http://labs.mbi.nus.edu.sg/abcd/research.html) (29.08.2018).

Stress fibers can be divided into three categories: dorsal stress fibers, ventral stress fibers and transverse arcs, which are illustrated in Figure 1.3. The three categories differ by their connection to focal adhesions, their localization in the cell and their assembly mechanisms [32] [33]. Focal adhesions describe areas in which the actin cytoskeleton of the cell is connected to the extracellular matrix (ECM) via many receptors, including integrins. One of the major components of focal adhesions on the cellular side is vinculin, which links F-actin to the cellular membrane. It can bind directly to α-actinin [34]. Dorsal stress fibers are connected to focal adhesions at one end. They grow from focal adhesions at the leading edge of the cell towards the cell center, where they interact with transverse arcs. Actin polymerization of dorsal stress fibers is mediated by the formin mDia1 [33]. Dorsal stress fibers, in contrast to transverse arcs, were shown to contain almost no myosin II [35]. Transverse arcs are not directly connected with focal adhesions. Their development starts as small actin bundles at the leading cell edge which condensate and contract while they move towards the cell center [35]. In this case, stress fiber formation is suggested to depend on the Arp2/3 complex, which is usually known to generate branched actin filaments [33]. Ventral stress fibers associate with focal adhesions at both ends. In contrast to dorsal stress fibers and transverse arcs, which develop by *de novo* actin polymerization, ventral stress fibers are generated by re-organization of already existing structures. It was observed that a transverse arc, associated with two dorsal stress fibers on opposite sites, contracts and depolymerizes to finally yield a ventral stress fiber bound to the focal adhesion sites which beforehand belonged to the dorsal stress fibers. It is important to mention that all these stress fiber categories form a network and are highly dynamic [33].

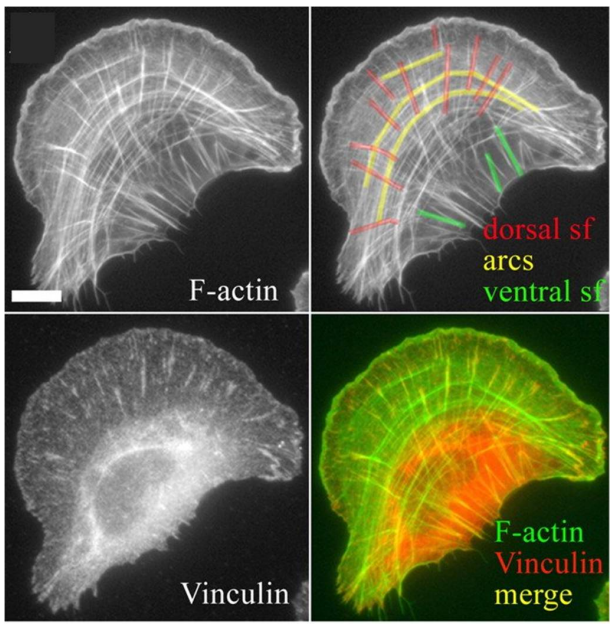

Figure 1.3: Stress fiber categories. Actomyosin stress fibers can be divided into three categories, illustrated in this image: dorsal stress fibers, ventral stress fibers and transverse arcs. Vinculin is a part of focal adhesions [33].

1.2 Rho GTPases

As mentioned above, the actin cytoskeleton is regulated by Rho GTPases. There are 20 different Rho GTPases in mammalian cells, which are shown in Figure 1.4. Many GTPases can be grouped according to their sequence similarities. Examples are RhoA, RhoB and RhoC, clustering tightly together, or also Rac1, Rac2 and Rac3. The best-characterized GTPases are RhoA, Rac1 and Cdc42, each regulating very specific actin structures in the cell.
Cdc42 for instance is involved in the formation of filopodia [36]. Lamellipodia on the other hand, and also membrane ruffles, are generated via Rac signaling [37] [38]. Membrane ruffling can also be induced by bacteria, such as *Salmonella enterica* serovar Typhimurium, to initiate uptake into non-phagocytic cells [39]. Finally, formation of stress fibers is mediated downstream of the Rho GTPases RhoA, RhoB and RhoC, which will be described in more detail in chapter 1.2.2 [40].

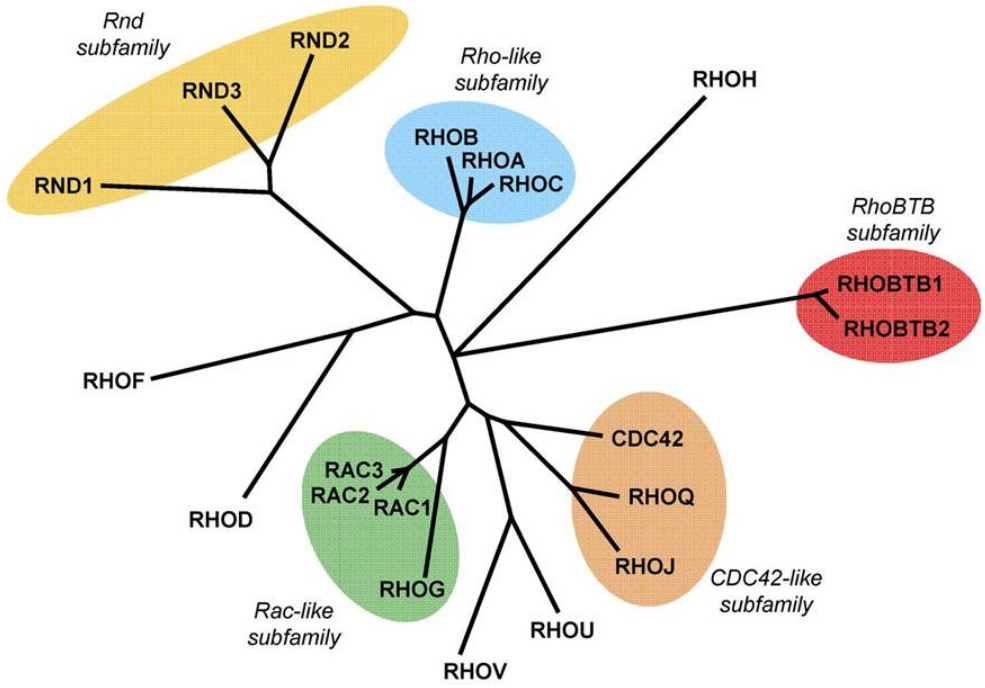

Figure 1.4: Overview of Rho GTPases. The phylogenetic tree shows sequence relations between all 20 mammalian Rho GTPases [41].

1.2.1 Rho GTPase regulation

Figure 1.5 shows how Rho GTPases themselves are regulated. Three different types of proteins are involved in this process. Rho guanine nucleotide exchange factors (GEFs) activate Rho GTPases by exchanging guanosine diphosphate (GDP) to guanosine triphosphate (GTP), whereas GTPase activating proteins (GAPs) are acting in the opposite direction. Rho GDP dissociation inhibitors (GDIs) protect the GTPases from degradation by binding them in the cytoplasm, which thereby also prevents activation via GEF proteins. Active GTPases are located on membranes [42].

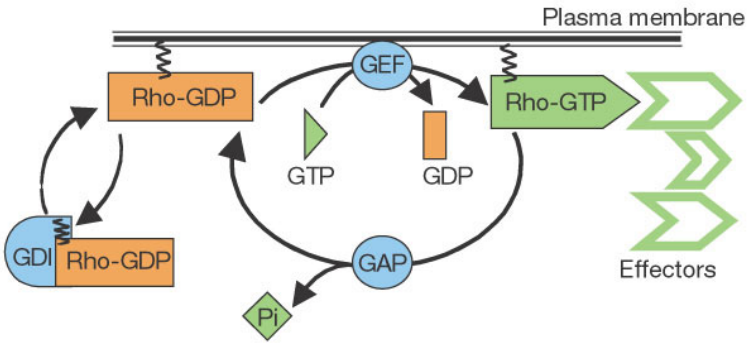

Figure 1.5: Activation cycle of Rho GTPases. Rho GTPases occur in an active, GTP bound, or inactive, GDP bound, state. Activation is initiated by GEFs and inactivation by GAPs. GDIs protect the inactive GTPases from degradation in the cytoplasm [42].

GEFs are classified in two different families, depending on the mechanism by which they induce nucleotide exchange. Dbl GEFs contain a DH/PH domain and, in contrast to DOCK GEFs, do not directly insert residues into the active site of the GTPase [43]. The proposed mechanism for nucleotide exchange via Dbl GEFs was analyzed in various studies [44] [45]. GEF binding induces transfer of the Mg^{2+} ion from the β- to the α-phosphate of GDP and subsequent release of both components. Displacement of Mg^{2+} from the β-phosphate destabilizes the connection between the GTPase and GDP. For GTPase activation via DOCK GEFs, an insert leads to conformational changes opening switch I in the GTPase and releasing GDP. Mg^{2+} bound GTP displaces the insert and yields an activated Rho GTPase [46]. It was shown that GEFs can simultaneously bind the GTPase and their respective effector protein to amplify the signal [47].

GAPs increase the hydrolytic activity of GTP when it is bound to the GTPase. Since the endogenous hydrolytic rate is rather slow, GAPs are able to inhibit or terminate signaling pathways very efficiently. There are three to four times more GAP proteins than Rho GTPases [48].

GDIs maintain a stable amount of inactive Rho GTPases in the cell. In addition to protecting the GTPases from degradation, Rho GDIs serve the function of mediating GTPase transport from the endoplasmic reticulum (ER) to the plasma membrane [49]. The ER is the final localization of Rho GTPase post-translational modifications. Modifications of Rho GTPases occur in three steps. First, the cysteine of the C-terminal CAAX tetrapeptide motif (C = cysteine, A = aliphatic amino acid and X = any amino acid) is either farnesylated or geranylgeranylated by farnesyltransferase or geranylgeranyltransferase type I, respectively [50]. This process, called prenylation, is necessary for the GTPases to associate with membranes and influences their localization. Degradation of Rho GTPases does not occur if the proteins are not prenylated yet [49]. Subsequently, the AAX motif is cleaved off by the Ras-converting enzyme 1 (Rce1) endoprotease. Finally, the cysteine is methylated by isoprenylcysteine-O-carboxyl methyltransferase (Icmt) [50]. An overview of the different Rho GTPase states and the role of GDIs is shown in Figure 1.6. There are three Rho GDIs in mammalian cells, namely GDIα, GDIβ and GDIγ. GDIα is the best characterized and most abundant protein of the three [51]. The *in vitro* affinity of GDIβ to Rho GTPases is lower than that of GDIα [52]. Also, expression of GDIβ was found predominantly but not exclusively in hematopoietic cells [53]. GDIγ localizes at the Golgi or other intracellular membranes and is expressed at low levels [54].

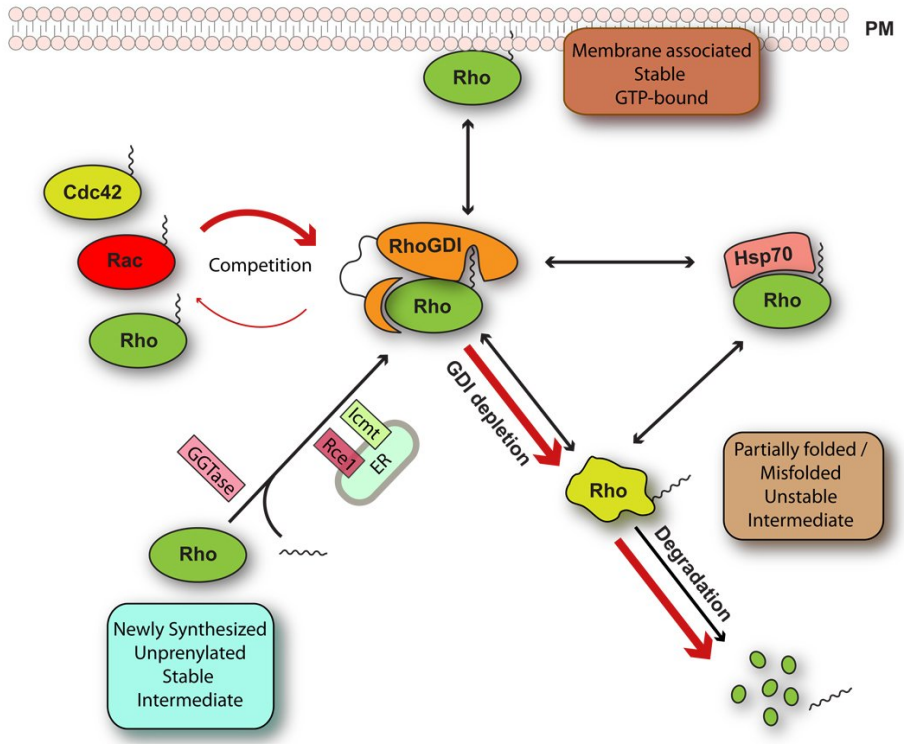

Figure 1.6: Role of Rho GDIs for GTPase stability. Newly synthesized Rho GTPases are modified by various proteins at the ER. Afterwards, Rho GDIs stabilize the prenylated form of Rho GTPases to protect them from degradation and shuttle them from the ER to the plasma membrane, where they reside in their active form. GDIs are capable of binding to various Rho GTPases, inducing binding competition. Furthermore, chaperones such as Hsp70 can stabilize Rho GTPases in the cytoplasm [49].

1.2.2 RhoA, RhoB and RhoC

The *rhoA* gene is longer and has more exons than those encoding for RhoB and RhoC. The *rhoB* gene in particular is rather short and has no introns (see also Figure 3.3). All three genes are located on different chromosomes, namely chromosomes 2, 5 and 3, respectively, in humans [55]. The amino acid sequence of the three proteins shows 85% identity with the variable regions being located at the C-terminus. The N-terminus contains the regions that are important for the binding of and switching between GDP and GTP [56].

The predominant localization of RhoB on endosomal membranes, in contrast to RhoA and RhoC which localize only at the plasma membrane, is mediated by the post-translational modification of two cysteins, upstream of the CAAX motif, by the fatty acid palmitate. This targets RhoB specifically to its desired location and is also found in a similar fashion in other GTPases that act on endosomal membranes. The localization of RhoB, to either the plasma membrane or endosomal membranes, is not depending on the first step of post-translational modifications, since RhoB can be farnesylated as well as geranylgeranylated. Inhibiting either farnesyltransferase or geranylgeranyltransferase does not induce specific localization of RhoB to either only endosomal membranes or only plasma membranes. RhoA and RhoC, as most GTPases, are exclusively geranylgeranylated.

It was also found that the cellular localization of RhoB depends on Rce1 modifications, whereas Icmt modifications are influencing RhoA localization [50].

RhoB expression can be induced upon DNA damage, for instance by UV radiation [57]. Its half-life is rather short and RhoB mRNA levels change during the cell cycle, suggesting a strict regulation [58]. RhoB becomes activated on endosomes by its GEF Vav2, which acts downstream of EGF receptor stimulation [59]. Activated RhoB recruits the formin mDia1 and the serine/threonine protein kinase PRK1 [60]. Actin polymerization by mDia1 leads to an actin coat around the endosome. The actin coat is linked to the cortical actin network and thereby prevents endosome transport on microtubules towards the perinuclear area. The role of PRK1 in this process in unknown. Rho associated protein kinase (ROCK), one of the best-studied downstream effectors of Rho proteins (see chapter 1.3.1), is not involved in RhoB mediated actin coats on endosomes [61]. A schematic model of the process is shown in Figure 1.7.

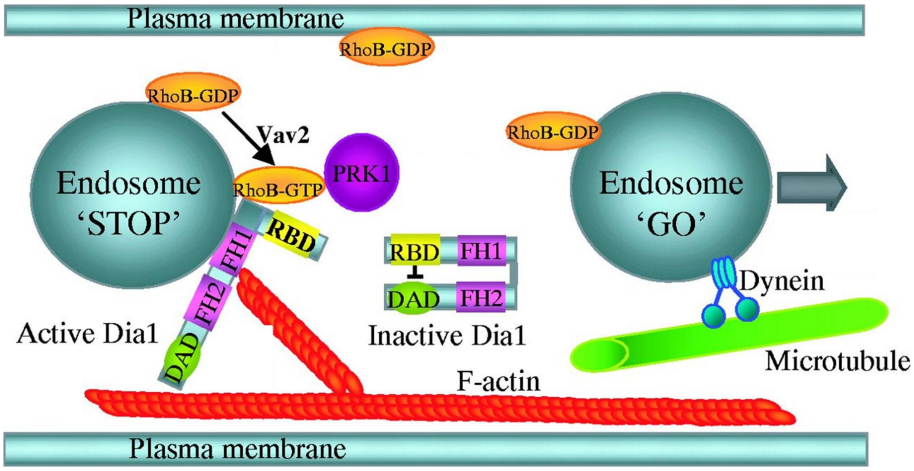

Figure 1.7: RhoB activity on endosomes. RhoB gets activated by Vav2 on endosomes and subsequently activates the formin Dia1. Dia1 induces actin polymerization and formation of an actin coat around the endosome, which prevents further transport along microtubules. If RhoB is inactive, motor proteins such as dynein can transport endosomes on microtubules [61].

Binding of the three Rho proteins to downstream effectors has only been analyzed to some extent in direct comparison. It seems that all three can bind to the same effectors, yet some differences occur in affinity and respective cellular localizations. Many studies on Rho proteins were performed using C3 toxin from *Clostridium botulinum*, which does not distinguish between the three proteins since it inactivates all of them [56].

Important cellular processes, regulated by RhoA, RhoB and RhoC, are cell migration, cell adhesion and cytokinesis. By activation of ROCK and thereby phosphorylation of myosin (see chapter 1.3.1), contraction of stress fibers is induced, which is needed during migration at the cell rear for detachment of the cell body [56]. Rho is needed for the contraction and abscission process during cytokinesis together with Anillin and Citron kinase, which is described below (see chapter 1.3.3).

In addition to directly regulating the actin cytoskeleton on protein level, RhoA was shown to regulate gene transcription via serum response factor (SRF). The transcription factor MAL binds to G-actin in the cytoplasm. Actin polymerization induced by Rho reduces G-actin levels, which leads to a translocation of MAL to the nucleus, where it acts as a cofactor of SRF and regulates gene expression of actin and vinculin for instance [62]. Also for RhoC a SRF dependent regulation of HOTAIR, a non-coding RNA strongly expressed in cancer tissues, was identified [63].

All three Rho proteins have been involved in cancer, yet in different ways. RhoA seems to be able to induce transformation of cells and was found to be upregulated in many cancer cells [56]. RhoC is not involved in transformation but was shown to specifically induce metastasis and cancer cell migration and invasion and is therefore also often upregulated in the respective cell types [64]. RhoB expression on the other hand is often decreased during late stages of cancer development, whereas it can also promote initial transformation [56].

In addition to regulation of GTPase activity by GEFs, GAPs and GDIs, phosphorylation of RhoA at Serine188 has been proposed to suppress Rho activity, but at the same time increases its stability. Binding of GDIs to phosphorylated active RhoA was shown to be enhanced in comparison to its unphosphorylated form [65]. Along the same line, RhoA phosphorylation led to a localization change of the GTPase, from the membrane to the cytoplasm, mediated by membrane extraction via GDIs [66]. Phosphorylation of RhoB on Serine185 was shown to occur via casein kinase 1 (CK1), inhibition of which induced RhoB activation and stress fiber formation. CK1 only phosphorylated RhoB, not RhoA or RhoC [67]. PKCϵ on the other hand was hypothesized to serine-phosphorylate and thereby inactivate RhoA and RhoC [68].

1.3 Downstream effectors of RhoA, RhoB and RhoC

1.3.1 ROCK and myosin II

ROCK1 and ROCK2 were identified as serine threonine kinases binding specifically to active RhoA [69] [70]. The Rho binding domain of ROCK mediates autoinhibition of the kinase, which is released by binding to Rho [71] [72]. Important signaling pathways downstream of ROCK include myosin II activation or inactivation of the actin depolymerizing factor Cofilin [73].

Non-muscle myosin II binds to F-actin and is responsible for contraction of stress fibers. The structure of the protein is shown in Figure 1.8.A. The globular head domain of myosin II binds F-actin and ATP. Hydrolysis of ATP induces movement of myosin II towards the barbed end of the filament, thereby moving the filament in the opposite direction (see Figure 1.8.B). There are three genes encoding for different heavy chains (see the tail in Figure 1.8.A), namely IIa, IIb and IIc [74]. Myosin IIa has the highest ATP hydrolysis rate of the three, whereas myosin IIb has a very high affinity to ADP and shows a very slow ADP release [75] [76]. Also, myosin IIa is found predominantly in dynamic areas such as protrusions or retraction areas at the back of the cell during migration, whereas myosin IIb incorporates in already existing actin bundles in the cell center or the cell rear [77]. Not much is known about myosin IIc so far, a much lower percentage of which is bound to actin in comparison to myosin IIa and IIb [78].

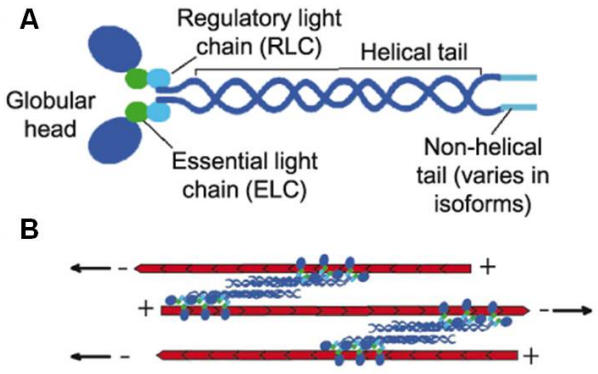

Figure 1.8: Myosin II and actin stress fibers. (A) Structure of myosin II. (B) F-actin in red. Myosin II moves towards the barbed end (+), thus initiating movement of the actin filament in the opposite direction [79].

Phosphorylation of the myosin II regulatory light chain increases its ATPase activity and thereby induces contraction in the presence of actin, even though the affinity for actin remains unchanged [80]. One of the most studied kinases phosphorylating and thereby activating myosin light chain (MLC) is ROCK [81] [82]. In addition to direct myosin II activation, ROCK inactivates myosin phosphatase, which would itself otherwise inhibit myosin light chain activation by dephosphorylation [83]. Myosin II phosphorylation does not only occur down-

stream of Rho and ROCK, but can also be mediated by myotonic dystrophy kinase related Cdc42 binding kinase (MRCK) downstream of Cdc42 [84], Citron-kinase and myosin light chain kinase [85]. Rac, being antagonistic to RhoA, is hypothesized to inhibit myosin II activation [74].

Incorporation of myosin II into dorsal stress fibers occurs at late elongation time-points. In the beginning, while dorsal stress fibers start growing towards the cell center, they are mainly decorated by α-actinin. At a certain length and after connection to transverse arcs, myosin II starts displacing α-actinin and incorporates into the stress fibers. The binding of myosin II and α-actinin to actin stress fibers is mutually exclusive. Transverse arcs on the other hand, contain higher amounts of myosin II and are more sensitive to myosin inhibition by blebbistatin [33] [35].

1.3.2 Cofilin

The Cofilin protein family consists of Cofilin 1, Cofilin 2 and actin depolymerizing factor (ADF). Cofilin 1 is the most abundant protein of the family [86]. Cofilin has at least two mechanistic functions to control F-actin levels, namely inhibiting binding of myosin II to F-actin and thereby controlling contraction mechanisms in the cell [87], and in addition severing of actin filaments. This occurs at boundaries between Cofilin-bound and undecorated filament areas [88]. These differences induce structural changes that are needed for the severing process [89]. Cofilin decorated actin filaments depolymerize faster at their pointed ends but also depolymerize slowly at their barbed ends. This effect is stronger when ADF is bound instead of Cofilin 1 or Cofilin 2 [90]. Another study also showed that Cofilin 2 and ADF are more efficient at induction of actin depolymerization than Cofilin 1, since lower amounts of these proteins are sufficient to initiate the severing process [91].

WD repeat containing protein (WDR)1, also called actin interacting protein (AIP) 1, caps barbed ends of Cofilin severed actin filaments, thereby increasing depolymerization efficiency of Cofilin [92]. Initially, it binds specifically to Cofilin decorated F-actin, enhances the severing process and then remains bound to the barbed end [93]. There are currently two theories about how WDR1 promotes severing. One is, that by displacing Cofilin on actin filaments, boundaries of Cofilin bound and unbound areas are created, which initiates severing. Alternatively, WDR1 binding could lead to structural changes at the F-actin binding site of Cofilin [89] [94] [95]. Figure 1.9 displays the two potential mechanisms.

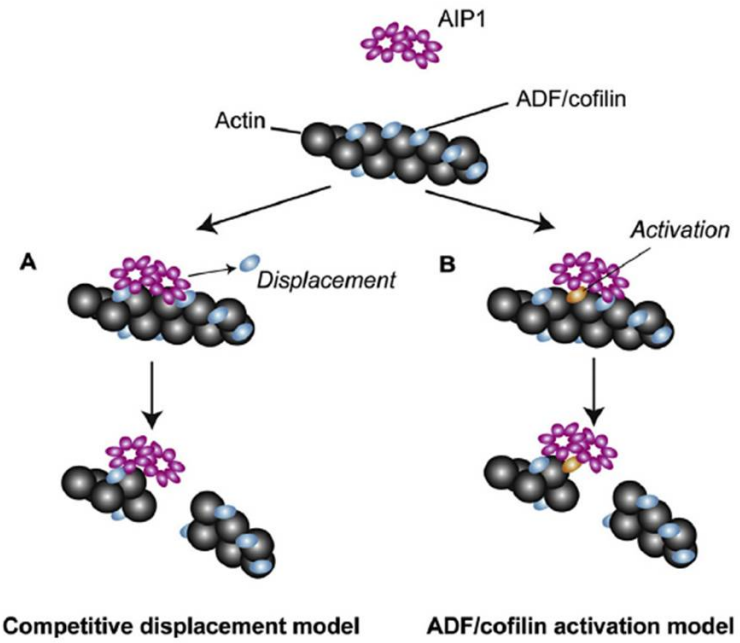

Figure 1.9: Actin severing by Cofilin and WDR1/AIP1. (A) WDR1/AIP1 displaces Cofilin from actin, thereby creating boundaries between Cofilin decorated and undecorated regions which promotes severing. (B) Binding of WDR1/AIP1 to Cofilin induces structural changes to activate actin severing properties of Cofilin [89].

Cofilin proteins are inactivated by phosphorylation at Ser3 by LIM kinase (LIMK). Dephosphorylated and thereby active Cofilin localizes clearly at lamellipodial protrusions, whereas the inactive form of the protein is distributed diffusely in the cell [96]. LIMKs themselves can be activated by various kinases, including ROCK downstream of Rho [97] and MRCKα downstream of Cdc42 [98]. RhoC regulates Cofilin phosphorylation locally and specifically in lamellipodial protrusions during cell migration. RhoC itself is strictly regulated by p190RhoGEF and p190RhoGAP during that process [99]. A recent study revealed phosphorylation of Cofilin mediated via WDR1 and LIMK, offering an additional level of regulation via WDR1 [100]. Another mechanism of Cofilin inactivation involves binding to phosphoinositides at the plasma membrane. This connection disables Cofilin from binding to actin as well as WDR1 [101].

1.3.3 Other Rho signaling pathways

RhoA has been shown to play an important role during two phases of cell division [102]. During prophase, when cells enter mitosis, RhoA mediates cell rounding and stiffening of the cellular cortex [103]. Later, RhoA is needed to induce contraction, mediating the abscission process [104]. There are no studies on RhoB or RhoC functions during cell division. Two proteins that are classified as RhoA downstream effectors mediating cell division are Anillin and Citron-kinase. The latter is actually needed for recruitment of RhoA and Anillin to the intercellular bridge during telophase and thereby essential for induction of the abscission process [105]. Another study also proposed that Citron-kinase is in fact an upstream regulator of RhoA, since RhoA inactivation only affects the

localization of Anillin, not of Citron-kinase. Depletion of Citron-kinase on the other hand displaces RhoA and Anillin from the midbody, which is the structure mediating the abscission process [106].

Rho can also, directly or indirectly, activate phospholipase D (PLD). Direct PLD activation occurs via binding of Rho to the C-terminus [107], whereas indirect activation is mediated via an additional Rho downstream effector, protein kinase N (PKN), which can also bind and activate PLD [108]. PLD is involved in many cellular processes such as trafficking, secretion, endocytosis and prevention of apoptosis [109] [110]. PKN, on the other hand, is involved in trafficking, cell migration and cortical actin formation downstream of Rho proteins [111] [112].

1.4 Pathogens manipulating the actin cytoskeleton

Many pathogens, bacteria as well as viruses, manipulate the actin cytoskeleton for their own benefit during the infection process. As an example, analysis by Alto *et al.* [113] revealed 24 bacterial proteins that share a common WxxxE motif. The WxxxE proteins can act as GEFs to activate Rho GTPases in infected host cells. The tryptophane (W) and glutamic acid (E) residues are conserved and do not show any variation throughout this protein family. Bacteria included in this list are enterohemorrhagic *E. coli*, enteropathogenic *E.coli*, *Citrobacter rodentium*, *Shigella flexneri*, *Shigella dysenteriae*, *Salmonella enterica* and *Salmonella enteritidis*. The WxxxE proteins are translocated into host cells via a type three secretion system (T3SS). This apparatus consists of a basal body residing in the bacterial membranes and a needle, whose tip is in contact with the host cell membrane, mediating formation of a pore and transport of bacterial virulence factors directly into the host cell [114].

Invasion of bacteria into host cells is classified in two mechanisms, one of which, the trigger-mechanism, involves the T3SS. Trigger-invasion depends on bacterial virulence factors being injected into the host cell and inducing uptake by manipulation of host cell proteins in the cytoplasm, which involves regulation of the actin cytoskeleton. Zipper-invasion on the other hand is mediated by bacterial surface proteins binding to receptors on the cell surface and influencing actin rearrangements by receptor signaling. Whereas *Listeria* and *Yersinia* species are well-known examples for the zipper-mechanism, *Shigella flexneri* and *Salmonella enterica* serovar Typhimurium use the trigger-pathway [115].

1.4.1 *Salmonella enterica* serovar Typhimurium

The gram-negative genus *Salmonella* of the family *Enterobacteriaceae* consists of two species, *S. enterica* and *S. bongori*. *S. enterica* is divided in multiple serovars, including Enteritidis, Paratyphi, Typhi and Typhimurium [116]. Some serovars, such as Typhi and Paratyphi can cause Typhoid fever and infect only humans. Non-typhoidal serovars, such as Typhimurium and Enteritidis cause salmonel-

losis, the main cause of gastroenteritis in humans and also animals, which causes around 155 000 deaths per year worldwide [117] [118]. *S. subterranea* used to be classified as a third *Salmonella* species, which has been revised due to new investigations [119].

Salmonellae infect humans and animals via contaminated food or water. Infection in the intestine occurs by transport of the bacteria through specialized M cells to the basolateral epithelial side. An important virulence factor is the flagellum, which provides bacterial motility and at the same time induces strong immune responses in the host [120]. On the basolateral side, bacteria are either taken up by macrophages or invade non-phagocytic enterocytes. After invasion, *Salmonella* resides in the *Salmonella* containing vacuole (SCV) to replicate in the host cell [121]. Two T3SSs, encoded on the *Salmonella* pathogenicity island (SPI)-1 and SPI-2, deliver effectors into the host cell to ensure bacterial invasion and survival. SPI-1 effectors facilitate entry into non-phagocytic cells, whereas SPI-2 is important for survival of bacteria residing in the SCV [122]. Three effectors relevant for the invasion process will now be described in further detail.

The *sopE* gene is found only in some *Salmonella* strains, but most of these have been epidemic [123]. SopE induces membrane ruffling in cells, which is mediated via Rac1 and Cdc42 activity. It was also shown that SopE increases the exchange of GDP to GTP on various Rho GTPases, including Rac1, RhoA and Cdc42. An increase was also detectable for RhoB and RhoC but it was more subtle since the basic level of GTP bound Rho GTPase without SopE was much lower [124]. SopE acts as a GEF by inserting its GAGA motif between switch I and switch II of the GTPase, which induces GDP release [125]. In addition, SopE promotes fusion of the SCV and early endosomes [126] to inhibit contact with the lysosome [127]. SCVs containing dead bacteria gain late endosomal markers such as Rab7 and later fuse with the lysosome which would lead to bacterial killing. SCVs with living bacteria do not acquire Rab7 or other late endosomal markers and thereby avoid killing by the lysosome [127]. The fusion of SCV and early endosomes is mediated via SopE binding to and activating Rab5 on the SCV surface. SopE is translocated to the cytosol, where it potentially activates Rab5, which can then in its GTP bound form be recruited by SopE to the phagosomal surface. Therefore, SopE also plays a role not only during invasion but also for later stages of infection [126].

SopE2 is conserved among various *Salmonella* strains and has 64% amino acid identity to SopE [128]. The effector protein activates Cdc42 and recruits the Arp2/3 complex to membrane ruffles, thereby promoting *Salmonella* invasion [129]. Invasion of a SopE2 mutant in HeLa cells was reduced to 17% [128].

The SopB protein from *Salmonella*, a phosphatidylinositol phosphatase, is secreted via the SPI1 type III secretion system. Phosphatidylinositoles can be phosphorylated at positions 3, 4 or/and 5 by phosphatidylinositol phosphatases, leading to the generation of phosphoinositides. These substrates regulate the

actin cytoskeleton in an indirect fashion. PtdIns(4,5)P_2 acts at the plasma membrane and can for example bind Cdc42, thereby supporting the generation of membrane ruffles [130]. After bacterial attachment to the cellular membrane, the phosphatidylinositol phosphatase activity of SopB leads to recruitment of the SNX18 host protein to the bacterial entry site. SNX (sorting nexin) proteins share a phospholipid-binding-domain and are involved in membrane trafficking and protein sorting [131]. SNX18 is important to form the SCV at the plasma membrane. This was shown to be independent of Rac1 and Cdc42 [132]. In addition, phosphatase activities of SopB recruit SNX9 to the bacterial entry site, which induces membrane ruffling by activation of the Arp2/3 complex activator N-WASP, leading to bacterial uptake [133] [134].

Figure 1.10 displays two mechanisms of *Salmonella* invasion and the respective implications of the effector proteins described above. The most studied pathway of entry is mediated by the Arp2/3 complex, although this mechanism was shown not to be essential for invasion [135]. A recently discovered pathway was shown to depend on SopB-mediated RhoA activation and myosin II-associated contraction [136]. The *S.* Typhimurium SL1344 strain was used for this study since it was shown to be highly invasive, induces large membrane ruffles and expresses the SopE protein [137].

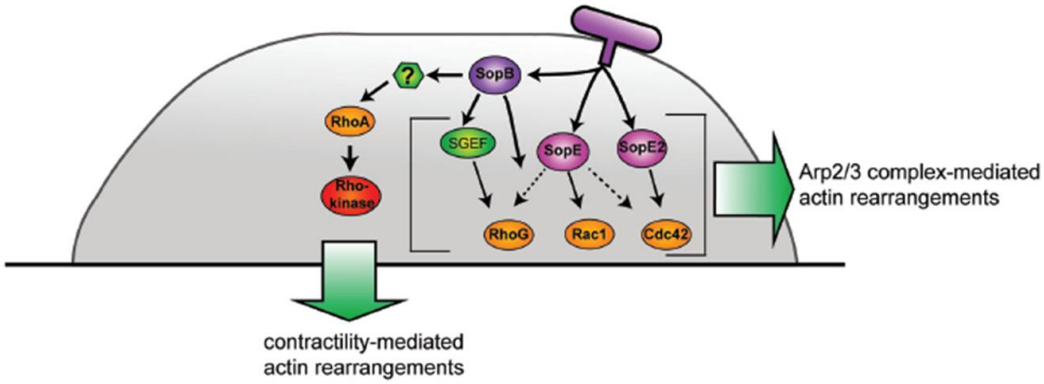

Figure 1.10: Invasion pathways of *Salmonella*. Virulence factors used by *S.* Typhimurium during two different invasion pathways are graphically displayed. SopB activates RhoA by a yet unknown mechanism, inducing contractility. On the other hand, SopB, SopE and SopE2 cooperate to induce membrane ruffling [138].

1.4.2 *Shigella flexneri*

Shigellae, as *Salmonellae*, are gram-negative bacteria belonging to the family of *Enterobacteriaceae*. There are four serogroups and also species, which are *S. boydii*, *S. dysenteriae*, *S. flexneri* and *S. sonnei*. The latter two are the predominant species causing shigellosis in developed and also developing countries [139]. *Shigella* species cause around 1 million deaths per year worldwide (http://www.who.int/immunization/topics/shigella/en/) (30.08.2018). The *S. flexneri* M90T strain was used in this study due to its virulence and invasiveness [140].

As *Salmonella*, *Shigella* species are food-borne pathogens that are taken up via contaminated nutrition. Once in the colon, bacteria breach the epithelial barrier by movement through M cells. On the basolateral site, they are either taken up by macrophages in which they induce cell death, or invade into epithelial cells [141]. After invasion, bacteria subsequently lyze the phagosomal membrane to escape into the cytoplasm. This is mediated by the haemolytic toxin IpaB [142]. Once in the cytoplasm, the bacteria use actin based motility, initiated via the IcsA protein [143], for spreading to neighboring cells while staying intracellular during the whole process. While entering the adjacent cell, a membrane forms around the bacterium developing into a vacuole. Finally *Shigella* escapes the vacuole and forms actin tails again [144].

Virulence factors of *Shigella* are encoded on the virulence plasmid pWR100 (see Figure 1.11). The mxi and spa proteins are important to form the T3SS, which translocates various effectors into the host cell to induce the invasion process. Additional genes encode regulators and chaperones for the effector proteins.

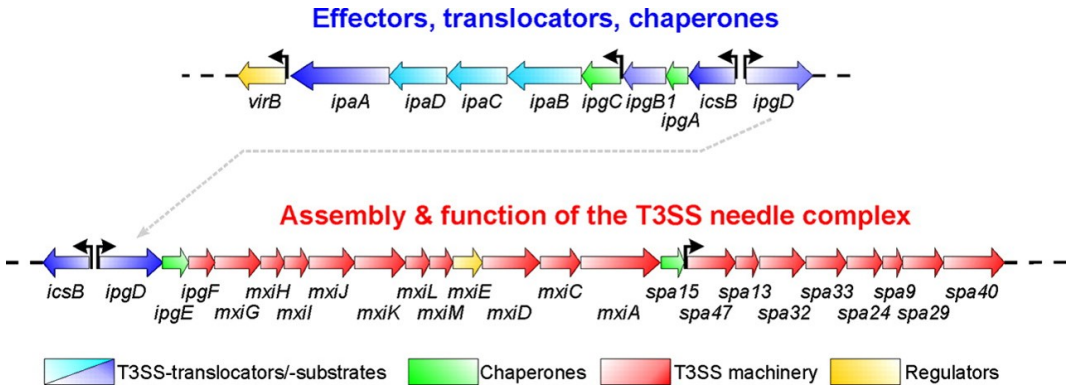

Figure 1.11: *Shigella* virulence plasmid pWR100. Virulence proteins of *Shigella* are encoded on the pWR100 plasmid and are either important to form the T3SS or are themselves effectors that are translocated into the host cell [145].

The virulence factor IpgB1, which is translocated via the T3SS, activates Rac1 and Cdc42. Subsequent generation of membrane ruffles, which are also formed upon overexpression of IpgB1 [146], aids in bacterial invasion into epithelial cells [147]. Activation of Rac occurs via the RhoG-ELMO-Dock180 pathway, in which IpgB1 is hypothesized to mimic RhoG [148]. Dock180 directly binds to and activates Rac1. RhoG binds to the ELMO protein and Dock180 to induce the activation [149].

IpgB2 induces the formation of stress fibers in cells [146]. Alto *et al.* [113] proposed that this process was independent of RhoA, but dependent on ROCK. Binding of IpgB2 to the Rho binding domain of ROCKI and ROCKII as well as mDia1 was thereby analyzed and verified [113]. Nevertheless, binding of IpgB2 to RhoA, acting as a Dbl-like GEF, was also confirmed a few years later [45]. The formation of stress fibers upon IpgB2 transfection is dependent on the WxxxE motif, since W62A and E66A mutations abolish the effect [113]. A collective role for IpgB1 and IpgB2 during invasion in epithelial cells was proposed [150].

IpgD shows 59% similarity and 41% identity to the amino acid sequence of SopB from *S.* Typhimurium. Similarly IpgE, the chaperone of IpgD, shares 57% sequence similarity and 29% identity to SigE, the chaperone for SopB [151]. As SopB, IpgD dephosphorylates PtdIns(4,5)P_2, thereby indirectly regulating the actin cytoskeleton and cell morphology [152]. Furthermore, IpgD induces long lasting Ca^{2+} signals during infection of epithelial cells and thereby delays focal adhesion disassembly [153]. Modification of Ca^{2+} fluxes by IpgD prevents activation of the protease calpain, so that cellular adhesions and cell-cell contacts are stabilized and not degraded by the protease [153] [154].

1.4.3 Other pathogens manipulating the actin cytoskeleton

In addition to *Shigella* and *Salmonella* strains, many other pathogens use the actin cytoskeleton of the host cell for their own benefit and manipulate Rho GTPase regulation. For instance, some strains of the enteropathogen *Yersinia pseudotuberculosis* express a protein called cytotoxic necrotizing factor $(CNF)_y$. This toxin activates RhoA, Rac1 and Cdc42. It was shown that RhoA activation by CNF_y increases effector translocation into the host cell via the T3SS [155].

Enteropathogenic and enterohaemorrhagic *Escherichia coli* (EPEC and EHEC) form pedestals on enterocytes in the gut instead of invasion into the cells. Pedestal formation and elongation are mediated by the bacterial virulence factor EspH, which induces actin polymerization via N-WASP and the Arp2/3 complex [156].

Belonging to the *Pneumoviridae* family, respiratory syncytial virus (RSV) induces lower respiratory tract infections, especially in children, the elderly and immunosuppressed patients. RSV has a negative sense RNA genome which is surrounded by a nucleocapsid and a lipid bilayer envelope [157]. One important protein embedded in the envelope is RSV-F.
The viral F-protein activates RhoA by increasing the amount of its isoprenylated and membrane-bound form. In addition, downstream signaling of RhoA, mediated by ROCK, was increased upon RSV infection [158]. RSV-F is able to bind GDP-RhoA and promotes syncytium formation, cell fusion and filamentous virion morphology. On the other hand, it is dispensable for infection efficacy and production of new virus particles [159][160]. The latter was shown to be dependent on Arp2. Filopodia formation and cell motility, promoting viral spread to uninfected cells, were also induced by RSV-F and facilitated by Arp2

[161]. Analysis of RhoA in the context of RSV infection described above was partially relying on the use of C3 toxin from *Clostridium botulinum*, which affects not only RhoA but also RhoB and RhoC [162]. Therefore, potential functions of RhoB and RhoC in RSV infection have not been analyzed in a distinct fashion in the past.

An example for a pathogen inhibiting RhoA is Vaccinia virus. Its F11 protein binds RhoA as well as Myosin-9A, which is a GAP for this GTPase. By bringing the GTPase and its respective GAP together, inactivation of RhoA is promoted, which facilitates viral spread [163]. Also Pseudorabies virus suppresses RhoA activity, in this case by phosphorylation of the GTPase via protein kinase A (PKA). This induces stress fiber breakdown and increases the amount of Rac1-mediated protrusions, supporting viral cell-to-cell spread [164].

1.5 Aim of the study

Rho proteins have been shown to be involved in important processes such as cell division and migration and are thus critical for cancer development. Furthermore, a recent study revealed a role for Rho in *Salmonella* invasion, in addition to Rho proteins being manipulated by many other pathogens. Nevertheless, most studies only focused on RhoA and neglected the closely related RhoB and RhoC proteins.

Therefore, the aim of this project was to analyze the specific contributions of RhoA, RhoB and RhoC to cellular as well as infection processes. For that purpose, knockout (KO) cell lines for the three proteins in various combinations were generated. Cell biological analysis was set out to distinguish the regulation of GTPases in the context with GDIs and also to investigate their distinct roles for the actin cytoskeleton and particularly for stress fiber formation. Global changes in mRNA expression depending on the specific Rho proteins as well as morphological changes upon Rho KO were elucidated to decipher the impact on gene regulation and the overall cellular phenotype, respectively.

In addition, infection studies with *Salmonella enterica* serovar Typhimurium in the context of Rho KOs gave further insight into the bacterial invasion process independent of Rac and membrane ruffling. Furthermore, infection studies with other pathogens expressing Rho activating factors, such as *Shigella flexneri*, were performed to discover potentially conserved mechanisms.

2 Materials and Methods

2.1 Chemicals, Buffers and Plastic ware

2.1.1 Chemicals

Chemicals, reagents and solvents used for this study were purchased from Addgene, Aobious, AppliChem, BD Biosciences, BioCision, Bioline, Bio-Rad, Biozym, Chromotech, Clontech Laboratories, Cytoskeleton, Dharmacon, Epicentre, Eurofins, Fluka, GE Healthcare, Gibco, Honeywell, Ibidi, J.T. Baker, Lonza, Macherey-Nagel, Merck, Millipore, Molecular Probes, NEB, Novagen, Qiagen, Promega, Roche, Roth, Serva, Sigma, Sino Biological, Thermo Fisher Scientific, Tocris, Toronto Research Chemicals and VWR. Details are stated in brackets whenever the reagent is mentioned during description of the methods.

2.1.2 Buffers

All buffers and media were prepared with deionized water (Milli-Q by Millipore). If not stated otherwise, H_2O will always refer to Milli-Q in the following chapters. Many buffers or media were sterilized by autoclaving before usage if necessary, for example phosphate buffered saline (PBS), which was used for many different experiments. It was prepared by dissolving a tablet from Gibco in 500 ml H_2O.

2.1.3 Plastic ware

Plastic tubes were ordered from Falcon and Sarstedt. Corning was the supplier for cell culture plastic, while petri dishes for bacteria were ordered from Greiner Bio-One.

2.2 Bacterial Culture

2.2.1 Bacterial Strains

Bacterial strains used for this study are listed in Table 2.1. *Salmonella enterica* serovar Typhimurium SL1344 wildtype (WT) will be referred to as *S.* Typhimurium in the following chapters. *Shigella flexneri* M90T WT will be termed *S. flexneri*. Details concerning the antibiotics, which are mentioned in table 2.1 are described in chapter 2.2.2.

Table 2.1: Bacterial strains

Strain	Resistance	Source
Escherichia coli TOP10	none	Zero Blunt TOPO PCR Cloning Kit (Thermo Fisher)
Salmonella Typhimurium SL1344 (wildtype)	none	Dirk Buhmann (University of Basel, Switzerland)
S. Typhimurium SL1344 ΔSopB	Spec	Wolf-Dietrich Hardt (ETH Zurich, Switzerland)
S. Typhimurium SL1344 ΔSopE/SopE2	Cm, Kan, Strep	Dirk Buhmann (University of Basel, Switzerland)
S. Typhimurium SL1344 ΔSopB/SopE/SopE2	Kan, Strep	Dirk Buhmann (University of Basel, Switzerland)
Shigella flexneri M90T (wildtype)	none	Philippe Sansonetti (Institut Pasteur, Paris)

2.2.2 Cultivation of Bacteria

Bacteria were cultivated in lysogeny broth (LB) medium (Table 2.2, Conc. means concentration), except for *Shigella* strains, which were grown in tryptic soy broth (TSB) medium (Table 2.3). Cultivation was performed in media containing respective antibiotics if necessary and was executed by agitation at 37°C (incubator from Thermo Fisher Scientific, IGS 400). Employed antibiotics were ampicillin (Amp), chloramphenicol (Cm), kanamycin (Kan), spectinomycin (Spec) and streptomycin (Strep) and are listed in Table 2.4. They were sterile filtered and stored at -20°C.
Bacterial colonies used for starting liquid cultures were picked from LB or TSB agar plates. For preparation of agar plates, media containing 16 g/l (LB) or 15 g/l (TSB) agar (BD Biosciences) were autoclaved and poured into ⌀10 cm plastic dishes (Greiner Bio-One). 500 ml agar-containing medium yielded ~20 dishes.
Long-term storage of bacteria was performed by mixing 600 µl overnight culture and 600 µl of 30% glycerol (Roth) in LB medium and stored at -70°C. For working cultures, bacteria were streaked on agar plates and incubated up-side down overnight at 37°C. The agar plates were stored up to 2 weeks at 4°C before new bacteria were thawed.

Table 2.2: LB medium

Compound	Company	Conc.
Bacto tryptone	BD	10 g/l
Bacto yeast extract	BD	5 g/l
NaCl	Roth	7.5 g/l

Table 2.3: TSB medium

Compound	Company	Conc.
Tryptic soy broth	BD	30 g/l

Table 2.4: Antibiotics

Antibiotic	Company	Working Concentration
Ampicillin (Amp)	Sigma	100 µg/ml
Chloramphenicol (Cm)	Sigma	20 µg/ml
Kanamycin (Kan)	Sigma	50 µg/ml
Spectinomycin (Spec)	Sigma	100 µg/ml
Streptomycin (Strep)	Sigma	90 µg/ml

2.2.3 Transformation of Chemically Competent Bacteria

Chemically competent *E. coli* TOP10 from the Zero Blunt TOPO PCR Cloning Kit (Thermo Fisher Scientific), were transformed by adding the respective deoxyribonucleic acid (DNA) (see chapter 2.3.7) and incubating the suspension on ice for 30 minutes. Afterwards, heat shocking of bacteria was achieved by a 1 minute incubation at 42°C (Thermocycler from Ditabis) to destabilize the bacterial membrane. Subsequently, bacteria were cooled on ice for 1 minute and, after adding 600 µl LB medium, transferred to 37°C at 500 rounds per minute (rpm) for 1 hour (Thermocycler from Eppendorf). Finally, bacteria were centrifuged at 10 000 x g for 2 minutes (Centrifuge Pico 17 from Thermo Fisher Scientific). Most of the supernatant was discarded and about 100 µl of the retaining supernatant was used to resuspend the bacteria, which were plated on LB agar plates containing the respective antibiotics using soda lime glass beads (⌀3 mm, Sigma). The plates were incubated up-side down at 37°C overnight and single colonies were used for further steps.

2.3 Molecular Biological Methods

2.3.1 Plasmid Preparation

Plasmid DNA was prepared using GeneJET Plasmid Miniprep Kit (Thermo Fisher Scientific). The preparation was done according to manufacturers protocol, except for the elution step, for which 50 µl of nuclease-free H_2O (Millipore) were used. DNA concentration and purity were controlled using Denovix DS-11+ at an optical density (OD) of 260 nm. Plasmid preparation for transfections was done using the Qiagen Plasmid Midi Kit. 75 ml overnight culture were used for the preparation and the rest of the procedure was performed according to manufacturers protocol. 150 µl of nuclease-free H_2O were used to dissolve the DNA pellet.
Plasmids used for this study are listed in Table 2.5. The pSpCas9(BB)-2A-GFP plasmids contain single guide ribonucleic acid (RNA) sequences for CRISPR-Cas9 mediated KO of RhoA, RhoB and RhoC (see chapter 2.3.10). sgRNA sequences were 5′-GAUAAGAGAGAGGCCGCAGG-3′ (RhoA), 5′-GCACCACCA-GCUUCUUGCGGA-3′ (RhoB) and 5′-GAUAUAGUUCUCAAAGACGGU-3′ (RhoC). Plasmid maps of pcDNA3 RSV-F, pCRBlunt II-TOPO vector and pSp-Cas9(BB)-2A-GFP are included in chapter 6.2.

Table 2.5: Plasmids

Name	Antibiotic Resistance	Source
pcDNA3	Ampicillin	Thermo Fisher
pcDNA3 RSV-F	Ampicillin	S. Haid [165]
pCRBlunt II-TOPO vector	Kanamycin	Zero Blunt TOPO PCR Cloning Kit (Thermo Fisher)
pEGFP-C1	Kanamycin	Clontech Laboratories
GFP-RhoA	Kanamycin	Addgene #23224
GFP-RhoB	Kanamycin	Addgene #23225
GFP-RhoC	Kanamycin	Addgene #23226
pSpCas9(BB)-2A-GFP RhoA	Ampicillin	J. Kollasser/ C. Brakebusch
pSpCas9(BB)-2A-GFP RhoB	Ampicillin	J. Kollasser/ C. Brakebusch
pSpCas9(BB)-2A-GFP RhoC	Ampicillin	J. Kollasser/ C. Brakebusch

2.3.2 Oligonucleotide Primers

Primers used for this study were ordered from Eurogentec and stored at -20°C as 100 µM stock solutions. A 1:10 dilution was used as working stock. The oligonucleotides are listed in Table 2.6. Rho primers were used to clone the respective genes for KO verification.

Table 2.6: Oligonucleotides

Name	Sequence 5′ to 3′	Purpose
M13 forward	GTAAAACGACGGCCAG	Sequencing
M13 reverse	CAGGAAACAGCTATGAC	Sequencing
RhoA forward	GGAAAGTCTGCACATGTATAGT	Cloning
RhoA reverse	AGGATCCAGGATACTAGATGT	Cloning
RhoB forward	AGCGGCAAGCAACAGGGA	Cloning
RhoB reverse	CCAGCTCCACCTGCTTGC	Cloning
RhoC forward	CTGCCTGCCAGTTTCAGCCAT	Cloning
RhoC reverse	GTGGTAAGGAAGGACATCCATG	Cloning

2.3.3 Polymerase Chain Reaction

Extracted DNA (see chapter 2.4.9) was amplified in a polymerase chain reaction (PCR) using Hot start KOD polymerase (Novagen) according to manufacturer's protocol (Table 2.7). KOD polymerase creates blunt-ended PCR products. Buffer, dNTPs and $MgSO_4$ were also purchased from Novagen. The respective PCR program is shown in Table 2.8. The PCR cycler used in this study was PeqSTAR 2x Gradient (Peqlab).
Amplification of DNA in a PCR reaction is accomplished in 3 steps. First, the double-stranded DNA is denatured at high temperatures to generate single strands. Next, the temperature is decreased to a specific point at which the respective primers anneal specifically to their complementary regions, flanking the target region. In the last step, the temperature is increased again to the optimal working temperature of the respective polymerase, which then elongates the double-stranded Primer-DNA regions to yield the target sequence. This cycle, which is repeated ~30 times, is shown in Figure 2.1.

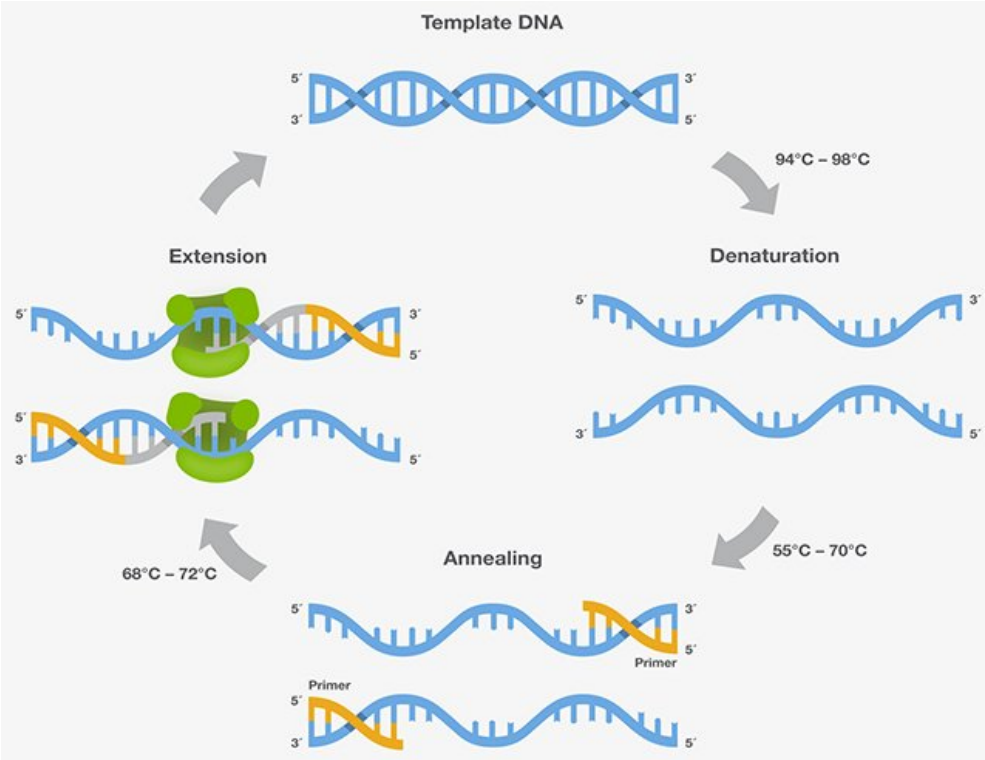

Figure 2.1: PCR cycle. Schematic representation of a PCR cycle, including denaturation, annealing and extension (https://www.thermofisher.com/de/de/home/life-science/cloning/cloning-learning-center/invitrogen-school-of-molecular-biology/pcr-education/pcr-reagents-enzymes/pcr-cycling-considerations.html) (26.03.2018).

Table 2.7: PCR reaction mix

Component	Stock concentration	Amount
Buffer	10x	2.5 µl
dNTPs	2 mM each	2.5 µl
$MgSO_4$	25 mM	1.5 µl
KOD polymerase	1 U/µl	0.5 µl
Primer forward	10 µM	0.75 µl
Primer reverse	10 µM	0.75 µl
DNA	-	~200 ng
H_2O	-	add up to 25 µl

Table 2.8: PCR program

Cycles	Denature	Annealing	Extension
1	95°C, 2 minutes		
10	95°C, 20 seconds	x°C*, 10 seconds	70°C, 10 seconds
25	95°C, 20 seconds	x°C**, 10 seconds	70°C, 10 seconds
1			70°C, 5 minutes

*: Annealing temperature starting with 65°C (RhoA), 68°C (RhoB), 70°C (RhoC) and decreasing 1°C per cycle
**: Annealing temperature 55°C for RhoA, 58°C for RhoB and 60°C for RhoC

2.3.4 qPCR

Isolated RNA from cells (described below in chapter 2.4.10) was used for quantitative polymerase chain reactions (qPCRs), which were performed by Silvia Prettin (HZI, Braunschweig). RNA was first mixed with 1 µl lysophosphatidic acid (LPA) (Thermo Fisher Scientific) and then with 50 µl NH_4OAc (Sigma) and 375 µl cold 100% ethanol. Precipitation was done for 30 minutes at -80°C. After centrifugation at 14 000 rpm for 20 minutes at 4°C, the pellet was washed twice with cold 80% ethanol and finally dried at 37°C. 11 µl DEPC (Roth) were used for dissolving the pellet.
The respective qPCR primers for murine RhoB were ordered from Sino Biological (Catalog number MP202540). The SensiFAST SYBR No-ROX One-Step Kit (Bioline) was used for the subsequent qPCR reaction in a LightCycler 480 (Roche) according to manufacturers protocol with 100 ng RNA. The PCR program is shown in Table 2.9.

Table 2.9: qPCR program

Cycles	Temperature	Time
1	45°C	10 minutes
1	95°C	2 minutes
45	95°C - 60°C - 72°C	5 seconds - 10 seconds - 5 seconds
1	95°C	5 seconds
1	65°C	1 minutes
1	40°C	30 seconds

2.3.5 Agarose Gel Electrophoresis

PCR products were subsequently mixed 5 : 1 with 6x loading dye (Thermo Fisher Scientific) and loaded on 1% agarose gels. Agarose gels were produced by dissolving agarose (AppliChem) in 1x Tris acetate EDTA (TAE) buffer (Table 2.10) and boiling the solution for complete solubility. The warm agarose solution was mixed with Midori Green (Biozym), of which 5 µl were used for 100 ml of TAE buffer, and poured into a gel chamber. The DNA ladder chosen for analysis was the 100 bp ladder from NEB (Figure 2.2). 3 µl ladder were used per gel. Midori Green intercalates into DNA, which can thereby be detected under ultraviolet (UV) light. The software used for analysis was Geljet Imager by Intas. Since DNA is negatively charged, it can be separated by size in an agarose gel by moving towards the positively charged pole. Smaller fragments move faster through the pores, which leads to separation of the molecules.

Table 2.10: TAE buffer 50x

Compound	Company	Concentration
Tris base	Roth	2 M
Acetic acid	VWR	1 M
EDTA	Fluka	50 mM

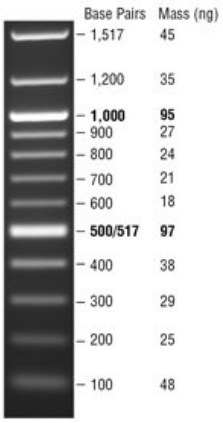

Figure 2.2: DNA ladder. The Quick load 100 bp ladder from NEB was used for analysis on agarose gels (https://www.neb.com/products/n0467-quick-load-100-bp-dna-ladder#ProductInformation) (22.03.2018).

2.3.6 DNA Purification

Amplified DNA fragments were cut with a scalpel out of agarose gels under UV light and subsequently purified using GeneJET Gel Extraction and DNA Cleanup Micro Kit (Thermo Fisher Scientific). The extraction was done according to manufacturer's protocol, except for the final elution, for which 10 µl of nuclease-free water (Millipore) were used.

2.3.7 TOPO Cloning

After purification, DNA fragments were cloned into pCRBlunt II-TOPO vector (see Table 2.5) according to manufacturer's protocols. 2 µl of DNA were mixed with 1 µl salt solution, 1 µl TOPO vector and 2 µl H_2O (all provided by Zero Blunt TOPO PCR Cloning Kit, Thermo Fisher Scientific). The solution was incubated at room temperature for 5 minutes and then cooled on ice. Transformation of the complete solution into chemocompetent bacteria was performed as described in chapter 2.2.3.

2.3.8 Enzymatic Digestion

After TOPO cloning, single bacterial colonies were picked and DNA was prepared as described in chapter 2.3.1. Before sequencing, DNA samples were screened by enzymatic digestion. For that purpose, 4 µl DNA were incubated with 1 µl EcoRI (cutting at 5′-GAATTC-3′, behind the guanine), 1 µl 10x FastDigest Green Buffer (Thermo Fisher Scientific) and 4 µl nuclease-free water (Millipore) at 37°C (Thermocycler from Ditabis) for 30 minutes. This was controlled by loading 5 µl of the mixture on a 1% agarose gel (see chapter 2.3.5). Due to usage of FastDigest Green Buffer no additional loading buffer was needed.

2.3.9 DNA Sequencing

Sequencing of DNA was performed by Eurofins. For that purpose, 5 µl DNA were mixed with 5 µl nuclease-free water (Millipore) and 10 µl of 10 µM M13 forward or M13 reverse primer (Table 2.6).

2.3.10 CRISPR/Cas9

The CRISPR/Cas9 technology, which is shown in Figure 2.3, can be used to induce defined gene KOs. CRISPR stands for Clustered regularly interspaced palindromic repeats, whereas Cas means CRISPR-associated proteins. For KO generation, specific single guide (sg) RNAs (see chapter 2.3.1) are designed, which are complementary to the target sequence that should be mutated. These sequences are cloned into the pSpCas9(BB)-2A-GFP plasmid, which is then used to transfect cells. Transfected cells are selected via fluorescence associated cell sorting (FACS) according to their green fluorescent protein (GFP) signal (see chapter 2.4.7). The Cas9 enzyme, which is coupled to the sgRNA, induces double strand breaks at the specific target sites, which can lead to mutations. A specific sequence motif, called protospacer adjacent motif (PAM), needs to be present downstream of the target region in order for the nuclease to cut the DNA [166]. In this project, the method was used to generate KO clones for RhoA, RhoB and RhoC.

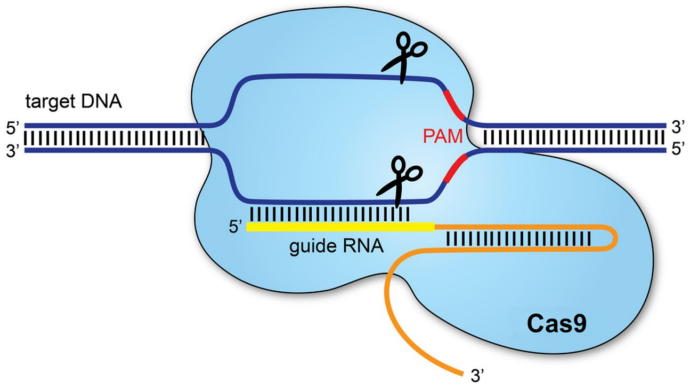

Figure 2.3: CRISPR/Cas9. The single-stranded guide RNA leads the Cas9 nuclease to the specific mutation site, where double strand breaks are induced, leading to gene KOs. PAM sites on the 3' end of the target region are necessary for cutting by the nuclease [166].

2.3.11 Microarray-Analysis

For analysis of RNA regulation in Rho KO cells, samples of all cell lines were resuspended in RLT buffer (Qiagen). For that purpose, 4 x 10^6 cells were centrifuged for 5 minutes at 1000 rpm (Centrifuge 5804 R from Eppendorf). The supernatant was discarded and the pellet was resuspended in 350 µl of buffer and stored at -70°C. After thawing, cells were vortexed for 1 minute and RNA was subsequently isolated using RNeasy Mini Kit (Qiagen). DNAse digestion was performed during RNA isolation as described in the protocol. Quality of the RNA was controlled afterwards using a Bioanalyzer (Agilent Technologies).

Labeling and scanning of samples was performed as described by Agilent Technologies (Scanner G2565CA). Agilent 4x44k_Mouse V2 design ID : 026655 was used for microarray analysis. From RNA isolation on, the procedure was done by Petra Hagendorff (GMAK, HZI, Braunschweig).

2.4 Cell Culture

2.4.1 Cell Culture Media

All cells mentioned in this study were cultured in DMEM with 4.5 g/L glucose (Gibco), 10% fetal bovine serum (FBS) (Sigma), 1% Glutamine (Gibco) and 1% MEM-Non-Essential-Amino-Acids (Gibco) at 37°C and 7.5% CO_2 in an i160 incubator from Thermo Fisher Scientific. Only Rac fl/fl and Rac $-/-$ cells (see Table 2.11) were grown in medium additionally containing 1% sodium pyruvate (Gibco). Media were sterile filtered through 0.22 µm pores of Corning filters.
For passaging, which was done every second day, cells were washed with PBS (Gibco) to get rid of medium remains (which could inhibit Trypsin functionality) and detached with Trypsin-EDTA (Gibco). The reaction was stopped by adding cell culture medium and diluting the cells appropriately. NIH-3T3 WT cells and RhoBC KO clones were usually diluted 1 : 10 for two days, whereas RhoAB KO clones were diluted 1 : 3 and RhoAC KO clones 1 : 4. Rac fl/fl cells were passaged at a 1 : 20 dilution, whereas Rac $-/-$ cells were diluted 1 : 6.

2.4.2 Cell Lines

The cell lines used in this study are listed in Table 2.11. Numbers of Rho KO cells are respective clone numbers.

Table 2.11: Cell lines

Name	Properties	Source
NIH-3T3 wildtype	mouse embryonic fibroblasts	ATCC CRL-1658
NIH-3T3 RhoA1	RhoA knockout	this study
NIH-3T3 RhoA2	RhoA knockout	this study
NIH-3T3 RhoA3	RhoA knockout	this study
NIH-3T3 RhoB1	RhoB knockout	this study
NIH-3T3 RhoB2.2	RhoB knockout	this study
NIH-3T3 RhoB3	RhoB knockout	this study
NIH-3T3 RhoC3	RhoC knockout	this study
NIH-3T3 RhoC6	RhoC knockout	this study
NIH-3T3 RhoC9	RhoC knockout	this study
NIH-3T3 RhoA3B6	RhoA & RhoB knockout	this study
NIH-3T3 RhoB1A1	RhoA & RhoB knockout	this study
NIH-3T3 RhoB1A5	RhoA & RhoB knockout	this study
NIH-3T3 RhoB3C4	RhoB & RhoC knockout	this study
NIH-3T3 RhoB3C5	RhoB & RhoC knockout	this study
NIH-3T3 RhoC3B4	RhoB & RhoC knockout	this study
NIH-3T3 RhoC3B6.7	RhoB & RhoC knockout	this study
NIH-3T3 RhoC9A2	RhoA & RhoC knockout	this study
NIH-3T3 RhoC9A3	RhoA & RhoC knockout	this study
Rac flox/flox	mouse embryonic fibroblasts, contain floxed Rac1 gene	A. Steffen [38]
Rac KO #3	Rac1 knockout	A. Steffen [38]

2.4.3 Freezing and Thawing of Cells

Long term storage of cells was done in tanks filled with liquid nitrogen. For thawing of cells, the vials were thawed in a waterbath (Grant) at 37°C and then transferred into a 15 ml tube with 4 ml of normal cell culture medium. The cells were centrifuged at 4°C for 5 minutes at 1000 rpm (Centrifuge 5804 R from Eppendorf). The supernatant was discarded and the pellet was resuspended in 7 ml of medium and transferred to a ⌀10 cm cell culture dish, which was then moved to the cell culture incubator with 37°C and 7.5% CO_2.
Confluent dishes of cells were used for freezing of backup stocks. Cells from a confluent ⌀10 cm dish were trypsinized and centrifuged for 5 minutes at 1000 rpm and 4°C. The supernatant was discarded and the pellet was resuspended in 1400 µl DMEM (containing 4.5 g/l glucose, from Gibco), 400 µl FBS (Sigma) and 200 µl DMSO. Cell solutions were transferred to cryo vials (1 ml solution per vial) and cooled down using CoolCell Cell Freezing Containers (BioCision) at -70°C, which cool 1°C per minute. The next day, cells were transferred to liquid nitrogen.

2.4.4 Counting of Cells

Cells were counted before seeding for experiments. After trypsinization, 10 µl out of 6 ml cell suspension were mixed with 90 µl Trypan Blue solution (Lonza). 25 µl of the mixture were transferred to a Fuchs-Rosenthal counting chamber, which is illustrated in Figure 2.4. The number of cells in one big square (the

magnification in Figure 2.4) was counted in four squares and the mean value was calculated. The mean value was multiplied with the dilution factor (10) and with 5000 (the chamber factor) to get the number of cells per ml. Afterwards, the needed number of cells was prepared in cell culture medium and seeded into well plates of needed formats for further incubation at 37°C and 7.5% CO_2.

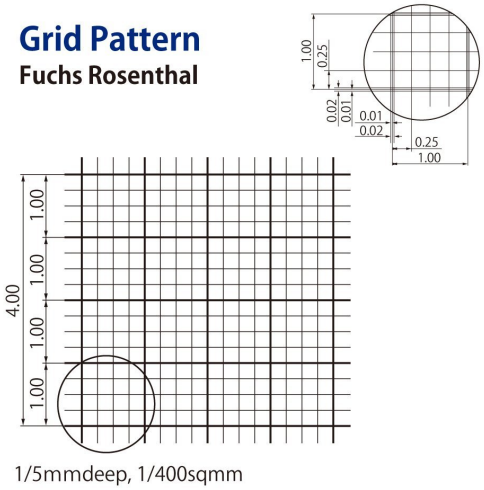

Figure 2.4: Fuchs-Rosenthal counting chamber. This chamber was used to count and calculate the number of cells per ml suspension (https://www.amazon.com/177-512C-Disposable-Counting-Rosenthal-10plates/dp/B01AU77P6E) (22.03.2018).

2.4.5 Transfection of Cells

For transfection with DNA, cells were seeded the day before to achieve subconfluent densities on the desired day. Cells were transfected with 1 µg of the respective plasmids per well in a 6 well plate using X-tremeGENE 9 DNA Transfection Reagent (Roche) at a 3:1 ratio according to manufacturer's instructions. DMEM (4.5 g/l glucose, from Gibco) was used to dilute DNA and the transfection reagent.

2.4.6 siRNA-induced Knockdown

Short interfering RNAs (siRNAs) can be used to downregulate gene expression. Therefore, double-stranded siRNA pools can be transfected into eukaryotic cells. These siRNAs then associate with the RNA induced silencing complex (RISC), which uses one strand of the siRNA to target the complementary mRNA and leads to its degradation. By degradation of the mRNA, respective protein levels are decreased.
SMARTpool siRNAs were ordered from Dharmacon. The pool for knockdown of Cofilin 1, Cofilin 2 and ADF is depicted in Table 2.12. Before transfection with siRNAs for cofilin family genes, cells were seeded at low densities in 24 well plates. For transfection, 2.5 µM per siRNA were added together and incubated for 5 minutes in serum-free Opti-MEM medium (Gibco). The same mixture was set up with nuclease-free water (Millipore) instead of siRNAs as mock control.

In parallel, 1 µl of Dharmafect transfection reagent per well was incubated in the same way. Next, both solutions were mixed and incubated for 20 minutes before adding normal culture medium and adding the solution to the cells. One day later, the same procedure was performed using only the siRNA for Cofilin 2 at a concentration of 5 µM. The next day, cells were plated on glass coverslips (NeoLab) coated with fibronectin (described in chapter 2.6.5). Three days after the first transfection, cells were fixed with 4% paraformaldehyde (PFA) (Sigma) in PBS for 20 minutes at room temperature and washed three times with PBS afterwards, before storage at 4°C or continuing immunofluorescence staining as described in chapter 2.6.5.

Table 2.12: siRNA for Cofilin knockdown

Target	Sequence
Cofilin 1	5′-CCAGAAGAAGUGAAGAAAC-3′
Cofilin 1	5′-CAGACCUGCUCUUGGGUGU-3′
Cofilin 1	5′-CUAACUGCUACGAGGAGGU-3′
Cofilin 1	5′-GUGUCAUCAAGGUGUUCAA-3′
Cofilin 2	5′-GGAAGUAAUUUGGGUAUAA-3′
Cofilin 2	5′-CUGAAAGUGCACCGUUAAA-3′
Cofilin 2	5′-UCUGAAUGAUUGCCGAUAU-3′
Cofilin 2	5′-AUGUAAGACAGGCGUGCUA-3′
ADF	5′-GAUGAAGUAUGUCGCAUUU-3′
ADF	5′-ACGACAUGAAAGUUCGGAA-3′
ADF	5′-CAGAAGACCUCAAUCGGAC-3′
ADF	5′-GUGCAUAGUCGAAGAAGAA-3′

2.4.7 FACS

FACS stands for fluorescent associated cell sorting. Single cells are analyzed by different lasers. Forward scattering is a measure for volume of cells, whereas the result of side scattering depends on granularity of the cell. The setup is illustrated in Figure 2.5. Fluorescently labeled cells can also be detected and sorted according to the result.

FACS sorting was used to specifically isolate cells that were GFP positive after transfection with pSpCas9(BB)-2A-GFP containing sgRNA sequences for Rho KO. This was done by Dr. Lothar Gröbe (HZI, Braunschweig). Single cells with high GFP levels were sorted directly into 96well plates containing 33.3% conditioned medium using the Aria-II SORP machine (BD Biosciences), grown to confluency and expanded.

To measure size/volume and granularity of cells, the LSR-II SORP from BD Biosciences was used. 1/3 of a confluent 10 cm dish was centrifuged for 5 minutes at 1000 rpm (Centrifuge 5804 R from Eppendorf) and the pellet was resuspended in 300 µl FACS buffer (Table 2.13). Samples were kept on ice until the actual measurement.

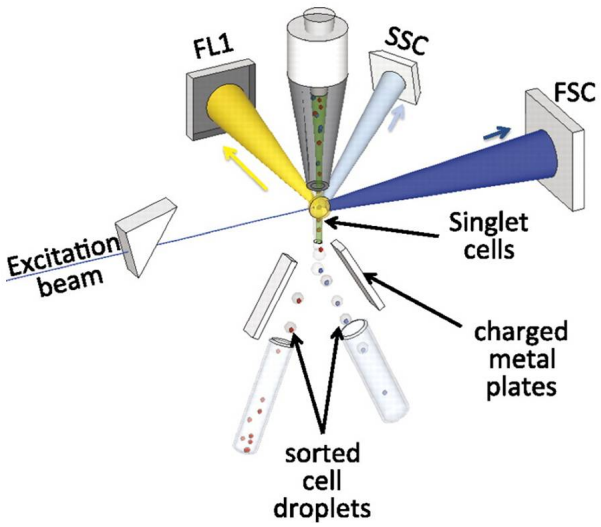

Figure 2.5: FACS. Figure shows how forward scatter (FSC) and side scatter (SSC) are positioned in a sorting machine and how single cells are analyzed and assigned according to the result. Fluorescent lasers (FL1) can be used to sort the cells depending on specific fluorescent signals [167].

Table 2.13: FACS buffer

Compound	Company	Concentration
PBS	Gibco	1x
EDTA	Fluka	2 mM
Fetal Bovine Serum	Sigma	10%

2.4.8 Generation of Cell Lysates

Cells were grown to confluency, subsequently trypsinized and transferred to a 2 ml tube. From this step forward, everything was carried out at 4°C. The suspension was centrifuged at 5000 x g for 5 minutes (Centrifuge Fresco 21 from Thermo Fisher Scientific) and washed three times with cold PBS in the same manner. Finally, the cell pellet was incubated in NP-40 lysis buffer for 20 minutes. The components of NP-40 lysis buffer are listed in Table 2.14. NaF, Na_3VO_4 and protease inhibitor cocktail were always added directly before usage. The buffer was solved in H_2O. For a confluent cell layer in a 6 well format, 250 µl lysis buffer were used. Another centrifugation step was carried out at 10 000 x g for 15 minutes and the supernatant containing the protein solution, was stored at -20°C.

Table 2.14: Content of NP40 lysis buffer

Compound	Company	Concentration
Glycerol	Roth	10%
NaCl	Roth	100 mM
NaF	Sigma	100 mM
Na_3VO_4	Sigma	1 mM
Nonidet P-40	Fluka	1%
$MgCl_2$	Roth	2 mM
Protease inhibitor cocktail	Cytoskeleton	1x
Tris HCl pH 8	Roth	50 mM

Cell extracts needed for phospho-antibodies were prepared with 1x Halt Protease and Phosphatase Inhibitor (Thermo Fisher Scientific) in 1x SDS loading buffer (see Table 2.17). The solution was pipetted directly on the adherent cells and after lysis, the solution was transferred to a tube and treated with 1 µl Benzonase (Merck) for 10 minutes at room temperature to digest the DNA before loading the sample on SDS gels (see chapter 2.5.2).

2.4.9 DNA Isolation from Cells

For sequencing of potential Rho KO clones, DNA was isolated using QuickExtract DNA Extraction Solution (Epicentre). From 6 ml cell suspension of a confluent 10 cm dish, 100 µl were used for DNA extraction. Cells were washed with PBS via centrifugation for 5 minutes at 5000 x g (Centrifuge Pico 17 by Thermo Fisher Scientifc). Subsequently, the pellet was resuspended in 50 µl QuickExtract solution and incubated first at 70°C for 20 minutes, followed by a 10 minutes incubation at 95°C (Thermocycler from Ditabis and Eppendorf). DNA was stored at 4°C.

2.4.10 RNA Isolation from Cells

To analyze mRNA expression in NIH-3T3 WT cells during *S.* Typhimurium infection via q-PCR (described in chapter 2.3.4), 200.000 cells per well were seeded the previous day in a 6 well plate. Right before infection with *S.* Typhimurium and 1 - 6 hours afterwards, cells were washed with PBS, lyzed with 500 µl lysis buffer and stored at -70°C. RNA isolation was performed by Silvia Prettin (HZI, Braunschweig) using the NucleoSpin RNA plus kit (Macherey-Nagel) according to manufacturers protocols. For elution of RNA, 60 µl elution buffer were used and sample concentration was measured using Denovix DS-11+ spectrophotometer.

2.4.11 Inhibitor Treatments

Cells were treated with various inhibitors, listed in Table 2.15 for two different experimental setups. For immunofluorescence stainings in the context of Cofilin siRNA knockdown (IF), treatment occured for 1 hour at 37°C and cells were

fixed with 4% PFA (Sigma) in PBS afterwards. In a different context, cells were treated with Rhosin for 24 hours or/and EHT 1864 for 4 hours before infection with bacteria (Bac) as described in chapter 2.4.14. All inhibitors were diluted in normal cell culture medium, with the exception of Rhosin which was diluted in DMEM only (4.5 g/l glucose, from Gibco) without any serum.

Table 2.15: Inhibitors

Compound	Target	Company	Working conc.
BDP5290	MRCK	Aobious	20 µM (IF)
(S)-Blebbistatin	myosin II	Toronto Research Chemicals	120 µM (IF)
EHT 1864	Rac1, Rac2, Rac3	Tocris	5 µM (Bac)
Rhosin	RhoA, RhoB, RhoC	Millipore	50 µM (Bac), 200 µM (IF)
Y-27632	ROCK1, ROCK2	BD Biosciences	50 µM (IF)

2.4.12 Treatments with Rho-Activating Proteins

For constitutive activation of RhoA, RhoB and RhoC, cells were seeded on coverslips with fibronectin (see chapter 2.6.5) and treated with 150 nM CNF_y (kindly provided by Paweena Chaoprasid, HZI, Braunschweig) for 4 hours at 37°C and 7.5% CO_2. After fixation with 4% PFA (Sigma) in PBS, cells were stained as described in chapter 2.6.5.

2.4.13 Transfections with RSV-F Protein

One day prior to transfection with pcDNA3 RSV-F, cells were seeded into 24 well plates. Transfection with X-treme Gene 9 (see chapter 2.4.5) was performed early in the morning and transfected cells were transferred on coverslips with fibronectin in the afternoon. Fixation of cells was done 24 hours after transfection. Immunofluorescence staining was done as described in chapter 2.6.5.

2.4.14 Gentamycin Protection Assay

For analysis of bacterial invasion into various cell lines, gentamycin protection assays were performed. Cells were seeded the day before into 24 well plates (4 replicates per condition). 50 000 cells per well were used (see counting and seeding of cells described in chapter 2.4.4). Bacteria were cultured overnight in 5 ml of their respective medium at 37°C. The next day, the overnight cultures were diluted in 5 ml medium (75 µl of *S. flexneri* or 70 µl of *S.* Typhimurium overnight culture) and grown to an optical density (OD) at 600 nm between 0.5 and 0.8 (which equals exponential growth phase, measured with Biophotometer Plus from Eppendorf), which took around 2 hours.
Subsequently, 2 ml of bacterial suspension were centrifuged at 10 000 x g for 2 minutes (Centrifuge Pico 17 by Thermo Fisher Scientific). The pellet was resuspended in 1 ml of PBS and the OD_{600} was measured again. Before infection, bacteria were diluted in DMEM (for details to cell culture medium see chapter 2.4.1) at a multiplicity of infection (MOI) of 100. An OD_{600} of 1 equals 5 x 10^8

bacteria for *S. flexneri* and 1 x 10^9 for *S.* Typhimurium. These numbers are based on experiments in which bacteria were plated on agar at multiple ODs in different dilutions, incubated overnight at 37°C and counted the next day.
For calculation of the actual inoculum, 10^{-4} and 10^{-5} dilutions of bacterial suspensions in PBS were plated on agar plates and incubated up-side down overnight at 37°C, as a control of bacterial numbers used for infection. 300 µl of bacterial suspension in DMEM were added to each well of cells. This was followed by centrifugation at 2000 rpm for 5 minutes (Eppendorf 5810 centrifuge) to define the starting point of infection. Infected cells were incubated at 37°C and 5% CO_2 for 30 minutes (incubator NuAire 5800-E), before 200 µl of gentamycin solution (Sigma) were added on top (final concentration of 50 µg/ml). After an additional incubation time of either 30 minutes or 5 hours and 30 minutes at 37°C, during which gentamycin killed all extracellular bacteria, cells were washed with PBS three times. Infected cells were lyzed with 250 µl of 0.5% Triton-X-100 (Bio-Rad) in PBS for 5 minutes at room temperature. Afterwards, bacterial suspensions were diluted in PBS and plated on agar plates. These were incubated up-side down at 37°C overnight and bacterial colonies were counted the next day. Depending on the experimental setup, one condition was chosen as control and all other conditions were normalized to it. Differences in bacterial inoculum were used to correct the values if multiple bacterial strains were used in one experiment.

2.4.15 CellTracker Stainings

Both NIH-3T3 WT and Rho KO cells were seeded for confluency on the next day and either one or the other was stained with CellTracker CMFDA (green) 7.5 µM or CellTracker CMPTX (red) 10 µM (Molecular Probes) diluted in Opti-MEM (Gibco) for 30 minutes at 37°C and 7.5% CO_2. Afterwards, stained and unstained cells were mixed on glass coverslips (NeoLab) coated with fibronectin (Roche). Immunofluorescence was performed as described in chapter 2.6.5. Cells were either stained with Alexa Fluor 488 coupled-phalloidin (in the case of red CellTracker) or ATTO 594 coupled-phalloidin (in the case of green CellTracker) and additionally with DAPI (see Table 2.19). Intensity and area measurements were carried out with Metamorph software. These experiments were performed by Franziska Grüner (HZI, Braunschweig).

2.5 Protein Biochemistry

2.5.1 Measurement of Protein Concentration

Protein concentrations needed for Western Blot analysis were measured using Pierce BCA Protein Assay Kit (Thermo Fisher Scientific) according to manufacturer's protocols. 10 µl of each sample were used in duplicates. Bicinchonic acid reacts with cuprous ions to form a purple complex. Cupric ions are reduced to cuprous ions by proteins, so that the intensity of the purple complex relates to the amount of protein in the sample. This process is depicted in Figure 2.6.

Figure 2.6: BCA reaction. Figure shows the reaction of Bicinchonic acid with proteins, leading to a purple dye (https://marylandmunch.wordpress.com/nutrients/protein/) (23.03.2018).

2.5.2 SDS-PAGE

Proteins can be separated according to their size via sodium dodecyl sulfate polyacrylamide gel electrophoresis (SDS-PAGE). The process is illustrated in Figure 2.7. SDS is a detergent that binds to denatured proteins with its hydrophobic part and is at the same time soluble in water due to its hydrophilic part. Since it is negatively charged, it moves towards an electrode with positive charge. On the way through the acrylamide gel, small proteins move faster than big proteins, which leads to a clear separation.

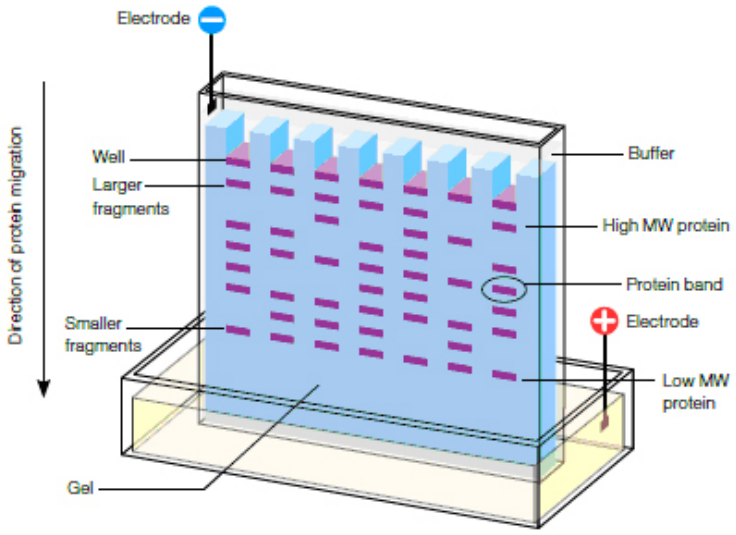

Figure 2.7: SDS-PAGE. Figure shows procedure of separating proteins according to their size via SDS-PAGE (http://www.bio-rad.com/de-de/applications-technologies/protein-electrophoresis-methods?ID=LUSOW4GRI) (23.03.2018).

SDS gels were poured with different acrylamid concentrations, depending on the size of proteins that needs to be analyzed. Higher concentrations of acrylamid were used for small proteins, such as Rho GTPases, with a size around 25 kDa. The composition of SDS gels at different concentrations is shown in

Table 2.16 (Res. stands for resolving gel). As acrylamide solution, 30% Acrylamide/ 0.8% Bisacrylamide (37.5:1) (Roth) was used. The resolving gel buffer consists of 1.5 M Tris and 0.4% SDS (Roth) pH 8.8, whereas the stacking gel buffer contains 0.5 M Tris and 0.4% SDS pH 6.8. TEMED and APS were ordered from Roth and Sigma, respectively. The BioRad system was used for pouring and running of gels. For the experiments of this study, glass plates with a space of 1.5 mm and combs with 15 wells were used. After pouring the resolving gel, isopropanol (Roth) was added on top to smoothen the edges. It was discarded after polymerization of the resolving gel, before the stacking gel was poured on top.

Table 2.16: Composition of 2 SDS gels

Compound	**7.5% Res.**	**10% Res.**	**12.5% Res.**	**15% Res.**	**Stacking**
Acrylamide	4 ml	5.34 ml	6.66 ml	8 ml	0.9 ml
Resolving gel buffer	4 ml	4 ml	4 ml	4 ml	
Stacking gel buffer					0.9 ml
H_2O	7.8 ml	6.6 ml	5.24 ml	3.9 ml	4 ml
TEMED	16 µl	16 µl	16 µl	16 µl	8 µl
APS	64 µl	64 µl	64 µl	64 µl	32 µl

Specific amounts of protein samples (20 µg if not stated otherwise) were mixed with the appropriate amount of 4x SDS loading dye (see Table 2.17) and boiled at 95°C for 5 minutes for denaturation (Thermocycler from Ditabis). Samples were afterwards centrifuged at 10 000 x g for 1 minute (Centrifuge Pico 17 from Thermo Fisher Scientific) before they were loaded on SDS gels. The ladder used for this study was Color Prestained Protein Standard, Broad Range, from NEB (shown in Figure 2.8). 5 µl ladder were used in one well. The separation process was performed at 200 V for about 1 hour. SDS running buffer consists of 25 mM Tris base (Roth), 192 mM Glycine (Serva) and 0.1% (v/v) SDS (Roth).

Table 2.17: SDS 4x loading dye

Compound	**Company**	**Concentration**
SDS	Roth	3.3%
Tris-HCl pH 6.8	Roth	25 mM
Glycerol	Roth	33.3%
β-Mercaptoethanol	AppliChem	3.3%
Bromphenolblue	AppliChem	0.041%

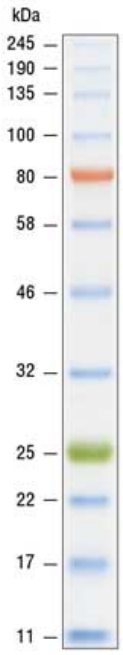

Figure 2.8: Protein Ladder. Color Prestained Protein Standard (Broad Range) from NEB was used as ladder on SDS gels (https://www.neb.com/products/p7712-color-prestained-protein-standard-broad-range-11-245-kda#Product Information) (23.03.2018).

2.5.3 Coomassie-Blue-Staining

To control protein amounts loaded onto SDS gels, they were stained after separation via electrophoresis. Therefore, the gels were incubated in Coomassie Brilliant Blue R-250 solution (0.1% Coomassie R-250 (w/v) (AppliChem), 10% Acetic Acid (v/v) (VWR), 25% Isopropanol (v/v) (Roth), 65% H_2O (v/v)). Coomassie binds to the basic side chains of amino acids and thereby stains proteins specifically. The solution was boiled in a microwave and incubated shaking afterwards for 30 minutes. To destain the gels, they were incubated in H_2O, which was boiled up a couple of times and refreshed after every boiling step. Finally, the gel was documented using a scanner (HP Scanjet G2710).

2.6 Immunological Methods

Immunostaining with antibodies can be used for various techniques. Primary antibodies are specific for an antigen and can then be detected by secondary antibodies, depending on which species they are from. These secondary antibodies are often coupled to dyes on their Fc region. The general structure of antibodies is shown in Figure 2.9.

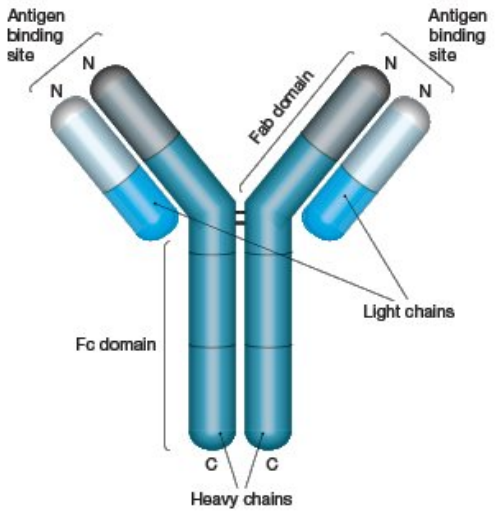

Figure 2.9: Antibody structure. This figure displays the general structure of an antibody (https://www.bio-rad-antibodies.com/immunoglobulin-antibody.html) (23.03.2018).

2.6.1 Primary Antibodies

Primary antibodies, used for Western Blots (WB) or immunofluorescence stainings (IF), are listed in Table 2.18. Pc stands for polyclonal and mc for monoclonal antibodies.

Table 2.18: Primary antibodies

Protein Target	Company	Catalog/ Clone	mc/pc	Species	Dilution
Actin	Sigma-Aldrich	A2066	pc	Rabbit	1 : 1000 (WB)
ADF	Walter Witke (University of Bonn)	7D10	mc	Mouse	1 : 5 (WB)
Cofilin 1	Walter Witke (University of Bonn)	KG60	pc	Rabbit	1 : 500 (WB)
Cofilin 2	Walter Witke (University of Bonn)	FHU1	pc	Rabbit	1 : 500 (WB)
GAPDH	Calbiochem	CB1001	mc	Mouse	1 : 10.000 (WB)
GDIα	Thermo Fisher	MA5-17032/ 2G3	mc	Mouse	1 : 1000 (WB)
GDIβ	abcam	ab227093	pc	Rabbit	1 : 1000 (WB)
GFP	Hybridoma (Barbara Behrendt, HZI)	101G4B2	mc	Mouse	undiluted (WB)
GM-130	BD	610823/ 35	mc	Mouse	1 : 200 (IF)
non-muscle myosin IIa	abcam	ab55456	mc	Mouse	1 : 100 (IF)
non-muscle myosin IIb	abcam	ab204358	pc	Rabbit	1 : 100 (IF)
p16	Hybridoma (Kerstin Schilling, HZI)	323H3	mc	Mouse	undiluted (IF)
phospho-Akt	Cell Signaling	9271	pc	Rabbit	1 : 1000 (WB)
phospho-Cofilin 1	Cell Signaling	3311	pc	Rabbit	1 : 1000 (WB)
phospho-MLC2	Cell Signaling	3675	mc	Mouse	1 : 1000 (WB)
Rac1	BD	610650/ 102	mc	Mouse	1 : 1000 (WB)
RhoA	Santa Cruz	sc-418/ 26C4	mc	Mouse	1 : 200 (WB)
RhoB	Santa Cruz	sc-180/ 119	pc	Rabbit	1 : 200 (WB)
RhoC	Cell Signaling	D40E4	mc	Rabbit	1 : 1000 (WB)
RSV-F (Synagis)	AbbVie	PZN 00639133	mc	humanized	1 : 1000 (IF)
ROCK1/2	Millipore	07-1458	pc	Rabbit	1 : 500 (WB)
Tubulin	Synaptic Systems	302 211/ 3A2	mc	Mouse	1 : 25.000 (WB)
WDR	Thermo Fisher	PA5-27645	pc	Rabbit	1 : 1000 (WB)

2.6.2 Secondary Antibodies/Fluorescent Dyes

Secondary antibodies, which were used for detection of the primary antibodies described in chapter 2.6.1, are listed in Table 2.19. They were coupled to fluorescent dyes or horseradish peroxidase to generate detectable signals for analysis. Phalloidin is a toxin from *Amanita phalloides* and binds directly to F-actin [168].

Table 2.19: Secondary antibodies

Name	Coupled to	Company	Dilution
A4a goat α-mouse	Peroxidase	Dianova	1 : 5000 (WB)
A13c goat α-mouse	Alexa 594	Invitrogen	1 : 200 (IF)
B4c goat α-rabbit	Peroxidase	Dianova	1 : 5000 (WB)
B13c goat α-rabbit	Alexa 594	Invitrogen	1 : 500 (IF)
DAPI (4,6-Diamidin-2-phenylindol)	–	Sigma	1 : 500 (IF)
Ph12 phalloidin	Alexa 488	Invitrogen	1 : 100 (IF)
Ph20 phalloidin	ATTO 594	ATTO-TEC	1 : 200(IF)

2.6.3 Western Blotting

Western Blotting was performed to transfer proteins from SDS gels to polyvinylidene difluoride (PVDF) membranes (Millipore). For that purpose, the membrane was activated in methanol (J. T. Baker) and then put between two Whatman papers (Roth) with the SDS gel. Everything was soaked in transfer buffer beforehand. Buffer and Western Blotting machine were used from Thermo Fisher Scientific (shown in Figure 2.10). The transfer was done for 15 minutes (20 minutes for large proteins) at 25 V and 1.3 A per membrane.

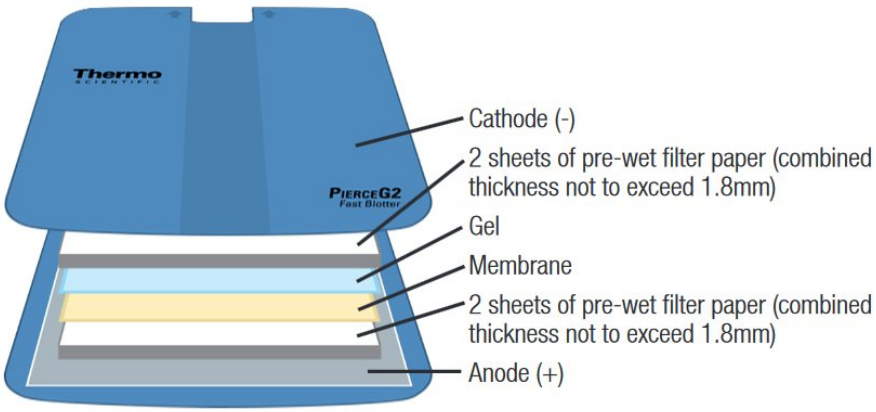

Figure 2.10: Western Blotting. The Fast Blotter from Thermo Fisher Scientific was used to transfer proteins from SDS gels to PVDF membranes. The setup is shown schematically (https://assets.thermofisher.com/TFS-Assets/BID/Product-Guides/2162534.pdf) (23.03.2018).

After the transfer, membranes were blocked with Tris buffered saline with Tween 20 (TBST) (see Table 2.20) containing 10% FBS for 1 hour. Incubation with primary antibodies occurred overnight at 4°C in TBST containing 5% FBS. After washing of membranes with TBST, secondary antibody incubation was performed for 1 hour in TBST. Subsequently, membranes were washed with TBST, followed by signal development with Lumi-Light Western Blotting Substrate (Roche) and recording with Intas ECL Chemocam Imager. Semi-quantitative analysis of Western Blots were performed using ImageJ software (BioVoxxel). For that purpose, rectangles of identical size were drawn around bands of interest and intensities were measured. These were adjusted corresponding to loading controls, such as GAPDH or tubulin, which are housekeeping genes.

WT bands were defined as 100% and intensities of KO clones were normalized to that value.

Table 2.20: 1x TBST buffer

Compound	Company	Concentration
Tris base pH 7.6	Roth	20 mM
5 M NaCl	Roth	137 mM
Tween20	Sigma	0.1%

2.6.4 Immunoprecipitation with GFP-Trap

Cells were transfected the day after seeding with 5 µg DNA (GFP plasmids from Table 2.5) per ⌀10 cm dish (see chapter 2.4.5). The following day, five ⌀10 cm dishes per condition were washed with cold PBS three times and the lyzed with 300 µl NP-40 buffer (see Table 2.14) per dish. After centrifugation at 20 000 x g for 15 minutes at 4°C (Centrifuge Fresco 21 from Thermo Fisher Scientific), 5% of the lysate were mixed with 4x SDS sample buffer and used as input control. 30 µl GFP-Trap beads (Chromotec), which were washed three times with 30 µl washing buffer (100 mM NaCl, 2 mM $MgCl_2$, 50 mM Tris HCl) via centrifugation at 1000 x g at 4°C for 5 minutes beforehand, were then mixed with the lysate and incubated at 4°C for 1 hour. After centrifugation at 1000 x g for 5 minutes, 5% of the supernatant were mixed with 4x SDS sample buffer and used as unbound control. Beads were then washed once with 1 ml washing buffer and subsequently mixed with 2x SDS sample buffer. These experiments were performed by Silvia Prettin (HZI, Braunschweig).

2.6.5 Immunofluorescence Staining

Glass coverslips from NeoLab (⌀12 mm) were washed under agitation in a solution of 60% ethanol (J. T. Baker) (v/v) and 40% HCl (Roth) (v/v) for 30 minutes for cleaning. After multiple washings steps with H_2O, coverslips were dried on Whatman paper (Roth) and sterilized by autoclaving. Before seeding of cells, glass coverslips in 24 well plates were coated with 100 µl 25 µg/ml fibronectin solution (Roche, stock concentration 1 mg/ml in 2 M Urea) in PBS for 1 hour at room temperature. After washing of coverslips with PBS three times, cells were seeded in normal culture medium onto the coverslips. The next day, cells were fixed with 4% PFA (Sigma) in PBS for 20 minutes at room temperature. Following fixation and washing of coverslips with PBS three times, cells were permeabilized with 0.05% Triton-X-100 (Bio-Rad) in PBS for 30 seconds and subsequently washed three times with PBS. Next, blocking solution, consisting of 5% horse serum (Cytogen) in PBS with 1% bovine serum albumin (BSA) (AppliChem) was added to the coverslips for 1 hour. For detection of specific cellular structures, the primary antibody was diluted according to Table 2.18 in PBS containing 1% BSA. Coverslips were added on a droplet of 30 µl of the antibody dilution and incubated in a dark humid chamber for 1 hour. After washing the coverslips with PBS three times, the same procedure was performed for secondary

antibody incubation, also for 1 hour in the dark humid chamber. Finally, the coverslips were washed three times with PBS and put on glass microscope slides (Thermo Fisher Scientific) on a droplet of prewarmed (60°C) Mowiol (aliquots were prepared in a former lab according to the protocol in Table 2.21 and stored at -20°C). Samples were stored at 4°C overnight and analyzed with a microscope the following day.

Table 2.21: Mowiol

Compound	Amount
Mowiol	2.4 g
87% Glycerol	6 g
H_2O	add to 6 ml
0.2 M Tris pH 8.5	200 µl
N-propylgalate	2.5 µg/ml

2.6.6 G-LISA Activity Measurements

For detection of active Rho GTPase levels, G-LISA RhoA and Rac1/2/3 Activation Kits (Cytoskeleton) were used. Confluent cells were trypsinized, washed with PBS via centrifugation at 4°C for 5 minutes at 5000 x g (Centrifuge Fresco 21 from Thermo Fisher Scientific) and lyzed in the appropriate amount of Cell Lysis Buffer (250 µl buffer for confluent cells in a 6 well plate). The assays were performed according to manufacturer's protocols.
Summarized, cell lysates were pipetted into a 96 well format in which only the GTP bound form of the respective GTPase was bound by the coating of the wells. After some washing steps, incubation with the primary antibody recognizing the respective GTPase was performed, followed by secondary antibody incubation. The secondary antibody was coupled to horseradish peroxidase so that colorimetric signal detection, measuring the amount of active GTPase, was possible. The procedure is therefore similar to an indirect enzyme linked immunosorbent assay (ELISA), which is shown in Figure 2.11. In this case, the antigen is provided by the company and specifically interacts with GTP-bound Rho GTPases.

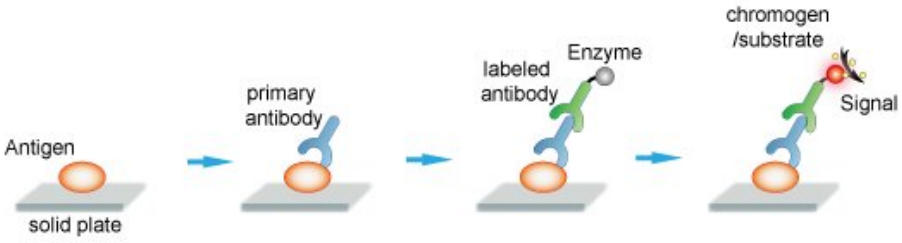

Figure 2.11: G-LISA procedure. This scheme shows the sequence of an indirect ELISA, which resembles the G-LISA protocol (https://www.creative-diagnostics.com/ELISA-guide.htm) (23.03.2018).

2.7 Microscopy

2.7.1 Epi-Fluorescence Microscopy

Image acquisition of fixed samples (see chapter 2.6.5) was performed using an inverted microscope (Axiovert 135TV, Zeiss) with a Photometrics CoolSnap K4 camera and Metamorph software. Images were obtained with 63x (Plan-NEOFLUAR, numerical aperture 1.25) or 100x oil objective (Plan-NEOFLUAR, numerical aperture 1.30) and were subsequently analyzed using ImageJ software.

2.7.2 Live Cell Imaging

NIH-3T3 WT and Rho KO cells were seeded at low densities on glass bottom dishes (Ibidi) coated with fibronectin (as described in chapter 2.6.5) and phase contrast videos were acquired at a rate of 6 frames/hour for 20 hours with a 20x objective. A Biostation from Nikon was used for that purpose, keeping the cells at 37°C and 7.5% CO_2 during measurements. Single cells were tracked via ImageJ using the manual tracking plugin.
Random migration experiments were also done in viscous medium, containing 0%, 1% or 2% polyvinylpyrrolidon (PVP) (Sigma). For these experiments, cells were seeded at low densities in 12 well plates and images were acquired with a SIM-E from Nikon. Normal cell culture medium was changed to PVP containing medium right before the recording started. Phase contrast images with a 10x objective were taken for 10 hours at a rate of 12 frames per hour.

2.8 Mathematical and Statistical Analysis

2.8.1 Statistical Analysis

For analysis of Western Blots as well as invasion assays with bacteria, values of the control group were set as 100% and results of other samples were normalized to that value. Graphs were generated with GraphPad Prism and One-Way ANOVA was used as statistical test for Western Blots, whereas invasion assays and random migration experiments were analyzed using the *t*-test.

2.8.2 Bioinformatical Analysis of Array-Data

Bioinformatical analysis of microarray results (described in chapter 2.3.11) was done by Dr. Robert Geffers. Expression results were displayed as binary logarithm. Again, Rho KO results were normalized to WT values.

3 Results

3.1 Small molecule inhibitors of Rho and Rac affect bacterial invasion

Rac [124], as well as Rho proteins [136], have been described to play a role in *Salmonella* infection by promoting bacterial uptake. However, previous studies did not dissect between RhoA, RhoB and RhoC. A first approach to assess the roles of Rac and Rho in combination was performed by utilizing Rac1 KO cells and/or the small molecule inhibitor Rhosin, suppressing RhoA, RhoB and RhoC functions at the same time. A more detailed analysis followed by using KO cell lines for the distinct Rho proteins, as described in chapter 3.4.1. For the first experiments, Rac1 fl/fl or Rac1 KO cells were either treated with 50 µM Rhosin for 24 hours or only incubated in serum-free medium before infection with *S.* Typhimurium WT for 30 minutes, followed by 30 minutes gentamycin treatment to get rid of extracellular bacteria and specifically assess invasion rates.
Results are shown in Figure 3.1. Inhibition of Rho proteins led to a 40% decrease in invasion, while bacterial invasion rates were decreased by more than 80% upon Rac1 deficiency when compared to Rac1 fl/fl control cells. Treatment of Rac1 KO cells with Rhosin reduced invasion to below 5%. These data revealed additive effects of Rac and Rho for invasion of *S.* Typhimurium.

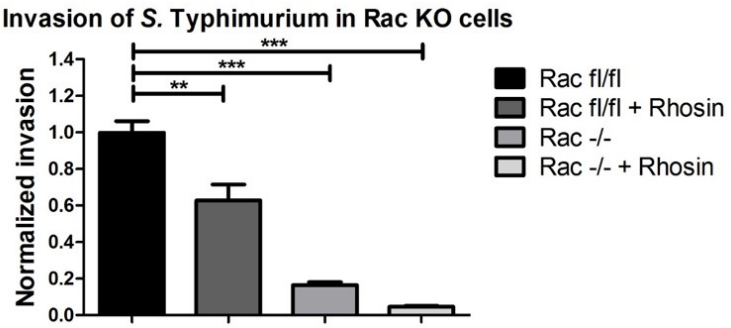

Figure 3.1: Invasion of *S.* Typhimurium WT in Rac1 KO cells with Rho inhibition. Rac1 fl/fl and Rac1 -/- cells were treated with 50 µM Rho inhibitor Rhosin for 24 hours and subsequently infected with *S.* Typhimurium WT for 30 minutes. Gentamycin was used to get rid of extracellular bacteria for additional 30 minutes. Cells were lyzed with Triton-X 100 and bacteria were diluted and plated on LB agar plates. Graph represents arithmetic means with standard error of the mean (SEM) from three independent experiments. Data were normalized to control levels. Unpaired *t*-test was used to calculate significances ($p < 0.05$).

Involvement of GTPases such as Rac and Rho in bacterial invasion has also been described for *S. flexneri* [169]. Therefore, the same experimental setup as described above was used for *S. flexneri* infection. The results are shown in Figure 3.2.A. Inhibition of Rho reduced bacterial invasion by 50%, whereas deletion of Rac1, with or without Rhosin, prevented invasion completely.

NIH-3T3 cells, which were used for a more detailed analysis by CRISPR/Cas9 mediated Rho KOs (see chapter 3.2), were investigated complementary to Rac1 fl/fl cells with Rho and Rac inhibitor treatments during *S. flexneri* invasion. Cells were treated with 50 µM Rhosin 24 hours before infection and/or with 5 µM EHT 1864, inhibiting Rac proteins, 4 hours before infection. The results are shown in Figure 3.2.B. Inhibition of Rho proteins decreased invasion to 40%, which was not further reduced upon Rac inhibition. Treatment with EHT 1864 alone led to an invasion rate of 60% compared to control levels. According to these experiments, deletion or inhibition of Rac and Rho proteins does not affect invasion of *S. flexneri* in an additive fashion, suggesting distinct pathways and mechanisms for the GTPases during the infection process.

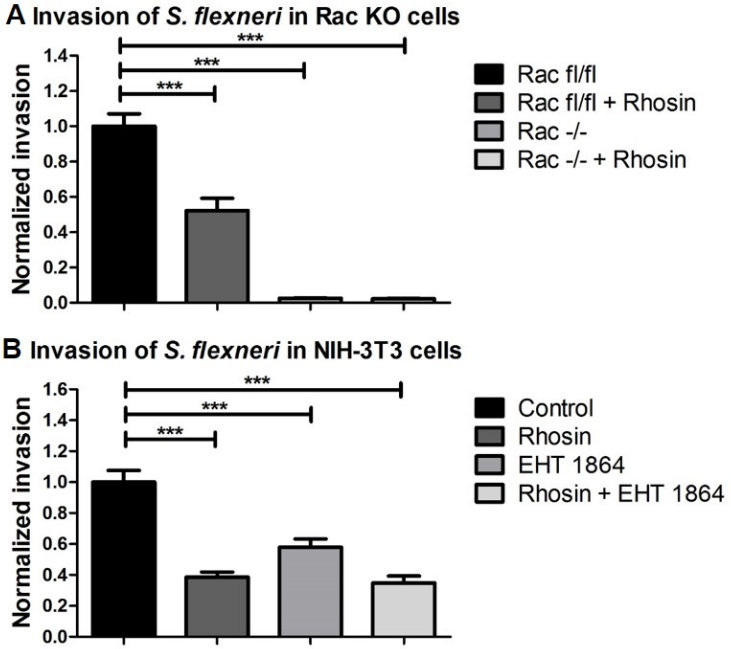

Figure 3.2: Invasion of *S. flexneri* WT in the absence of Rac1 and Rho. (A) Rac1 fl/fl and Rac1 -/- cells were treated with 50 µM Rho inhibitor Rhosin for 24 hours and subsequently infected with *S. flexneri* WT for 30 minutes. Afterwards, gentamycin was added for 30 minutes to kill extracellular bacteria. After lysis with Triton-X 100, bacteria were diluted and plated on TSB agar plates. Graph shows arithmetic means and SEM from three independent experiments. Significances were calculated with unpaired *t*-test ($p < 0.05$). All data were normalized to the control condition, namely Rac1 fl/fl without Rhosin. (B) NIH-3T3 cells were treated with Rho inhibitor Rhosin for 24 hours and/or Rac inhibitor EHT 1864 for 4 hours and subsequently infected with *S. flexneri* WT for 30 minutes. Graph shows arithmetic means and SEM from three independent experiments. Gentamycin was used to get rid of extracellular bacteria for additional 30 minutes. Cells were lyzed with Triton-X 100 and bacteria were diluted and plated on TSB agar plates. Data were normalized to control levels. The unpaired *t*-test was used to calculate significances ($p < 0.05$).

3.2 Knockout of RhoA, RhoB and RhoC in NIH-3T3 fibroblasts

Initial infection experiments with various inhibitors from this project and previous studies [136] suggested important roles for Rho proteins in bacterial infections, which could not be completely dissected by the use of small molecule inhibitors. Differential contributions of the single proteins RhoA, RhoB and RhoC could not be analyzed with inhibitors targeting all three proteins at once. Therefore, KO cell lines for RhoA, RhoB and RhoC were generated using the CRISPR/Cas9 technology. The murine cell line NIH-3T3 was used for these experiments, since all three Rho genes are highly expressed (see Table 6.1, Supplements) and potential effects of the deletions can therefore be analyzed easier. Gene KOs in NIH-3T3 fibroblasts were induced at the target sites shown in Figure 3.3 by transfection with pSpCas9(BB)-2A-GFP plasmids containing the respective RhoA, -B or -C sgRNA sequences (see chapter 2.3.1). Single cells were sorted according to their GFP intensities by FACS (Dr. Lothar Gröbe, HZI, Braunschweig) and expanded to analyze DNA sequences and protein expression for KO verification.

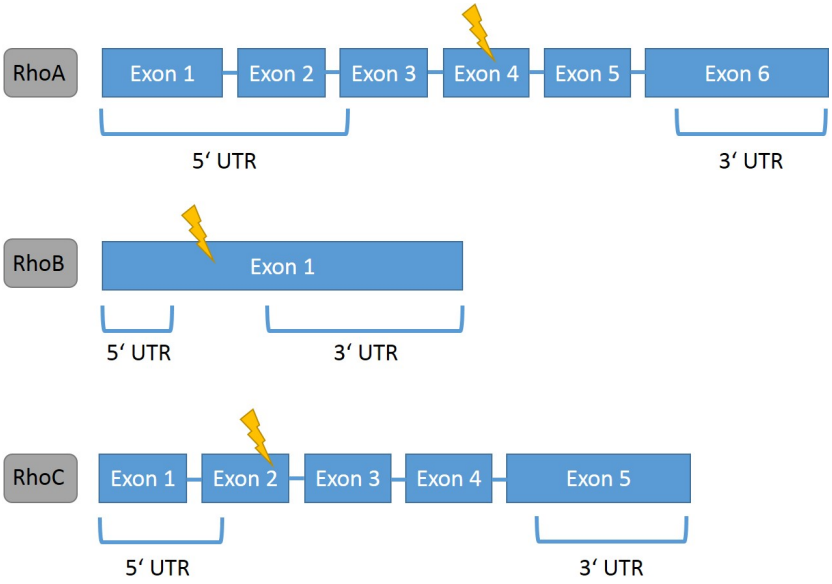

Figure 3.3: CRISPR/Cas9 mediated KO of RhoA, RhoB and RhoC. Target regions for mutations leading to KOs in the three Rho genes are labeled by yellow flashs. UTR = untranslated region

The generation of RhoA, RhoB and RhoC single KO cells yielded three KO clones per condition. KO clones were labeled by numbers. For the generation of double KO clones, two different single KO clones were used. For the generation of RhoBC double KOs for instance, RhoB KOs were induced in a RhoC KO clone termed RhoC3 and RhoC KOs were induced in a RhoB KO clone termed RhoB3. This led to four KO clones for RhoBC, two from each single KO clone, which was done to increase the probability that observed phenotypes were specific to the induced KOs and not due to off target effects. If the KO procedure leads to off

target effects, these should differ between the clones and thus not appear in all the combinations with different backgrounds. The KO of RhoA and RhoC only resulted in double KOs, if cells harbored a RhoC KO first. Inducing RhoC KOs in RhoA KOs did not yield surviving KO cells. For RhoAB KOs, the problem was similar. Inducing a RhoA KO in a RhoB KO yielded two clones, whereas RhoB KO in RhoA KO cells only led to one surviving KO clone. Even though this was repeated a couple of times, no additional RhoAB KO clones, originating from a RhoA KO, could be generated. Triple KOs could not be obtained at all. After FACS sorting of potential triple KO clones, single cells divided a few times in a 96 well plate and then died.

For screening of potential KO clones, cell extracts were analyzed via Western Blotting (see Figure 3.4) with RhoA, -B or -C-specific antibodies. The Figure shows Western Blots from one screening of potential double KO cells. Respective Western Blots of all KO clones which were used during the experiments of this study are displayed in Figure 3.13 and Figure 6.7 (Supplements). Clones which did not contain detectable levels of the respective protein were further analyzed on DNA level.

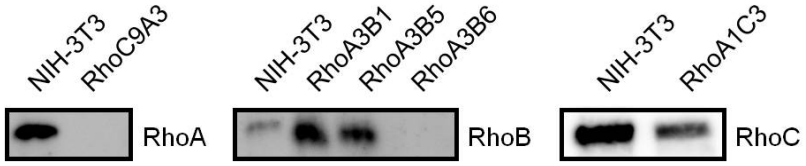

Figure 3.4: Rho KO verification by Western Blotting. Potential Rho KO clones were lyzed and analyzed on 15% SDS gels, followed by Western Blotting with respective Rho antibodies, as indicated. NIH-3T3 WT cells were used as control.

Sequencing results of Rho KO clones are listed in Table 3.1, showing all clones that were generated during this study and used for all experiments described in the next chapters. Deletions of DNA base pairs are marked by Δ, whereas $+$ labels an insertion. RhoB2.2 and RhoC3B6.7 carry an additional subclone number, since sequencing of initial clones revealed three or more different sequences. As only two different alleles should be present in one clone, these results pointed towards a mixture of clones. Subcloning was performed to generate distinct single clones with a defined genotype. All DNA and respective amino acid sequences of the generated KO clones are shown in chapter 6.1.2 (Supplements).

Table 3.1: Sequencing of Rho KOs

Clone	Mutation in allele 1	Mutation in allele 2
RhoA1	Δ1	Δ86
RhoA2	Δ18	Δ17
RhoA3	Δ10	Δ1
RhoB1	+1	identical to allele 1
RhoB2.2	Δ14	Δ12
RhoB3	+1	Δ11
RhoC3	Δ16	Δ2
RhoC6	+1	Δ21
RhoC9	+1	identical to allele 1
RhoA3B6	Δ1	Δ11
RhoB1A1	+1	Δ10
RhoB1A5	Δ7	Δ11
RhoB3C4	Δ2	Δ2
RhoB3C5	+1	Δ1
RhoC3B4	+1	identical to allele 1
RhoC3B6.7	+1	+1
RhoC9A2	+1	Δ10
RhoC9A3	Δ2	Δ2

Table 3.1 reveals that, since three DNA bases encode one amino acid, most mutations induce a frame shift in the amino acid sequences of the protein. Only in the case of RhoA2, RhoB2.2 and RhoC6 the number of deletions in one allele can be divided by three and did not lead to a frame shift but instead to a shortened amino acid sequence. Since no protein could be detected via Western Blotting for these clones, they were still used for experiments, though not for the generation of double KO clones. Figure 3.5 shows how the mutation in RhoA3 affects the open reading frame and yields premature stop codons. This is assumed to lead to degradation of the protein.

Figure 3.5: Rho KO DNA and protein sequence mutations. (A) DNA sequences of the target region are shown and aligned for NIH-3T3 WT and RhoA3. Red region depicts the deletion of 10 base pair (bp). (B) Translated RhoA amino acid sequences of NIH-3T3 WT and RhoA3. * shows stop codons, which appear only at the end of the sequence for WT cells but at earlier positions in the RhoA KO sequence, yielding a truncated protein.

3.3 Cellular characterization of RhoA-, RhoB-, and RhoC-KO cells

3.3.1 Morphology of Rho KO cells

To assess global morphological parameters of different Rho KOs, cellular volume and area were analyzed, as shown in Figure 3.6. Cells were grouped in four categories by FACS analysis, depending on size and granularity. The percentage of cells categorized as big is depicted in Figure 3.6.A. In RhoB KOs, a significantly lower amount of big cells was observed. In line with this result, in RhoAC KOs expressing only RhoB, the percentage of big cells was increased but showed high variation between replicates.
The cell area on the other hand, measured with the help of Franziska Grüner (HZI, Braunschweig), showed no dramatic changes in most cases (see Figure 3.6.B). Only RhoA, RhoAB und RhoBC double KO cells were shown to be larger than WT cells. All these cell types appear larger without an increase of volume, which points towards a very flat morphology. The same is true for RhoB KOs, which show the same cellular area but a reduction of volume and are assumed to be flat as well.

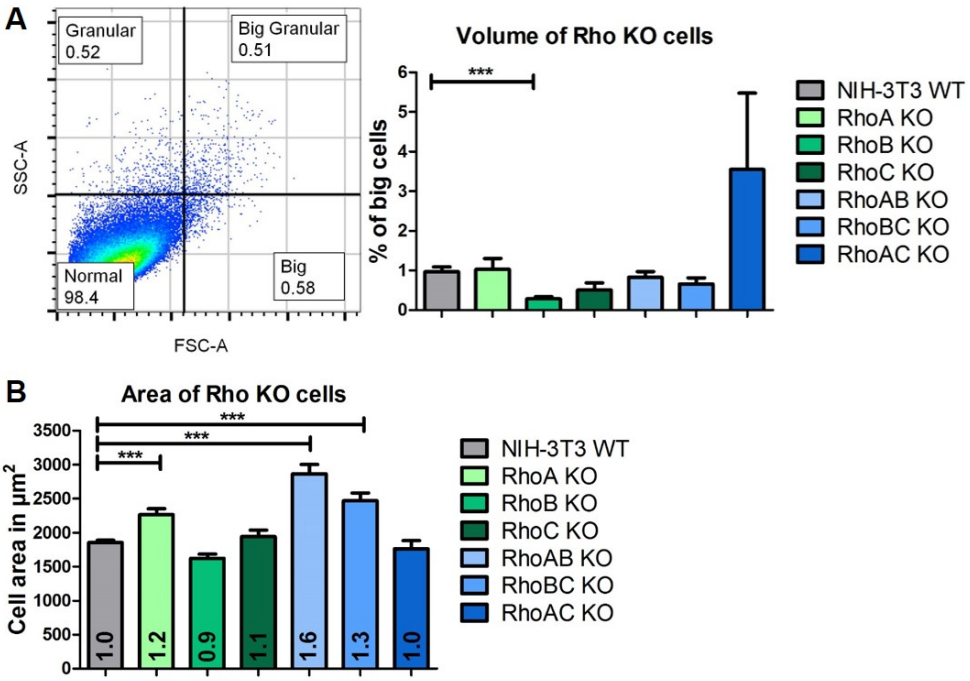

Figure 3.6: Volume and area of Rho KO cells. (A) NIH-3T3 and Rho KO clones were analyzed via FACS and grouped in four categories according to size and granularity measured via forward and side scatter. Each clone was measured twice, whereas six measurements were executed for WT cells. The pooled results are graphically depicted as arithmetic mean with SEM. Unpaired *t*-test was used to calculate the significance ($p < 0.05$). (B) Either NIH-3T3 WT or Rho KO cells were stained with CellTracker and mixed on the same glass coverslip for direct comparison and stained with phalloidin and DAPI. Area of cells was measured using the phalloidin staining with Metamorph. At least 60 cells were measured per KO phenotype and cells from all KO clones were included. At least two replicates per clone were used. Graph shows arithmetic means with SEM and significance was measured via 1way ANOVA ($p < 0.05$). Data were in addition normalized to WT levels and the respective numbers are displayed in the bars. These experiments were performed with the help of Franziska Grüner (HZI, Braunschweig).

After analyzing the size of the whole cell, are of nuclei was investigated with the help of Franziska Grüner (HZI, Braunschweig). Area of nuclei was increased in RhoBC KO cells, in line with an increased cell size (see Figure 3.7.A). Nuclear area of RhoAB double KOs is unchanged even though the cellular area is enlarged. This correlates nevertheless to the number of nuclei per cell, which is increased in all cell lines lacking RhoA (see Figure 3.7.B). A RhoAB KO therefore induces more and also smaller nuclei. The same was observed for RhoA KOs, with increased cellular area and decreased nuclear area. More nuclei per cell point towards a defect in cell division, which is in line with the fact that the same cell lines that display multiple nuclei per cell also grow slower in cell culture, which was a preliminary observation without further quantification.

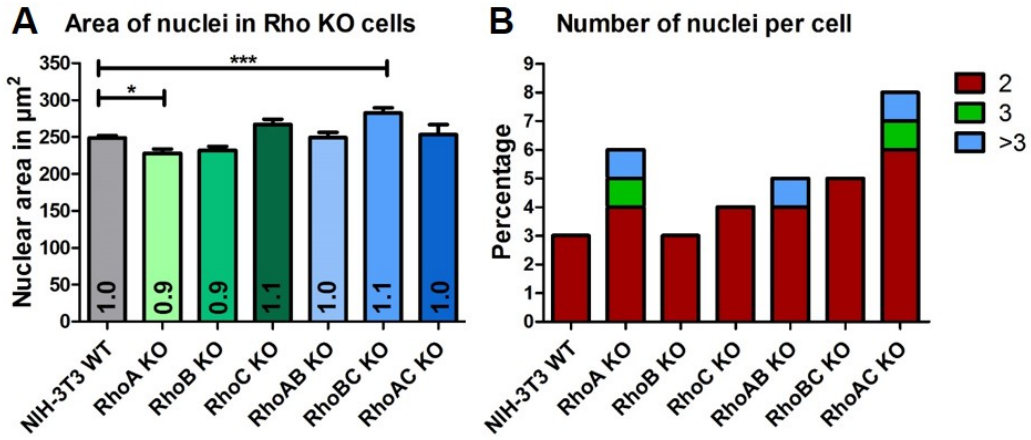

Figure 3.7: Area and number of nuclei in Rho KO cells. (A) NIH-3T3 WT and Rho KO cells were analyzed together on the same glass coverslip and distinguished by CellTracker staining. After fixation, cells were stained with phalloidin and DAPI. Area of nuclei, labeled via DAPI staining, was measured with Metamorph for at least 60 cells per KO phenotype and cells from all KO clones were included. At least two replicates per clone were used for the analysis. Graph shows arithmetic means and SEM and data normalized to WT levels are written in the bars. Significance values were calculated with 1way ANOVA ($p < 0.05$). These experiments were performed with the help of Franziska Grüner (HZI, Braunschweig). (B) Number of nuclei per cell was analyzed by DAPI staining of at least 600 fixed cells from three independent experiments per KO phenotype. Graph shows percentage of cells with more than one nucleus.

FACS measurements of Rho KO cells revealed not only information about cell volume but also about granularity. Figure 3.8.A shows an increase in number of cells with high granularity for all cell lines lacking RhoA, whereas the effect is most dramatic in the respective double KO cells. A decrease in granularity was on the other hand observed in RhoB KO cells. A correlation between RhoA levels and granularity, potentially correlating with cell division and multinucleation, can thereby be assumed.
Due to the involvement of RhoB in vesicular trafficking [61], the Golgi structure of all cell lines was analyzed via immunofluorescence stainings (see Figure 3.8.B). The Golgi structure was divided in two categories, compact or dispersed. In NIH-3T3 WT cells around 40% of cells contained a compact Golgi, the other 60% were dispersed. The number of cells with a compact Golgi phenotype was increased in RhoB KO cells to 50% and decreased in RhoAC KOs, expressing only RhoB, to 25%. In all other cases, the distribution was similar to WT levels with a tendency to less compact Golgi structures, especially in RhoA single KOs. These data suggest a direct correlation between RhoB levels and Golgi structure, showing rather dispersed structures upon high RhoB levels.

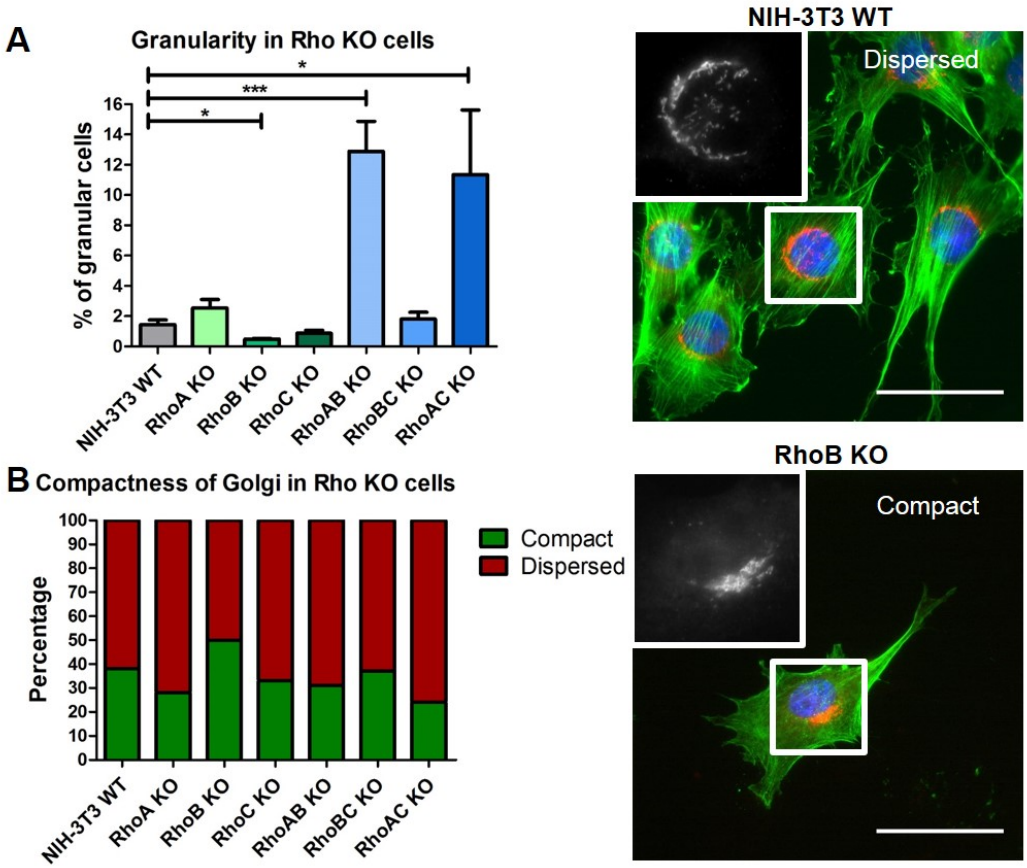

Figure 3.8: Granularity and Golgi structure in Rho KO cells. (A) Granularity of NIH-3T3 WT and Rho KO cells was measured via FACS as depicted in Figure 3.6.A. Graph shows pooled arithmetic means with SEM of two replicates per clone and data were all normalized to WT levels. Unpaired *t*-test was used for calculation of significance ($p < 0.05$). (B) Golgi structure of NIH-3T3 WT and Rho KO cells was analyzed by staining of fixed cells with phalloidin (green), DAPI (blue) and a GM-130 antibody labeling the Golgi apparatus (red). Golgi structures were categorized as compact or dispersed and graph shows arithmetic means of at least 160 cells per KO phenotype, analyzed during at least two independent experiments per clone. Scale bar shows 50 µm.

Rho proteins have long been investigated in the context of cell migration [170]. Hence, random migration assays with all KO cell lines were performed to address their migration capacities (see Figure 3.9.A). Velocity of almost all Rho KO cells was strongly decreased compared to WT levels. The weakest effect was observed for RhoAC double KOs, whereas velocity in RhoA single KOs was reduced to only 50% of WT levels. Directionality of migration was decreased in all cell lines except for RhoB KOs.
Since cells lacking only RhoA were most affected in cell migration, these cell lines were used for an additional investigation, in which random migration was analyzed in viscous medium containing different concentrations of polyvinylpyrrolidon (PVP) (see Figure 3.9.B). PVP is a water-soluble polymer increasing viscosity of liquids. This experimental setup was used to analyze the ability of Rho KO cells to generate enough force for migration with increased resistance of the environment. Whereas velocity of NIH-3T3 WT cells was only moderately affected by an increasing PVP concentration, RhoA KOs migrated much

slower in 2% PVP than in normal medium. Taken together, these data reveal an important role for RhoA in migration speed and overcoming environmental resistances during migration.

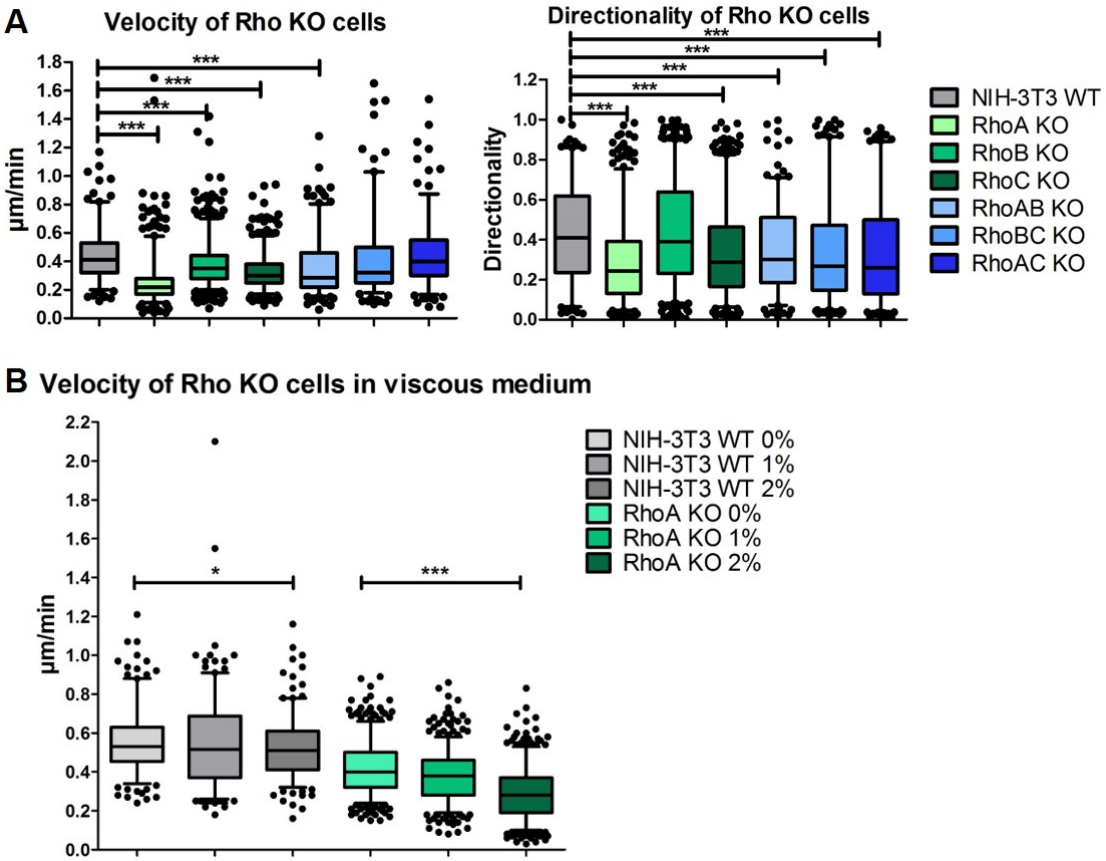

Figure 3.9: Migration capacity of Rho KO cells. (A) NIH-3T3 and Rho KO cells were seeded on Ibidi glass bottom dishes with fibronectin and phase contrast images were taken every 10 minutes for 20 hours. Random migration was tracked via ImageJ for at least 180 cells per phenotype, measured during three independent experiments. Graphs for velocity and directionality show box plots with 95/5 percentiles. Unpaired *t*-test was used for calculation of significances ($p < 0.05$). (B) RhoA KO cells and NIH-3T3 WT cells as control were seeded in 12 well plates and phase contrast videos were recorded for 10 hours, by taking an image every 5 minutes. Immediately before the recording was started, the medium was changed to different concentrations of PVP, increasing the viscosity of the environment. Graph shows pooled results of at least 240 cells per phenotype, measured during three independent replicates. As in (A), box plots with 95/5 percentiles are shown and unpaired *t*-test shows significance values ($p < 0.05$).

3.3.2 Differential regulation of RhoA, RhoB, RhoC and respective GDIs in Rho KO cells

For a detailed investigation of gene regulation in cells lacking one or two Rho proteins, microarray analysis after RNA isolation was performed in cooperation with Petra Hagendorff and Dr. Robert Geffers (HZI, Braunschweig) to compare Rho KO cell lines to NIH-3T3 WT cells. Three WT control replicates were included during the analysis of single as well as double KO clones, respectively. Figure 3.10 displays heat maps of the most regulated genes. The conclusion that

can be drawn from this dataset is, that gene regulation in RhoA and RhoB KOs is antagonistic. Surprisingly, gene regulation in RhoC KOs looks quite similar to WT levels. In the double KO datset, RhoBC KOs expressing only RhoA show no dramatic changes compared to WT cells. RhoAB and RhoAC KOs on the other hand also seem to be regulated in an antagonistic fashion.

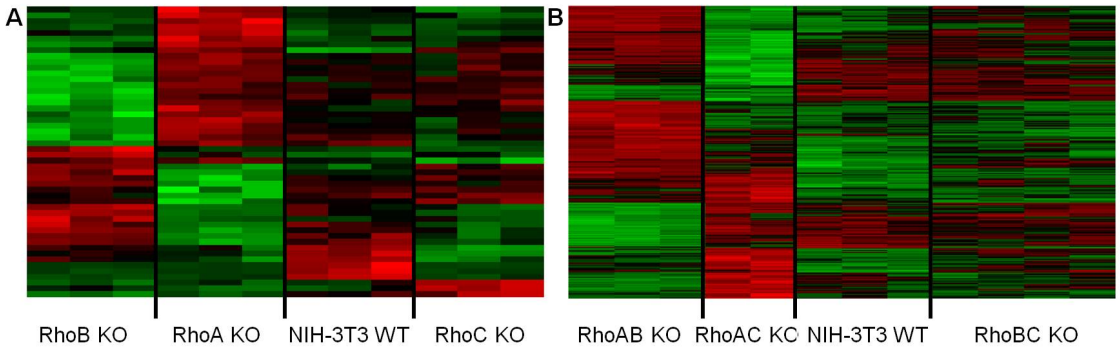

Figure 3.10: Heat maps of gene regulation in Rho KO cells. Microarray analysis, performed by Petra Hagendorff and Dr. Robert Geffers (HZI, Braunschweig) revealed mRNA regulation in Rho KOs. Each horizontal line displays one of the top regulated genes. Green shows downregulation whereas red depicts upregulation of mRNA levels. One experimental setup measured all single KO clones and three replicates of WT cells and another one all double KO clones and again three replicates of WT cells. (A) Single KO cells top 50 regulated genes. (B) Double KO cells top 500 regulated genes.

The most regulated mRNAs were expressed from genes involved in cell proliferation, cell migration and adhesion to the extracellular matrix (ECM). Examples for mRNA regulation of genes potentially involved in Rho signaling or its regulation are shown in Figure 3.11. Expression of the micro-RNA 377, which was shown to be involved in cell proliferation [171], was strongly downregulated in all Rho KO cell lines. mRNA levels of Rhophilin 2, encoding for a protein connected with RhoB activity on late endosomes [172], were increased specifically in RhoA and RhoAC KO cells, which express high levels of RhoB (see Figure 3.13). mRNA expression of Tropomyosin 4, which was shown to recruit myosin II to stress fibers [173], was increased in RhoB and RhoC KO cells, expressing high levels of RhoA (see Figure 3.13), and decreased in RhoAC double KO cells. Expression of phosphatase of regenerating liver (PRL) genes revealed differences between PRL1, which has already been shown to be involved in RhoA activation [174], PRL2 and PRL3. PRL1 levels were increased in particular in RhoB KO cells, whereas an increase of PRL3 expression was observed in RhoA and RhoC KO cells. PRL2 mRNA levels on the other hand were decreased in RhoBC and RhoAC double KO cells. A detailed analysis of these genes and their potential involvement in Rho pathways will follow in the discussion. Other genes which were analyzed based on the microarray dataset are described throughout the next chapters.

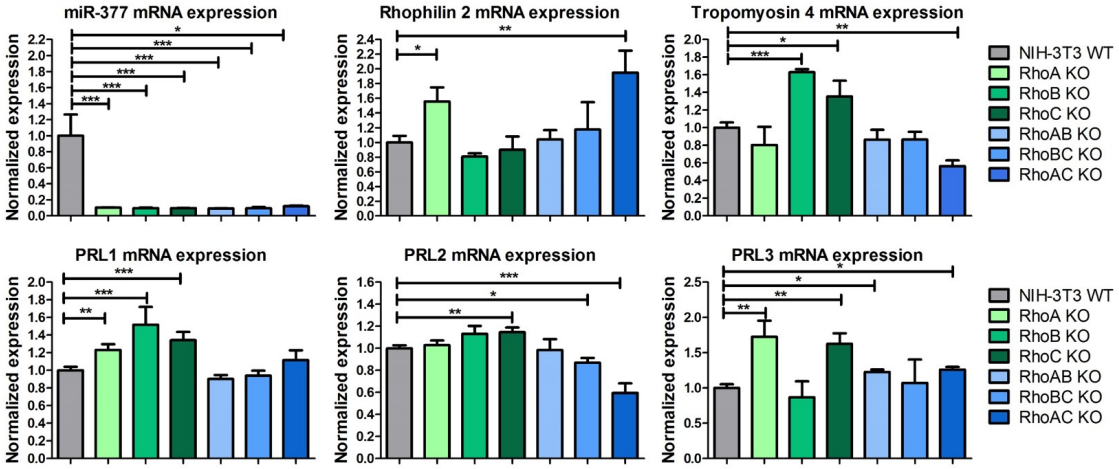

Figure 3.11: Regulated genes in Rho KO cells. Microarray data from Rho KO cells were used to analyze the amount of miR-377, Rhophilin 2, Tropomyosin 4 and PRL mRNA. Graphs show arithmetic means with SEM. Significance values were calculated with unpaired *t*-test ($p < 0.05$). Data were normalized to WT levels.

The microarray analysis was also used to investigate mRNA levels of Rho genes. RhoA mRNA levels were strongly decreased in all cell lines lacking the RhoA protein, whereas no changes in other cell lines were observed (see Figure 3.12.A). Interestingly, RhoB mRNA levels were decreased only in RhoB single KOs, but increased in RhoA and RhoAC KO cell lines. Accordingly, more RhoC mRNA was observed in RhoAB KO cells. In all other cell lines, especially the ones where RhoC was deleted, RhoC mRNA levels were reduced. This investigation thereby revealed that RhoA and RhoC mRNAs were degraded upon genetical KO, which was not as efficient upon RhoB KO, probably due to differences in the gene structure (see Figure 3.3). An additional analysis revealed the relative distribution of Rho mRNAs in NIH-3T3 WT cells (see Figure 3.12.B). 82% of Rho mRNA were coding for RhoC, while only 2% encoded RhoB and 16% RhoA.

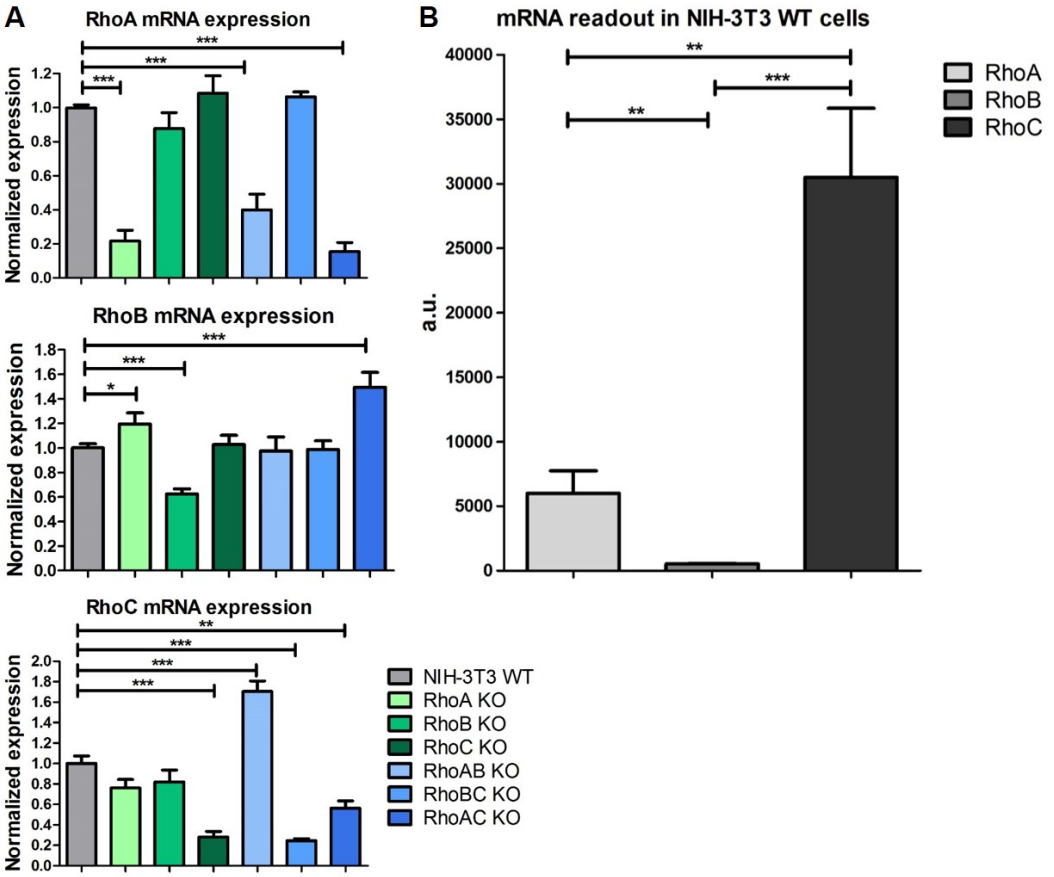

Figure 3.12: RhoA, -B and -C mRNA levels in Rho KO cells. Microarray data were used to analyze mRNA levels of RhoA, -B and -C in the respective KO cell lines and also in NIH-3T3 WT cells. (A) Arithmetic means with SEM of RhoA, -B and -C mRNA levels are shown for all Rho KO cells, normalized to WT levels. Significance was calculated with unpaired *t*-test ($p < 0.05$). (B) Relative amounts of RhoA, -B and -C in NIH-3T3 WT cells are depicted based on mRNA readout. Arithmetic means are shown with SEM and significance values were calculated with unpaired *t*-test ($p < 0.05$).

Since upregulation of some Rho mRNAs was detected in the absence of one or more Rho proteins, Western Blotting was performed to analyze Rho protein levels in Rho KO cells (see Figure 3.13). Data revealed that RhoA protein levels were increased around 2-fold in RhoB, RhoC and RhoBC KO cell lines. Upregulation of RhoB levels was even more dramatic, with a 5-fold increase in RhoC KOs and a 15-20 fold enhanced expression in RhoA and RhoAC KO cells. RhoC levels on the other hand showed no changes in RhoA or RhoB single KOs, while protein expression was enhanced 5-fold in RhoAB KOs. These data point towards a strong compensatory effect of the respective Rho proteins.

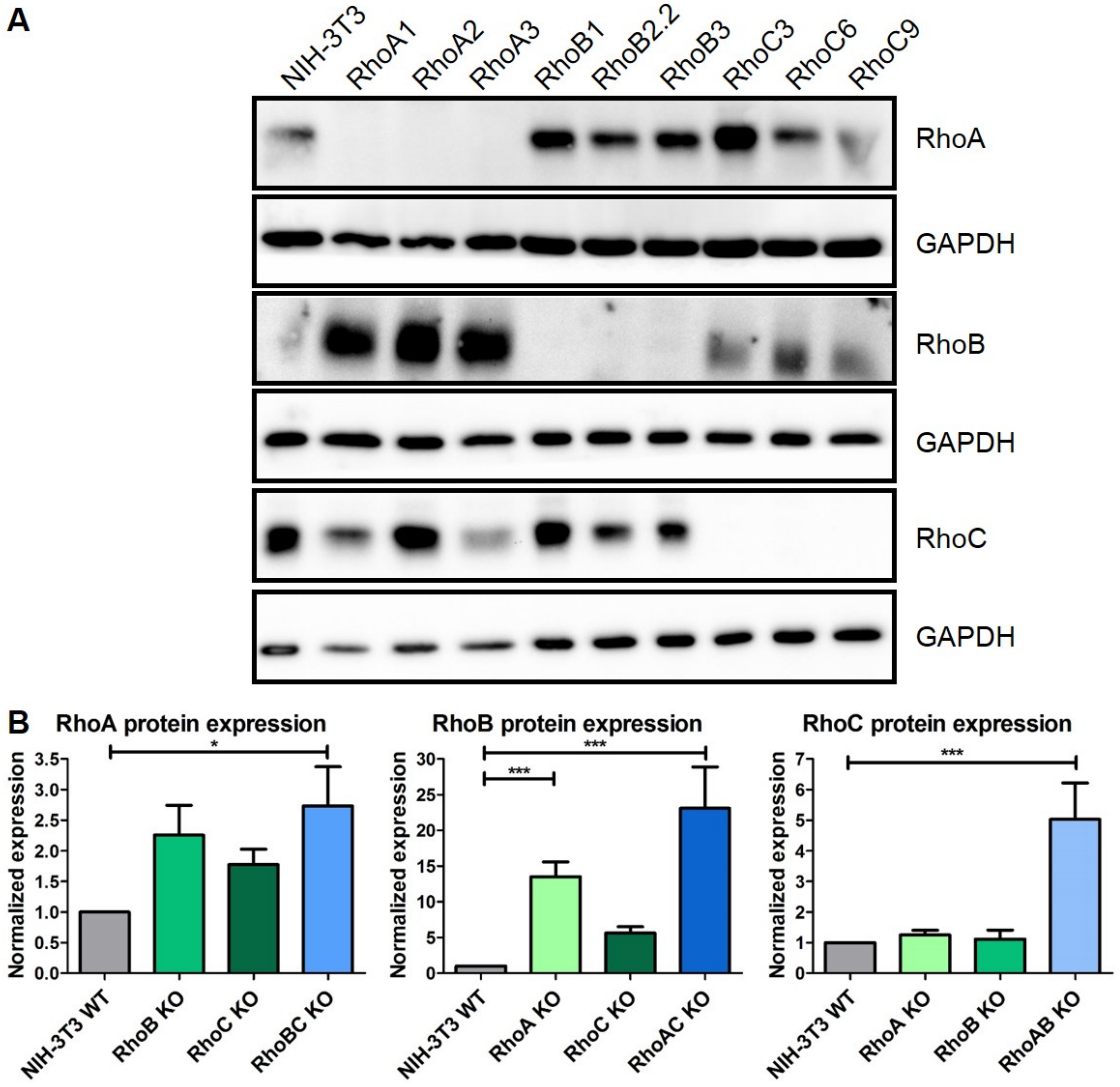

Figure 3.13: RhoA, -B and -C protein levels in Rho KO cells. (A) Lysates of single and double Rho KO cells were analyzed via Western Blotting with RhoA, -B and -C antibodies, as indicated. GAPDH was used as loading control and Rho KO lysates were compared to NIH-3T3 cells. Blots for single KOs are shown here, whereas Western Blots for Rho double KO cells are displayed in Figure 6.7 (Supplements). (B) Graphs show arithmetic means with SEM from at least 5 independent experiments per clone. Data were analyzed with 1way ANOVA ($p < 0.05$) and normalized to WT levels.

Total protein levels of Rho GTPases do not necessarily correlate with protein activity, which is why G-LISA analysis was performed (see Figure 3.14). The kit that was used was supposed to be specific for GTP bound RhoA. Even though, G-LISA values in cell lines lacking RhoA were not clearly decreased. Since clear absence of RhoA was shown at the protein level (see Figure 3.13), no difference in activity measurements of RhoA KOs by the G-LISA kit could be explained be detection of all three Rho proteins. Activity levels were increased in RhoB and especially RhoBC KOs, which express more RhoA according to Western Blotting. Also, higher Rho GTP levels were observed for RhoAC double KOs. A reduction in active GTP levels was observed in RhoC KO cell lines. The experiment thereby provides the tendency that RhoA activity is higher in the absence of RhoB.

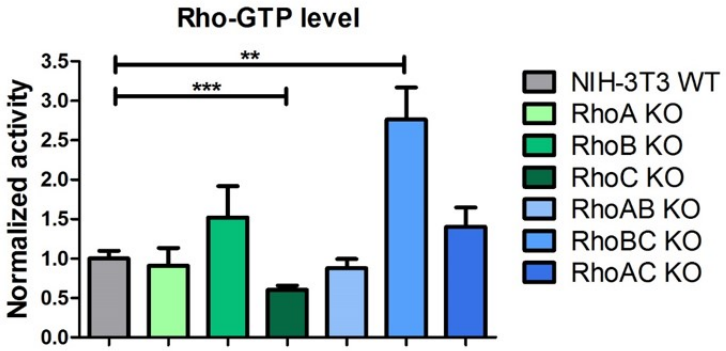

Figure 3.14: Rho GTP levels in Rho KO cells. Rho GTP levels were analyzed via Rho G-LISA. Graph shows arithmetic means and SEM from four independent experiments per clone, which were normalized to WT levels. Unpaired *t*-test was used to calculate significance values ($p < 0.05$).

Endogenous Rho protein levels upon Rho overexpression were dissected in addition to analysis in KO cell lines. Figure 3.15 shows that RhoA levels slightly increase upon RhoC overexpression and vice versa. No significant changes could be observed. These data suggest a correlation between RhoA and RhoC regulation.

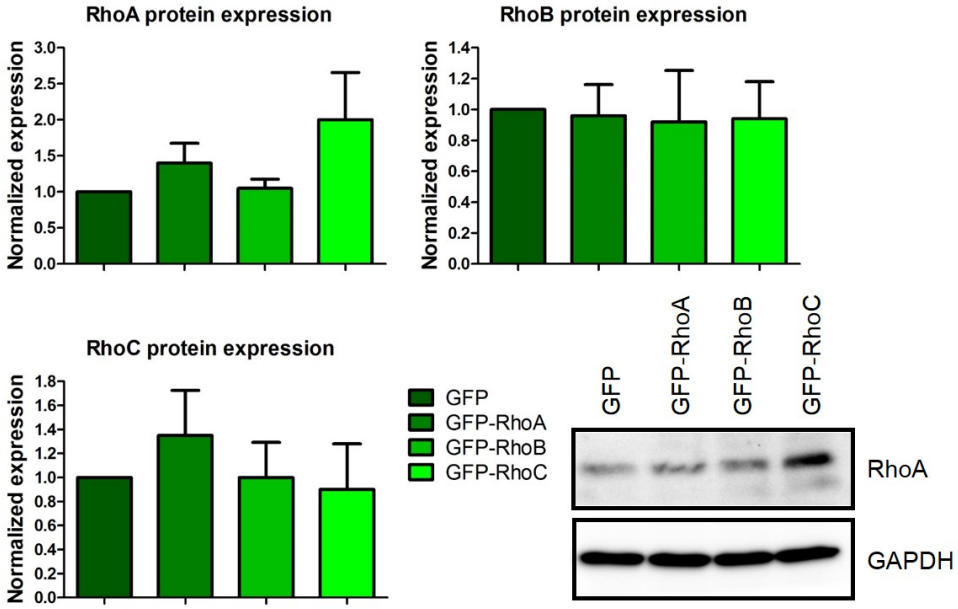

Figure 3.15: Rho levels upon Rho over-expression. Endogenous RhoA, RhoB and RhoC levels were analyzed with lysates of GFP-transfected cells. GAPDH was used as loading control for Western Blotting. Graphs show arithmetic mean and SEM from at least four independent experiments. Significance values were calculated with 1way ANOVA ($p < 0.05$) but did not show significant changes.

Since GDIs play an important role in Rho GTPase regulation by protecting the proteins from degradation [49], potential changes in Rho GDI levels were analyzed subsequently. Microarray analysis revealed that only GDIα and GDIβ were expressed in NIH-3T3 cells, whereas GDIγ levels were below the detection limit (data not shown). No significant changes in GDIα mRNA expression were

observed in Rho KO cells, whereas mRNA levels of GDIβ were decreased in Rho double KOs (see Figure 3.16.A). Further analysis showed that 68% of GDI mRNA in NIH-3T3 WT cells encoded for GDIα and only 32% for GDIβ (see Figure 3.16.B).

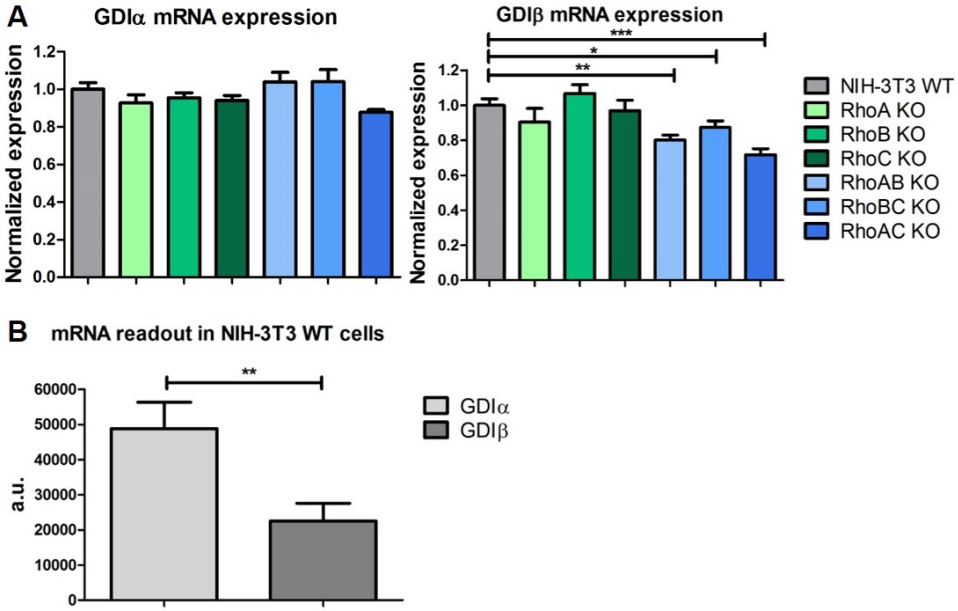

Figure 3.16: GDI mRNA levels in Rho KO cells. (A) mRNA levels of Rho GDIs were analyzed based on microarray data. Expression of GDIγ was below the detection limit (data not shown). Expression levels of GDIα and GDIβ were normalized to WT levels. Graphs show arithmetic means and SEM. Unpaired *t*-test was used to calculate significance values ($p < 0.05$). Changes of GDIα expression were not significant. (B) Direct mRNA readout of GDIα and GDIβ from microarray data are displayed as arithmetic means with SEM. Significance values were calculated with unpaired *t*-test ($p < 0.05$).

Western Blot analysis displayed an increase in GDIα levels in RhoBC double KOs and no significant changes in the other cell lines (see Figure 3.17.A). GDIβ protein expression was slightly increased in all cell lines except for RhoA KOs (see Figure 3.17.B). Upregulation of GDI levels could be due to increased Rho protein levels as compensation for the loss of one or two Rho proteins.
Upregulation of the three Rho proteins upon deletion of one or two raised the question of how exactly the increased amounts of proteins are stabilized. RhoA and RhoC are suggested to bind to GDIα and GDIβ, whereas RhoB was shown to bind GDIγ [53]. Since GDIγ was not expressed in NIH-3T3 cells, the interactions between GDIs and Rho proteins were analyzed with GFP-Trap IP experiments, performed by Silvia Prettin (HZI, Braunschweig). Data revealed that RhoB does not interact with GDIα or GDIβ upon overexpression, whereas binding of RhoA and RhoC to both GDIs was confirmed (see Figure 3.18.A). Binding of RhoB to GDIs was additionally analyzed by transfection of RhoAC double KOs with GFP-RhoB and a subsequent GFP-Trap IP. Even in the absence of RhoA and RhoC, RhoB did not bind to GDIα or GDIβ (see Figure 3.18.B). Stability of increased Rho protein amounts can therefore partially be correlated with increased GDI levels, but a so far unknown additional mechanism has to be considered.

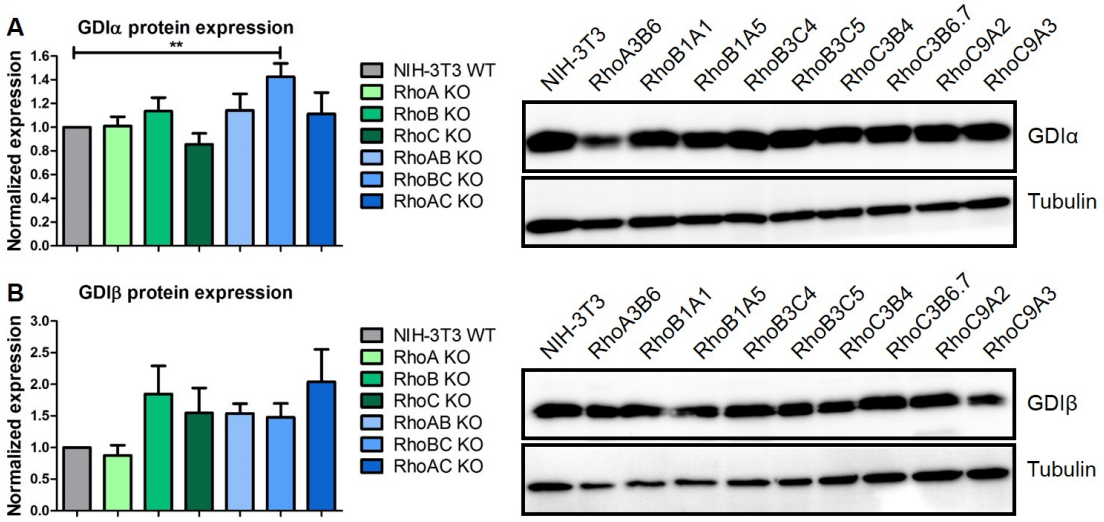

Figure 3.17: GDIα and GDIβ proteins in Rho KO cells. (A) Protein levels of GDIα were analyzed via Western Blotting of Rho KO and WT lysates. Tubulin was used as loading control. Blot for double KOs is shown. Graph depicts arithmetic means and SEM from at least four independent experiments. Data were analyzed with 1way ANOVA ($p < 0.05$). (B) GDIβ protein levels were analyzed via Western Blotting with tubulin as loading control. The Western Blot shows Rho double KOs. Graph shows arithmetic means and SEM from at least four independent experiments with 1way ANOVA analysis ($p < 0.05$). Data revealed no significant changes.

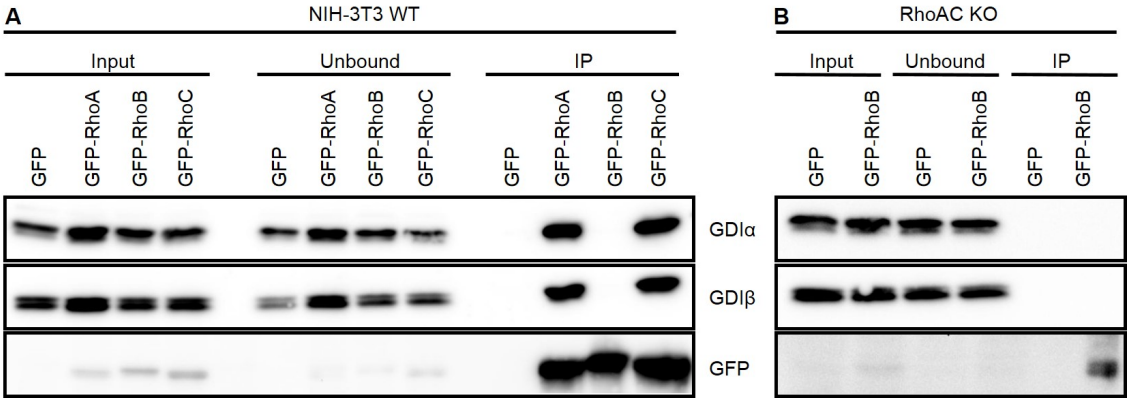

Figure 3.18: GDI interactions with RhoA, RhoB and RhoC. (A) NIH-3T3 cells were transfected with GFP only, GFP-RhoA, GFP-RhoB or GFP-RhoC. The next day, cells were lyzed and and GFP-Trap IP was performed by Silvia Prettin (HZI, Braunschweig). Input and unbound control as well as IP samples were analyzed via Western Blotting with GDIα, GDIβ and GFP antibodies, as indicated. This experiment was performed at least three times independently. (B) RhoAC double KOs were transfected with GFP only or GFP-RhoB. Further processing was performed as in (A). The experiment was performed once.

3.3.3 Regulation of other GTPases in Rho KO cells

Rac family GTPases have shown to act antagonistically to Rho family GTPases [175], so that Rac levels in Rho KOs were analyzed subsequently. Cdc42, as the third well-studied GTPase in addition to Rac1 and RhoA, was included in the analysis. Only Rac1 and Rac3 mRNA were expressed in NIH-3T3 cells, whereas the values for Rac2 mRNA were below the detection limit during microarray

analysis (data not shown). There were no obvious changes in Rac mRNA levels in the Rho KO cells. The only noticeable difference was observed for Rac3 mRNA levels, which were decreased in RhoA and RhoC KO cells. Cdc42 mRNA levels in Rho KOs were also similar to WT levels and only showed moderate downregulation in RhoB and RhoAC KOs and moderate upregulation in RhoAB double KOs (Figure 3.19.A.)
Protein levels were analyzed by usage of an antibody recognizing all Rac family members as well as Cdc42. An increase in protein levels was observed in almost all Rho KOs, but was only significant for RhoBC KOs, where 2.5 x more protein was detected (see Figure 3.19.B). Finally, Rac activity was analyzed by using a G-LISA kit for Rac1, Rac2 and Rac3. Again, a weak increase in Rac-GTP levels was measured for all Rho KO cells, which did not reveal to be significantly different (see Figure 3.19.C). Taken together, these data reveal a moderate increase in Rac/Cdc42 protein levels in the absence of Rho proteins.

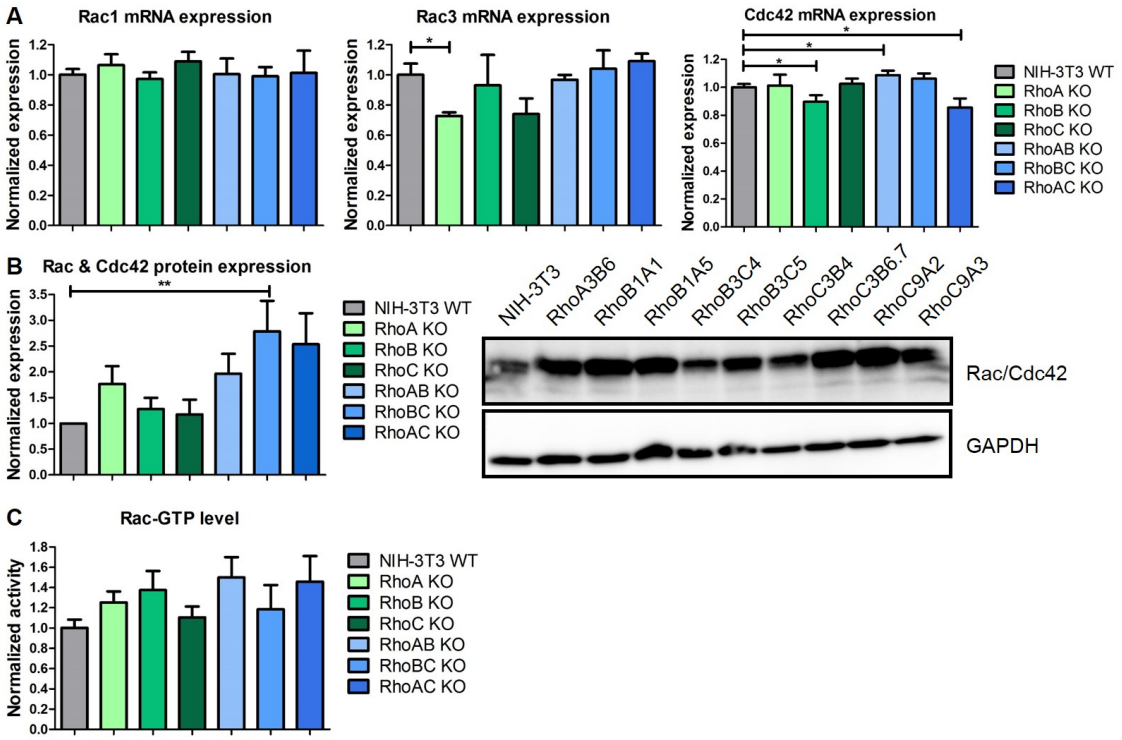

Figure 3.19: Rac and Cdc42 levels in Rho KOs. (A) mRNA levels of Rac and Cdc42 were analyzed via microarray. Rac2 mRNA levels were below detection limit (data not shown). Graphs show arithmetic means and SEM and significance values were calculated with unpaired *t*-test ($p < 0.05$). Rac1 data showed no significant changes. All data were normalized to WT levels. (B) Cell lysates of NIH-3T3 WT and Rho KOs were analyzed via Western Blotting with an antibody recognizing all Rac paralogs and Cdc42. GAPDH was used as loading control. Graph depicts arithmetic means and SEM from at least three independent experiments. Significances were calculated with 1way ANOVA ($p < 0.05$). Western Blot for Rho double KOs is shown. (C) Rac GTP levels were analyzed via G-LISA. Graph shows arithmetic means with SEM from four independent experiments per clone. Significances were calculated with unpaired *t*-test ($p < 0.05$), with no significant results. All data were normalized to WT levels.

In addition to analysis of protein levels via Western Blotting, morphology of Rho KO cells was also investigated by staining specifically for lamellipodia, which

are regulated by active Rac proteins [37]. For this purpose, a p16 antibody, binding to the subunit of the Arp2/3 complex downstream of Rac signaling and localizing at lamellipodial tips, was used. In all Rho KO cell lines, lamellipodial structures could still be observed (see Figure 3.20).

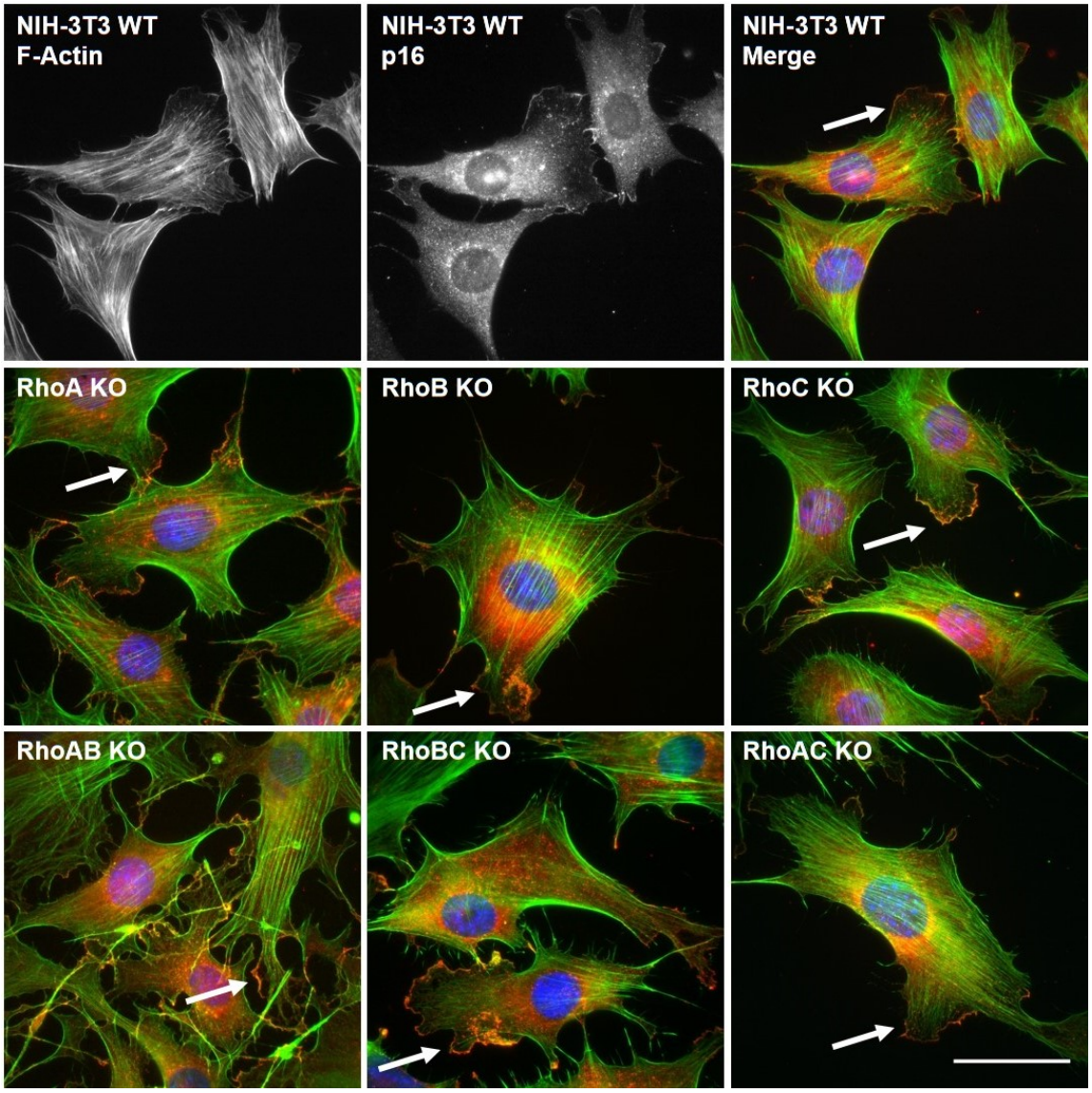

Figure 3.20: Lamellipodia in Rho KOs. NIH-3T3 WT and Rho KO cells were fixed and stained with phalloidin (green) and DAPI (blue). p16 (red) was used to highlight Lamellipodia. Arrows point towards lamellipodial structures. Merged images are shown for Rho KOs. Furthermore, the single channels for phalloidin and p16 are shown for NIH-3T3 WT. At least one clone per KO phenotype was analyzed. Scale bar represents 50 µm.

3.3.4 The actin cytoskeleton in Rho KO cells

Since Rho proteins regulate the actin cytoskeleton and especially stress fiber formation [176], the following experiments address this topic.
Total actin levels were analyzed via Western Blotting (see Figure 3.21.A). Interestingly, all Rho KO cells show the tendency of higher actin expression, which is significantly increased in RhoBC and RhoAC double KOs. To distinguish

between G- and F-actin, CellTracker stainings, performed by Franziska Grüner (HZI, Braunschweig), were used to measure the F-actin intensity by phalloidin staining. RhoA single KOs and RhoAB double KOs displayed a decrease in F-actin intensity, which was only 70% of WT levels in the case of RhoAB KOs (see Figure 3.21.B). When F-actin intensities are correlated to the cell area, differences appear much more dramatic. RhoB single KOs are the only cell type where the intensity per cell area is much higher than in WT cells. In RhoC KOs, the relation is quite close to control levels, whereas the strongest reduction can be observed in RhoAB double KOs, which are larger but contain less F-actin. Increased actin levels in RhoBC and RhoAC double KOs, expressing only RhoA or only RhoB, are therefore probably due to increased G-actin amounts. RhoC alone, namely in RhoAB double KOs, was accordingly the least able to maintain normal F-actin levels.

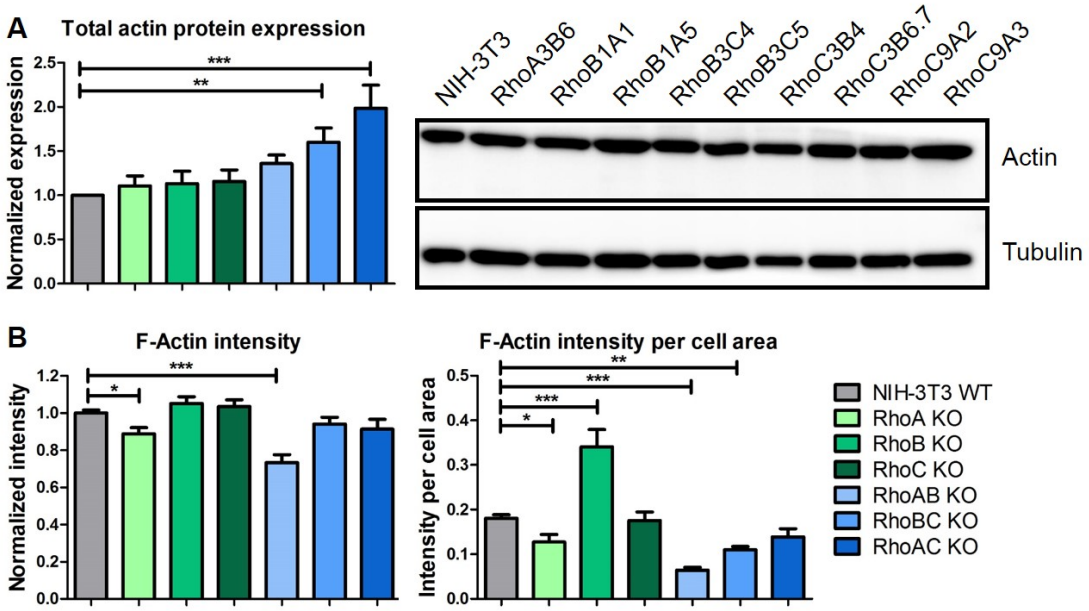

Figure 3.21: Total and F-Actin levels in Rho KO cells. (A) Total actin levels were measured via Western Blotting with tubulin as loading control. Graph shows arithmetic means and SEM from at least three independent experiments. Data were normalized to WT levels and analyzed with 1way ANOVA ($p < 0.05$). Western Blot of Rho double KOs is shown. (B) F-Actin intensities of Rho KO cells in direct comparison to NIH-3T3 WT cells were analyzed via CellTracker and phalloidin stainings by Franziska Grüner (HZI, Braunschweig). Intensities of at least 60 cells per KO phenotype from at least two independent experiments were measured with Metamorph software. Measured intensity values were correlated with cell area shown in Figure 3.6.B. Graphs show arithmetic means and SEM and data were analyzed with 1way ANOVA ($p < 0.05$). Intensities were normalized to WT values. These experiments were performed with the help of Franziska Grüner (HZI, Braunschweig).

Stress fiber formation was addressed by starving the cells in serum-free medium, followed by a short stimulation with the addition of serum. The serum component lysophosphatidic acid (LPA) is thought to lead to Rho activation and thereby stress fiber formation [176]. In NIH-3T3 WT cells as well as all single KO cells, starvation led to a reduction of stress fibers, whereas serum stimulation induced stress fibers, which were localized mainly at the cell border (see

Figure 3.22). This effect was less dramatic in RhoA KO cells, in which stress fiber formation at the cell border upon serum stimulation was much weaker.

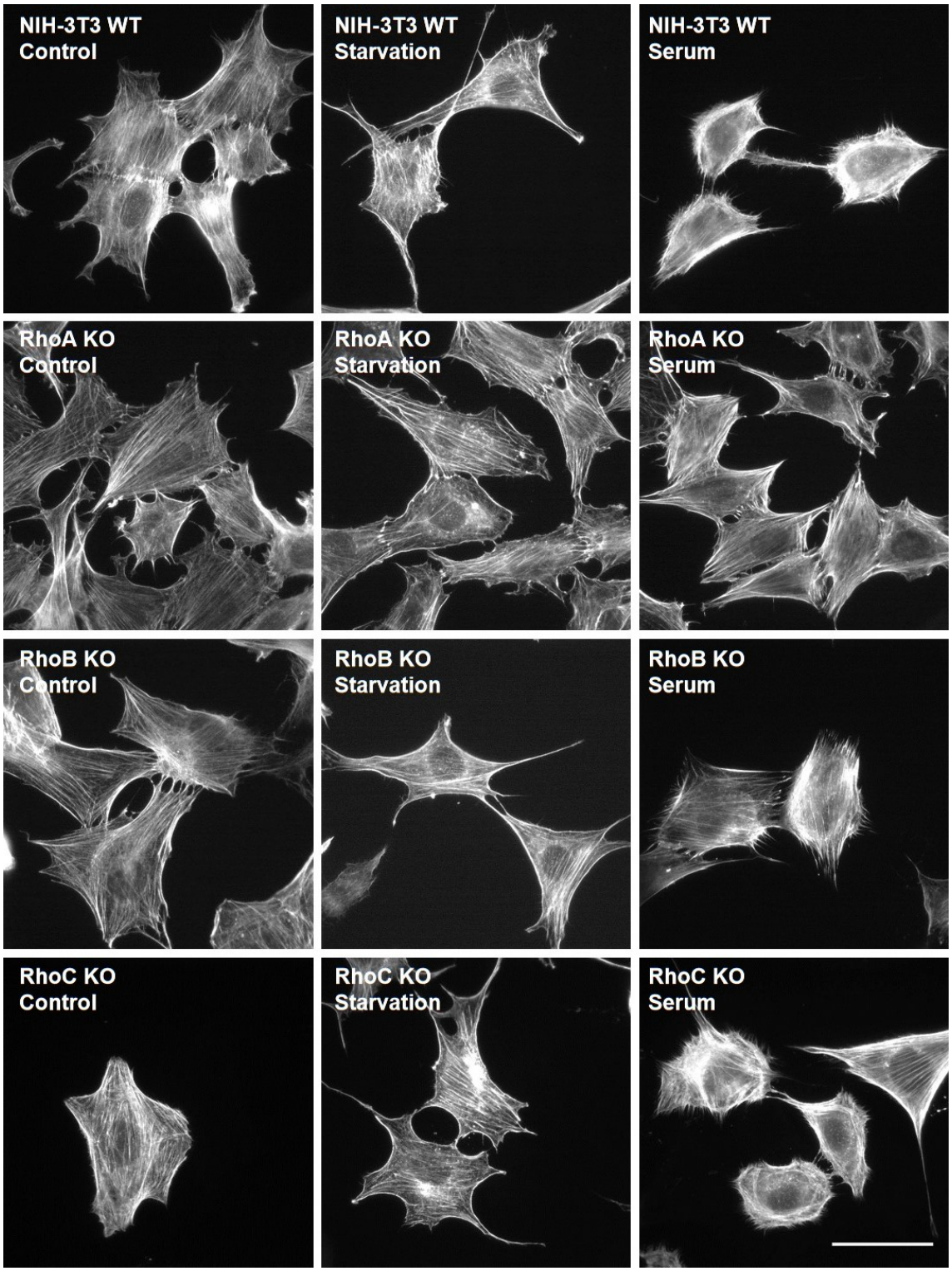

Figure 3.22: Serum stimulation in Rho single KOs. NIH-3T3 WT and Rho single KO cells were starved with serum-free medium for 24 hours and subsequently stimulated with 10% FBS for 15 minutes. Cells were fixed and stained with phalloidin. This was performed at least once with all singe KO clones. Scale bar depicts 50 µm.

The same experiment as described above was performed with Rho double KO cells (see Figure 3.23). Similar phenotypes were observed, although the starvation effect on RhoAB KO cells appeared less dramatic since the cells show reduced stress fiber formation already under control conditions. Serum stimulation in RhoAC double KOs also lead to increased stress fiber formation, but not predominantly at the border as in the other cell lines. Stress fiber formation thereby shows impairment in the absence of RhoA, with the impact depending on the presence of the other two Rho proteins.

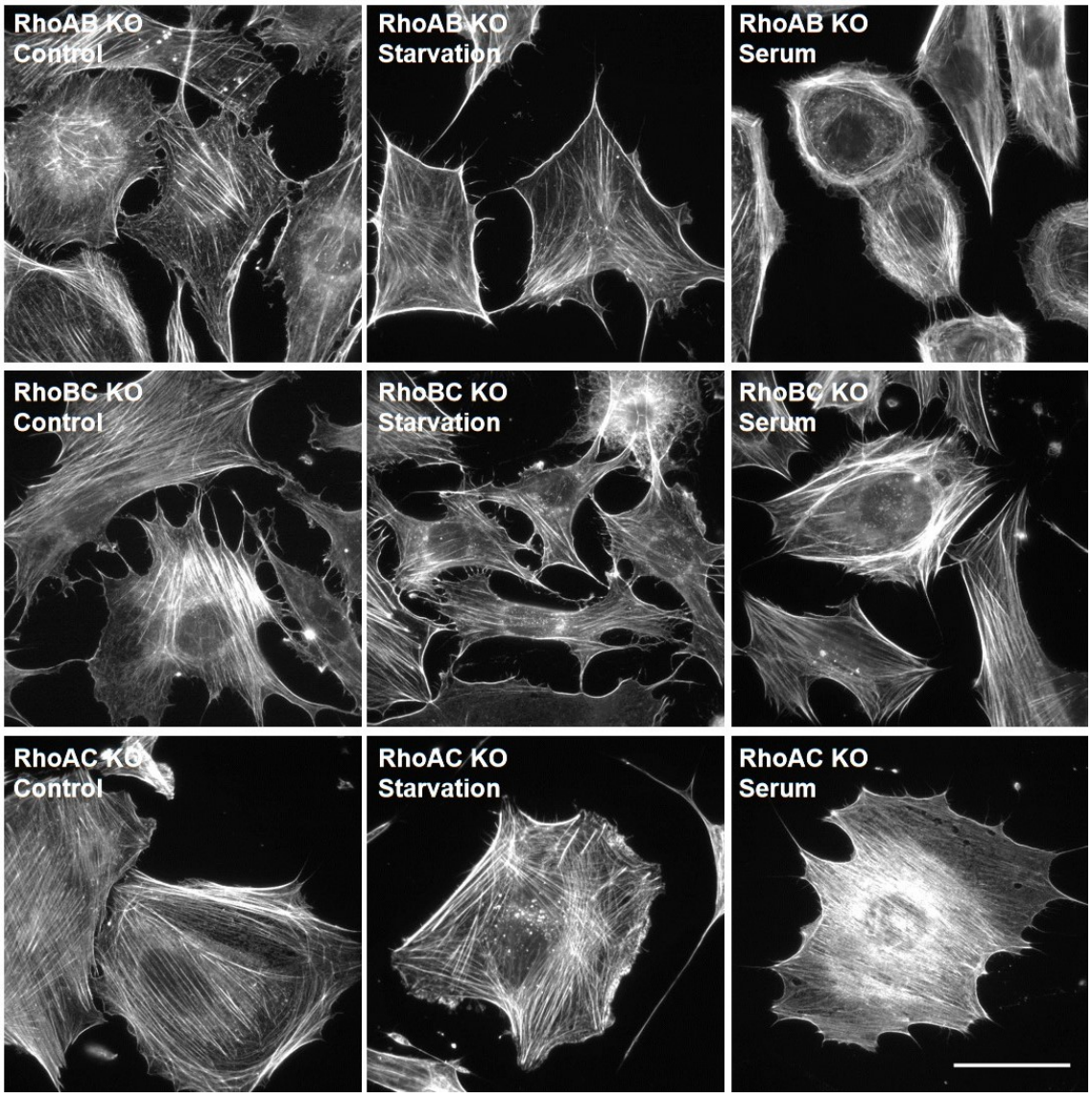

Figure 3.23: Serum stimulation in Rho double KOs. Rho double KO cells were starved for 24 hours with serum-free medium and then stimulated with 10% FBS for 15 minutes. Subsequently, cells were fixed and stained with phalloidin. The experiments were performed at least once with at least two clones per KO phenotype. Scale bar represents 50 µm.

Stress fiber formation downstream of Rho is mediated via ROCK proteins 1 and 2 [177]. Therefore, ROCK1 and ROCK2 levels were also investigated. Microarray analysis revealed a decrease of ROCK1 mRNA in RhoAB KO cells, the cell type with the lowest amount of F-actin (see Figure 3.24.A). ROCK2 mRNA was

increased in RhoA, RhoC and RhoAB KO cells. A moderate decrease was observed in RhoB, RhoBC and RhoAC KO cells. Protein levels of ROCK1/ROCK2 combined were increased in all single KO cells (see Figure 3.24.B), with twice as much protein in RhoB KO cells. The highest ROCK amounts were thereby induced by high RhoA levels in the absence of RhoB and the presence of RhoC. RhoAB and RhoAC KO cells showed a slight reduction of ROCK protein levels. RhoB or RhoC alone could therefore not maintain normal ROCK levels.

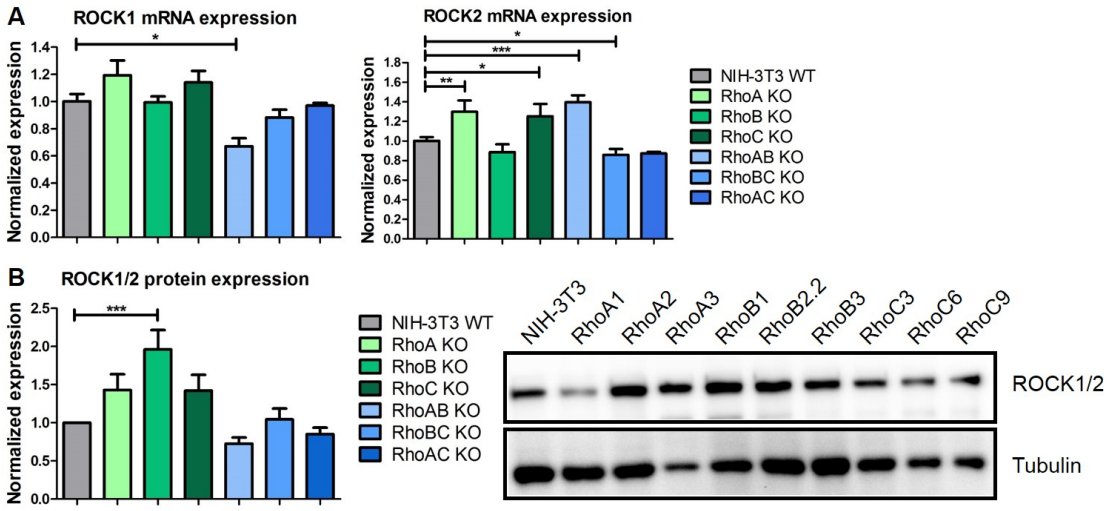

Figure 3.24: ROCK levels in Rho KO cells. (A) ROCK mRNA levels were analyzed using microarray data. Graphs show arithmetic means and SEM, normalized to WT control levels. Significance values were calculated with unpaired *t*-test ($p < 0.05$). (B) Protein levels for ROCK1 and ROCK2 in Rho KO cells were analyzed via Western Blotting, where tubulin was used as loading control. Western Blot for single KOs is shown. Graph depicts arithmetic means and SEM from at least three independent experiments. 1way ANOVA was used to calculate significances ($p < 0.05$).

Stress fiber formation and myosin II phosphorylation occurs not only downstream of Rho but also via Cdc42 and MRCK proteins [84]. Therefore, levels of MRCK mRNA from microarray analysis were also evaluated (see Figure 3.25). MRCKγ was not expressed in NIH-3T3 cells (data not shown). MRCKα mRNA levels were reduced in RhoBC and RhoAC double KOs, while MRCKβ mRNA was decreased to 60-70% in RhoB and RhoBC KO cells. These data reveal that MRCKβ levels were decreased in cells with high RhoA levels in the absence of RhoB.

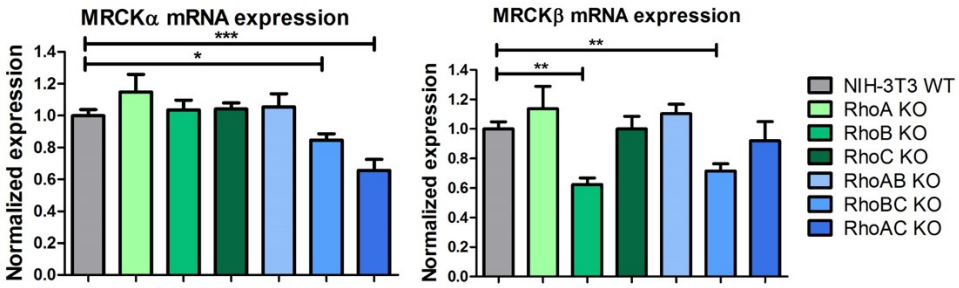

Figure 3.25: mRNA levels of MRCK in Rho KO cells. mRNA expression levels of MRCK genes were analyzed via microarray for Rho KO cells. MRCKγ levels were below the detection limit (data not shown). Graphs of MRCKα and MRCKβ depict arithmetic means and SEM, normalized to NIH-3T3 WT levels. Unpaired *t*-test was used to analyze significance values ($p < 0.05$).

Stress fibers and contractility are closely associated with phosphorylation of myosin II light chain downstream of ROCK and MRCK [178] [84]. First, localization of myosin IIa and myosin IIb were investigated in Rho KO cells. Figure 3.26 shows how myosin IIa co-localizes with actin stress fibers also in Rho double KO cells. The respective images of Rho single KO cells, not revealing any obvious differences, are shown in Figure 6.8 (Supplements).
Myosin IIb localization is shown in Figure 3.27 for Rho single KOs. Even though myosin IIb was in general more diffusely distributed in the cytoplasm, a co-localization with actin stress fibers was clearly visible for all Rho KO cells. This is true for single KOs as well as double KOs, the latter of which are shown in the supplements in Figure 6.9.
In addition to myosin IIa and IIb localization, phosphorylated myosin light chain was stained in all Rho KO cells. Figure 3.28 displays how pMLC2 localizes at stress fibers also in Rho single KOs. The same stainings were also performed with Rho double KOs (see Figure 3.29). Co-localization of pMLC2 and actin stress fibers was clearly visible in all cell lines. Myosin localization, including myosin IIa, myosin IIb and phosphorylated myosin light chain, was thereby unchanged in the absence of one or two Rho proteins.

In addition to immunofluorescence stainings, Western Blotting revealed the level of activated MLC in Rho KO cells (see Figure 3.30). Phosphorylation of MLC was strongly enhanced in RhoB KO cells and also increased in RhoBC double KO cells, namely in cells with high RhoA and low RhoB levels. In all other cell lines, phosphorylation levels were similar NIH-3T3 WT cells.

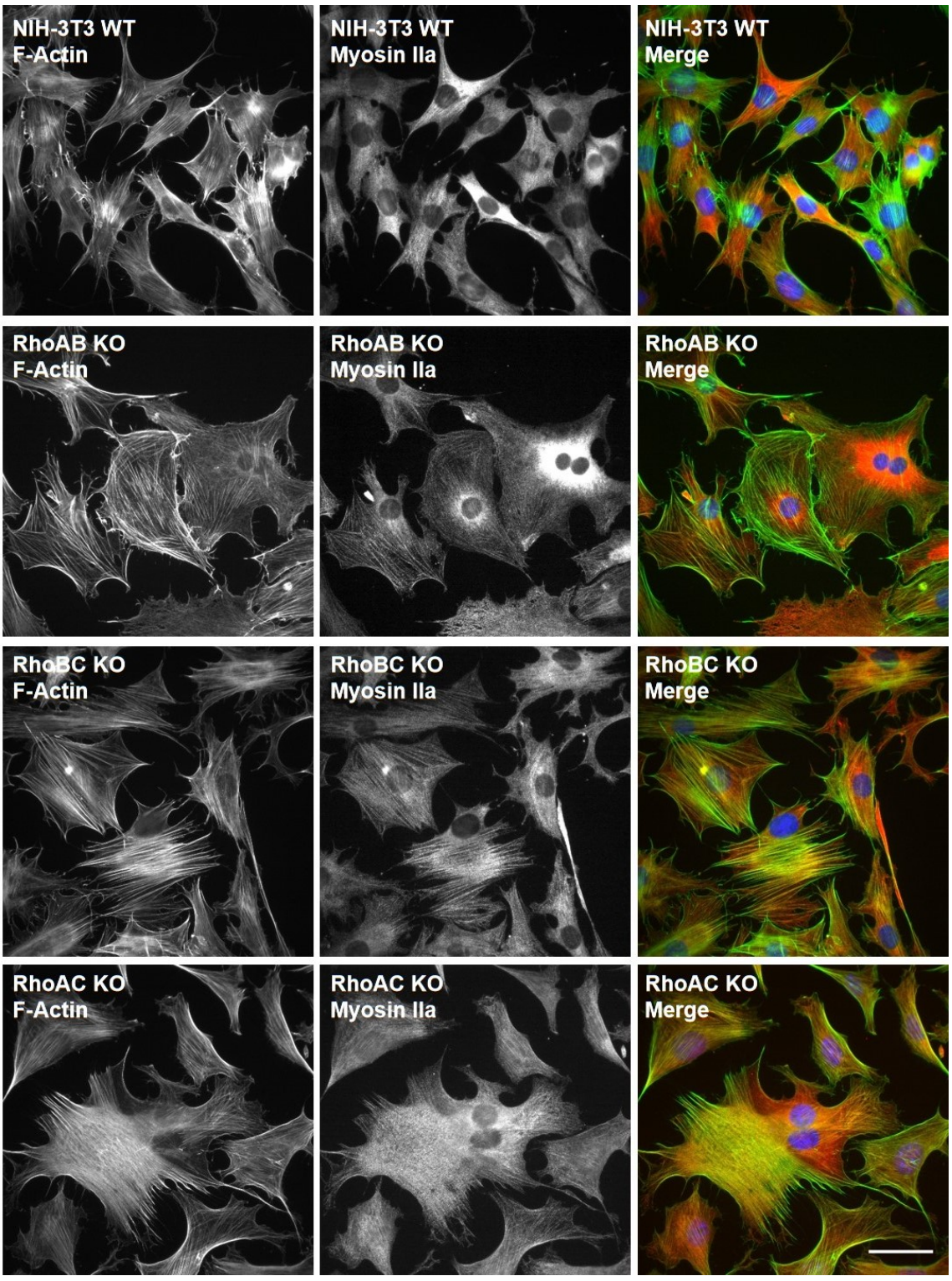

Figure 3.26: Localization of myosin IIa in double KOs. NIH-3T3 WT and Rho KO cells were fixed and stained with phalloidin (green), myosin IIa antibody (red) and DAPI (blue). Figure shows phalloidin, myosin IIa and the merged image with DAPI for double KO cells. Two clones per KO condition were analyzed. Stainings of single KO cells are shown in Figure 6.8 (Suuplements). Scale bar shows 50 µm.

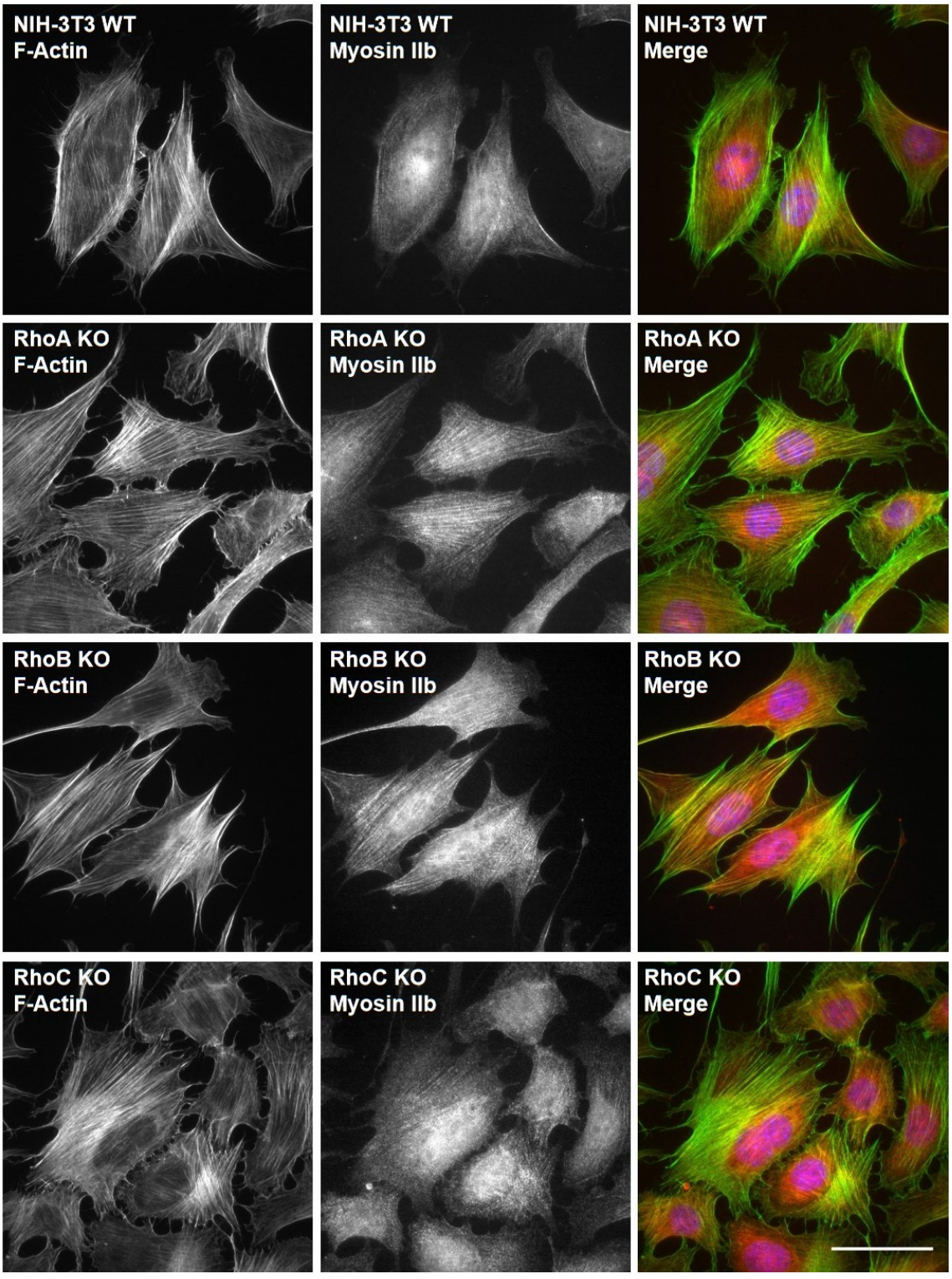

Figure 3.27: Localization of myosin IIb in single KOs. Rho KO and NIH-3T3 WT cells were fixed and stained with phalloidin (green), myosin IIb antibody (red) and DAPI (blue). This figure shows phalloidin, myosin IIB and the merged image with DAPI for Rho single KO cells. Two clones per KO phenotype were analyzed. Double KO cells, stained for myosin IIB, are shown in Figure 6.9. Scale bar represents 50 μm.

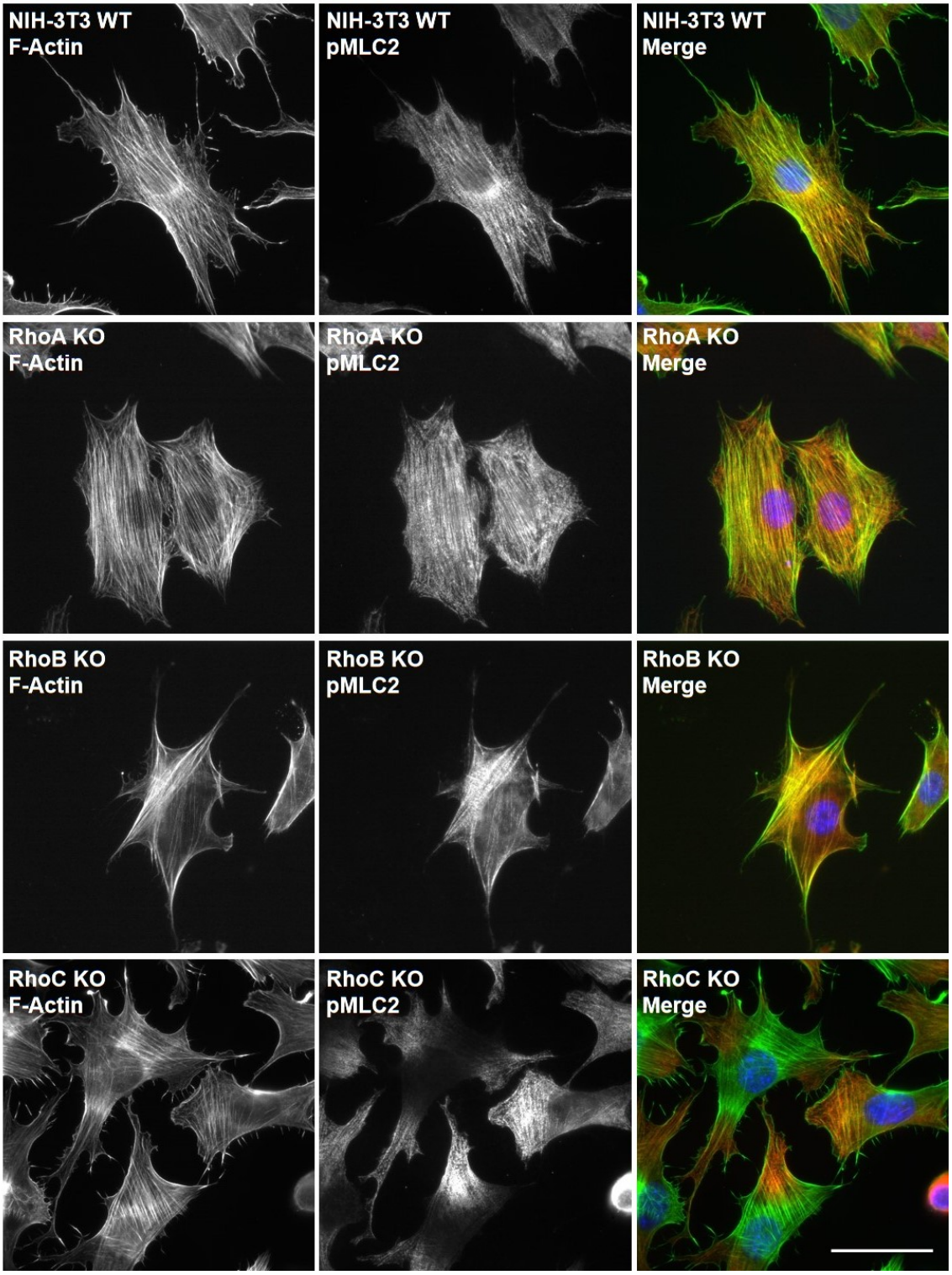

Figure 3.28: Localization of pMLC in single KOs. NIH-3T3 WT and Rho single KOs were fixed and subsequently stained with phalloidin (green), pMLC2 antibody (red) and DAPI (blue). Figure shows single images for phalloidin and pMLC2 and then the merged image with DAPI. At least one clone per KO phenotype was analyzed. Scale bar shows 50 μm.

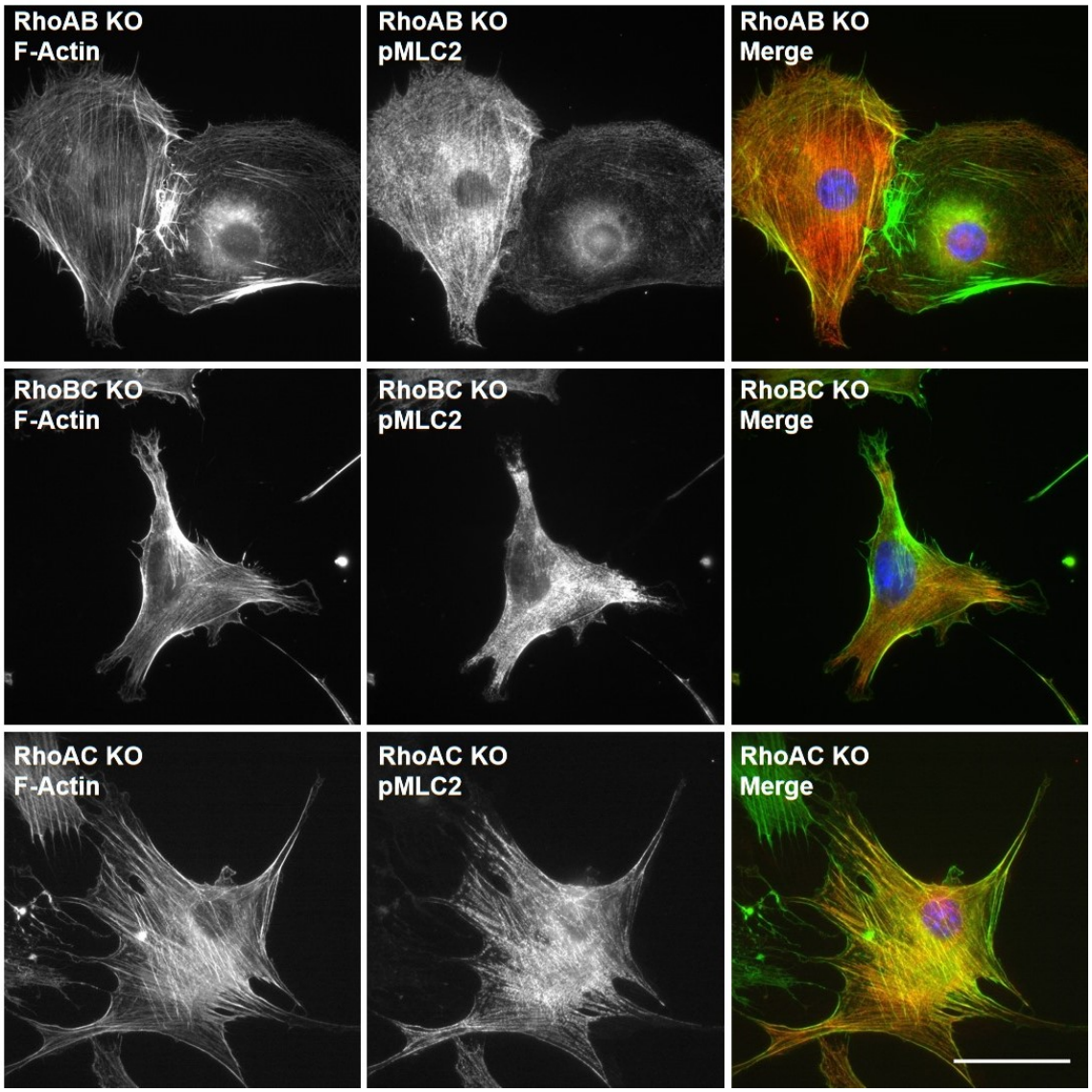

Figure 3.29: Localization of pMLC double KOs. Staining of fixed Rho double KO cells was performed with phalloidin (green), pMLC2 antibody (red) and DAPI (blue). Single images of phalloidin and pMLC2 stainings are shown and followed by the merged images with DAPI. At least one clone per KO phenotype was analyzed. Scale bar depicts 50 µm.

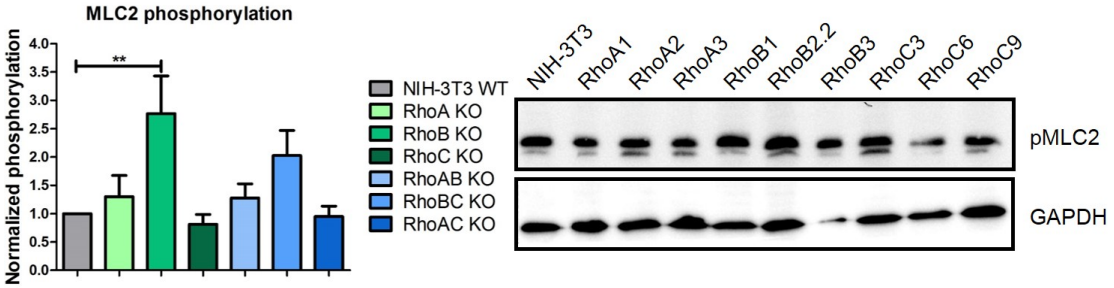

Figure 3.30: Myosin light chain phosphorylation in Rho KO cells. pMLC2 levels were measured via Western Blotting of Rho KO cell lysates with GAPDH as loading control. Figure shows Western Blot for single Rho KOs. Graph depicts arithmetic means and SEM of three independent experiments with all data normalized to WT levels. 1way ANOVA was used to calculate significance values ($p < 0.05$).

One gene which showed dramatic changes at the mRNA level during microarray analysis was ADF, a member of the Cofilin family, which contains proteins responsible for actin depolymerization. Therefore, mRNA levels of Cofilin 1 and Cofilin 2 were evaluated (see Figure 3.31). For Cofilin 1 and Cofilin 2, only moderate changes were observed on mRNA level, such as a reduction of Cofilin 1 in RhoAC KOs or a decrease of Cofilin 2 in RhoBC KOs. RhoC KOs showed moderate increase of both mRNAs, while the tendency for RhoA and RhoB single KOs was a reduction of mRNA for both genes. On the other hand, ADF mRNA levels were increased in all Rho KO cells, especially in RhoA and RhoC single KOs. Compared to mRNA changes for other proteins analyzed so far, the 4-fold increase in RhoA KOs is much more dramatic. In NIH-3T3 WT cells, 77% of Cofilin mRNA encode for Cofilin 1, 7% for Cofilin 2 and 16% for ADF (see Figure 3.31.B).

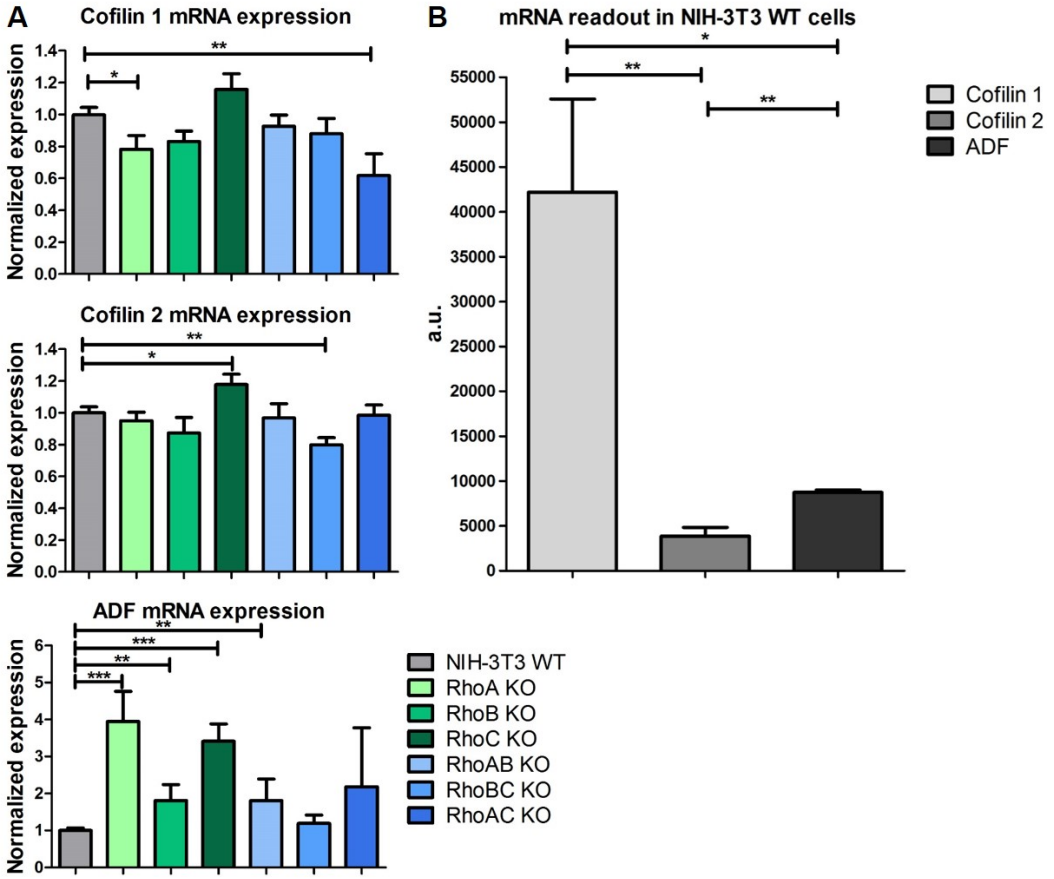

Figure 3.31: mRNA levels of Cofilin in Rho KOs. (A) mRNA levels of Cofilin family genes were analyzed according to microarray data of Rho KO cells. Graphs display arithmetic means with SEM and data are normalized to WT levels. Significance values were calculated with unpaired *t*-test ($p < 0.05$). (B) mRNA readout of Cofilin 1, Cofilin 2 and ADF in NIH-3T3 WT cells was compared to analyze relative gene expression. Graph depicts arithmetic means with SEM and unpaired *t*-test was used for calculation of significance values ($p < 0.05$).

Protein levels of Cofilin family members were analyzed via Western Blotting (see Figure 3.32). Surprisingly, in contrast to mRNA levels, Cofilin 1 protein expression was increased in all cell lines except for RhoA KOs, though the differences

were not significant. Phosphorylation and thereby inactivation of Cofilin 1 was increased mainly in RhoB and RhoBC KO cells. This is thereby specific for situations with high RhoA and low RhoB levels. Correlation of Cofilin 1 phosphorylation to increased Cofilin 1 levels reveals that the amount of phosphorylated and thereby inactivated Cofilin 1 is unchanged in most cases, with the exception of RhoA KOs. Here, inactive Cofilin 1 levels increase further than total Cofilin 1 levels. Cofilin 2 was upregulated around 2-fold in Rho double KOs, but values in single KOs resembled WT levels. ADF expression was increased 4-fold in Rho double KOs and around 2-fold in RhoB and RhoC single KOs. The general upregulation of Cofilin family proteins in the absence of Rho suggests increased actin depolymerization, potentially explaining decreased F-actin intensities described earlier.

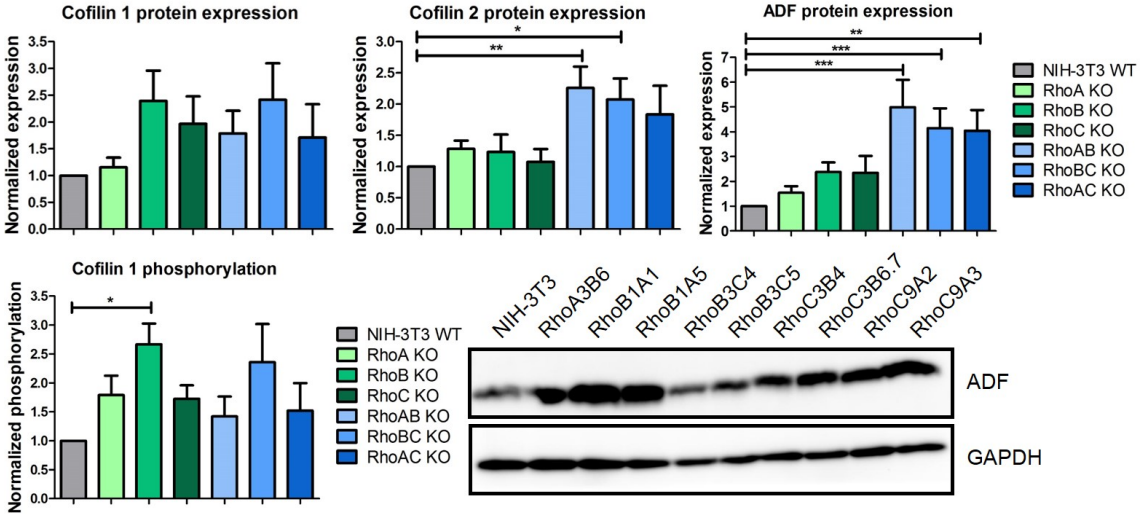

Figure 3.32: Protein levels of Cofilin family proteins in Rho KOs. Cell lysates of Rho KO clones and NIH-3T3 WT cells were analyzed via Western Blotting with antibodies against Cofilin 1, Cofilin 2, ADF and phosphorylated Cofilin 1. GAPDH was used as loading control. Western Blot of ADF with Rho double KOs is shown. Graphs show arithmetic mean and SEM for at least three independent experiments. The only exception is the graph for Cofilin 1 phosphorylation, for which only two values for one RhoAC KO were used. All data were normalized to WT levels and were analyzed with 1way ANOVA ($p < 0.05$). Data for Cofilin 1 showed no significant changes.

Since Cofilin levels were increased upon deletion of Rho, the effects of Rho overexpression in NIH-3T3 WT cells upon transfection with GFP constructs were analyzed via Western Blotting. The results in Figure 3.33 surprisingly revealed an increase of Cofilin family proteins when RhoA, RhoB or RhoC were overexpressed in WT cells. Even though, no significant changes were observed and levels of phosphorylated Cofilin 1 showed a moderate increase as well. Since Cofilin levels increase upon Rho KO but do not decrease upon Rho overexpression, the correlation between Rho and Cofilin is probably indirect and involves other factors, which are so far unknown.

WDR1, also called Aip1, was found to work together with Cofilin to depolymerize actin filaments [179]. Therefore, WDR1 mRNA and protein levels were inves-

tigated as well (see Figure 3.34). According to microarray data, WDR1 mRNA levels were increased in RhoAB and RhoAC double KOs. Western Blotting revealed an increase of protein expression in RhoBC and even more in RhoAC double KOs. Depolymerizing activity by Cofilin family proteins was thereby probably supported by WDR1 in the absence of Rho.

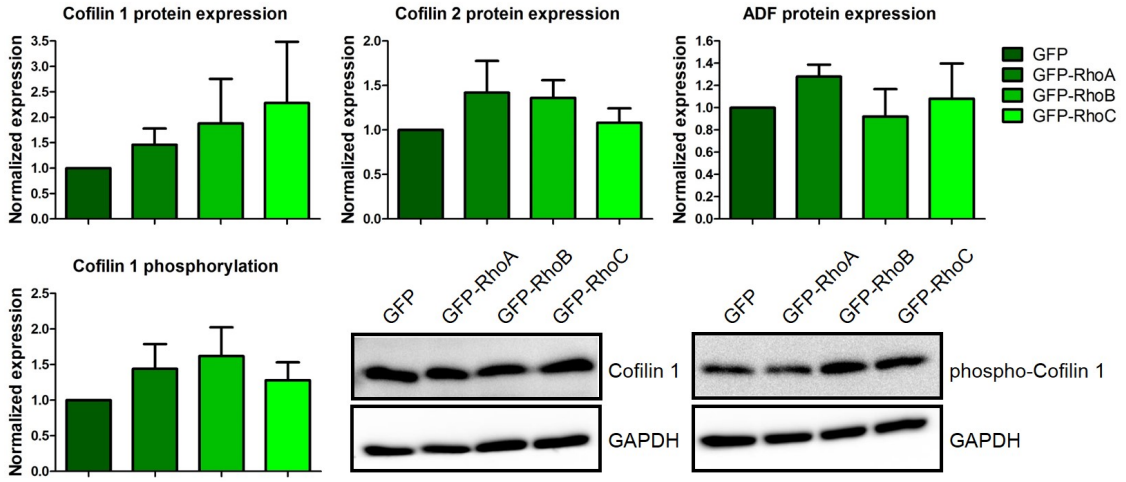

Figure 3.33: Cofilin levels upon Rho overexpression. Cofilin levels upon GFP-Rho overexpression in NIH-3T3 WT cells were analyzed via Western Blotting. GAPDH was used as loading control. Graphs show arithmetic means and SEM from five independent experiments. Significance values were calculated with 1way ANOVA ($p < 0.05$), but results were not significantly different.

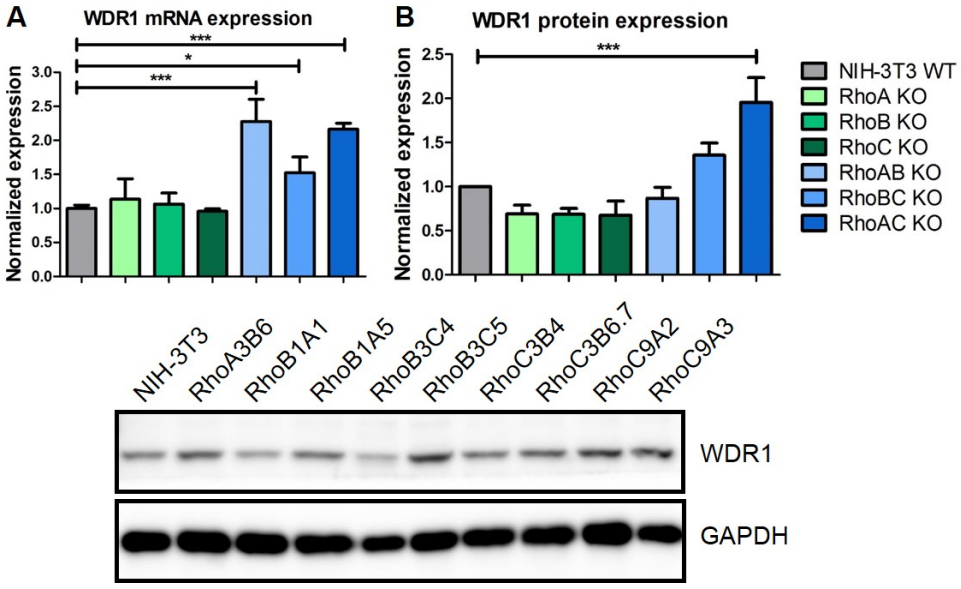

Figure 3.34: WDR1 expression levels in Rho KOs. (A) WDR1 mRNA expression was investigated via microarray analysis. Graph displays arithmetic means with SEM. All data were normalized to WT levels and analyzed with unpaired *t*-test ($p < 0.05$). (B) Protein levels of WDR1 were analyzed via Western Blotting, which is shown for Rho double KOs in comparison to NIH-3T3 WT. GAPDH was used as loading control. Graph shows arithmetic means and SEM from at least three independent experiments. All data were normalized to WT levels and analyzed with 1way ANOVA ($p < 0.05$).

Cofilin depolymerizes actin and lower F-actin levels could potentially be explained by increased Cofilin levels. The next experiments were set out to evaluate if Rho KO cells can generate more stress fibers if Cofilin is knocked down via siRNA, which has been described previously under control conditions in the presence of Rho [180]. Figure 3.35 depicts how protein levels of all three Cofilin family members were reduced upon siRNA knockdown. Transfections with all three siRNAs were performed on day 0, with a second transfection of only Cofilin 2 siRNA on day 1. Without the second transfection, ADF levels decreased further but Cofilin 2 was strongly upregulated for compensation (data not shown), which is the reason why the procedure with two transfections was finally chosen.

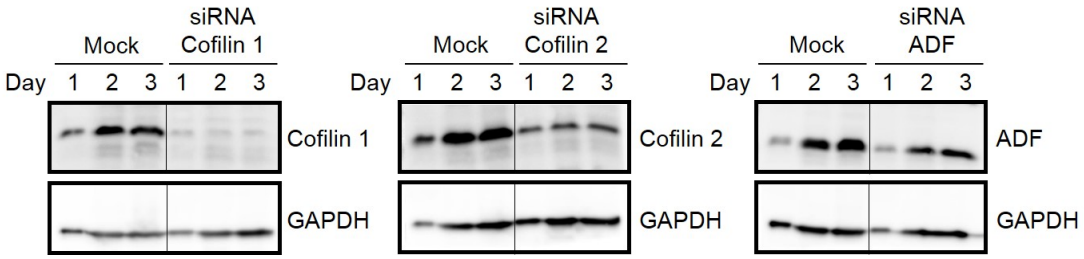

Figure 3.35: Cofilin knockdown with siRNA. NIH-3T3 WT cells were transfected with 2.5 µM siRNA of Cofilin 1, Cofilin 2 and ADF one day after seeding and once again with 5 µM Cofilin 2 siRNA the next day. Control cells were transfected with nuclease-free water instead of RNA. Cell lysates were generated each day after the first transfection and analyzed via Western Blotting with GAPDH as loading control. This exact experimental setup was performed once as a control before immunofluorescence stainings were started.

Knockdown of Cofilin family proteins induced dramatic stress fiber formation, increased cell size and increased and deformed nuclei (see Figure 3.36). To dissect if generation of stress fibers, under control conditions as well as upon Cofilin knockdown, arises by ROCK activation downstream of Rho or MRCK activation downstream of Cdc42, all cell lines were treated with small molecule inhibitors diminishing Rho proteins (Rhosin), ROCK (Y-27632), myosin II (Blebbistatin) or MRCK (BDP5290).
Figure 3.36 displays the effect of Cofilin knockdown in combination with various inhibitors of the stress fiber signaling pathways on NIH-3T3 WT cells. Under control conditions without Cofilin knockdown, Rho inhibition, ROCK inhibition, myosin II inhibition as well as MRCK inhibition all strongly reduce stress fibers. The strongest reductions are observed when ROCK or myosin II are inhibited, while MRCK and Rho inhibition yielded many dead cells, but also cells expressing still a few stress fibers. Starvation in serum-free medium, which was included since the inhibitor Rhosin has to be used in serum-free medium, showed a much weaker reduction of stress fibers than the inhibitors.

Upon Cofilin knockdown, reduction of stress fiber formation by using the different inhibitors was very subtle and no inhibitor was able to diminish the massive stress fiber formation that was triggered by Cofilin siRNA. A few cells with normal stress fiber amounts were observed, but this was also the case after Cofilin siRNA without further inhibitor treatment, since not every single cell was affected as strongly by the knockdown.
Similar results could be observed for RhoA KO cells (see Figure 3.37), as well as for RhoB, RhoC and RhoBC KOs (Supplements, see Figures 6.10, 6.11 and 6.12). Inhibitor treatments for ROCK and myosin II were very efficient in the reduction of stress fibers under control conditions but only worked partially in the Cofilin knockdown environment, where also the KO cells showed dramatic stress fiber formation and increased cell and nuclear size.
In RhoAB KO cells (see Figure 3.38), showing the lowest stress fiber amount of all cell lines in this study, the results were slightly different. Here, Rho and MRCK inhibitors affected the actin cytoskeleton stronger than ROCK and myosin II inhibitors under control conditions. Cofilin knockdown also induced stress fibers in these cells, however the effect was much less dramatic. Again, inhibition of the stress fiber signaling pathway only partially affected cells treated with Cofilin siRNA.
Also in RhoAC double KO cells, results were comparable to NIH-3T3 WT effects (see Figure 3.39). Again, ROCK and myosin II inhibition had the strongest impact under control conditions and Cofilin knockdown led to a similar massive stress fiber formation. Upon Cofilin knockdown in RhoAC double KO cells, myosin II inhibition was the only way to at least partially reduce stress fiber formation in some cells.
Taken together, Cofilin knockdown induces dramatic stress fiber formation, even in the absence of one or two Rho proteins. Since inhibitors of Rho, ROCK, MRCK or myosin II only partially diminished this effect, stress fibers were probably generated by both signaling pathways, mediated by ROCK as well as MRCK.

The final analysis considering stress fiber formation via Rho proteins included constitutive Rho activation by the toxin CNF_y from *Y. pseudotuberculosis*. NIH-3T3 WT and Rho double KO cells, each of the latter expressing only one of the three Rho proteins, were treated with CNF_y. Figure 3.40 shows stress fiber formation in all cases. RhoBC and RhoAC double KOs as well as NIH-3T3 WT cells already contain many stress fibers under control conditions, so that the effect is rather subtle. On the other hand, the change in RhoAB double KOs, expressing only RhoC, is dramatic. Many stress fiber bundles are formed upon CNF_y treatment, whereas particularly these cell lines show only a very low amount of stress fibers in the control status. These data suggest that RhoC, when constitutively active, is able to induce stress fiber formation even in the absence of RhoA and RhoB.

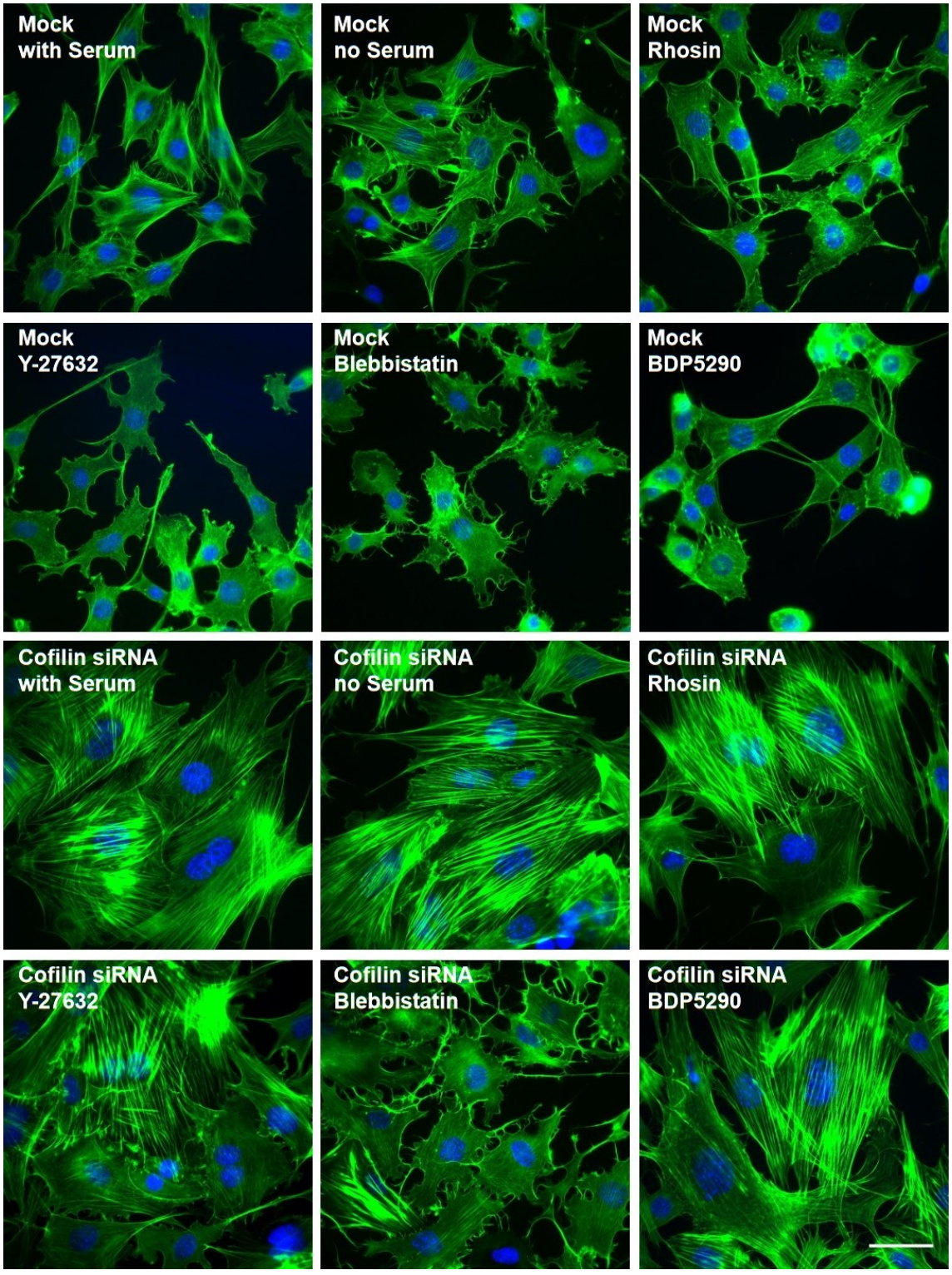

Figure 3.36: Cofilin knockdown in NIH-3T3 WT cells. NIH-3T3 WT cells were treated with 2.5 μM of Cofilin 1, Cofilin 2 and ADF siRNA one day after seeding of cells and again with 5 μM Cofilin 2 siRNA one day later. Two days after that, cells were treated with various inhibitors or serum-free medium for 1 hour before fixation. Inhibitors were 200 μM Rhosin to inhibit Rho proteins, 50 μM Y-27632 to inhibit ROCK, 120 μM Blebbistatin inhibiting myosin II and 20 μM BDP5290 to inhibit MRCK. Subsequently, cells were fixed and stained with phalloidin (green) and DAPI (blue). These experiments were performed twice independently. Merged images are shown. Scale bar represents 50 μm.

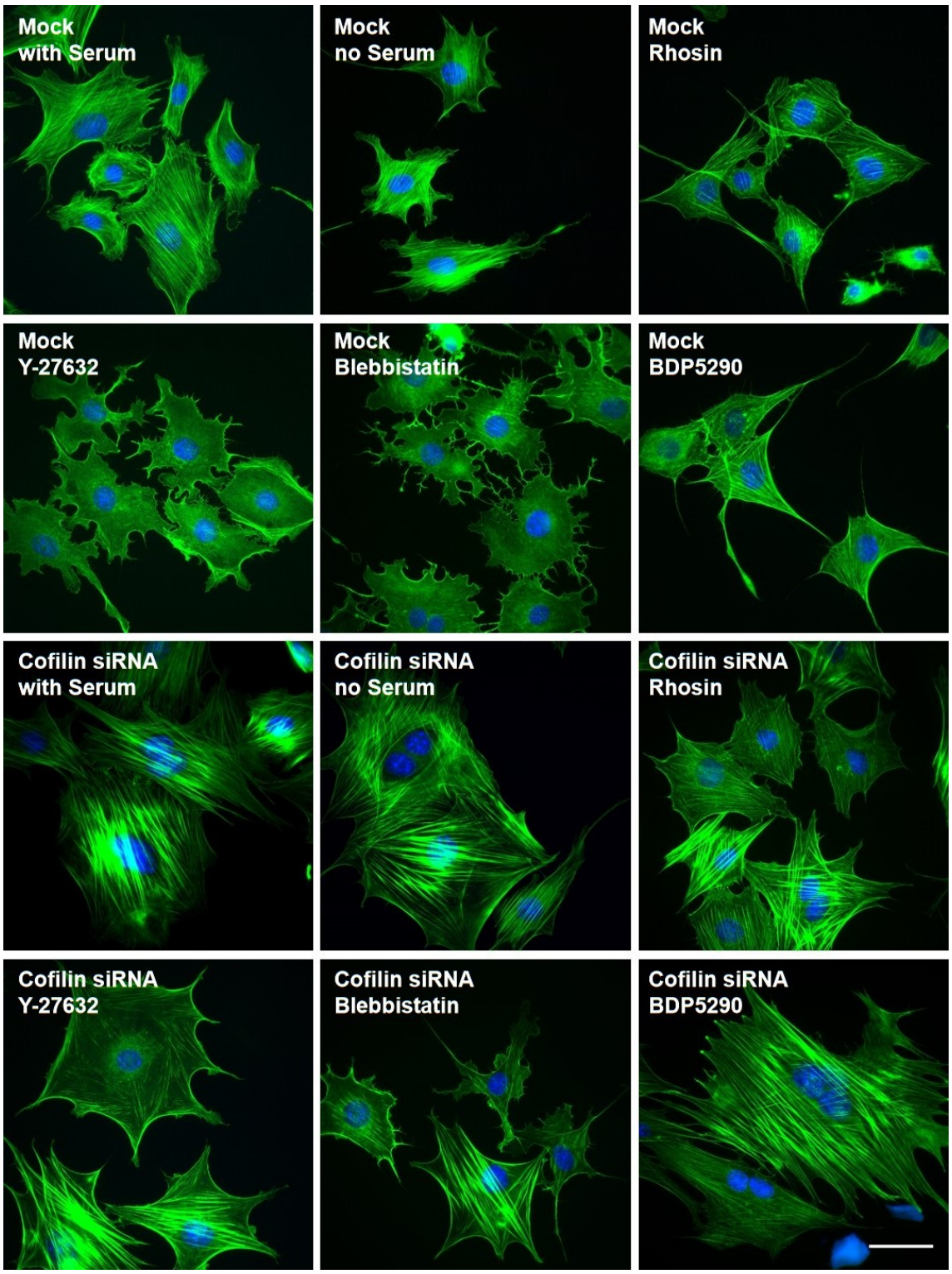

Figure 3.37: Cofilin knockdown in RhoA KOs. RhoA KO cells were seeded into 24 well plates and transfected with 2.5 µM of Cofilin 1, Cofilin 2 and ADF siRNA the next day. One day later, they were again transfected with 5 µM Cofilin 2 siRNA. Two days after the second transfection, cells were treated with various inhibitors or serum-free medium for 1 hour before fixation. Used inhibitors were 200 µM Rhosin to inhibit Rho proteins, 50 µM Y-27632 to inhibit ROCK, 120 µM Blebbistatin inhibiting myosin II and 20 µM BDP5290 to inhibit MRCK. Finally, cells were fixed and stained with phalloidin (green) and DAPI (blue). Figure shows merged images. Two clones were included in the analysis. Scale bar equals 50 µm.

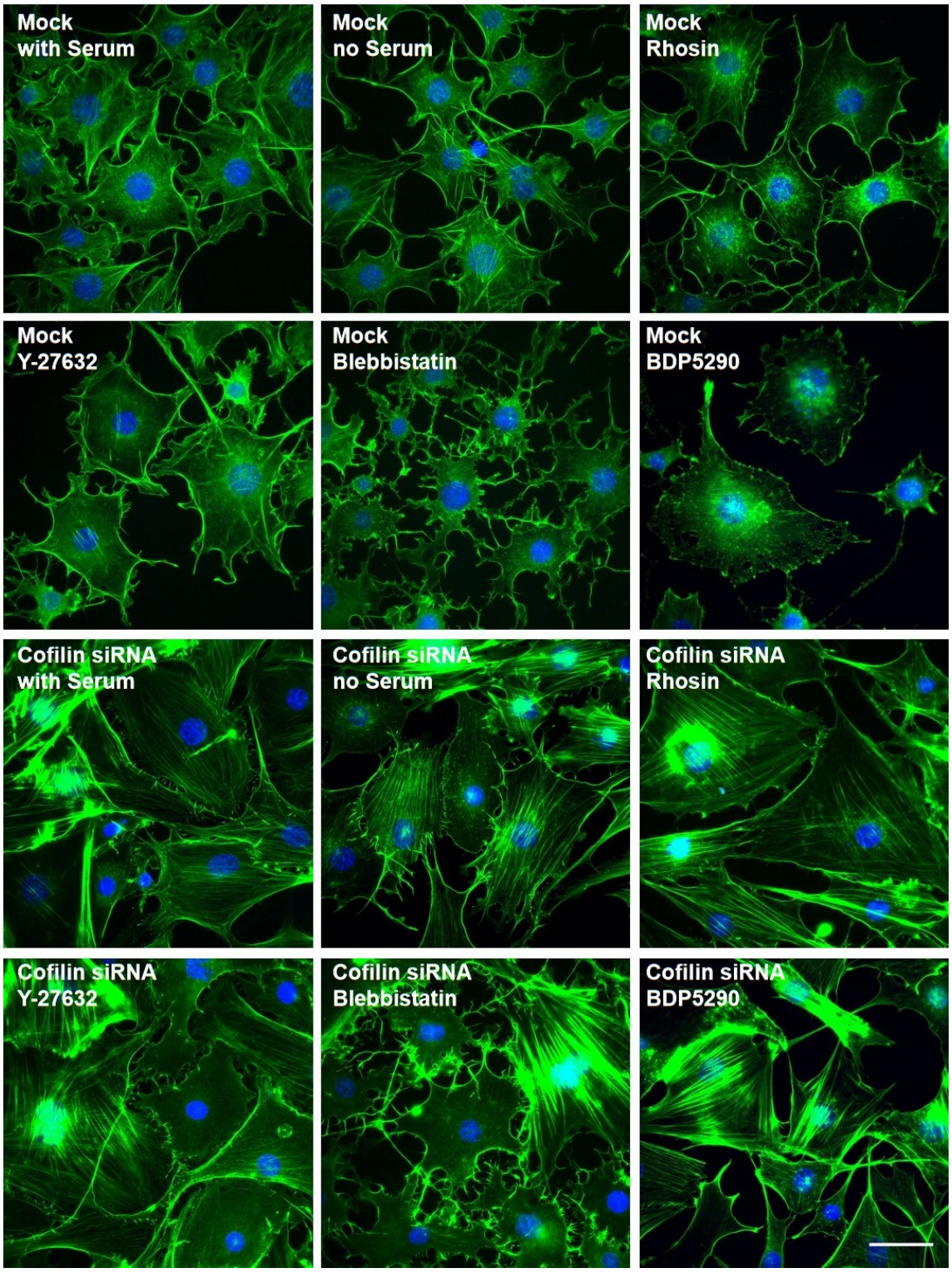

Figure 3.38: Cofilin knockdown in RhoAB KOs. In RhoAB double KO cells, Cofilin 1, Cofilin 2 and ADF were knocked down with 2.5 µM siRNA one day after seeding of cells and again with 5 µM Cofilin 2 siRNA one day after that. Two days later, transfected cells were treated with various inhibitors or serum-free medium for 1 hour before fixation. Inhibitors were 200 µM Rhosin to inhibit Rho proteins, 50 µM Y-27632 inhibiting ROCK, 120 µM Blebbistatin to inhibit myosin II and 20 µM BDP5290 inhibiting MRCK. After inhibitor treatment, cells were fixed and stained with phalloidin (green) and DAPI (blue). Only merged images are shown. Two KO clones were analyzed. Scale bar displays 50 µm.

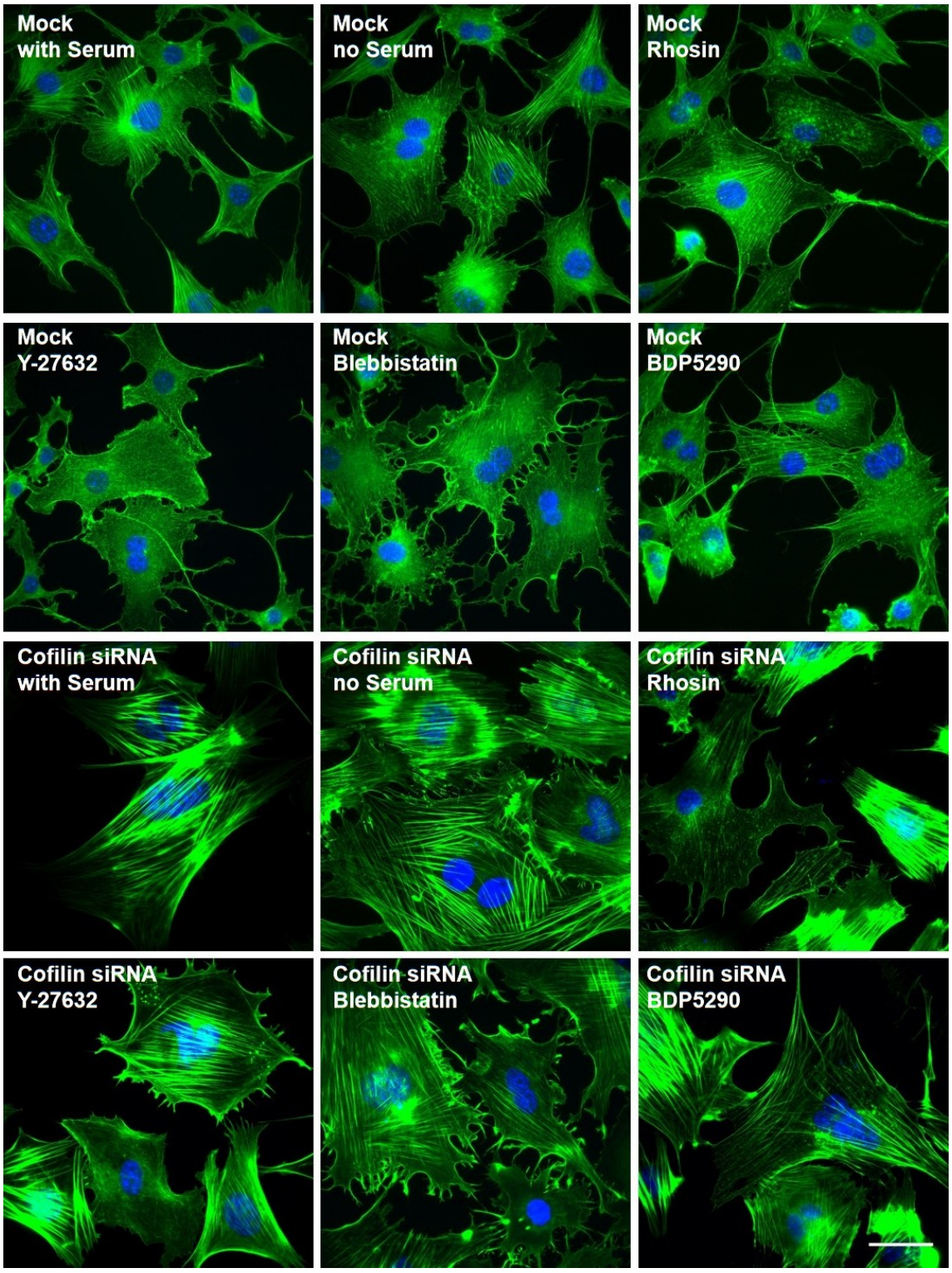

Figure 3.39: Cofilin knockdown in RhoAC KOs. RhoAC double KO cells were treated with 2.5 µM of Cofilin 1, Cofilin 2 and ADF siRNA one day after seeding of cells and again with 5 µM Cofilin 2 siRNA one day later. Two days after the second transfection, cells were treated with various inhibitors or serum-free medium for 1 hour before fixation. Inhibitors were 200 µM Rhosin to inhibit Rho proteins, 50 µM Y-27632 inhibiting ROCK, 120 µM Blebbistatin to inhibit myosin II and 20 µM BDP5290 inhibiting MRCK. Afterwards, cells were fixed and stained with phalloidin (green) and DAPI (blue). Figure displays merged images. Both RhoAC KO clones were analyzed. Scale bar shows 50 µm.

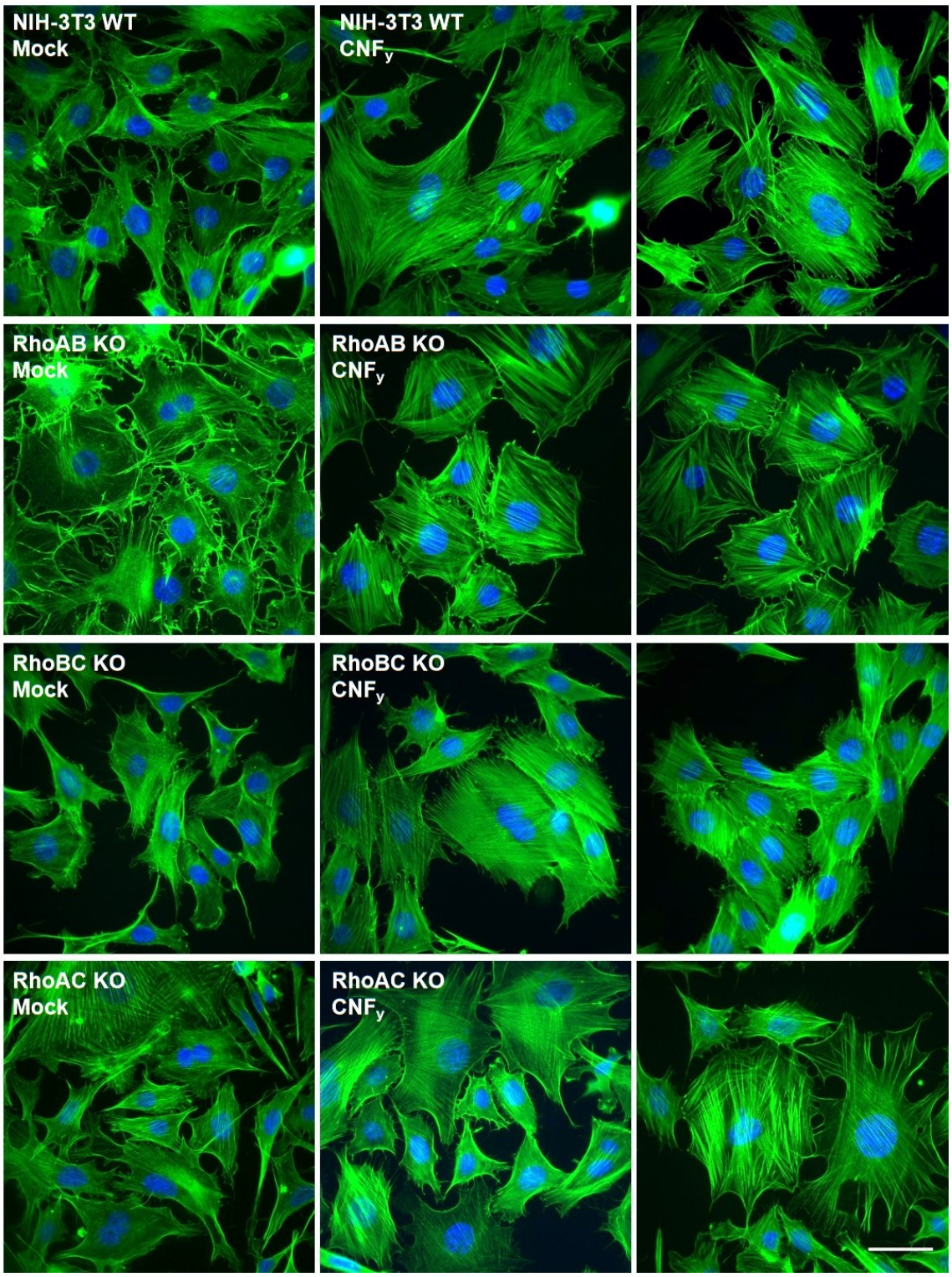

Figure 3.40: Stress fiber induction with CNF_y. NIH-3T3 and Rho double KO cells were treated with 150 nm CNF_y for 4 hours. Subsequently, they were fixed and stained with phalloidin (green) and DAPI (blue). Only merged images are shown, of which two examples are displayed for CNF_y treated cells. All double KO clones were analyzed once. Scale bar represents 50 µm.

3.4 Bacterial and viral infections in RhoA-, RhoB-, and RhoC-KO cells

3.4.1 Invasion of *Salmonella enterica* serovar Typhimurium in Rho KO cells

Complementary to small molecule inhibitor experiments (see chapter 3.1), CRISPR-Cas9 mediated Rho KO cells were assessed during *S.* Typhimurium invasion. The generated Rho KO cells were infected with *S.* Typhimurium WT for 30 minutes, followed by a 30 minutes gentamycin treatment to kill extracellular bacteria, so that invaded bacteria could be analyzed specifically.
Results are depicted in Figure 3.41. Besides RhoB single KOs, invasion was decreased in all Rho KO clones. RhoA single KO had the strongest impact and reduced invasion to 40%. Interestingly, RhoBC double KOs, expressing only RhoA, showed the lowest reduction. Bacteria still invaded at a rate of 90% compared to NIH-3T3 WT levels. Invasion in RhoAC KOs showed similar results with rates of 80%. In cells expressing only RhoC, namely RhoAB KOs, but also RhoC single KOs, invasion rates were around 60%. Taken together, a deletion of RhoA had the biggest impact on *S.* Typhimurium invasion, whereas RhoB did not reveal an obvious function during bacterial uptake.

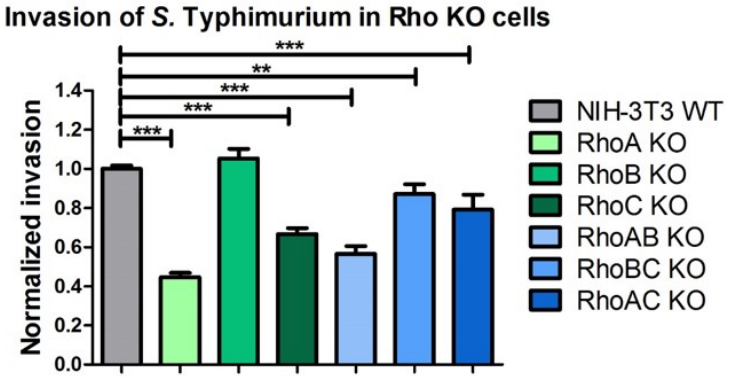

Figure 3.41: Invasion of *S.* Typhimurium WT in Rho KO cells. NIH-3T3 WT and Rho KO cells were infected with *S.* Typhimurium WT for 30 minutes. Gentamycin was used to kill extracellular bacteria for additional 30 minutes. Cells were lyzed with Triton-X 100 and bacteria were diluted and plated on agar LB plates. Bars represent arithmetic means with SEM from pooled clones and at least 3 independent experiments per clone. Data were normalized to NIH-3T3 WT levels. Significances were calculated with unpaired *t*-test ($p < 0.05$).

S. Typhimurium infection induces membrane ruffles for bacterial uptake, which are mediated by Rac activation [124]. Since Rho KO cells should still be able to form ruffles, this was verified in all single KOs by immunofluorescence. Cells were infected for 30 minutes with *S.* Typhimurium WT and subsequently fixed and stained with DAPI and phalloidin. Formation of membrane ruffles on bacterial infection sites could be observed for all cell lines. Figure 3.42 shows NIH-3T3 WT and RhoA KO. Thereby, the invasion deficiencies described above are not due to diminished membrane ruffling.

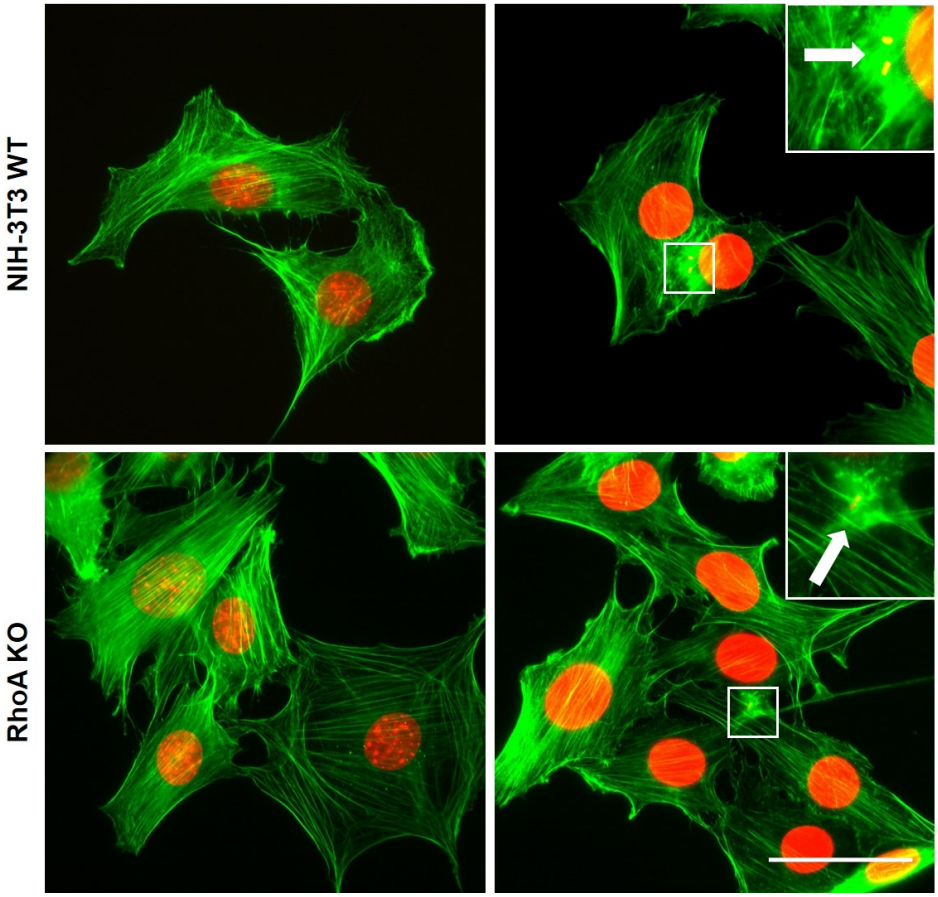

Figure 3.42: *S.* Typhimurium WT induces membrane ruffles in Rho KO cells. NIH-3T3 WT and RhoA KO cells were infected with *S.* Typhimurium WT for 30 minutes. Cells were fixed and stained with phalloidin (green) and DAPI (red). Scale bar represents 50 µm. The same experiment was performed with RhoB and RhoC KOs, but only RhoA is shown here. Experiments were performed twice with all single KO clones. Left panel = uninfected cells. Right panel = cells infected with *S.* Typhimurium WT.

In addition to *S.* Typhimurium WT, mutants lacking virulence factors which were shown to be involved in bacterial invasion were used for infection of Rho single KO clones and NIH-3T3 WT. Cells were accordingly infected for 30 minutes with *S.* Typhimurium ΔSopB, *S.* Typhimurium ΔSopE/SopE2 and *S.* Typhimurium ΔSopB/SopE/SopE2. SopE and SopE2 act as GEFs and activate Rac and/or Cdc42 [124] [129]. SopB is a phosphatase, indirectly regulating the actin cytoskeleton, which was shown to be involved in the Rho associated invasion pathway of *S.* Typhimurium [136]. Extracellular bacteria were killed by gentamycin treatment for additional 30 minutes to specifically analyze invaded bacteria.

Figure 3.43 shows the respective results. Invasion of *S.* Typhimurium WT was used as control and all other data were normalized to its values. *S.* Typhimurium ΔSopB/SopE/SopE2 was used as negative control and showed invasion rates below 5% in all experimental setups. In all cell lines, NIH-3T3 WT as well as all single Rho KO clones, *S.* Typhimurium ΔSopB invaded at rates around 40% but still better than *S.* Typhimurium ΔSopE/SopE2, which showed only around

20% invasion. This suggests that bacteria unable to use the Rho pathway, namely ΔSopB mutants, are less affected by Rho KOs than bacteria depending mostly on the Rho pathway, namely bacteria expressing only SopB and not SopE and SopE2.

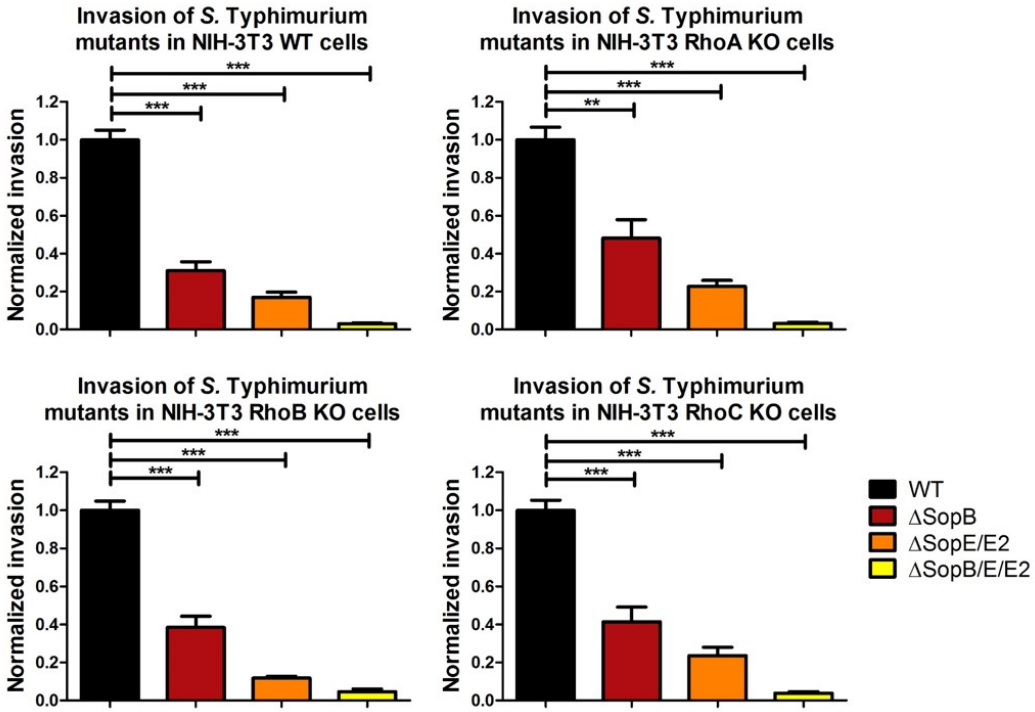

Figure 3.43: Invasion of *S.* Typhimurium mutants in Rho KO cells. NIH-3T3 WT and single Rho KO cells were infected with *S.* Typhimurium WT and mutants lacking effectors involved in bacterial uptake, namely SopB, SopE and/or SopE2, for 30 minutes. Gentamycin was used to get rid of extracellular bacteria for additional 30 minutes. Cells were lyzed with Triton-X 100 and bacteria were diluted and plated on LB agar plates. Graphs show pooled results from at least three independent experiments each and display arithmetic means with SEM. Data were normalized to *S.* Typhimurium WT levels. Significances were calculated with unpaired *t*-test ($p < 0.05$).

RhoB KO did not lead to decreased invasion of *S.* Typhimurium WT as seen in Figure 3.41. Since RhoB, in contrast to RhoA and RhoC, is involved in endosomal trafficking [61], an experiment was set up to analyze RhoB levels during later stages of infection, when the bacteria replicate in the SCV. Therefore, NIH-3T3 WT cells were infected with *S.* Typhimurium WT or *S.* Typhimurium ΔSopB, since SopB was shown to be involved in Rho activation at least during earlier time points [136], and SDS samples were taken briefly before infection and then every hour for up to 6 hours. Samples were analyzed via Western Blotting with RhoA, RhoB and RhoC antibodies. Figure 3.44 shows strong upregulation of RhoB upon infection with WT bacteria. This was depending on SopB, since the respective mutant did not lead to an increase in RhoB levels. RhoA and RhoC levels only showed a moderate increase over 6 hours compared to RhoB levels. These data indeed suggest a specific role for RhoB during intracellular survival of bacteria instead of the invasion process.

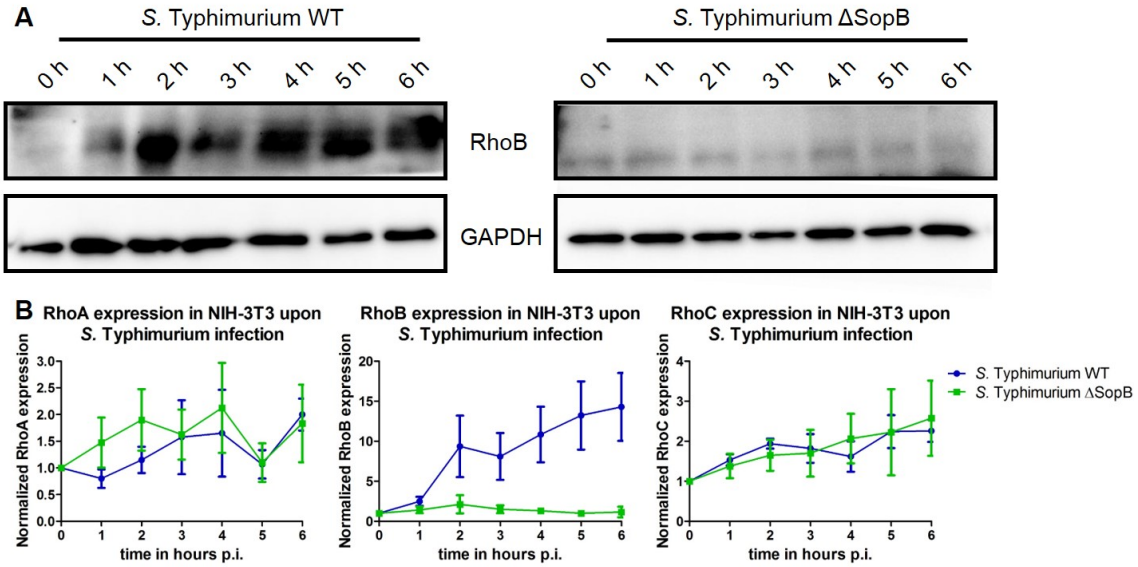

Figure 3.44: Infection with *S.* Typhimurium WT increases RhoB protein levels. NIH-3T3 WT cells were infected with *S.* Typhimurium WT or *S.* Typhimurium ΔSopB. Gentamycin was added after 30 minutes. Right before infection and $1-6$ hours after infection, cells were lyzed in 4x SDS sample buffer. (A) Western Blotting was performed using RhoB antibody and GAPDH as loading control. (B) Western Blots were also performed with RhoA and RhoC antibodies. Quantifications from at least four independent experiments were pooled and are depicted in the graphs. The basal level before infection was set as 1 and all other data were normalized to this control.

To analyze if the increase of RhoB during *S.* Typhimurium WT infection is regulated at the RNA or the protein level, RNA was isolated during infection and qPCR was performed with primers for RhoB by Silvia Prettin (HZI, Braunschweig). Figure 3.45 shows that indeed RhoB mRNA levels increased strongly right after bacterial invasion and then stayed at a two-fold increased level over at least 5 hours. Upregulated RhoB levels were therefore at least partially due to increased mRNA expression.

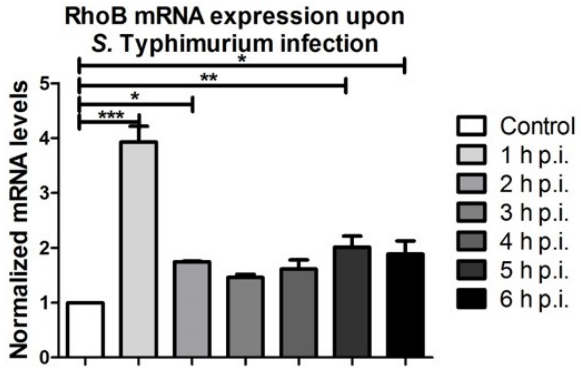

Figure 3.45: RhoB mRNA levels during *S.* Typhimurium WT infection. NIH-3T3 WT cells were infected with *S.* Typhimurium WT and gentamycin was added after 30 minutes. RNA was isolated right before infection and 1-6 hours afterwards. qPCR was performed with RhoB primers by Silvia Prettin (HZI, Braunschweig). Graph displays arithmetic means with SEM from three independent experiments.

It was previously suggested that SopB plays a role in the activation of Akt signaling [181]. Akt signaling influences many cellular processes such as proliferation, cell survival and migration [182]. Since SopB was responsible for the increase of RhoB levels, it was further analyzed if Akt phosphorylation was also changed upon *S.* Typhimurium infection. First, basal Akt levels in Rho KO cells were investigated.
Figure 3.46.A shows that mRNA levels of Akt are only slightly changed in Rho KO cells. Akt1 mRNA levels are decreased in RhoB KOs, whereas they are increased in RhoAB KOs. Akt2 mRNA levels are also decreased in RhoB KOs, whereas an increase was detected in RhoA and RhoAC KOs, both containing high RhoB protein amounts. Akt3 mRNA is only increased in cells expressing only RhoB. These results were obtained via microarray analysis. Akt phosphorylation was analyzed via Western Blotting of Rho KO cell lysates. A slight increase was observed in all Rho KOs, surprisingly with the strongest difference in RhoC KOs, with almost three times more phosphorylated Akt (Figure 3.46.B). Even though mRNA and protein levels showed some differences, a tendency towards increased Akt activity was observed in Rho KO cells.
As described above, lysates were obtained from NIH-3T3 cells infected for 6 hours with *S.* Typhimurium WT and *S.* Typhimurium ΔSopB. Western Blotting with phospho-Akt antibody revealed an increase in phosphorylation 1 hour after infection, which then decreased back to control levels. This effect was visible for both bacterial strains, but the increase was slightly higher when cells were infected with WT bacteria (see Figure 3.46). Akt is thereby probably involved in the initial invasion process but does not seem to be completely dependent on SopB.

Since data from Figure 3.44 point towards a role for RhoB in later stages of *S.* Typhimurium infections, replication of bacteria in RhoB KO cells was analyzed and compared to NIH-3T3 WT cells. For that purpose, cells were infected with *S.* Typhimurium WT and *S.* Typhimurium ΔSopB for 6 hours. Gentamycin was added after 30 minutes to constrain replication of extracellular bacteria. Results are shown in Figure 3.47. Even though bacterial load after 1 hour post infection (p.i.) is unchanged in comparison to NIH-3T3 WT cells (see Figure 3.41), a reduction of 35% can be detected after 6 hours. *S.* Typhimurium ΔSopB levels were below 3% after 6 hours, in NIH-3T3 WT and RhoB KO cells, compared to WT control levels. This suggests not only a role for SopB in the invasion process but also during intracellular replication and survival, whereas RhoB seems to be specifically involved in the latter.

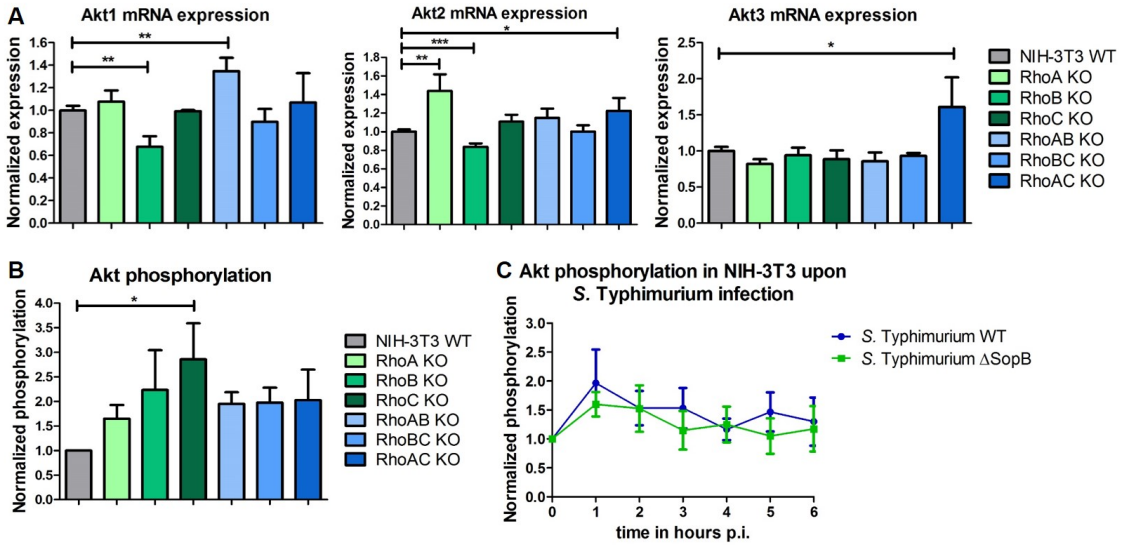

Figure 3.46: Akt phosphorylation in Rho KOs and NIH-3T3 WT upon *S.* Typhimurium infection. (A) mRNA levels of Akt1, Akt2 and Akt3 were measured via microarray analysis and normalized to NIH-3T3 WT levels. Unpaired *t*-test was used to calculate significances ($p < 0.05$). (B) NIH-3T3 WT and Rho KO cells were lyzed and subsequently analyzed via Western Blotting with phospho-Akt antibody and GAPDH as loading control. Graph shows quantifications from four independent experiments. Data were normalized to NIH-3T3 WT levels. Significances were calculated with 1way ANOVA ($p < 0.05$). (C) NIH-3T3 WT cells were infected with *S.* Typhimurium WT or *S.* Typhimurium ΔSopB. Right before infection and $1 - 6$ hours after infection, cells were lyzed in 4x SDS sample buffer. Lysates were analyzed via Western Blotting with phospho-Akt antibody and GAPDH as loading control. Graphs show data from three independent experiments. All data were normalized to control levels before infection.

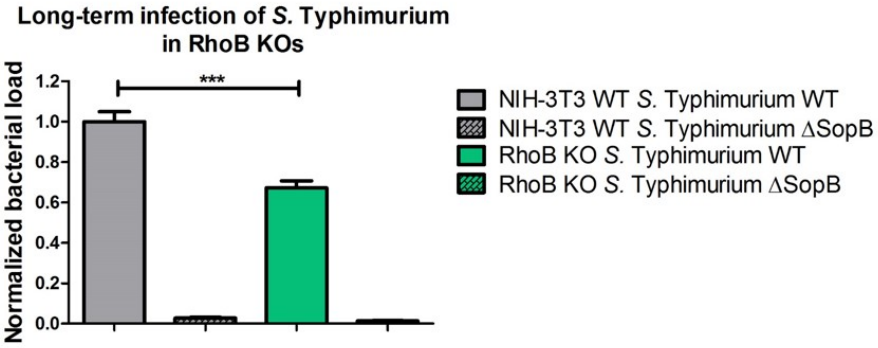

Figure 3.47: Long-term infection with *S.* Typhimurium in RhoB KOs. NIH-3T3 WT and RhoB KO cells were infected with *S.* Typhimurium WT and *S.* Typhimurium ΔSopB. After 30 minutes, gentamycin was added to kill extracellular bacteria. 6 hours p.i. cells were lyzed and bacterial load was analyzed. Graph shows arithmetic means and SEM from four independent experiments for *S.* Typhimurium WT and three experiments for *S.* Typhimurium ΔSopB. Unpaired *t*-test was used for calculation of significances ($p < 0.05$). All data were normalized to WT/control levels.

3.4.2 Invasion of *Shigella flexneri* in Rho KO cells

Following invasion experiments of *S. flexneri* WT in context with Rho inhibition (see chapter 3.1), infection experiments were also performed in Rho KO cells. Cells were infected for 30 minutes, followed by a 30 minutes gentamycin treatment to kill extracellular bacteria and specifically analyze invaded bacteria. As shown in Figure 3.48, all combinations of Rho KO led to significantly reduced bacterial invasion. Deletion of RhoA alone and in combination with RhoB decreased invasion to 20%. The weakest effects on invasion rates were observed in RhoB and RhoBC KO cells, where 70% invasion, compared to NIH-3T3 WT levels, were achieved. 60% invasion were observed for RhoC KOs and 50% for RhoAC double KOs. Of the three Rho proteins, RhoA seems to affect invasion of *S. flexneri* the strongest, compared to RhoB and RhoC.

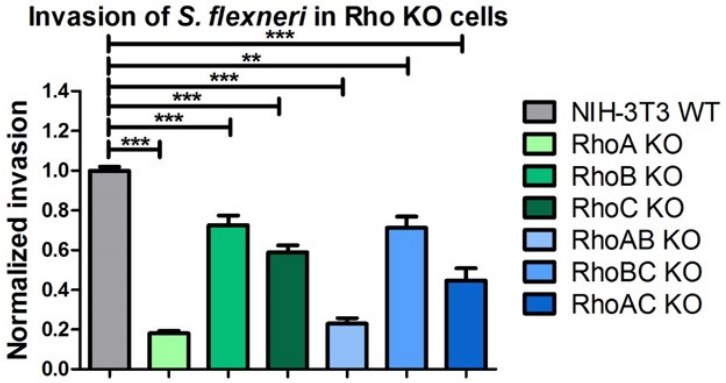

Figure 3.48: Invasion of *S. flexneri* in Rho KO cells. NIH-3T3 WT and Rho KO cells were infected with *S. flexneri* WT for 30 minutes. Gentamycin was used to get rid of extracellular bacteria for additional 30 minutes. Cells were lyzed with Triton-X 100 and bacteria were diluted and plated on TSB agar plates. Data show pooled arithmetic means and SEM from at least three independent experiments per clone. All results were normalized to NIH-3T3 WT levels. Unpaired *t*-test was used to calculate significances ($p < 0.05$).

Subsequently it was analyzed, if actin tail formation, induced by the virulence factor IcsA [143], as well as membrane ruffling, mediated by Rac signaling [146], were still observed upon *S. flexneri* WT infection in the absence of Rho. Therefore, NIH-3T3 WT and Rho single KO cells were infected with WT bacteria for 30 minutes and subsequently fixed and stained with DAPI and phalloidin. Ruffling and actin tails could be observed in all cell lines. NIH-3T3 WT and RhoA KO are shown in Figure 3.49. This confirmed that the reduction of bacterial invasion upon Rho KO is independent of Rac-induced membrane ruffling and intercellular spread is probably also not affected, since the role of Rho proteins in *S. flexneri* infection is specifically involved in the uptake process.

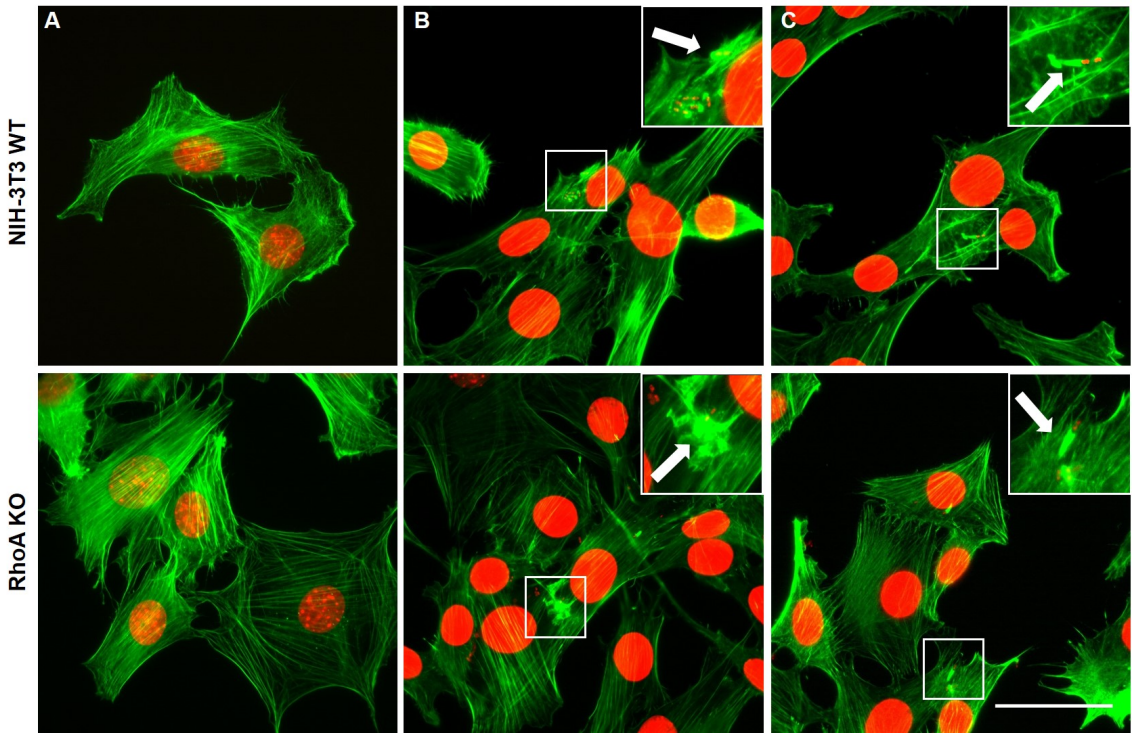

Figure 3.49: *S. flexneri* induces actin tails and membrane ruffles also in Rho KO cells. NIH-3T3 WT and RhoA KO cells were infected with *S. flexneri* WT for 30 minutes. Cells were fixed and stained with phalloidin (green) and DAPI (red). This was performed twice with all single KO clones, whereas only RhoA KO is shown as an example. (A) Uninfected cells. (B) Infection with *S. flexneri* WT inducing membrane ruffles. (C) Actin tails generated by *S. flexneri* WT. Scale bar represents 50 µm.

3.4.3 RSV infection in Rho KO cells

Implications of Rho GTPases and the actin cytoskeleton in the infection process of respiratory syncytial virus (RSV) have been described previously [160] [161]. While RhoA was shown to be involved in syncytium formation and cell fusion, the roles of RhoB and RhoC were neglected in this study [160]. Due to RhoBs involvement in endosomal trafficking [61], which could be important for the transport of viral components in the cell, and the already mentioned role of RhoA for RSV, RhoAB double KO clones were analyzed by Svenja Wiechert in the group of Prof. Dr. Thomas Pietschmann (Twincore, Hannover) in the context of RSV infections. The cells were infected with mCherry-tagged virus and the potential increase of mCherry-labeled cells was analyzed 18, 24, 48 and 72 hours p.i. via FACS analysis. The viral strain used for these experiments was HRSV subgroup A, strain Long [183]. The results of these experiments are displayed in Figure 3.50. The data clearly show that following infection, the amount of RSV-infected cells increases in NIH-3T3 WT cells, whereas it stagnates in RhoAB double KOs.

Since RhoA was shown to be involved in cell fusions mediated by RSV [159], while RhoB and RhoC were not analyzed, all Rho KO cells, as well as NIH-3T3 WT, were transfected with the viral fusion protein RSV-F for 24 hours. Immunofluorescence stainings of the cells are depicted in Figure 3.51. Several phe-

notypical changes could be observed upon RSV-F transfection. Virus filaments budding from the cells were detectable, as well as cell fusions, noticeable by multiple nuclei per cell. In addition, some transfected cells revealed RSV-F accumulations in the perinuclear area. Most of these structural changes appeared in all cell lines tested, while particularly cell fusions were hardly detectable in RhoA and RhoAB KO cells and less frequent in RhoAC KO cells. Also, the accumulations in the perinuclear area seemed to appear more often in RhoA, RhoB and RhoAB KOs. Due to time constraints, data were not quantified. However, these experiments support the proposed role for RhoA in RSV-F induced cell fusions and suggest a role for RhoB in intracellular transport of the RSV-F protein.

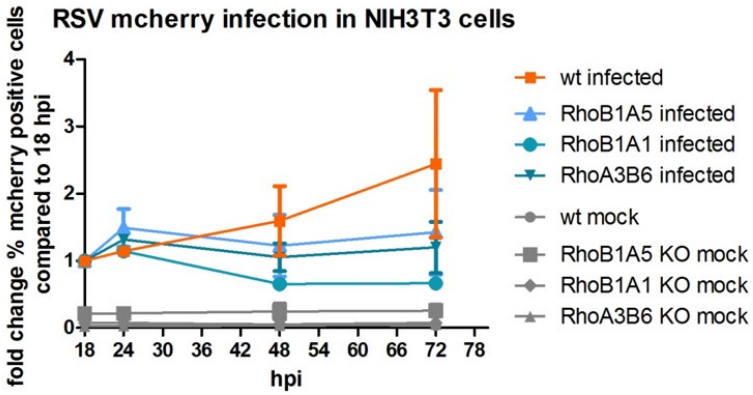

Figure 3.50: RSV spreading in RhoAB KO cells. NIH-3T3 WT and RhoAB double KO cells were infected with mCherry-tagged RSV and the percentage of mCherry-positive cells was measured after 18, 24, 48 and 72 hours via FACS analysis. These experiments were performed by Svenja Wiechert in the group of Prof. Dr. Thomas Pietschmann at the Twincore in Hannover.

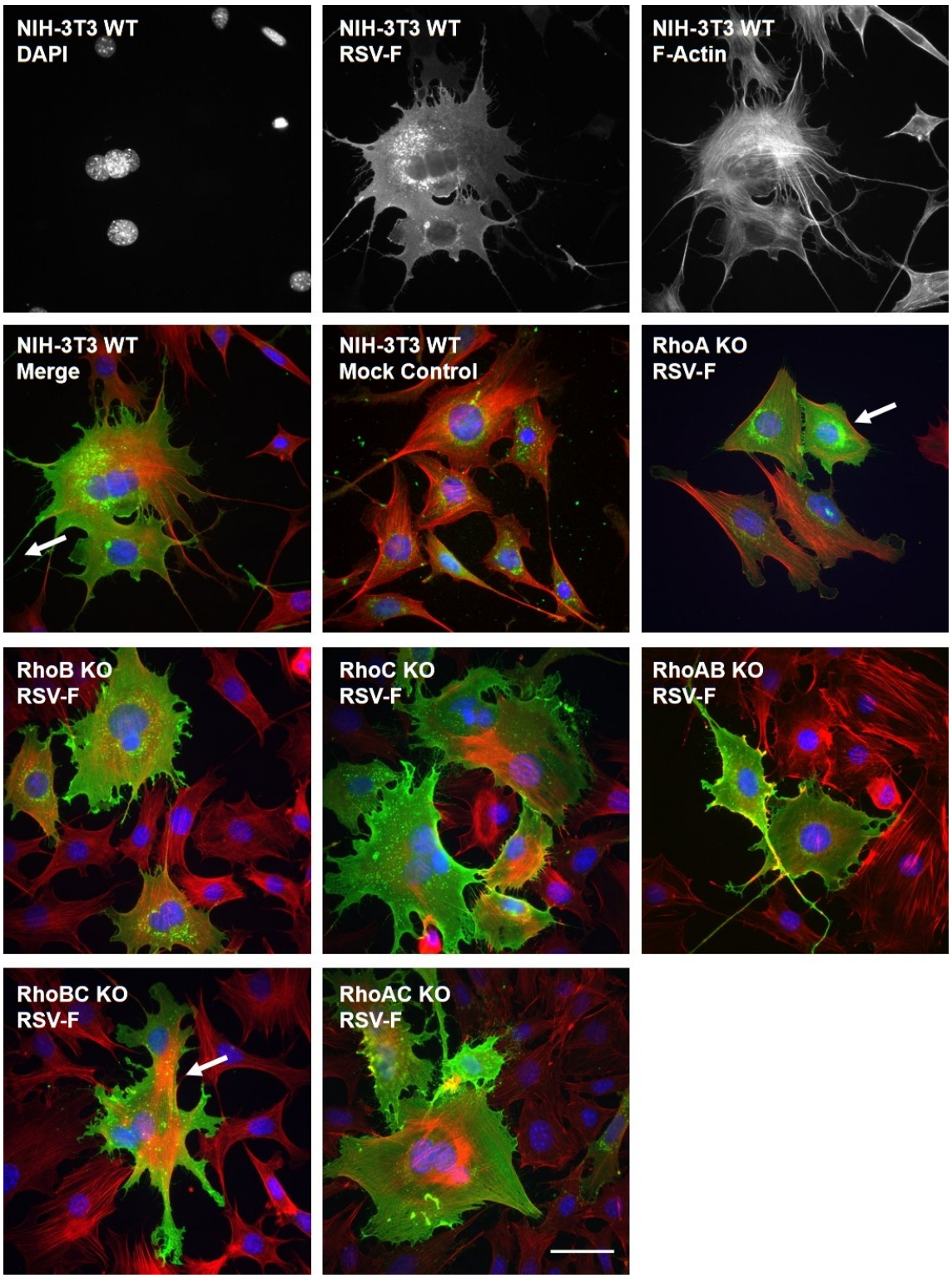

Figure 3.51: RSV-F induces cell fusion dependent on RhoA. NIH-3T3 WT and Rho KO cells were transfected with RSV-F or the respective control plasmid for 24 hours. Cells were fixed, permeabilized and stained with RSV-F antibody (green), phalloidin (red) and DAPI (blue). Single and merged channels are shown for NIH-3T3 WT transfected with RSV-F, whereas only the merged images are depicted for Rho KOs and the mock control. White arrows label virus filaments (NIH-3T3 WT), perinuclear accumulations (RhoA KO) and cell fusions (RhoBC KO). The experiment was performed with two clones per KO. The scale bar represents 50 µm.

4 Discussion and Outlook

4.1 CRISPR/Cas9 mediated KO of RhoA, RhoB and RhoC

To dissect the roles of the three Rho proteins during various processes, this study was set out to generate KO cell lines for RhoA, RhoB and RhoC. As described in chapter 3.2, CRISPR/Cas9 mediated KO of Rho proteins yielding single KO cell lines was successfully done. Generation of double KO clones revealed the first difficulties, which turned out to be even more dramatic when KO of all three proteins was assessed. Most of the isolated single cells did not proliferate to establish stable cell lines. It was very ineffective to generate double KO cells when RhoA was the protein that was deleted first, with clone A3B6 being the only positive cell line derived. The same phenomenon as with potential triple KOs appeared: sorted KO cells only divided a few more times and subsequently died.
The role of RhoA in cell division has been analyzed previously and is thought to be essential for successful cytokinesis [184]. RhoB and RhoC can, as proven by the generation of dividing KO cell lines, substitute for RhoA in this process, yet at least one of the three is obviously essential for the division process since Rho triple KO cells did not proliferate. Also cells lacking RhoA proliferate slower in cell culture, which shows that the compensation via RhoB or RhoC is less efficient than RhoA. Sorted triple KO clones probably still contained low numbers of remaining Rho proteins and could therefore divide a few times but then failed to do so as soon as the previously expressed protein was degraded and no new protein was expressed. Considering the difficulties of double KO generation upon initial RhoA depletion, a reason could be that RhoA KO changed the regulation in the cells in a way that they were strongly depending on RhoB and RhoC to compensate. Additional deletion of one of the compensating factors was then not tolerable anymore. Initial deletion of RhoB or RhoC therefore probably had less dramatic effects on regulation in the fibroblasts. Microarray analysis (discussed in chapter 4.2.2) confirmed that gene regulation was indeed only mildly affected upon RhoC KO (see Figure 3.10). Interestingly, RhoA as well as RhoB KO both induced strong changes. It still remains to be elucidated which genes are specifically involved in the compensation of a RhoA KO and are essential for the described phenomenon. So far there are no studies on the functionality of RhoB or RhoC during cytokinesis.
In contrast, Königs *et al.* analyzed cells lacking all three Rho proteins [185]. This study was done with macrophages, in which RhoA and RhoB were deleted, while RhoC was not expressed in this cell type. Macrophages, in contrast to the immortalized fibroblast cell lines used in this study, are post-mitotic and therefore do not divide anymore. During differentiation of precurser cells to terminally differentiated macrophages, the growth factor that stimulates prolif-

eration is specifically degraded [186]. This explains why the problem occurring during triple KO generation in fibroblasts does not apply to the situation in macrophages. A study by Melendez *et al.* investigated primary mouse embryonic fibroblasts in which RhoA was depleted using Cre-Lox recombination. In this case, RhoA KO cells stopped proliferation after 24 hours, even though RhoB and RhoC were expressed and upregulated, which led the authors to the conclusion that RhoA is absolutely essential for cell division [187]. It is well known that survival and proliferation of primary cells are extremely sensitive to culture medium components and incubation conditions [188]. Since transformed cell lines such as NIH-3T3 cells are more robust in this context than primary cells, this would explain why NIH-3T3 cells can proliferate without RhoA. The conclusion could be that RhoB and RhoC have the potential to partially compensate for RhoA during cell division, but only under specific growth conditions. Therefore this study offers, in contrast to many others, the chance to analyze cells in the absence of RhoA continuously and furthermore provides cell lines expressing only one of the three Rho proteins. On the other hand, these data reveal a significant difference between *in vitro* studies and the usage of primary cells, thereby suggesting that RhoA might indeed be essential for cell division *in vivo*. Knockout mice for RhoB or RhoC exist and are viable [189] [190], whereas knockout mice for RhoA only exist with the deletion being restricted to a certain cell type, for instance keranocytes [191], which confirms the essential role for RhoA.
Alternative mechanisms to analyze cells in the absence of all Rho proteins are knockdown of the third one or over-expression of Citron kinase, which is hypothesized to regulate RhoA during cytokinesis [106]. This might however, at least in the latter case, lead to unknown side effects and render potential results not very reliable. Knockdown of the third protein would only reduce protein levels but could not abolish them completely, since one Rho protein seems to be essential for cellular survival. Therefore, the results would only give vague tendencies.

4.2 Cellular characteristics of Rho KO cells

Rho KO cells revealed a strong upregulation of the respective other Rho proteins, except for RhoC in RhoA and RhoB single KOs, see Figure 3.13. Even though the details concerning Rho protein levels and their connection with regulation via GDIs will be discussed in detail later in chapter 4.2.2, this information needs to be kept in mind and will be referred to in the following discussions.

4.2.1 Morphology of Rho KO cells

Initial experiments were set out to measure volume and area of Rho KO cells. Cellular volume was decreased in RhoB KO cells and increased in RhoAC double KOs, expressing only RhoB (see Figure 3.6.A). The cellular area was only increased in RhoA, RhoAB and RhoBC KO cells (see Figure 3.6.B). It can thereby

be concluded that RhoB KO cells are flat, whereas cells expressing only RhoB are thicker compared to WT cells. In both cases, the size of the cellular area was unchanged. RhoA, RhoAB and RhoBC KO cells are larger without an increase in volume, which also leads to a flat phenotype. Cellular volume and spread are connected with adhesion to the substrate and actomyosin contractility [192]. RhoAC KO cells, expressing only RhoB, are therefore probably not able to induce strong contractility, which is why their volume increases. Cells expressing either only RhoC or only RhoA, which get larger without an increase in volume, thereby flatten out and show low contractility. If on the other hand RhoA and RhoC are both expressed (in RhoB KOs), contractility in the cell seems to be increased, since the cells get thinner without changing the size of their surface area. A possible conclusion from these data would be that RhoA, in contrast to RhoB, induces contractility, but much more efficient in the presence of RhoC.

The area of nuclei was slightly decreased in RhoA KO cells and increased in RhoBC KOs (see Figure 3.7.A). In the case of the latter, this is in line with the enlarged cellular area. RhoA KO cells are larger with smaller nuclei, which could be explained by an increased number of nuclei per cell, see Figure 3.7.B. Counting of nuclei per cell revealed a strong correlation between RhoA, cell division and multinucleated cells (see Figure 3.7.B). Cells with three or more nuclei were only observed in the absence of RhoA, in single as well as double KOs. These are the same cell lines which were observed to grow slower in cell culture. As described in chapter 4.1, RhoA is known to play an important role during cell division [184]. Non-functional cytokinesis can be a reason for multinucleation of cells [193]. RhoA has been shown to be involved in the abscission process during cytokinesis [106], which explains the present data, even though the mechanism of cytokinesis in the absence of RhoA and presence of RhoB and/or RhoC still remains to be understood.

During FACS analysis of Rho KO cells, not only cellular volume was analyzed but also granularity. This dataset revealed strong differences in the absence of Rho proteins (see Figure 3.8.A). In RhoB KO cells, the percentage of cells categorized as granular was decreased, whereas around ten times more granular cells were found in the RhoAB and RhoAC populations. Increased granularity can point towards processes such as senescence, apoptosis or autophagy [194]. The two double KO cell types showing increased granularity also contained many cells which were extremely large and had multiple nuclei, which was frequently observed during various immunofluorescence analyses. These could be signs of senescence and growth arrest [195]. Senescence can be induced by high activities of tumor suppressors, which is also the reason why cancer cells proliferate efficiently in the absence of these proteins [196]. Both double KO cell lines grew slower than WT cells in cell culture and for instance in RhoAC double KOs, RhoB as the only Rho protein was strongly upregulated and was shown to be a tumor suppressor [197]. This would also explain decreased granularity in RhoB KO cells. In addition, data of this study point towards important roles for RhoA and RhoB during cellular processes, whereas the role of RhoC might

only be indirect, maybe through stimulation of RhoA. Concluding, RhoAB KO cells, depending completely on RhoC, have an increased probability of promoting apoptosis, thereby potentially justifying the high granularity levels.

Due to RhoBs involvement in endosomal trafficking and a connection between granularity and RhoB, the Golgi apparatus was analyzed in relation to Rho protein levels (see Figure 3.8.B). Golgi structures of cells stained via immunofluorescence were categorized as compact or dispersed. Both phenotypes were observed in all cell lines. Nevertheless, a clear connection between RhoB levels and Golgi structure was confirmed, see Figure 3.8. When RhoA levels were increased in the absence of RhoB and the presence of RhoC, the Golgi was more often compact (RhoB KOs). In RhoBC double KO cells, with high RhoA levels in the absence of RhoC, the structure was similar to WT levels. If either only RhoC was present (RhoAB KOs) or RhoA and RhoB at high levels (RhoC KO) a tendency towards more dispersed Golgi structures could be observed. This effect became more evident in the absence of RhoA and had the biggest impact if only RhoB was expressed (RhoAC KOs). Concluding, RhoB induces a dispersed Golgi, whereas RhoA promotes compact Golgi structures. RhoA activity seems to be supported by the presence of RhoC, which was not the case for RhoB. Also RhoA and RhoB obviously displayed antagonistic activities. A previous study investigated Golgi dynamics depending on RhoA [198]. The nomenclature of phenotypes differed from this study, since their specification of dispersed meant that the Golgi had many small fragments, which were thereby closer together and resembled the phenotype named compact in this study. This was induced via mDia1 downstream of RhoA and is thereby in line with the experimental data from this project. Still, the exact roles for RhoA and RhoB concerning Golgi structure and the downstream effectors involved in this mechanics need further investigations.

Since RhoB was shown to be specifically involved in granularity and Golgi structure, analysis of RhoB effectors potentially involved in these processes pointed towards Rhophilin 2. This protein was found to bind RhoB [199] and to be recruited to late endosomes connected with RhoB activity [172]. Microarray analysis of Rhophilin 2 mRNA showed a significant upregulation upon increased RhoB levels in the absence of RhoA (see Figure 3.11). RhoC KOs, expressing high levels of RhoA as well as RhoB, revealed no difference in Rhophilin 2 mRNA regulation. In contrast, another study proposed binding of Rhophilin 2 to RhoA [200]. Nevertheless, in line with the results from Steuve *et al.* [172], the mRNA levels upon Rho KO point towards a connection with RhoB activity, which needs further analysis on protein level in the future.

Due to the well known involvement of Rho GTPases and the actin cytoskeleton in cell migration, random migration analysis of Rho KO cells was performed, see Figure 3.9.A. Velocity of all Rho KO cells was decreased, with the strongest impact induced by RhoA single KO and only a mild decrease for RhoBC and RhoAC KOs. Specific effectors and tasks have been proposed for the three pro-

teins during migration [201]. RhoA acts through both ROCK proteins inducing retraction of the cell rear. RhoC is especially needed for invasion of cancer cells, whereas RhoB mediates adhesion to the ECM via regulation of integrins and focal adhesions. The strong defect in migration of RhoA KO cells could therefore be due to inefficient retraction of the cell rear and strong adhesion to the current cellular position, since RhoB is strongly upregulated in these cells. The second slowest of single and double Rho KO cell lines tested here were RhoAB KOs, which expressed only RhoC and were therefore potentially ineffective in integrin mediated adhesion and retraction of the rear. Surprisingly, cells expressing only RhoA or only RhoB, as well as RhoB KOs expressing RhoC and high RhoA levels, migrated almost as fast as WT cells. As shown for instance in cancer cells, in which RhoA is upregulated and RhoB levels are decreased, the two proteins seem to be regulated antagonistically [56]. Therefore it is possible that their specific functionality during cell migration is more efficient if the other one is absent, whereas the presence of RhoC seems to increase efficiency for RhoA but not RhoB.
Directionality was impaired in all cells except for RhoB KOs, expressing high RhoA and normal RhoC levels (see Figure 3.9.A). It was shown that contractility and integrin signaling affect directionality in an additive fashion [202]. Integrin signaling was expected to be impaired in the absence of RhoB [203], but upregulated RhoA activity and thereby increased contractility might compensate the effect.
As discussed above, deletion of RhoA had the strongest impact on velocity during migration. Incubation of WT and RhoA KO cells in viscous medium, which was performed to get an idea if cells lacking RhoA show a defect in force generation, decreased migration speed even stronger. The impact of increasing viscosity was much more significant in the absence of RhoA than in the WT situation (see Figure 3.9.B). Migration of epithelial cells on a viscous substrate has been linked to vinculin re-localizing away from focal adhesions and actomyosin contractility [204]. Impairment of this process in the absence of RhoA can be hypothesized but the details will have to be elucidated in further experiments. Without RhoA the ability to move against the force of the viscous environment seems to be diminished, which might be correlated with contractility defects.

4.2.2 Interactions and regulation of Rho proteins and GDIs

Microarray analysis of Rho KO cells revealed that RhoA and RhoB, in contrast to RhoC, play important roles in gene regulation by acting antagonistically (see Figure 3.10). Genes which were upregulated in the absence of RhoA, were downregulated in the absence of RhoB. Data from Rho double KOs pointed towards a more important function for RhoA. RhoBC double KOs, in which RhoA is still expressed, showed no dramatic changes compared to WT cells in the heat map. If only RhoB was expressed, changes were observed antagonistically to RhoAB double KOs with only RhoC expression. Taking the results for single and double KOs together, the roles of RhoA and RhoC might correlate since both act antagonistically towards RhoB.

Taking a closer look at the top 50 regulated genes, in particular for the single KO analysis, the list included mainly proteins involved in cell proliferation, adhesion to the ECM and vesicular trafficking. All these processes are known to be regulated via the actin cytoskeleton and Rho GTPases. Examples are ribosomal protein S6 kinase, involved in cell growth and proliferation [205], fibrillin-1, a glycoprotein involved in ECM adhesion [206] and sorting nexin 6, involved in vesicular trafficking [207].

One important experiment was to determine how RNA and protein levels of the respective other Rho genes were regulated in the KO cell lines to analyze potential compensatory effects. Interestingly, mRNA of the mutated genes was not completely downregulated (see Figure 3.12.A), at least not for RhoB in double KOs. A cellular mechanism, known as nonsense mediated decay, degrades mRNA when premature stop codons are present, which was the case in the Rho KO cell lines. This is hypothesized not to work properly if the gene contains no introns [208], as found in the *rhoB* gene. This is probably the reason why RhoA and RhoC mRNAs were decreased upon the respective KO, while RhoB mRNA was not as dramatically. On the other hand, upregulation was only observed for RhoB in RhoA and RhoAC KOs and for RhoC in RhoAB KOs, not for RhoA. As reviewed by Nomikou *et al.*, many proteins as well as micro-RNAs regulate gene expression of *rhoA*, *rhoB* and *rhoC* and the possible combinations and implications are too complex to draw clear conclusions [209]. In addition to regulation of gene expression by micro-RNAs and other proteins, it was also found that high RhoA protein levels suppress transcription of the *rhoB* gene, pointing towards close interactions of the *rho* genes and their respective proteins themselves [210]. One micro-RNA was found to be strongly downregulated in all Rho KO cells, which was miR-377 (see Figure 3.11). Interestingly, from what is known so far, miR-377 is involved in the regulation of Rac, not Rho proteins. miR-377 inhibits T-cell lymphoma invasion and metastasis inducing protein (TIAM)1, a GEF for Rac. The micro-RNA was classified as a tumor suppressor, inhibiting cell proliferation [171] [211]. Downregulation of miR-377 in the absence of one or two Rho proteins could thereby potentially increase Rac activity.
In addition, directly comparing microarray readouts revealed that much more mRNA encoding for RhoC is present than for RhoA or RhoB (see Figure 3.12.B). It would be important to know if this also correlates with protein levels, which is why mass spectrometry should be performed to quantify and compare the absolute protein amounts of RhoA, RhoB and RhoC.

What did correlate with RNA regulation was the increase of Rho protein levels, in particular in double KOs with only one Rho protein left. Furthermore, RhoA and RhoB were also upregulated in respective single KOs (see Figure 3.13.B). Upregulation of RhoB upon silencing of RhoA and/or RhoC has been described previously. It was shown that half-life of RhoB was increased under these conditions and that this was somehow mediated by GDP-RhoA and the presence of GDIα [212]. Increase of RhoA levels upon RhoB KO were also observed in macrophages [185], whereas a mild upregulation of RhoC in RhoA KO cells was

found in primary fibroblasts [187]. These compensatory effects have been observed quite often, yet the mechanisms behind them need further clarification, particularly in connection with GDIs. Also, RhoA was upregulated upon RhoC overexpression and vice versa, which points towards a positive correlation between the two proteins (see Figure 3.18.C).
Activity of Rho proteins was analyzed with G-LISA kits, which were supposed to only recognize RhoA. This was disproved by the usage of cell lines lacking RhoA, which led to signals close to WT levels (see Figure 3.14). However, it is not known if the affinities to the three GTPases are comparable, so that the experiments only provide a tendency. This tendency shows increased activity in cell lines expressing high RhoA levels in the absence of RhoB, namely RhoB and RhoBC KOs. The experiments showed higher signals for RhoBC KOs, in which RhoA is the only Rho protein. Other results from this study suggest higher RhoA activities in the presence of RhoC. In this case, the difference could be due to the experimental setup, in which RhoC somehow manipulates the signal outcome of the assay, since its specificity is not as indicated. Rho activity is decreased in RhoC KOs, where RhoA and RhoB are upregulated and potentially inhibit each other.

Upregulation of Rho proteins raises the question of regulation by GDIs, since the excessive amount of protein needs to be protected from degradation. GDIγ mRNA levels were below the detection limit. GDIα was not regulated on mRNA level, whereas GDIβ was downregulated in Rho double KOs (see Figure 3.16.A). In addition it was observed that WT cells contain twice as much GDIα mRNA than GDIβ mRNA (see Figure 3.16.B). Again, it should be addressed how protein levels compare to mRNA levels and also if GDIγ protein is really not expressed. On protein level, GDIα was midly upregulated in RhoBC KOs, which contain high levels of RhoA (see Figure 3.17.A). GDIβ protein levels were upregulated in all Rho KO cells except for RhoA KOs, yet not significantly (see Figure 3.17.B). Since protein levels of GDIβ increased, whereas they were decreased on mRNA level, the regulation behind GDI amounts needs further clarification.
Whatever the case, in order to address which GDI isoforms bound to the respective Rho proteins, GFP-Trap IPs were performed. These showed that RhoA and RhoC both bind to GDIα and GDIβ, whereas RhoB does not bind to any of them, even not in the absence of RhoA and RhoC (see Figure 3.18.A&B). GDIα and GDIβ were previously proposed to bind RhoA and RhoC, whereas RhoB was suggested to bind GDIγ [53]. So far, these results correspond to the data from this study. Since GDIγ mRNA levels were below the detection limit in microarray analysis, this protein was neglected during Western Blot analysis. If GDIγ is really absent in NIH-3T3 fibroblasts, which should be verified, the question arises how RhoB levels are maintained, particularly in those Rho KO cell lines in which the protein is upregulated. In the WT situation, RhoB shows a short half-life and is specifically upregulated when it is needed [58]. Therefore, a stabilizing GDI for RhoB might not be as essential in the WT situation, but the protein levels are so high upon KO of RhoA and/or RhoC, that there has to be a mechanism protecting RhoB from degradation. Ho *et al.* proposed that RhoB

stability depends on GDIα [212], which can be excluded, at least via a direct interaction, due to the GFP-Trap IP data.

To get an overview of the complex interactions and regulations of Rho proteins and GDIs, the group of Prof. Dr. Michael Meyer-Herrmann, specifically Lito Papaxenopoulou, Dr. Gang Zhao and Dr. Haralampos Hatzikirou, analyzed the Western Blot expression data and microarray results to generate a mathematical model of the interactions between Rho proteins and the GDIs. Therefore, a kinetic model was formulated which was subsequently fitted to experimental data and adjusted until an agreement between experimental data and previous assumptions was found. The assumption that RhoC basal protein levels are higher than those for RhoA and RhoB was based on the microarray data and used for the model but needs further proof by mass spectrometry. The outcome is shown in Figure 4.1. The models propose that protection of RhoB from degradation by GDI interactions is quite strong and that the already mentioned antagonism between RhoA and RhoB also showed strong effects (see Figure 4.1.A). In addition, it is hypothesized that RhoB and RhoC influence RhoA activity and degradation by either inhibiting RhoA inactivation and binding of inactive RhoA to the GDI or by supporting RhoA activation and release from GDIs (see Figure 4.1.B). Various data from this study promote a role for RhoC in RhoA activation, but not for RhoB. The antagonism between RhoA and RhoB fits to the conclusions from this study, whereas the strong interaction between RhoB and GDIs, as mentioned above, needs further specification.

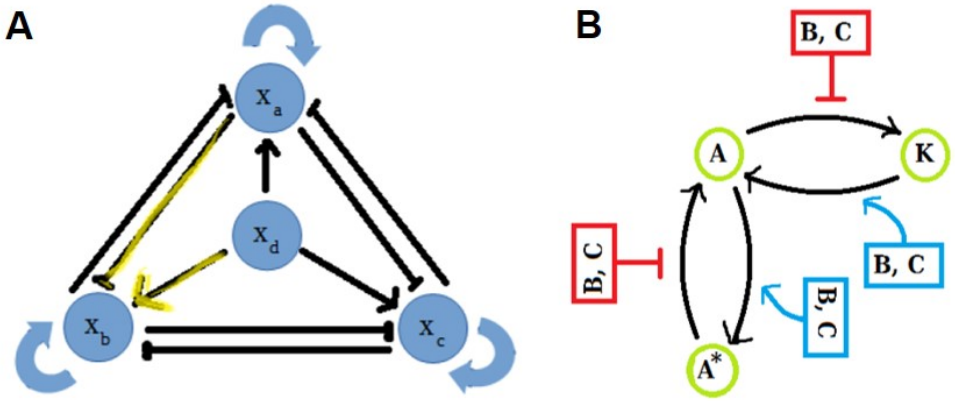

Figure 4.1: Model of Rho and GDI interactions. These models were generated by Lito Papaxenopoulou, Dr. Gang Zhao and Dr. Haralampos Hatzikirou from the group of Prof. Dr. Michael Meyer-Hermann, HZI. (A) Reactions between RhoA, RhoB and RhoC with GDI as buffer. X_a = amount of RhoA, X_b = amount of RhoB, X_c = amount of RhoC, X_d = amount of GDI. Yellow arrows show very strong interactions. Arrows from GDI to the GTPases mean that the Rho protein is protected from degradation by the GDI. (B) Suppressive reactions between the Rho proteins. X_a, described above, is the sum of A (inactive state of RhoA) + A* (active state of RhoA) + K (complex of RhoA with GDI). Red color represents direct suppression, whereas blue arrows indicate indirect suppression. RhoB and RhoC can either directly inhibit inactivation of RhoA or complex formation of inactive RhoA with the GDI. Indirectly, RhoB and RhoC can promote RhoA activation or separation of RhoA from the GDI.

Activity of Rho proteins can also be regulated by other proteins than GDIs, GEFs and GAPs. The PRL family, consisting of the three tyrosine phosphatases PRL1, PRL2 and PRL3 has been implicated in the activation of RhoA. The mechanisms of this process are still under investigation. PRL1 was shown to increase RhoA activity by binding to and thereby inhibiting the p115 Rho GAP [174]. Not much is known about PRL2 so far, but knockdown of its mRNA decreased vinculin expression and also migration and invasion capacities in cancer cells [213]. PRL3 overexpression led to an increase of active RhoA and RhoC which depended on its phosphatase activity [214]. As mentioned earlier, Rho proteins can be phosphorylated and thereby inactivated [68]. A direct interaction between PRL phosphatases and phosphorylated Rho proteins can therefore not be excluded. mRNA levels of the three PRL genes in Rho KOs, extracted from the microarray dataset, revealed an interesting regulation shown in Figure 3.11. PRL1 mRNA levels are increased particularly in RhoB and RhoC KOs, in which RhoA levels are upregulated. PRL2 mRNA is strongly downregulated in RhoAC double KO cells, containing high RhoB protein amounts. PRL3 mRNA levels on the other hand are strongly increased in RhoA and RhoC KOs, where again RhoB is present at high levels. This points towards very specific functions of the three proteins, potentially regulating either RhoA, as PRL1 or/and PRL2, or rather activating RhoB, as PRL3. The background for this conclusion is the fact that RhoA and RhoB are antagonistically regulated (see Figure 3.10).

4.2.3 Regulation of Rac and Cdc42 upon Rho deletion

Rac and Cdc42 proteins are, besides RhoA, the best-studied Rho GTPases involved in regulation of the actin cytoskeleton. Since Rac is also known to be antagonistic to RhoA [215], mRNA and protein levels of Rac and Cdc42 were analyzed in the absence of Rho. Also for Cdc42 and RhoA, opposing activities have been proposed, at least in the regulation of metalloproteinases [216]. Cdc42 mRNA levels were mildly decreased in RhoB and RhoAC KO cells and slightly increased in cells expressing only RhoC (see Figure 3.19.A). Rac2 mRNA was below the detection limit and Rac1 showed no significant changes. Rac3 mRNA was decreased in RhoA KO cells. The only significant difference of Rac/Cdc42 protein levels was an increase observed in RhoBC KOs, but all other KO clones also showed a similar tendency (see Figure 3.19.B). Activity of Rac1, Rac2 and Rac3 combined was mildly increased in all Rho KO cells, but not significantly (see Figure 3.19.C). All experiments on protein level only give a rough overview since multiple proteins are simultaneously included in the analysis. Furthermore it should be considered that not only RhoA is antagonistic towards Rac1, but also Rac1 and Rac3 have been suggested to carry out opposing functions considering adhesion and contraction [217], which makes the data more difficult to interpret. The tendency of a mild increase in protein level and activity of particularly Rac proteins can be observed and would fit to an antagonism towards the deleted Rho proteins. For detailed conclusions, a more specific analysis differentiating between the GTPases would be necessary.

Due to the expression data, it was not surprising that lamellipodia, induced by Rac signaling [37], could be observed in all cell lines depleted in Rho proteins (see Figure 3.20), since Rac activity was not diminished.

4.2.4 F-actin, stress fibers and myosin in the absence of Rho

Due to the direct connection between Rho GTPases and the actin cytoskeleton, total actin levels in the absence of Rho were analyzed via Western Blotting (see Figure 3.21.A). Interestingly, total actin levels were increased, especially in RhoBC and RhoAC double KOs. Measurements of F-actin intensities on the other hand revealed a decrease in most Rho KO cells, with the exception of RhoB KOs (see Figure 3.21.B). There, more F-actin per cell area was observed, which could be due to high RhoA levels in the presence of RhoC and the absence of RhoB. The lowest amount of F-actin per cell area was observed in RhoAB KOs, expressing only RhoC. RhoBC KOs, in which more total actin was found, might contain a high amount of G-actin, since F-actin intensity per cell area was also strongly reduced here. Yet, increased cell area has to be considered. RhoA alone, even when upregulated, does not seem to be able to maintain a high stress fiber content in the cell. The same is true for RhoAC double KOs, expressing only RhoB. In conclusion, generation of F-actin is most efficient if RhoA and RhoC are active, appears to keep the balance if RhoB is upregulated, slightly less effective if RhoA is the only Rho protein and the least efficient if RhoC is the only Rho protein. Aspenström *et al.* observed that all three Rho proteins, when overexpressed and constitutively active, were able to induce stress fibers [218], which is why a more detailed analysis on stress fibers was followed up.
All cell lines used for this study showed a reduction of stress fibers upon starvation but generated strong stress fibers at the cell border upon serum stimulation (see Figures 3.22 and 3.23). The only exception were RhoA and RhoAC double KOs, in which stress fiber formation upon serum stimulation was not mainly at the cell border or not as strong. Peripheral stress fibers are rather mediated via MRCK whereas central stress fibers are generated via ROCK signaling [219]. This points towards a differential regulation of myosin activation in RhoA and RhoAC double KOs. Reduction of stress fibers upon serum starvation has frequently been used for investigations in the past [220], since for instance the serum component LPA is responsible for induction of stress fibers [176].
Treatment of all double KO cell lines with CNF_y showed that all three Rho proteins alone were able to induce stress fiber formation (see Figure 3.40). Previous analyses of CNF_y revealed that it predominantly activates RhoA, but also affects Rac1 and Cdc42 [221] [222]. Therefore, stress fiber generation upon CNF_y treatment via Cdc42 and MRCK can not be excluded. On the other hand, all three double KOs contain strongly increased amounts of the respective Rho protein and, as just mentioned, CNF_y seems to prefer Rho over Cdc42 as substrate. This promotes the hypothesis that the single Rho proteins, when constitutively active, can induce stress fibers.

Stress fibers are induced downstream of kinases like ROCK or MRCK, with ROCK inducing myosin light chain phosphorylation downstream of Rho and MRCK downstream of Cdc42 [84]. ROCK mRNA levels showed mild variations upon Rho KO, but this did in most cases not reflect the protein level (see Figure 3.24). ROCK protein levels were mainly increased in cells with high RhoA levels, in the absence of RhoB and the presence of RhoC, namely RhoB KOs. Again, these results suggest a cooperative role for RhoA and RhoC in activation of contractility and stress fiber formation. Melendez *et al.* also observed no significant increase in ROCK levels and activity upon RhoA single KO [187].
mRNA levels of MRCK were decreased in a few cell lines, especially double KOs and RhoB KOs (see Figure 3.25). An explanation could be that upon upregulation of RhoA, especially in the absence of RhoB, the ROCK pathway was predominantly used and myosin activation relied less on MRCK activity. The two kinases have been shown to work in cooperation [223], so that it could be possible that one pathway is downregulated when the other one is predominantly used. Of course, MRCK protein levels and activity need to be analyzed to draw clear conclusions.

Myosin IIa and IIb, as well as phosphorylated myosin, localized to stress fibers in all Rho KO cells and this localization revealed no obvious differences to NIH-3T3 WT cells (see Figures 3.26 − 3.29). Stress fibers contain myosin, independent of activation via ROCK and Rho or MRCK and Cdc42 [84]. Therefore, myosin content of stress fibers was not expected to change as much as the amount of stress fibers themselves upon Rho KO. For instance RhoAB KOs contain only a very low amount of stress fibers, but the few that are present contain myosin. Recruitment of myosin II to stress fibers is mediated via Tropomyosin 4 [173]. mRNA levels of Tropomyosin 4 are strongly increased in RhoB KOs and decreased in RhoAC KOs (see Figure 3.11). RhoB KO cells have previously been proposed to contain increased F-actin amounts and contractility by results from this study (see chapter 4.2.1). This is in line with increased Tropomyosin 4 levels. The opposite has been proposed for RhoAC KO cells, containing only RhoB. This confirms that RhoA together with RhoC is the most important factor for contractility and stress fiber formation. Tropomyosin 4 levels should be verified on protein level.

Phosphorylation of myosin light chain was increased strongly in RhoB KOs and to a lesser extent in RhoBC KOs (see Figure 3.30). As already described for other experiments, the Rho contraction pathway is therefore at its optimum when RhoA is upregulated in the absence of RhoB. The presence of RhoC seems to improve RhoA activity, which is why the increase in phosphorylation was weaker in RhoBC double KOs. The lowest level of myosin phosphorylation was observed in RhoC KOs, containing high amounts of RhoA and RhoB, probably inhibiting each other. An increase of myosin light chain phosphorylation was already observed in other studies when RhoB was deleted in addition to RhoC [185].

4.2.5 Role of cofilin in Rho KO cells

One gene that was strongly regulated upon Rho KO at the mRNA level was the actin depolymerizing factor ADF. It was particularly upregulated in RhoA and RhoC KO cells (see Figure 3.31.A). The other cofilin family members, Cofilin 1 and Cofilin 2, displayed only moderate regulation at the mRNA level. Interestingly, the total levels of Cofilin1 mRNA in NIH-3T3 WT cells were much higher than those encoding ADF and in particular Cofilin 2 (see Figure 3.31.B). Since it was previously observed that Cofilin 2 and ADF disassemble actin filaments more efficiently than Cofilin 1, it can be hypothesized that higher amounts of Cofilin 1 are needed to generate the respective level of activity [91].
Analysis of Cofilin family members at the protein level confirmed the upregulation in the absence of Rho (see Figure 3.32). Particularly in Rho double KOs, ADF was upregulated, as well as Cofilin 2, even though less dramatically in case of the latter. Upregulation of Cofilin 1 reflected partially the increase of Cofilin 1 phosphorylation and thus inactivation, suggesting that increased expression levels are compensated by decreasing Cofilin 1 activity. Higher amounts of Cofilin 1 phosphorylation were especially observed in RhoB and RhoBC KO cells, which contain high amounts of RhoA in the absence of RhoB.
Interestingly, even though deletion of Rho proteins led to an increase of Cofilin family member expression, overexpression of Rho did not induce decreased cofilin family expression (see Figure 3.33). Instead, a moderate increase in Cofilin family expression was observed, which was again also true for Cofilin 1 phosphorylation. These data suggest that the correlation between Rho protein and Cofilin family member expression likely involves an additional regulation besides LIMK mediated Cofilin family member inactivation. In previous studies, Cofilin expression was observed to be induced by cyclic stretching of cells and thereby concluded to respond to changes in mechanotransduction [224]. Therefore it is not unlikely that the contractile activity in cells has an influence on Cofilin expression. Consistent with this view, ADF was most strongly upregulated in Rho double KO cells, which, as discussed above due to increased cell area or volume, might contain reduced levels of contractility. However, it should also be considered that Cofilin does not act alone, but operates together with many other proteins, such as Coronin [225], Memo [226] or WDR1 [89].

WDR1 (also called Aip1) was also upregulated in Rho double KO cells. This was most evident at the protein level in RhoAC double KO cells, expressing only RhoB (see Figure 3.34). WDR1 was previously found to be implicated in cytokinesis [227]. It is therefore possible that RhoAC double KO cells display upregulated WDR1 expression levels to compensate for the loss of RhoA, in particular during cytokinesis. Further localization studies would be needed to verify this hypothesis.

siRNA induced knockdown of all Cofilin family members reduced their expression but did not completely abolish it (see Figure 3.35). This might be due to probably similar problems as observed for Rho proteins: it is not possible to

erase all three Cofilin family members since they might be essential for cell survival. As also observed in the current study, Hotulainen *et al.* previously noticed upon knockdown of one family member, a strong upregulation of a remaining one, suggesting a compensatory mechanism [228]. It is likely that ADF/Cofilin activity is important for cell motility and cytokinesis, all of which require dynamic turnover of cellular actin filaments, and thereby not dispensable for cellular survival.

Knockdown of Cofilin family proteins, suggested to reduce actin depolymerization, induced massive stress fiber formation, increased cell size and multiple and deformed nuclei in all cell lines, not only in NIH-3T3 WT but also in Rho KOs (see Figures 3.36 − 3.39). For WT cells in the presence of Rho, similar observations upon elimination of Cofilin expression have been described earlier [180]. However, RhoAB KOs showed a different behavior, as Cofilin knockdown in these cells did not induce stress fiber formation as dramatically as in other cell lines. While RhoC and Cdc42 are both expressed in RhoAB KOs, these proteins alone apparently can not trigger efficient stress fiber formation. Furthermore, the difference of capability to form stress fibers in WT cells versus RhoAB KOs was even more evident upon Cofilin knockdown, confirming differential signaling in these distinct cell lines. Since prominent stress fiber formation by Cofilin siRNA was observed in all other Rho KO cell lines except for RhoAB KO, the presence of either RhoA or RhoB might be sufficient for stress fiber formation upon ADF/Cofilin inactivation.
In order to explore the pathway that mediates the pronounced stress fiber formation observed upon ADF/Cofilin knockdown, Rho, ROCK, MRCK or myosin II were inhibited under these conditions. None of these inhibitors was able to completely abolish the stress fiber phenotype induced by Cofilin siRNA. However, the same inhibitor treatments strongly diminished stress fiber formation under control conditions (i.e. without Cofilin knockdown), suggesting that more than one pathway is involved in stress fiber formation upon ADF/Cofilin inactivation. The strongest reduction of stress fiber formation in cells treated with Cofilin siRNA was observed upon myosin II inhibition, in WT as well as Rho KO cells. Since stress fibers contain myosin II irrespective of the upstream signaling pathway, the disassembly of stress fibers upon myosin II inhibition was not unexpected [84]. Interestingly, the second strongest inhibition of stress fiber formation was induced by inhibiting ROCK but not Rho proteins. Therefore a second, perhaps indirect, pathway of ROCK activation might contribute to the strong stress fiber formation upon ADF/Cofilin inactivation. For instance, activation of ROCK through the NOTCH receptor has been described previously [229], showing that alternative pathways should be considered.
Under control conditions (i.e. without Cofilin knockdown), inhibition of myosin II or ROCK also had the strongest impact on stress fiber formation in most cell lines. As an exception however, this was not observed in RhoAB KOs, in which MRCK or Rho inhibition had the strongest impact. The few stress fibers left in RhoAB KOs are therefore likely generated through RhoC as well as Cdc42 signaling, whereas ROCK seems to be more relevant in the other cell lines. Nev-

ertheless, the fact that ROCK inhibition reduced stress fiber formation more strongly than Rho inhibition could be due to an alternative, Rho independent pathway of ROCK activation, or alternatively, differential inhibitor efficiencies at given concentrations. Future experiments will have to distinguish between these possibilities.
Taken together, the data obtained with this experimental setup suggest that both Rho and ROCK as well as Cdc42 and MRCK are capable of inducing stress fiber formation when actin depolymerization by Cofilin proteins is reduced. However, RhoA and RhoB seem to be more efficient than RhoC and Cdc42 during this process.

4.3 Infection studies in the absence of Rho proteins

4.3.1 Role of Rho and Rac proteins during *S.* Typhimurium infections

Invasion of *S.* Typhimurium was shown to depend on Rac as well as Rho proteins and the contributions seemed to be additive [136]. Nevertheless, previous studies on the role of Rho proteins were performed with C3 toxin from *C. botulinum*, not distinguishing between RhoA, RhoB and RhoC since all three are inhibited by the toxin. Rac KO cells and the Rho inhibitor Rhosin were utilized to verify previous data. Rho inhibition decreased invasion to 60%, whereas Rac KO yielded an invasion rate of only 16% (see Figure 3.1). Confirming the additive effect, 5% of bacteria invaded in Rac KO cells treated with Rhosin. These data could point towards a stronger contribution of Rac, yet a genetic KO can not be directly compared with inhibition via small molecule inhibitors. As shown for Rhosin, RhoA activation is reduced upon treatment but not completely diminished, since small molecule inhibitors are competing with GEFs for binding to the GTPase [230].
Table 4.1 displays invasion rates of *S.* Typhimurium in the absence of one or two Rho proteins in context with expression levels of the respective other Rho and Rac/Cdc42 proteins. Rho KO cell lines are sorted according to the resulting invasion rates (see Figure 3.41). + signs are used to display fold protein changes compared to NIH-3T3 WT levels, according to Figures 3.13.B and 3.19.B. − displays deletion of the respective gene and = stands for the same levels as in NIH-3T3 WT cells, representing the control condition.

Table 4.1: Rho and Rac/Cdc42 protein levels and resulting invasion of *S.* Typhimurium

Cell line	RhoA levels	RhoB levels	RhoC levels	Rac/Cdc42 levels	Invasion
NIH-3T3 WT	=	=	=	=	100%
RhoB KO	++	−	=	=	105%
RhoBC KO	++	−	−	++	87%
RhoAC KO	−	+++++	−	++	79%
RhoC KO	++	+++	−	=	67%
RhoAB KO	−	−	+++	=	57%
RhoA KO	−	++++	=	=	45%

The table reveals different roles for RhoA, RhoB and RhoC. In RhoB KO cells, with increased RhoA levels and RhoC still present bacteria invaded as efficient as in WT cells (RhoB KO). An additional RhoC depletion slightly reduced the invasion rate, even though Rac/Cdc42 levels were higher than in WT cells (RhoBC KO). Invasion was even less efficient when cells expressed RhoB as the only Rho protein, but in strongly increased amounts, and showed increased Rac/Cdc42 levels compared to WT cells (RhoAC KO). An even lower invasion rate was induced when only RhoA and RhoB were expressed, even though protein levels of both were quite high (RhoC KO). The second weakest invasion rate was observed in cells expressing RhoC as the only Rho protein, despite its increase in expression (RhoAB KO). The lowest invasion rate of 40% was observed in cells expressing high RhoB levels but also WT levels of RhoC (RhoA KO).
In conclusion these data suggest that all three Rho proteins are able to facilitate *S.* Typhimurium invasion, since all KO cell lines lead to invasion rates that are still higher than in Rac KO cells (16%). However, the three Rho proteins show different efficiencies. RhoA has the strongest impact on the invasion pathway but is more efficient if RhoC is present and RhoB is absent. Antagonistic functions for RhoA and RhoB have already been proposed based on the microarray data (see Figure 3.10). RhoB is more efficient at inducing invasion than RhoC and in contrast to RhoA, RhoB acts more efficient in the absence of RhoC.
Hänisch *et al.* showed that the Rho dependent entry pathway involves myosin II activity and stress fiber formation [136]. All three Rho proteins alone are able to induce stress fibers (see Figure 3.40), yet the exact mechanism of how stress fiber formation induces uptake is still unknown. Additive effects of Rho and Rac in *S.* Typhimurium have been confirmed by the experiments described above. Also, ruffle formation during infection with *S.* Typhimurium was not abrogated upon deletion of one Rho protein (see Figure 3.42). This confirmed that bacterial entry in the absence of Rho could occur without hindrance via the well studied Rac induced membrane ruffling pathway [39].

It was previously found that the Rho entry pathway depends on the bacterial effector protein SopB, whereas SopE, SopE2 and SopB all induce the Arp2/3 complex mediated ruffling pathway [136]. To further dissect the roles of RhoA, RhoB and RhoC in context with the virulence factors, Rho single KO cells were infected with the respective *S.* Typhimurium mutants (see Figure 3.43). Bacteria lacking all three effectors were non-invasive in all cell lines. Bacteria defective in either SopB or SopE/SopE2 expression all showed reduced invasion in WT

and Rho KO cells compared to WT bacteria. Yet in all cases, bacteria lacking only SopB invaded better than bacteria expressing SopB as the only one of the three virulence factors initiating invasion. In NIH-3T3 WT cells, the invasion rate of *S.* Typhimurium ΔSopE/SopE2 is similar to the invasion of bacteria in Rac KO cells, thereby confirming the link between Rac and the two effectors. Also, infection experiments in Rac KOs suggested a more important role for the Rac pathway during invasion. *S.* Typhimurium ΔSopE/SopE2 can still use the Rho pathway and partially the Rac pathway via SopB [133]. The SopB mutant on the other hand can not induce Rho activation but has still two proteins capable of activating membrane ruffling and therefore invades better. Even though, the difference between invasion of the two mutant strains in the different Rho KO cell lines depended on RhoA expression levels.
It is well known that RhoA and Rac1 activities are antagonistic [231] [215]. There are currently no studies revealing this effect between RhoB or RhoC and Rac. In RhoA KO cells, an inhibitor of the Rac pathway is therefore missing, suggesting increased Rac1 efficiencies. In RhoC KO cells, RhoA levels are increased but potentially suppressed by high RhoB levels and RhoC, as a supporter of RhoA activation, is missing. Thereby, in both cell lines bacteria lacking SopE and SopE2 and thereby depending on SopB for invasion have better chances of using the Rac pathway in the absence of Rho proteins. In RhoB KOs on the other hand, which express high levels of RhoA and therefore should highly suppress Rac activity, *S.* Typhimurium ΔSopE/SopE2 shows strong invasion defects. This is interesting, since SopB and RhoA are both expressed and should lead to an efficient invasion via the Rho pathway. Also it has to be considered that WT bacteria invade as good in RhoB KO cells as in WT cells. Therefore, a potential connection between SopB and RhoB during bacterial infection should be elucidated.

The role of RhoB during *S.* Typhimurium infection remains unclear since a RhoB KO did not reduce invasion rates. Since RhoB differs from RhoA and RhoC in its localization and is involved in vesicular trafficking [61], experiments were set out to analyze RhoB levels in late stages of infection, when *S.* Typhimurium resides in the SCV (see Figure 3.44). Whereas RhoA and RhoC levels were only slightly increased over 6 hours of infection, RhoB levels were strongly upregulated. This increase showed the strongest rise between 1 and 2 hours p.i. with WT bacteria. Interestingly, in particular considering the latest discussion about SopB and RhoB in the previous paragraph, the increase in RhoB was completely abolished if the cells were infected with *S.* Typhimurium ΔSopB. These data lead to the hypothesis that RhoA might play a role in the early invasion process while RhoB is important for later intracellular steps of the infection. Additional experiments showed that RhoB upregulation partially depends on an early increased mRNA expression, even though the increase in protein by far exceeds the increase in mRNA levels, with the latter stagnating after the initial increase (see Figure 3.45). An additional regulation of RhoB protein stability independent of mRNA levels therefore needs to be present and has to be analyzed in more detail.

It was previously shown that SopB protects infected cells from apoptosis by Akt activation [232]. Another investigation revealed a role for RhoB during that process, at least during early stages of infection [233]. Therefore, Akt phosphorylation was analyzed in all Rho KO cell lines and during infection in NIH-3T3 WT cells (see Figure 3.46). Microarray data revealed that Akt mRNA levels were either decreased in the absence of RhoB or increased in cell lines with high RhoB levels. Akt phosphorylation on the other hand was increased in all Rho KO cells, with the strongest increase in RhoC KO cells, where RhoB levels are high and RhoA activity can not be supported by RhoC anymore. Nevertheless, infection experiments showed a slight increase in Akt phosphorylation after 1 hour p.i. and subsequently decreasing and stagnating levels. There was no strong difference between WT bacteria and *S.* Typhimurium ΔSopB, even though the increase in Akt phosphorylation after 1 hour was not quite as strong in the absence of SopB. It can therefore be suggested, that the upregulation of RhoB via SopB during infection is not involved in Akt activation.
Confirmation that RhoB is important for later stages of infection was given by comparing bacterial load after 6 hours p.i. in NIH-3T3 WT and RhoB KO cells (see Figure 3.47). Infection of RhoB KO cells yielded a reduction of bacterial load by 30%. Furthermore, bacteria lacking SopB failed to replicate efficiently in both cell lines. Of course earlier invasion rates are already lower for *S.* Typhimurium ΔSopB, but bacterial numbers after 6 hours were so low, that this points towards a defect not only in invasion but also in intracellular replication. It should be considered that bacteria lacking SopB also grow slightly slower during normal cultivation in LB medium, compared to all other strains used for this study (data not shown). The exact contribution of RhoB and SopB to bacterial replication and SCV formation and stability remains to be established. Previous studies revealed a role for SopB during trafficking of the SCV to inhibit fusion with the lysosome [234]. Another investigation showed that myosin activity downstream of ROCK was important for positioning of the SCV, also in context with SopB activity. A potential connection via a constitutively active RhoA construct was shown, but RhoB was not included in the study [235]. Since RhoB was shown to regulate endosomal trafficking by inhibiting transport to and via microtubules by building an actin cage around the vesicles [61], a potential connection to SCV positioning seems plausible and needs a detailed analysis in the future.

4.3.2 Invasion of *S. flexneri* and the roles of Rho and Rac proteins

Invasion of *S. flexneri* in non-phagocytic host cells is an important step during bacterial infection. It has been shown previously that activation of the GTPase Rac via the bacterial virulence factor IpgB1, acting as a GEF, induces membrane ruffling and thereby uptake of the bacteria [147]. Since an additional RhoA dependent invasion mechanism has already been discovered for *S.* Typhimurium [136] and *S. flexneri* expresses IpgB2, a GEF for RhoA [45], experiments were set up to analyze the contributions of Rho and Rac to bacterial invasion. In initial experiments, we made use of small molecule inhibitors for Rho and Rac proteins.

Treatment of NIH-3T3 WT fibroblasts with the inhibitors revealed that both GTPase families are involved in the invasion process since invasion was reduced to around 40% in both cases. The reduction was stronger for Rho inhibition and was not further decreased upon usage of both inhibitors at the same time (see Figure 3.2.B).
Small molecule inhibitors are competitive and never able to inhibit all target proteins in the cell [230]. Therefore, complete deletion of proteins via gene KO is in the end necessary to draw definite conclusions. A Rac KO in mouse embryonic fibroblasts has been generated previously [38]. In this cell line, Rho inhibition reduced invasion by 50%, which was slightly less than in NIH-3T3 cells. Interestingly, invasion in Rac KO cells, with or without Rho inhibition, was completely abolished (see Figure 3.2.A).
Strikingly, invasion of *S. flexneri* in Rho KO cells, which express high amounts of Rac proteins as shown previously, confirmed a role also for Rho proteins in the invasion process (see Figure 3.48). Table 4.2 gives an overview of the situation in the different Rho KO cell lines, which are sorted by the resulting invasion rates. + signs are used to display fold protein changes compared to NIH-3T3 WT levels, according to Figures 3.13.B and 3.19.B. − stands for deletion of the respective gene and = displays control levels as in NIH-3T3 WT cells.

Table 4.2: Rho and Rac/Cdc42 protein levels and resulting invasion of *S. flexneri*

Cell line	RhoA levels	RhoB levels	RhoC levels	Rac/Cdc42 levels	Invasion
NIH-3T3 WT	=	=	=	=	100%
RhoB KO	++	−	=	=	73%
RhoBC KO	++	−	−	++	71%
RhoC KO	++	+++	−	=	59%
RhoAC KO	−	+++++	−	++	45%
RhoAB KO	−	−	+++	=	23%
RhoA KO	−	++++	=	=	18%

The table reveals differential roles for RhoA, RhoB and RhoC. Compared to control levels, invasion is most effective if RhoA levels are increased, RhoB is absent, and RhoC is still present (RhoB KO). Invasion is reduced slightly when RhoC is deleted in addition even though Rac/Cdc42 levels are mildly increased (RhoBC KO). Reduction of invasion is even stronger when RhoC is absent and RhoB is upregulated in the presence of RhoA (RhoC KO). The next decreasing step appears when Rac/Cdc42 levels are increased but only RhoB is present, even though the latter is strongly upregulated (RhoAC KO). The second-strongest invasion defect occurs when only RhoC is expressed, even though its levels are increased (RhoAB KO). The lowest invasion rate was found when RhoA was absent, RhoC levels were unchanged and RhoB was strongly upregulated.
In conclusion these data show that even though the exact contribution of Rho proteins to *S. flexneri* invasion is not known, RhoA can perform this function the most efficient. RhoC helps RhoA to execute its function, whereas the presence of RhoB, which was already shown in the microarray analysis to be antagonistically regulated to RhoA (see Figure 3.10), impedes RhoA activity. RhoB alone is able to promote invasion, even though not as good as RhoA, but this is more

efficient without RhoC. RhoC alone is not able to efficiently facilitate invasion. Upregulated Rac/Cdc42 levels seem to have a mild positive effect on invasion in the situation described above.
The hypothesis that Rho as well as Rac are both directly involved in the mechanisms of bacterial uptake for *S. flexneri*, yet by alternative mechanisms, is not convincing. Invasion is strongly reduced when either Rac or RhoA are depleted, even though the other one is still expressed and the alternative pathway should therefore be possible. The contribution of Rac to membrane ruffling inducing bacterial invasion has been described previously [148], but the functionality of Rho proteins in this process needs further clarification. One possibility is that Rho proteins are inducing effector translocation via the bacterial T3SS. This mechanism, even though the details are still unknown, has already been found in *Y. pseudotuberculosis* [155] [222]. In this case, the bacterial toxin CNF_y gets into the cell by a yet unknown pathway, activates Rho GTPases and thereby induces secretion of virulence factors through the T3SS. Assuming this hypothesis for *S. flexneri* could explain the current datasets. Without Rho proteins, there would be no effector translocation and therefore no Rac activation and subsequent membrane ruffling and invasion. Invasion was never completely abolished in Rho KO cells since all three proteins seem to be able to exert the function, yet with different efficiencies. In the absence of Rac, effector translocation would be possible but membrane ruffling can not be induced so that bacterial uptake is not possible. Looking at small molecule inhibitor treatments in NIH-3T3 cells, using both inhibitors at the same time did not further decrease invasion compared to only Rho inhibition, since Rac activation can not occur anyway if the effector IpgB1 can not be translocated. Therefore, *S. flexneri* invasion depends on Rho for the initiation and on Rac for the execution of the invasion process. This theory naturally needs experimental evidence, so that future experiments should analyze effector translocation in the absence of Rho proteins.

Formation of membrane ruffling during *S. flexneri* invasion and actin tails for intracellular movement was not expected to change upon deletion of Rho proteins. Membrane ruffling depends on Rac activation [169], whereas actin tails are mediated via binding of the virulence factor IcsA to cellular N-WASP, one of the NPFs for Arp2/3 [236]. Even in the absence of one Rho protein, as discussed above, the other respective Rho proteins can to a certain extent compensate and in the case that effector translocation is induced, invasion will occur via membrane ruffling. Nevertheless, Rho single KO cells infected with the bacterial WT strain were fixed and stained to check for potential morphological differences. As hypothesized, both types of actin structures were detectable even in the absence of Rho and no other morphological changes could be observed (see Figure 3.49). This supports the hypothesis that invasion defects upon Rho KO are not due to impaired membrane ruffling but specifically changed by the absence of Rho proteins.

4.3.3 RSV infection in Rho KO cells

The roles of Rho GTPases and the actin cytoskeleton during respiratory syncytial virus (RSV) infections have been studied earlier [161] [160]. Specific contributions of RhoB and RhoC were not addressed in the past, while RhoA was shown to induce syncytium formation. The FACS experiments performed by Svenja Wiechert revealed that viral spread is inefficient in the absence of RhoA and RhoB (see Figure 3.50).
This inefficiency could be due to reduced cell fusions. To further analyze this, NIH-3T3 WT and all Rho KO cells were transfected with the viral fusion protein RSV-F. Our data show that syncytium formation was found rather infrequently in cells lacking RhoA, whereas accumulations of RSV-F in the perinuclear area were observed more frequently in cells lacking RhoA or RhoB (see Figure 3.51). These data confirm the role of RhoA in RSV-F mediated cell fusions but also reveal a potential role for RhoB in transport of the RSV-F protein to the cellular surface, since it needs to get embedded in the plasma membrane to interact with neighboring cells. RSV-F is expressed as a precurser protein in the cytoplasm, which is triggered by a so far unknown mechanism to change its structure and get into the membrane with its hydrophobic region [237]. RSV-F co-localization with RhoA at lipid rafts on the plasma-membrane has been shown, but the analysis of RSV-F transport to the lipid rafts was executed with C3 toxin from *Clostridium botulinum*, which, as mentioned earlier, inhibits all three Rho proteins. RSV-F was not able to localize at lipid rafts after C3 treatment, which, despite its co-localization at the rafts with RhoA, does not exclude a role for RhoB in the transport [238]. Future studies should include the other Rho KO clones in the FACS experiments to clearly distinguish between the roles of RhoA and RhoB but also to uncover if there is a role for RhoC that is not known so far. Co-localization studies of RSV-F and RhoB should also be performed. In addition, the Rho KO cells provide a nice tool to analyze the exact contributions of RhoA and RhoB for RSV infections in more detail.

4.4 Concluding Remarks

This study provided new insights into the specific roles and the interplay between RhoA, RhoB and RhoC via genetic knockouts of the single GTPases as well as two at the same time, leaving only one Rho protein in the cell. The overall hypothesis that could be drawn out of various experiments is that RhoA and RhoB have antagonistic functions and are more efficient in the absence of the respective other protein. Importantly, the genetic and cell biological toolbox generated in this work was able to reveal a very specialized functional role of RhoC, since the protein alone can only partially compensate for the loss of the others. Instead, the data propose that it supports RhoA activity by a yet unknown mechanism, but does not support RhoB. mRNA data revealed that RhoC is expressed in much larger amounts than RhoA or RhoB, which should be verified on protein level in future experiments by mass spectrometry. This might confirm the hypothesis that RhoC is quite inefficient itself but promotes RhoA

activity by blocking Rho GDIs due to its high amounts and thereby pushes RhoA out of the Rho GDIs and towards an active state.
The typical pathways downstream of Rho proteins, via ROCK or LIMK, were shown to be mediated mainly via RhoA, probably together with RhoC. For instance, RhoB KO cells, containing increased RhoA protein levels, were the cell line with the highest level of F-actin and contractility, as was concluded due to morphological changes. Furthermore, cell growth was slowed down in the absence of RhoA and the roles of RhoB or RhoC during cytokinesis in the absence of RhoA need to be analyzed. RhoB specific functions were found to be involved in Golgi structure and granularity. Yet, the mechanism behind RhoB stability upon upregulation in the absence of RhoA or RhoC is so far unknown and at least not due to GDIα or GDIβ, since RhoB was shown not to interact with the two proteins.
Infection studies revealed pathogen-specific roles for Rho GTPases. RhoA and RhoC mediate bacterial invasion during the early phase of infection of *S.* Typhimurium, while RhoB is strongly upregulated during later stages of infection and influences bacterial replication and survival. The role for Rho proteins in *S. flexneri* infection still remains to be validated, since a direct mechanic effect on invasion is not very likely. However, even though Rho proteins are suggested to perform different functions during invasion of *S.* Typhimurium and *S. flexneri*, the specific contributions and efficiencies of RhoA, RhoB and RhoC were found to be very similar. Data on RSV in the absence of Rho proteins gave promising insights into specific roles for RhoA and RhoB promoting syncytium formation which also needs further experimental analysis.

5 Summary

Mammalian Rho GTPases play a key role in regulating the actin cytoskeleton during processes such as cellular trafficking or cell division. RhoA, Rac1 and Cdc42 have been studied extensively in the past. The closely related RhoB and RhoC proteins share 85% sequence identity with RhoA [56]. RhoB localizes at endosomal membranes and is thought to be involved in endosomal trafficking, while RhoA and RhoC accumulate at the plasma membrane [50]. Aside from these differences, RhoB and RhoC have mostly been neglected in the past, since many studies failed to distinguish between Rho subfamily members. Moreover, various pathogens activate or inactivate Rho family GTPases during infection processes to manipulate the actin cytoskeleton for their own benefit. RhoA was studied in this context [163], but little is known in case of RhoB and RhoC.

For a distinct analysis of RhoA, RhoB and RhoC functions in cellular and infection processes, genetic knockouts of all three proteins were generated, as single deletions and in double combinations, in the murine fibroblast cell line NIH-3T3. Elimination of RhoA, alone or in combination with RhoB or RhoC, slowed down cellular growth and increased the number of multinucleated cells. Deletion of one or two proteins led to an upregulation of the remaining Rho proteins, which was most prominent for RhoB in the absence of RhoA and/or RhoC. Changes of F-actin content were subtle in most cases, while stress fiber formation in RhoAB double KO cells was strongly reduced. However, generation of stress fibers could be restored even in RhoAB double KOs upon constitutive Rho protein activation using the bacterial toxin CNF_Y. In the presence of RhoA and RhoC and the absence of RhoB, namely in RhoB KO cells, Rho kinase expression as well as myosin light chain phosphorylation were increased the most, which is in line with increased F-actin intensities in the same cell type. Moreover, the actin depolymerizing factor Cofilin was found to be upregulated in the absence of Rho. Knockdown of all three Cofilin proteins led to massive induction of stress fibers, increased cell size and multiple nuclei per cell. *Salmonella enterica* serovar Typhimurium required RhoA together with RhoC for efficient invasion at early time points. Interestingly, RhoB was strongly upregulated during later stages of infection, which was dependent on the *S.* Typhimurium inositol phosphate phosphatase SopB. The invasion capacity of *Shigella flexneri* was found to decrease to 20% in the absence of RhoA. An initial set of experiments with respiratory syncytial virus revealed an influence of RhoA and RhoB on viral fusion and syncytium formation, which is hypothesized to result from defective transport of the RSV-F fusion protein to the cell surface.

In conclusion, the data from this study reveal antagonistic roles for RhoA and RhoB. Furthermore, RhoC appears to promote RhoA activity. Taken together, the Rho single and double KO cell lines generated during this study allow for the first time precise dissection of respective Rho subfamily functions and their differential contributions to fundamental cell biological processes as well as to bacterial or viral infections.

6 Appendix

6.1 Supplementary Data

6.1.1 Rho GTPase expression in different cell lines

Microarray analysis performed during studies of Block *et al.* [239] revealed mRNA expression levels of genes encoding for Rho GTPases in three murine cell lines. The normalized analysis for Rho and Rac genes shown in Table 6.1 was done by Prof. Dr. Theresia Stradal (HZI, Braunschweig).

Table 6.1: Rho GTPase mRNA expression in murine cell lines

Gene	B16-F1 cells	NIH-3T3 cells	Swiss3T3 cells
RhoA	+++++	+++++	+++++
RhoB	+++	++++	++++
RhoC	+++	+++	++++
Rac1	+++++	+++++	+++++
Rac2	−	−	−
Rac3	+++	++	++

6.1.2 Sequences of Rho KO clones

DNA sequences of Rho KO cell lines are shown in Figures 6.1 - 6.6. Green boxes highlight the target sequences for gene KO. Mutations in the KO sequences are labeled in red. Only the regions which were amplified for genomic sequencing, containing the target sequence, are shown instead of the complete RhoA-, RhoB- or RhoC DNA sequences. The two alleles are shown separately, while only one is displayed in the case that both harbor the same mutation, which was shown for RhoB1, RhoC9, and RhoC3B4. Respective amino acid translations of the complete Rho genes are depicted in Tables 6.2 - 6.4. Sequences labeled in red show amino acids that differ from the WT sequence. Numbers in yellow display number of missing amino acids at this exact position, compared to the WT sequence. The * at the end of the sequences represents a stop codon.

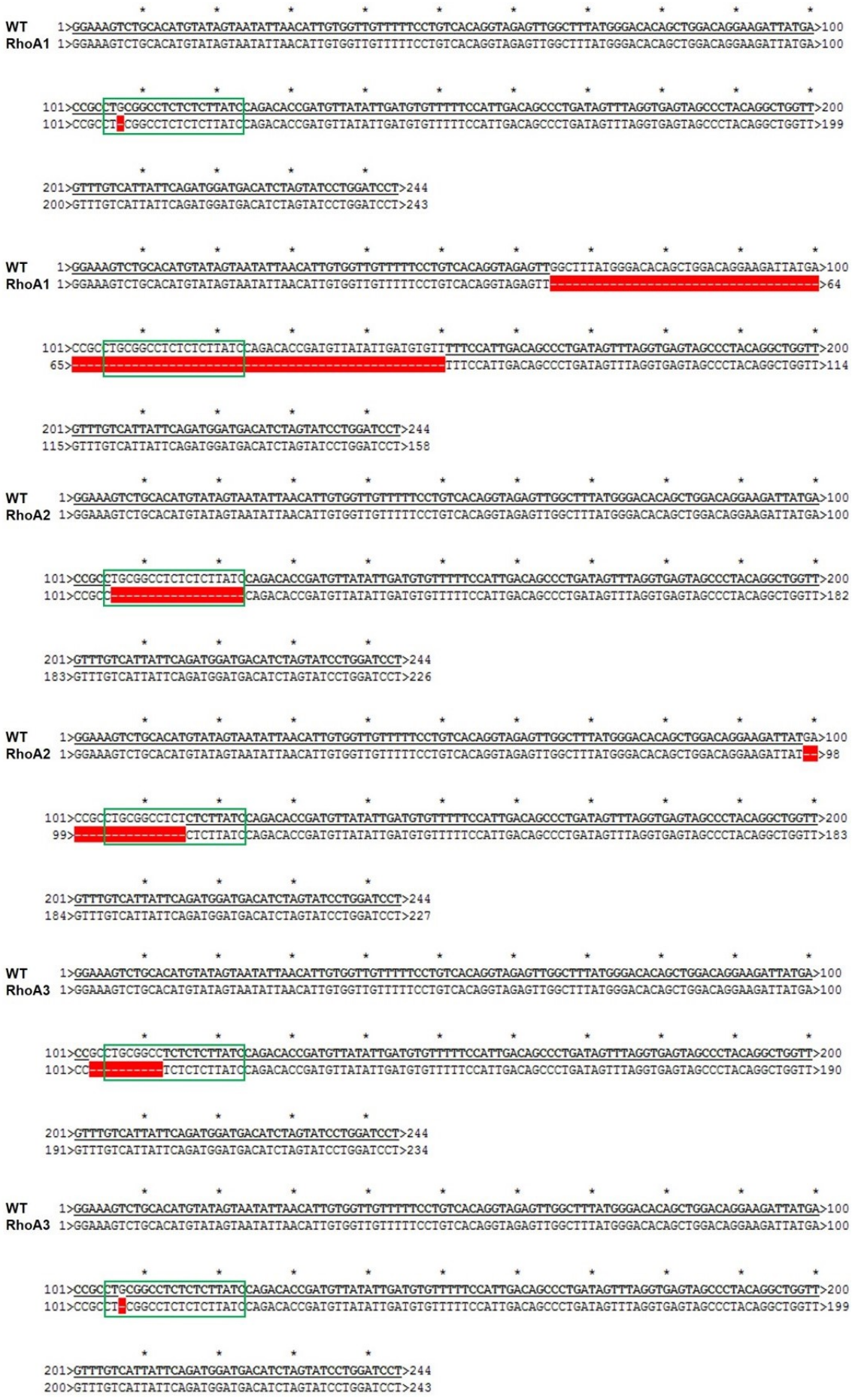

Figure 6.1: DNA sequences of RhoA single KOs. Sequences of RhoA single KOs were aligned to the NIH-3T3 WT RhoA sequence. Green boxes highlight the target sequences for RhoA KO. Mutations are shown in red.

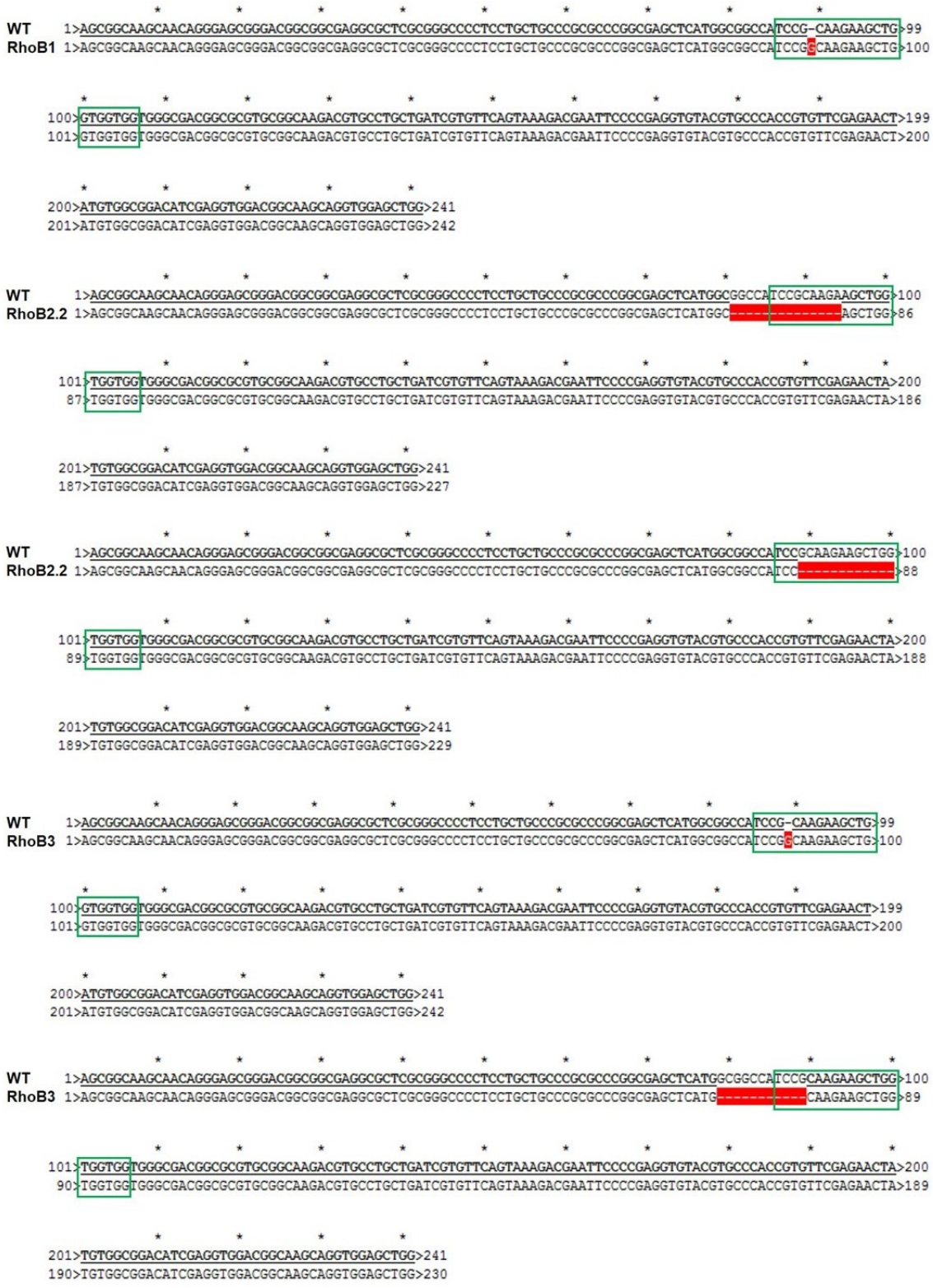

Figure 6.2: DNA sequences of RhoB single KOs. Sequences of RhoB single KOs are compared to NIH-3T3 WT RhoB sequences. Green boxes highlight target sequences for RhoB KO and respective mutations are shown in red.

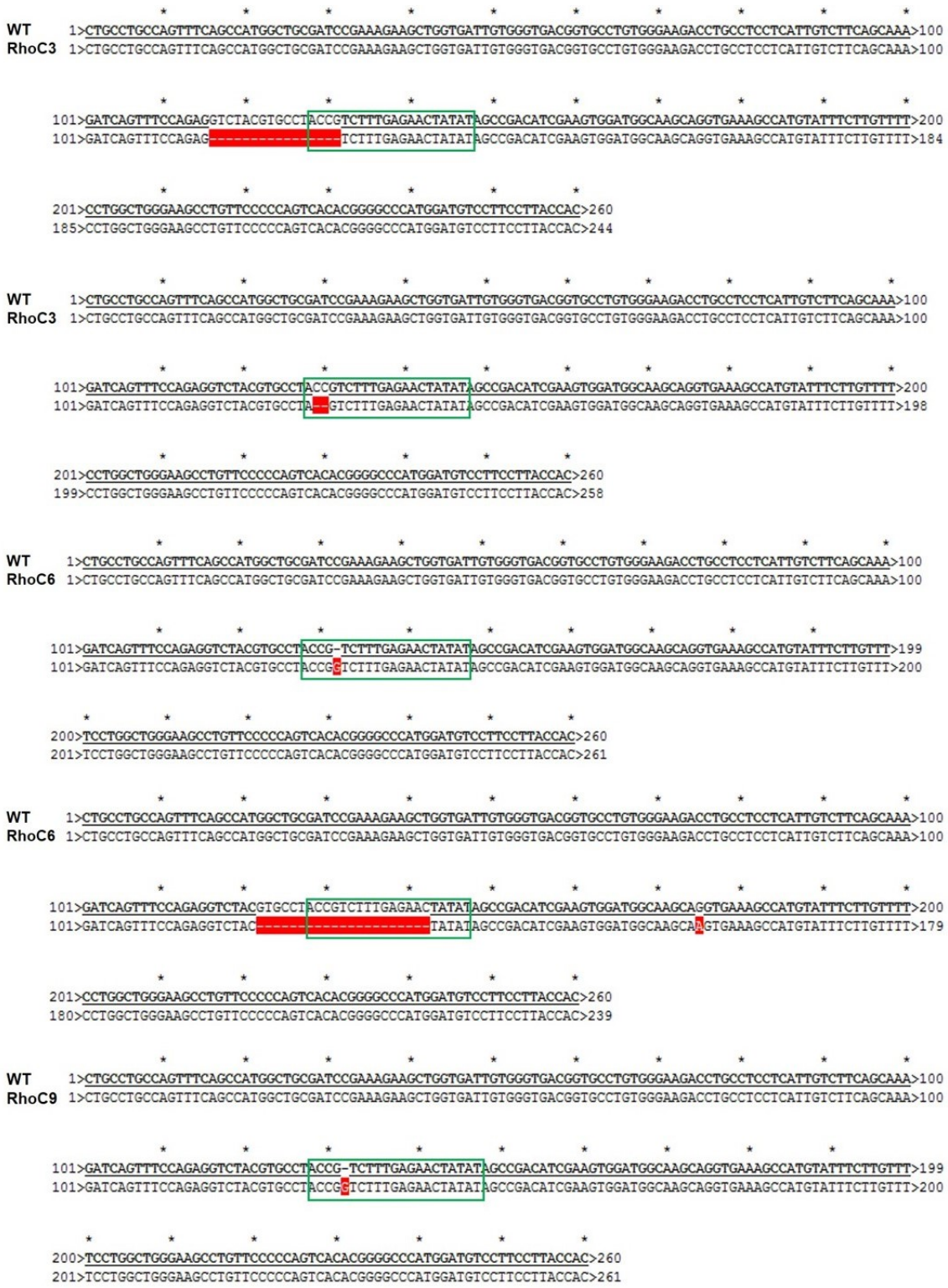

Figure 6.3: DNA sequences of RhoC single KOs. Sequences of RhoC single KOs were aligned to the NIH-3T3 WT RhoC sequence. Green boxes label target sequences for CRISPR-Cas9 mediated RhoC KO. Mutations are shown in red.

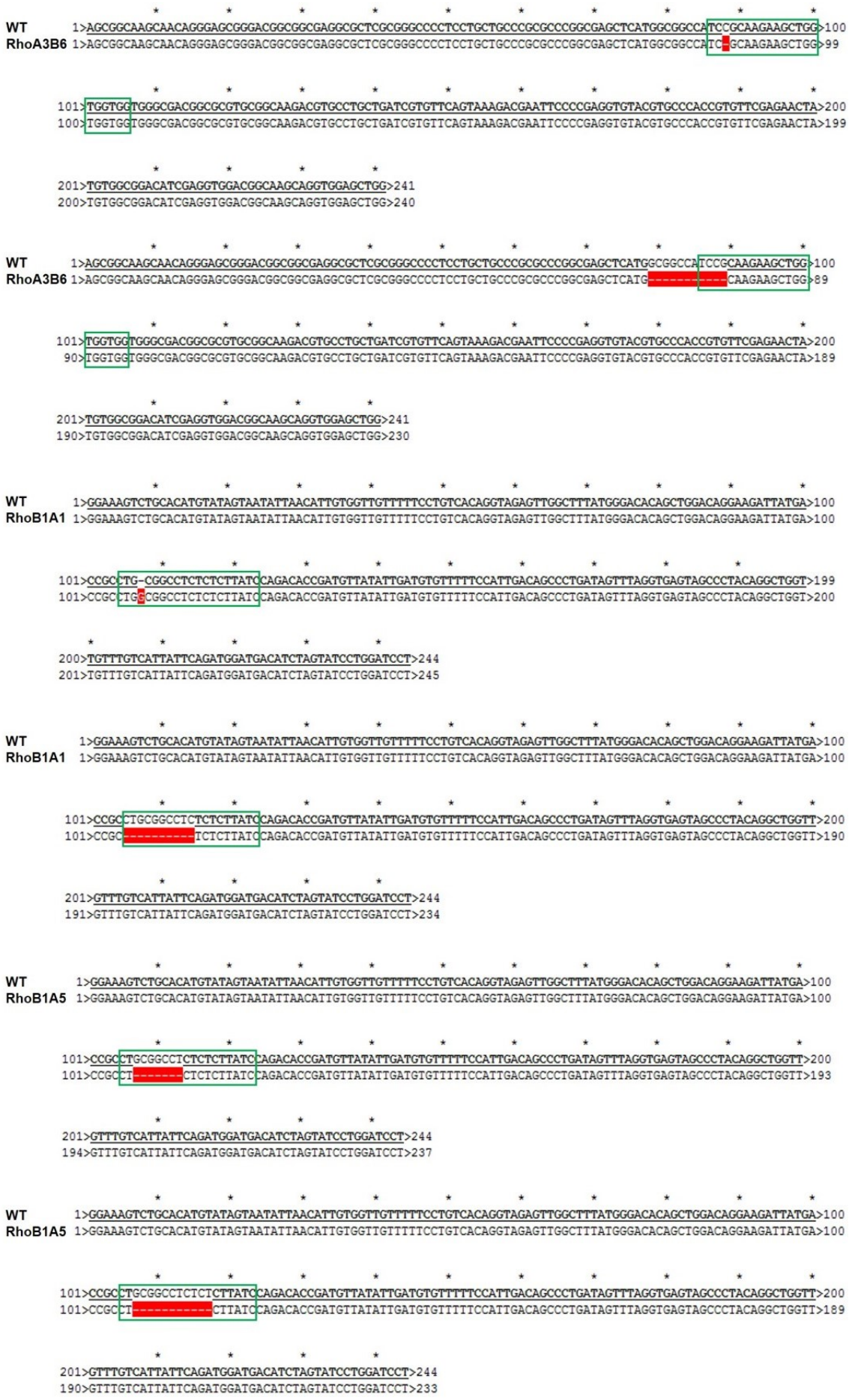

Figure 6.4: DNA sequences of RhoAB double KOs. Sequences of RhoAB double KOs aligned to the respective RhoA or RhoB WT DNA sequence. Green boxes highlight respective target sequences. Mutations are shown in red.

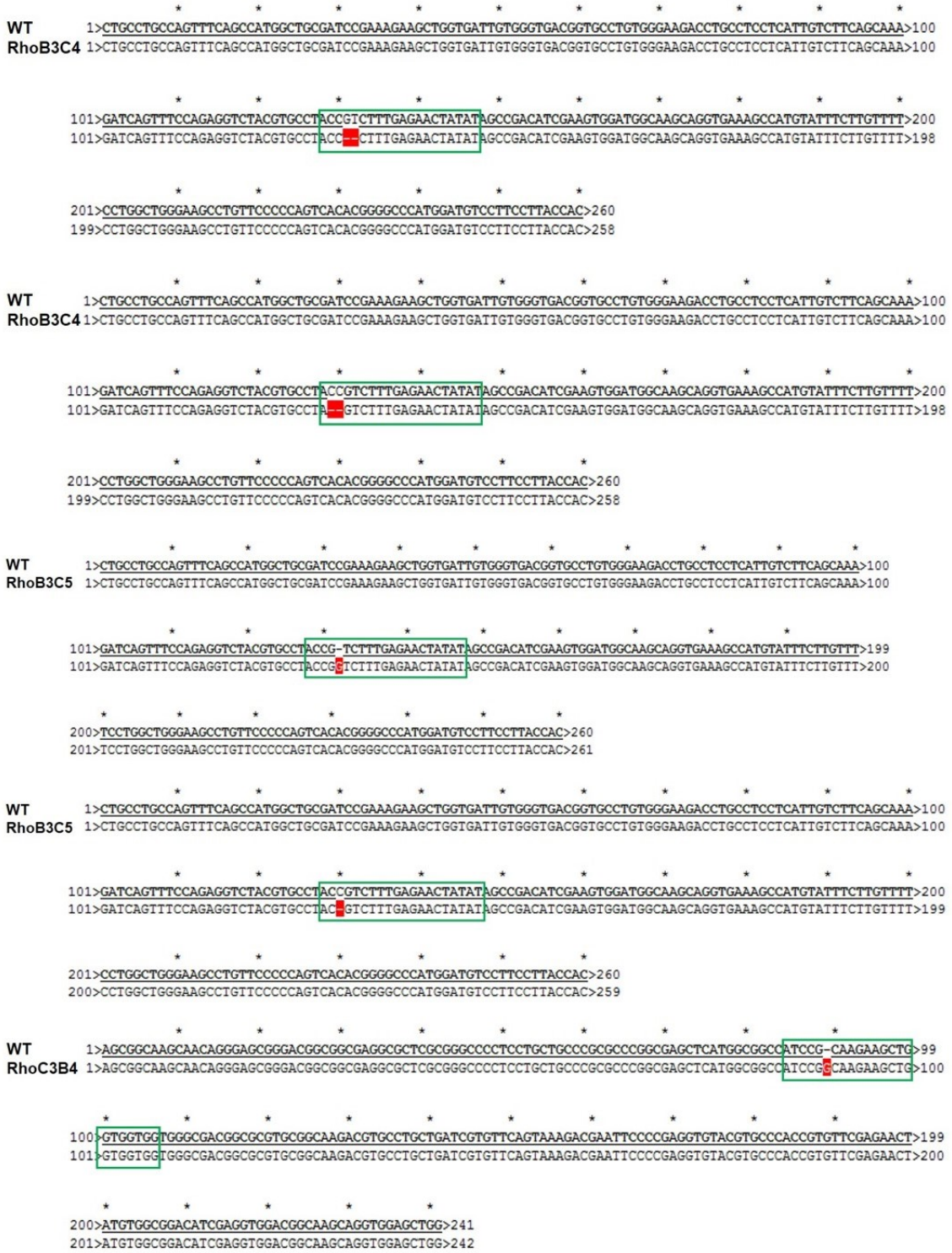

Figure 6.5: DNA sequences of RhoBC double KOs. Sequences of RhoBC double KOs are compared to the respective WT sequences of RhoB or RhoC. Green boxes label respective target sequences and mutations are shown in red. This Figure shows three of four RhoBC double KOs.

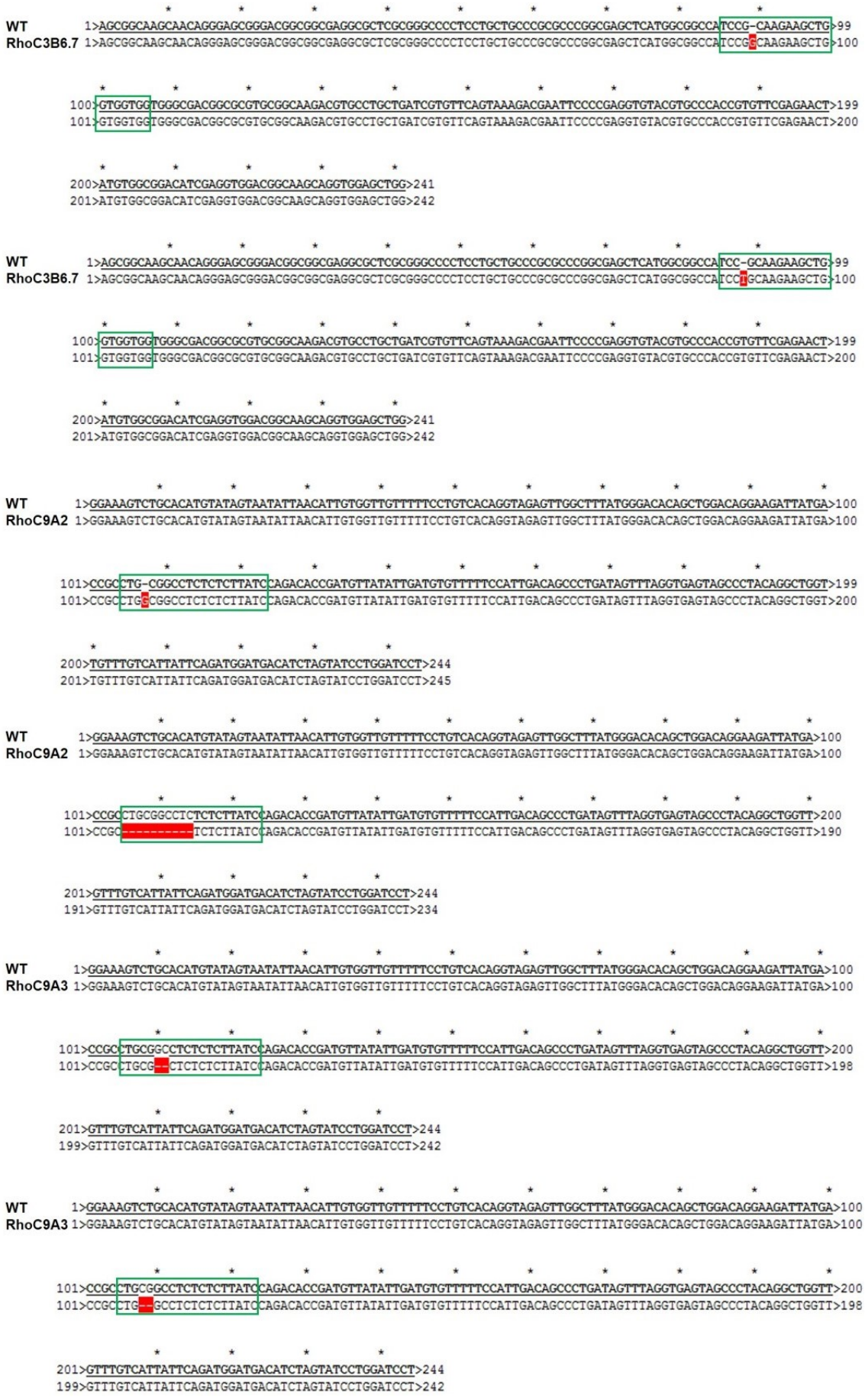

Figure 6.6: DNA sequences of RhoAC double KOs. Sequences of RhoAC double KOs and one RhoBC double KO are aligned to the respective RhoA or RhoB WT DNA sequences. Green boxes highlight respective target sequences. Mutations are shown in red.

Table 6.2: Amino acid sequences of RhoA in WT and RhoA KO cells

Cell line	Sequence
NIH-3T3 WT	MAAIRKKLVIVGDGACGKTCLLIVFSKDQFPEVYVPTVFENYVADIEVDG KQVELALWDTAGQEDYDRLRPLSYPDTDVILMCFSIDSPDSLENIPEKWT PEVKHFCPNVPIILVGNKKDLRNDEHTRRELAKMKQEPVKPEEGRDMA NRIGAFGYMECSAKTKDGVREVFEMATRAALQARRGKKKSGCLIL*
RhoA1 Allele 1	MAAIRKKLVIVGDGACGKTCLLIVFSKDQFPEVYVPTVFENYVADIEVDG KQVELALWDTAGQEDYDRL GLSLIQTPMLY *
RhoA1 Allele 2	MAAIRKKLVIVGDGACGKTCLLIVFSKDQFPEVYVPTVFENYVADIEVDG KQVE FFH *
RhoA2 Allele 1	MAAIRKKLVIVGDGACGKTCLLIVFSKDQFPEVYVPTVFENYVADIEVDG KQVELALWDTAGQEDYDR 6 PDTDVILMCFSIDSPDSLENIPEKWT PEVKHFCPNVPIILVGNKKDLRNDEHTRRELAKMKQEPVKPEEGRDMA NRIGAFGYMECSAKTKDGVREVFEMATRAALQARRGKKKSGCLIL*
RhoA2 Allele 2	MAAIRKKLVIVGDGACGKTCLLIVFSKDQFPEVYVPTVFENYVADIEVDG KQVELALWDTAGQEDY LLSRHRCYIDVFFH *
RhoA3 Allele 1	MAAIRKKLVIVGDGACGKTCLLIVFSKDQFPEVYVPTVFENYVADIEVDG KQVELALWDTAGQEDYD LSLIQTPMLY *
RhoA3 Allele 2	MAAIRKKLVIVGDGACGKTCLLIVFSKDQFPEVYVPTVFENYVADIEVDG KQVELALWDTAGQEDYDRL GLSLIQTPMLY *
RhoB1A1 Allele 1	MAAIRKKLVIVGDGACGKTCLLIVFSKDQFPEVYVPTVFENYVADIEVDG KQVELALWDTAGQEDYDRL AASLLSRHRCYIDVFFH *
RhoB1A1 Allele 2	MAAIRKKLVIVGDGACGKTCLLIVFSKDQFPEVYVPTVFENYVADIEVDG KQVELALWDTAGQEDYDR SLIQTPMLY *
RhoB1A5 Allele 1	MAAIRKKLVIVGDGACGKTCLLIVFSKDQFPEVYVPTVFENYVADIEVDG KQVELALWDTAGQEDYDRLS LIQTPMLY *
RhoB1A5 Allele 2	MAAIRKKLVIVGDGACGKTCLLIVFSKDQFPEVYVPTVFENYVADIEVDG KQVELALWDTAGQEDYDRL LSRHRCYIDVFFH *
RhoC9A2 Allele 1	MAAIRKKLVIVGDGACGKTCLLIVFSKDQFPEVYVPTVFENYVADIEVDG KQVELALWDTAGQEDYDRL AASLLSRHRCYIDVFFH *
RhoC9A2 Allele 2	MAAIRKKLVIVGDGACGKTCLLIVFSKDQFPEVYVPTVFENYVADIEVDG KQVELALWDTAGQEDYDR SLIQTPMLY *
RhoC9A3 Allele 1	MAAIRKKLVIVGDGACGKTCLLIVFSKDQFPEVYVPTVFENYVADIEVDG KQVELALWDTAGQEDYDRLR SLLSRHRCYIDVFFH *
RhoC9A3 Allele 2	MAAIRKKLVIVGDGACGKTCLLIVFSKDQFPEVYVPTVFENYVADIEVDG KQVELALWDTAGQEDYDRL ASLLSRHRCYIDVFFH *

Table 6.3: Amino acid sequences of RhoB in WT and RhoB KO cells

Cell line	Sequence
NIH-3T3 WT	MAAIRKKLVVVGDGACGKTCLLIVFSKDEFPEVYVPTVFENYVADIEVDG KQVELALWDTAGQEDYDRLRPLSYPDTDVILMCFSVDSPDSLENIPEKWV PEVKHFCPNVPIILVANKKDLRSDEHVRTELARMKQEPVRTDDGRAMAVR IQAYDYLECSAKTKEGVREVFETATRAALQKRYGSQNGCINCCKVL*
RhoB1 Allele 1 & 2	MAAIR QEAGGGGRRRVRQDVPADRVQ *
RhoB2.2 Allele 1	MAA GGGGRRRVRQDVPADRVQ *
RhoB2.2 Allele 2	MAAI 3 LVVGDGACGKTCLLIVFSKDEFPEVYVPTVFENYVADIEVDG KQVELALWDTAGQEDYDRLRPLSYPDTDVILMCFSVDSPDSLENIPEKWV PEVKHFCPNVPIILVANKKDLRSDEHVRTELARMKQEPVRTDDGRAMAVR IQAYDYLECSAKTKEGVREVFETATRAALQKRYGSQNGCINCCKVL*
RhoB3 Allele 1	MAAIR QEAGGGGRRRVRQDVPADRVQ *
RhoB3 Allele 2	M QEAGGGGRRRVRQDVPADRVQ *
RhoA3B6 Allele 1	MAAI ARSWWWWATARAARRAC *
RhoA3B6 Allele 2	M QEAGGGGRRRVRQDVPADRVQ *
RhoC3B4 Allele 1 & 2	MAAIR QEAGGGGRRRVRQDVPADRVQ *
RhoC3B6.7 Allele 1	MAAIR QEAGGGGRRRVRQDVPADRVQ *
RhoC3B6.7 Allele 2	MAAI LQEAGGGGRRRVRQDVPADRVQ *

Table 6.4: Amino acid sequences of RhoC in WT and RhoC KO cells

Cell line	Sequence
NIH-3T3 WT	MAAIRKKLVIVGDGACGKTCLLIVFSKDQFPEVYVPTVFENYIADIEVDG KQVELALWDTAGQEDYDRLRPLSYPDTDVILMCFSIDSPDSLENIPEKWT PEVKHFCPNVPIILVGNKKDLRQDEHTRRELAKMKQEPVRSEEGRDMANR ISAFGYLECSAKTKEGVREVFEMATRAGLQVRKNKRRRGCPIL*
RhoC3 Allele 1	MAAIRKKLVIVGDGACGKTCLLIVFSKDQFPE SLRTI *
RhoC3 Allele 2	MAAIRKKLVIVGDGACGKTCLLIVFSKDQFPEVYVP SL *
RhoC6 Allele 1	MAAIRKKLVIVGDGACGKTCLLIVFSKDQFPEVYVPT GL *
RhoC6 Allele 2	MAAIRKKLVIVGDGACGKTCLLIVFSKDQFPEVY 7 YIADIEVDG KQVELALWDTAGQEDYDRLRPLSYPDTDVILMCFSIDSPDSLENIPEKWT PEVKHFCPNVPIILVGNKKDLRQDEHTRRELAKMKQEPVRSEEGRDMANR ISAFGYLECSAKTKEGVREVFEMATRAGLQVRKNKRRRGCPIL*
RhoC9 Allele 1 & 2	MAAIRKKLVIVGDGACGKTCLLIVFSKDQFPEVYVPT GL *
RhoB3C4 Allele 1	MAAIRKKLVIVGDGACGKTCLLIVFSKDQFPEVYVPT L *
RhoB3C4 Allele 2	MAAIRKKLVIVGDGACGKTCLLIVFSKDQFPEVYVP SL *
RhoB3C5 Allele 1	MAAIRKKLVIVGDGACGKTCLLIVFSKDQFPEVYVPT GL *
RhoB3C5 Allele 2	MAAIRKKLVIVGDGACGKTCLLIVFSKDQFPEVYVPT SLRTI *

6.1.3 Expression levels of RhoA, RhoB and RhoC in Rho double KO cells

As addendum to Figure 3.13, Western Blots for Rho double KO cells with specific antibodies for RhoA, RhoB or RhoC are shown in Figure 6.7.

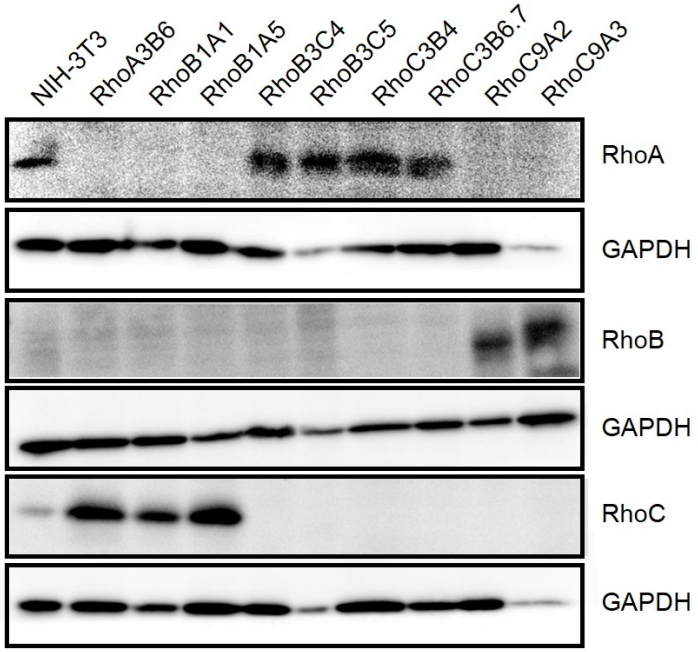

Figure 6.7: Protein expression of RhoA, -B and -C in Rho double KO cells. Cell extracts of Rho double KO cells were analyzed via Western Blotting with RhoA, -B and -C antibodies, as indicated. GAPDH was used as loading control.

6.1.4 Myosin II localization in Rho KO cells

Immunofluorescence stainings of Rho single KOs with myosin IIa and Rho double KOs with myosin IIb are displayed in Figures 6.8 and 6.9, respectively. These data are an addendum to the images shown in chapter 3.3.4.

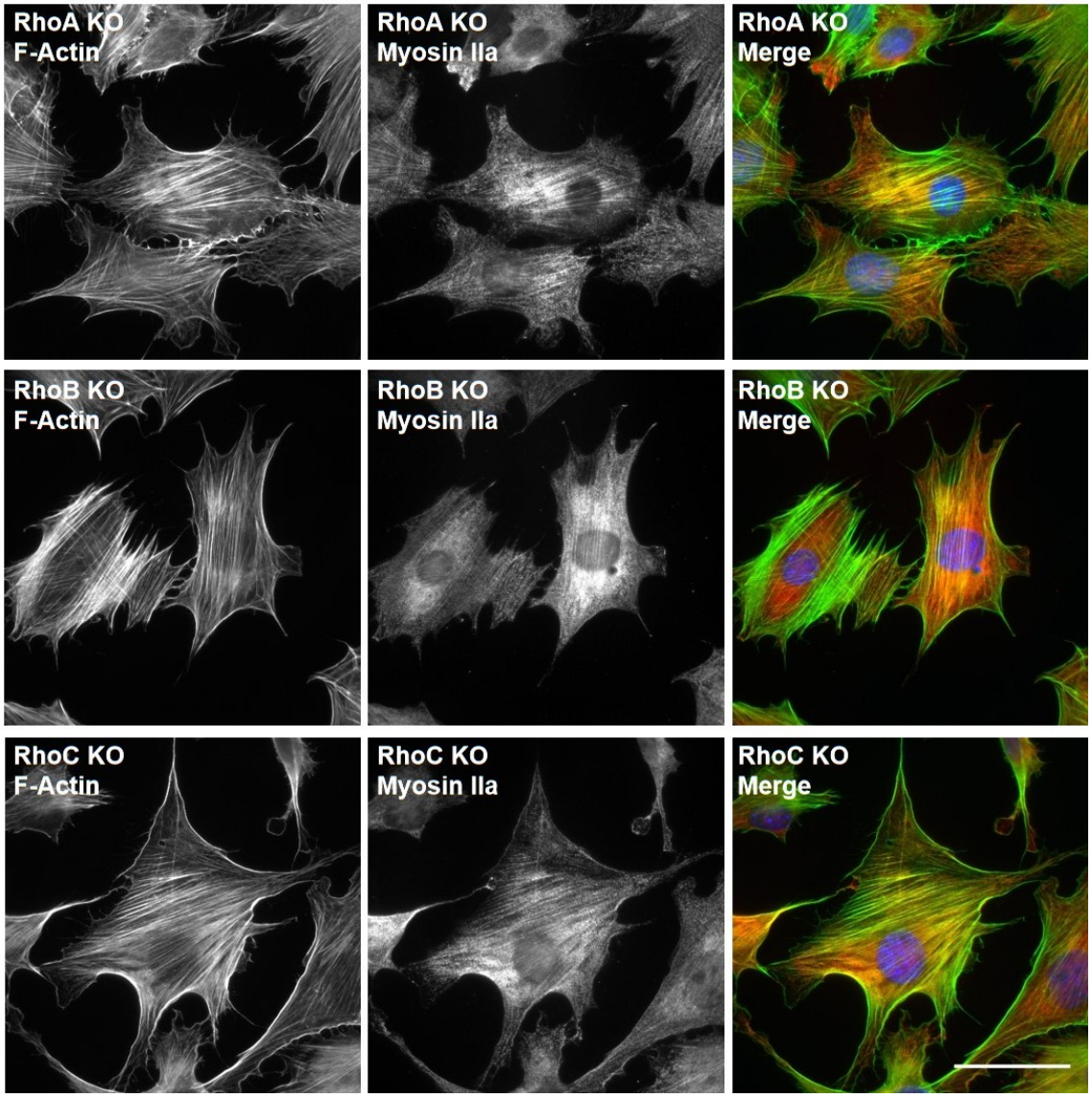

Figure 6.8: Myosin IIa localization in Rho single KOs. Rho single KOs were fixed and stained with phalloidin (green), myosin IIa antibody (red) and DAPI (blue). Figure shows single images for phalloidin and myosin staining together with the merged image including DAPI. Two clones were analyzed per KO condition. Scale bar equals 50 µm.

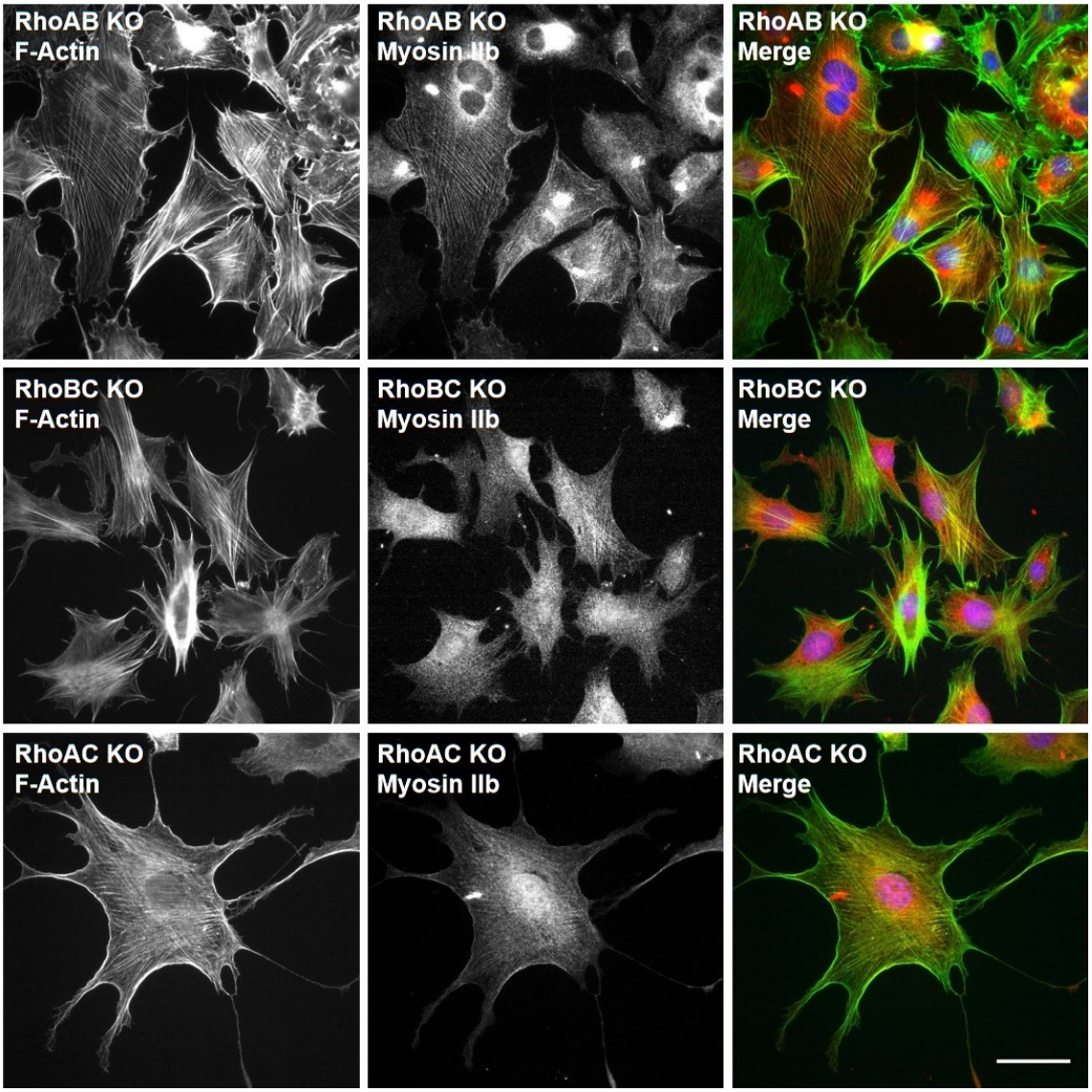

Figure 6.9: Myosin IIb localization in Rho double KOs. Immunofluorescence staining of Rho double KOs after fixation was performed with phalloidin (green), myosin IIb antibody (red) and DAPI (blue). Single images for phalloidin and myosin IIb are displayed, followed by the merged image with DAPI. Two clones per KO phenotype were included in the analysis. Scale bar represents 50 µm.

6.1.5 Cofilin knockdown in Rho KO cells

Immunofluorescence images of Cofilin knockdown in RhoB, RhoC and RhoBC KOs combined with inhibitor treatments for Rho, ROCK, MRCK and myosin II are shown in Figures 6.10, 6.11 and 6.12, respectively. These are supplementary data to the Figures described in chapter 3.3.4.

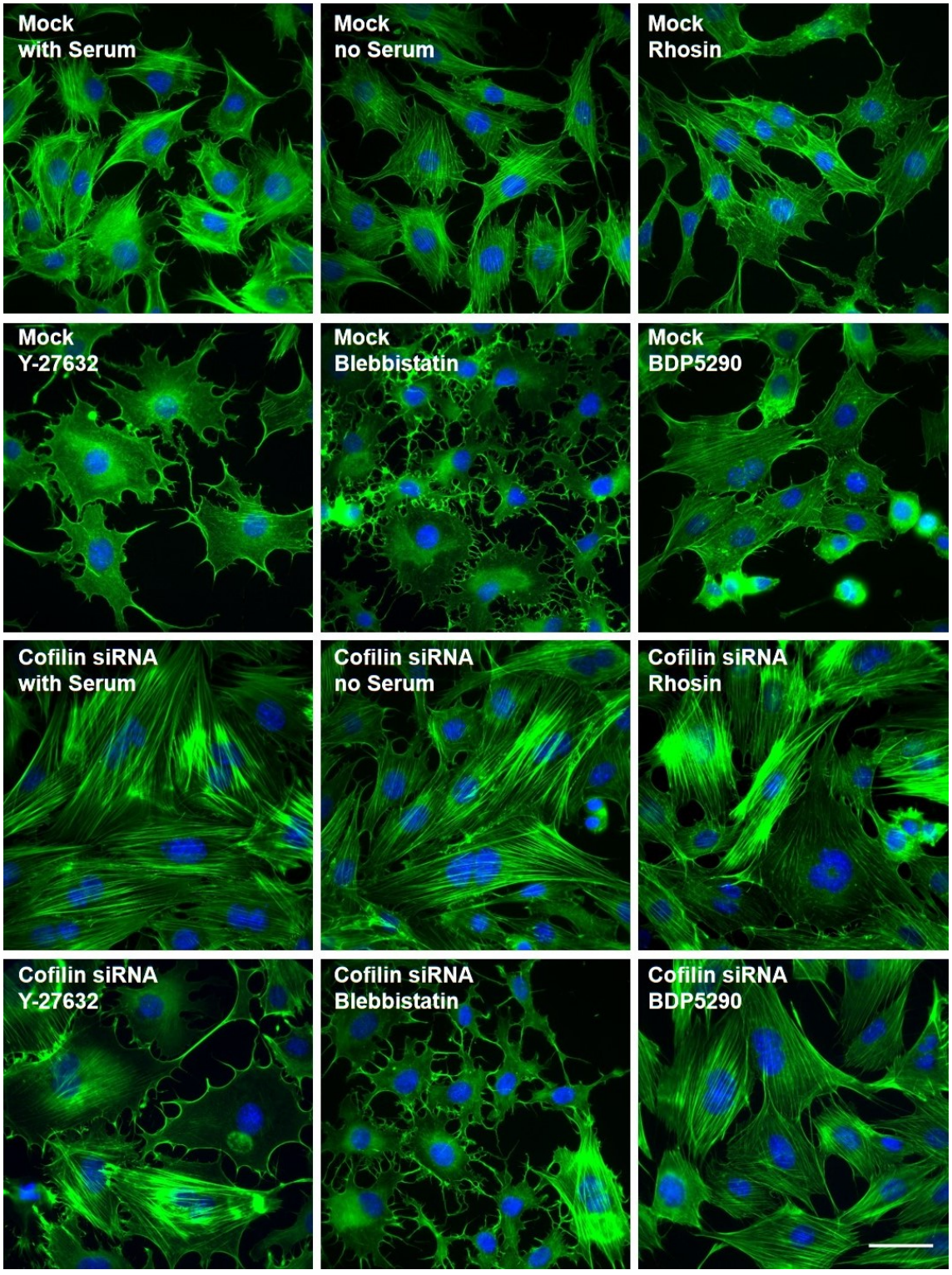

Figure 6.10: Cofilin knockdown in RhoB KOs. RhoB single KO cells were treated with 2.5 μM of Cofilin 1, Cofilin 2 and ADF siRNA one day after seeding of cells and again with 5 μM Cofilin 2 siRNA one day later. Two days after the second transfection, cells were treated with various inhibitors or serum-free medium for 1 hour before fixation. Inhibitors were 200 μM Rhosin to inhibit Rho proteins, 50 μM Y-27632 inhibiting ROCK, 120 μM Blebbistatin to inhibit myosin II and 20 μM BDP5290 inhibiting MRCK. After fixation, cells were stained with phalloidin (green) and DAPI (blue). Figure displays merged images. Two clones were analyzed per KO phenotype. Scale bar shows 50 μm.

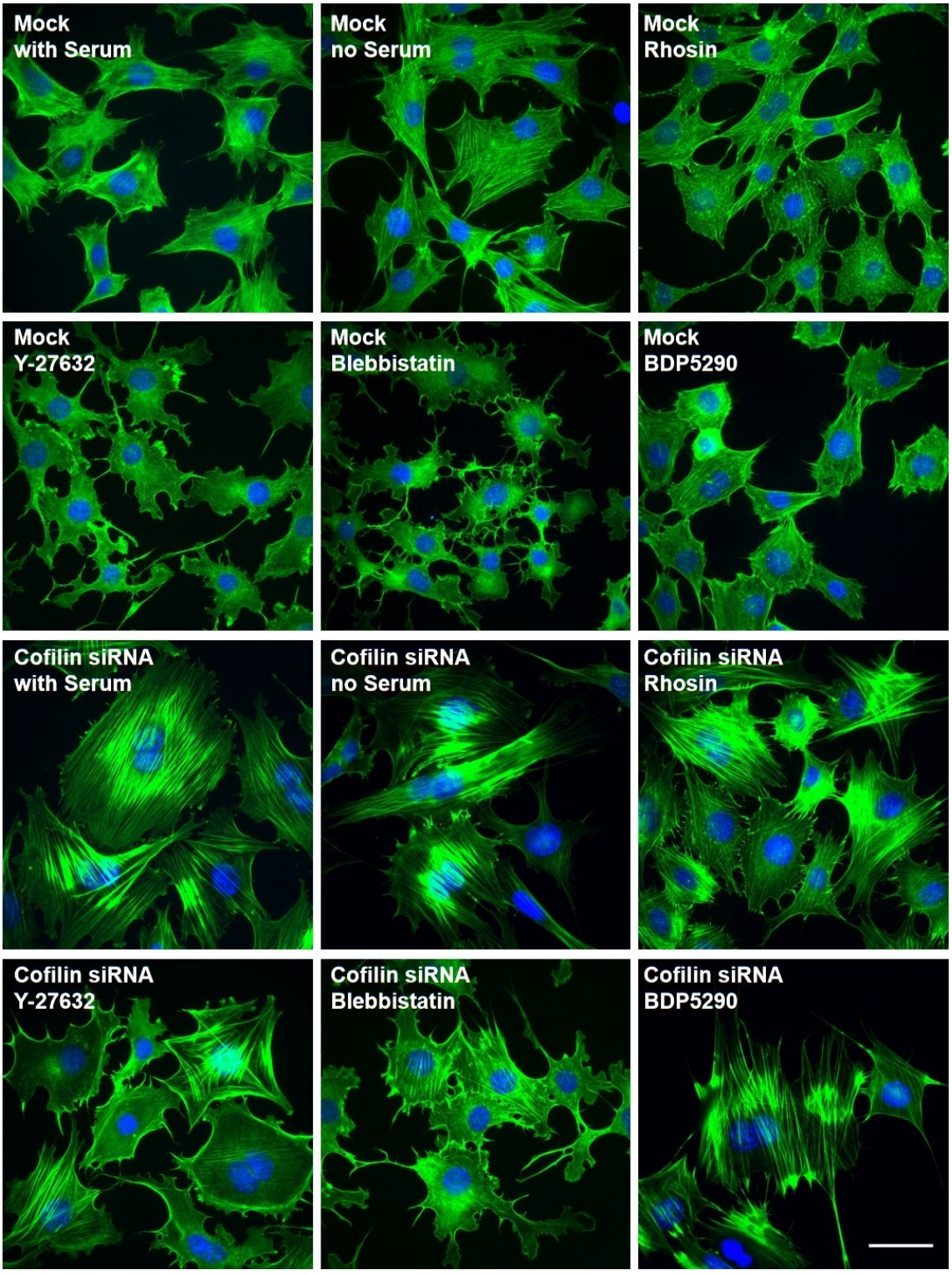

Figure 6.11: Cofilin knockdown in RhoC KOs. One day after seeding of cells, RhoC KOs were transfected with 2.5 µM of Cofilin 1, Cofilin 2 and ADF siRNA. In addition, transfection with 5 µM Cofilin 2 siRNA was performed one day later. Two days after that, cells were treated with various inhibitors or serum-free medium for 1 hour before fixation. Inhibitors were 200 µM Rhosin to inhibit Rho proteins, 50 µM Y-27632 inhibiting ROCK, 120 µM Blebbistatin to inhibit myosin II and 20 µM BDP5290 inhibiting MRCK. After fixation, cells were stained with phalloidin (green) and DAPI (blue). Only merged images are shown. Two clones per KO phenotype were included in the analysis. Scale bar equals 50 µm.

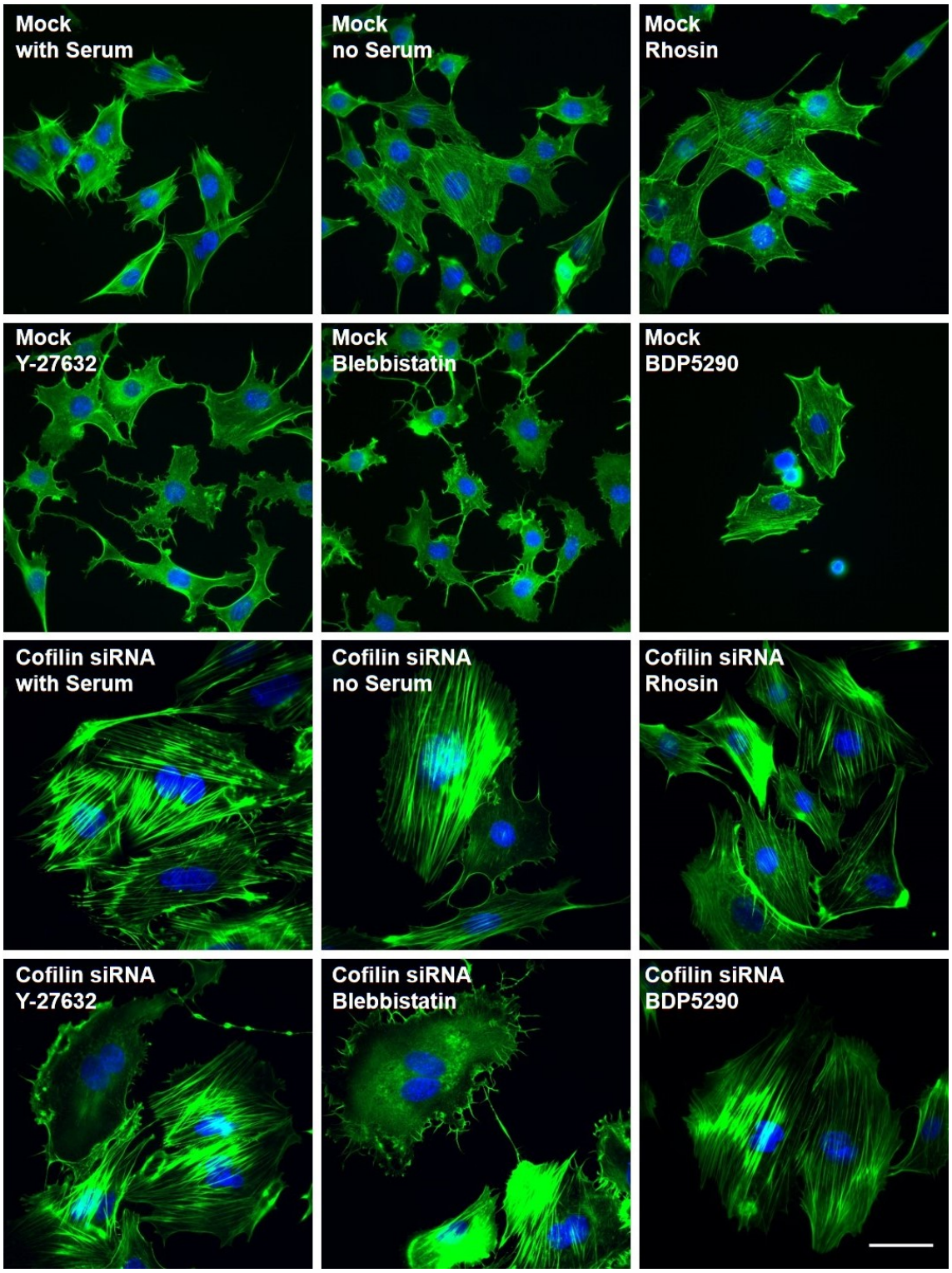

Figure 6.12: Cofilin knockdown in RhoBC KOs. Transfection of RhoBC double KO cells with 2.5 µM of Cofilin 1, Cofilin 2 and ADF siRNA was performed one day after seeding of cells and again with 5 µM Cofilin 2 siRNA one day after that. Two days after the second transfection, cells were treated with various inhibitors or serum-free medium for 1 hour before fixation. Inhibitors were 200 µM Rhosin to inhibit Rho proteins, 50 µM Y-27632 inhibiting ROCK, 120 µM Blebbistatin to inhibit myosin II and 20 µM BDP5290 inhibiting MRCK. Finally, cells were stained with phalloidin (green) and DAPI (blue). Merged images are shown. Two clones per KO phenotype were analyzed. Scale bar displays 50 µm.

6.2 Plasmid Maps

Maps of plasmids used in this study are shown in Figures 6.13, 6.14 and 6.15. The map of restriction sites in Figure 6.14 shows how the PCR product is flanked by EcoRI sites upstream and downstream. Therefore, test digestions before sequencing of potential KO clones were performed with this respective enzyme.

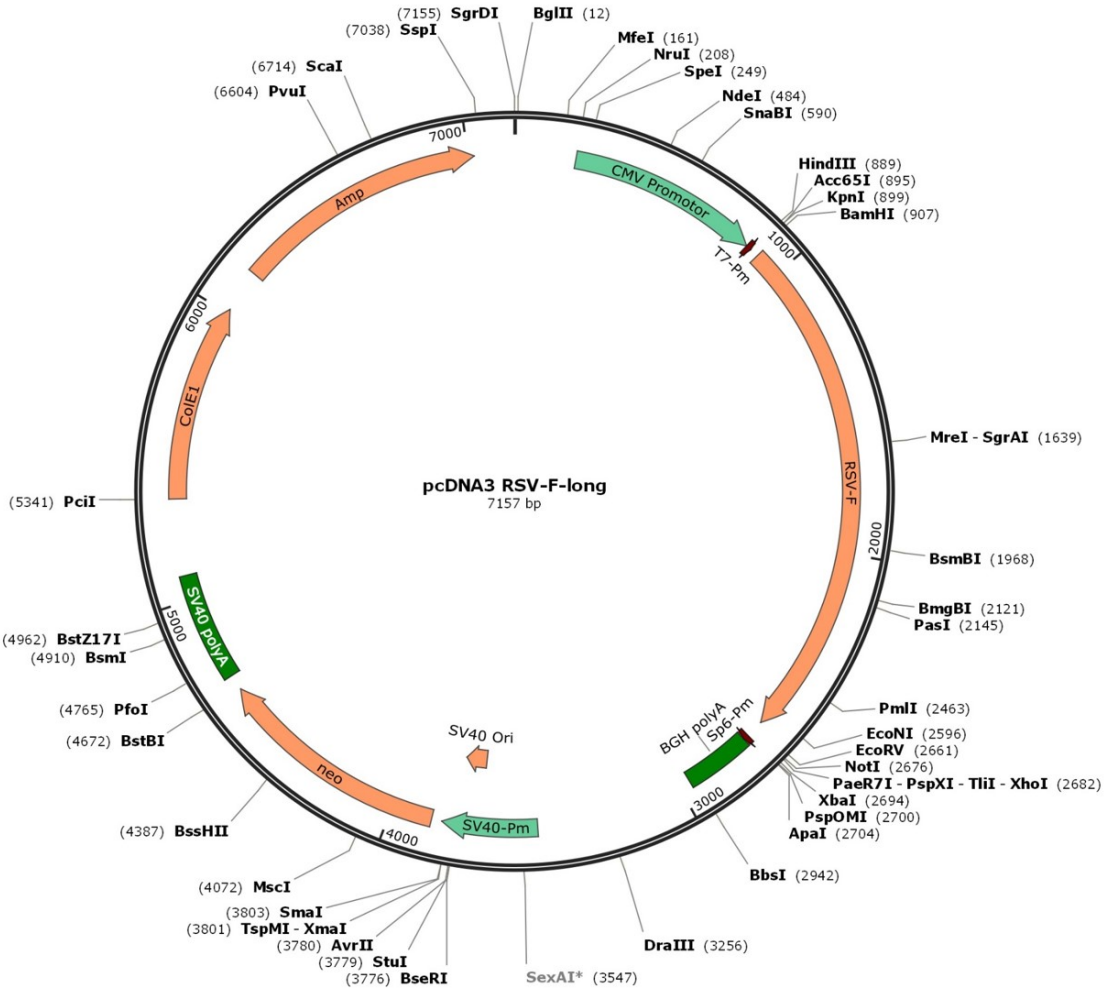

Figure 6.13: pcDNA3 RSV-F. Figure shows pcDNA3 RSV-F, which was kindly provided by the group of T. Pietschmann and cloned by S. Haid (Twincore, Hannover). The RSV-F protein is encoded after a CMV promoter and the plasmid harbors an ampicillin resistance.

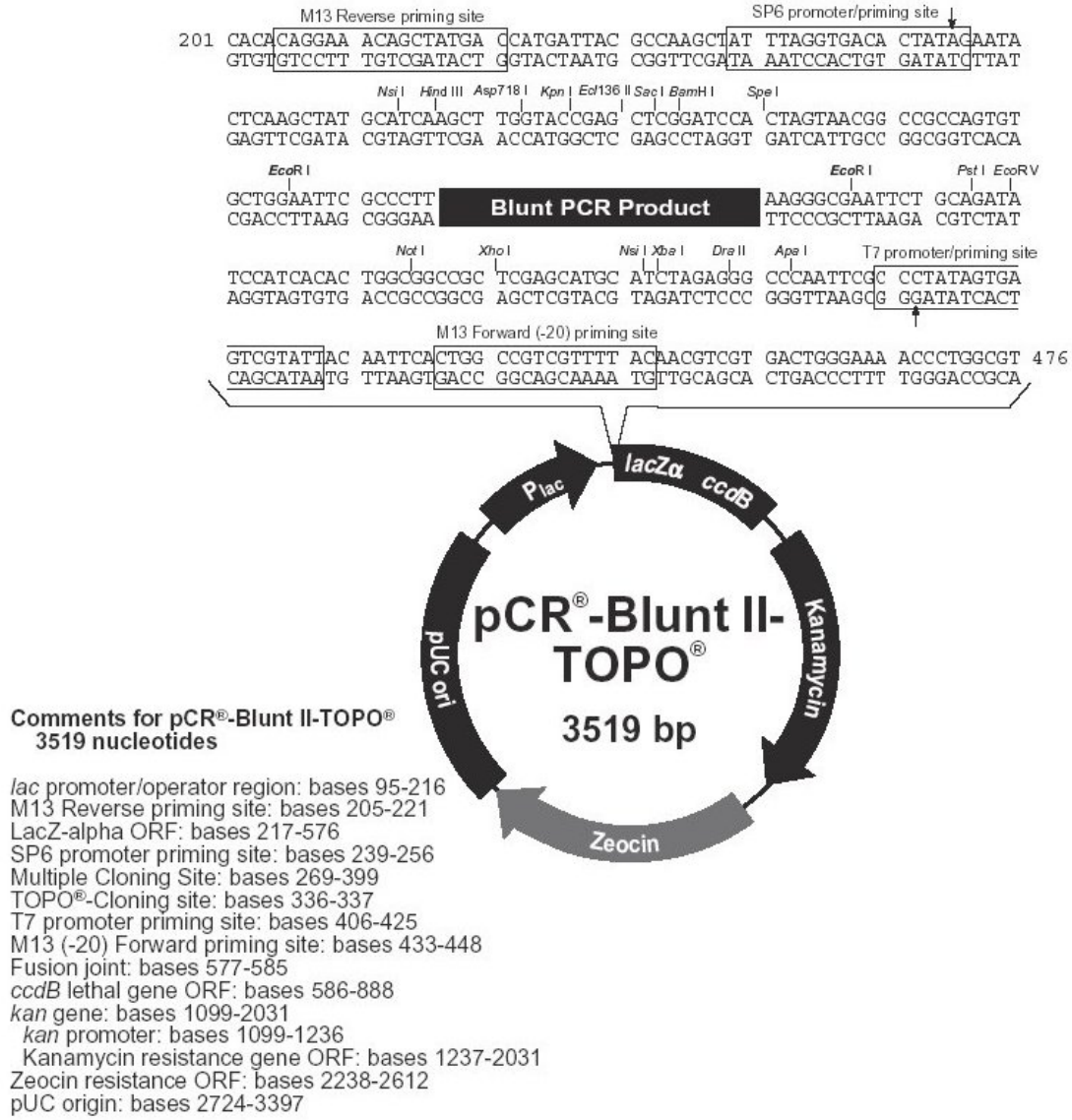

Figure 6.14: pCRBlunt II-TOPO vector. Map of pCRBlunt II-TOPO vector, showing EcoRI restriction sites, which were important for test digestions before sequencing of potential Rho KO clones (Zero Blunt TOPO PCR Cloning Kit - User Guide).

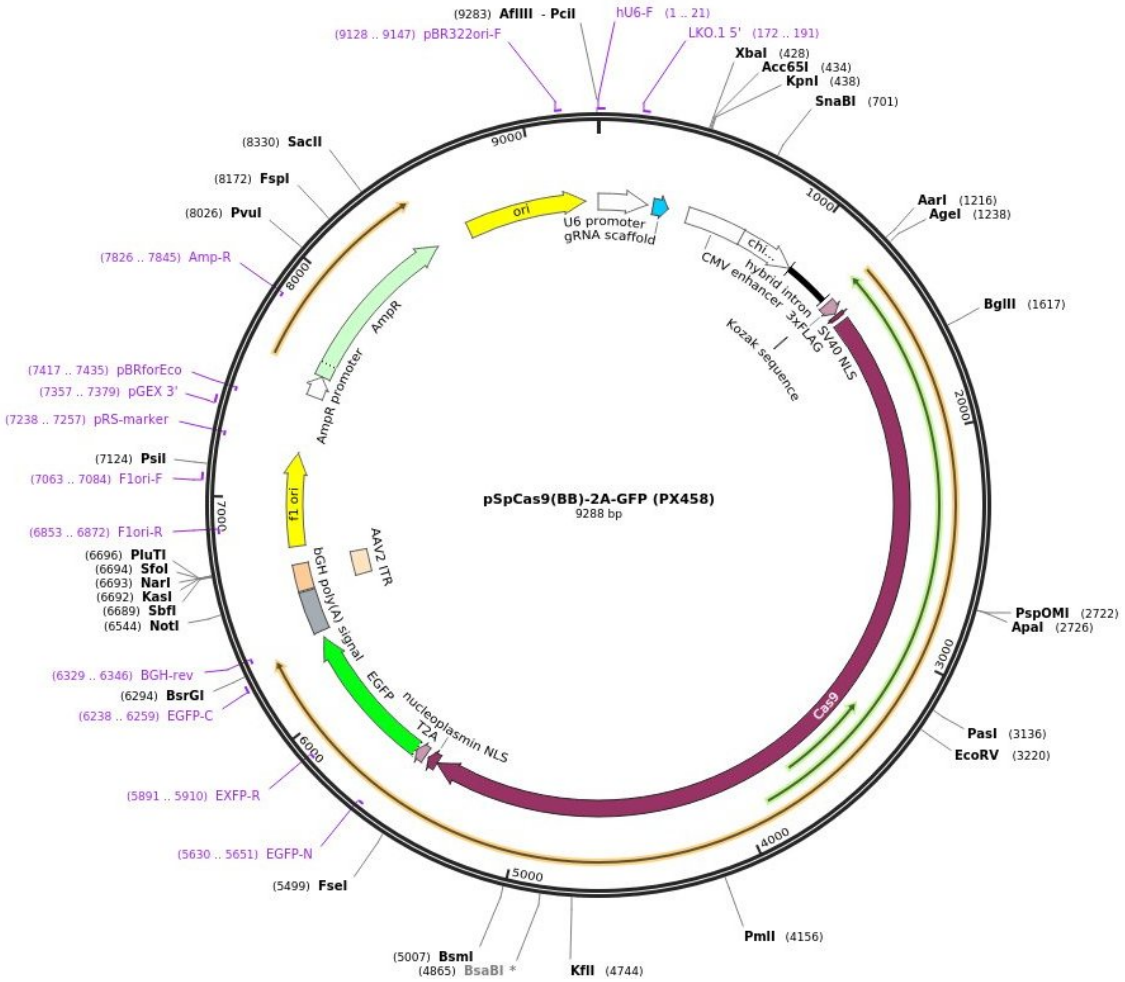

Figure 6.15: pSpCas9(BB)-2A-GFP. Figure shows pSpCas9(BB)-2A-GFP, which was used for CRISPR/Cas9 mediated gene knockout. The plasmid encodes Cas9 nuclease and the GFP protein and harbors a resistance to ampicillin (https://www.addgene.org/48138/) (26.03.2018).

References

[1] Daniele Fanale, Giuseppe Bronte, Francesco Passiglia, Valentina Calò, Marta Castiglia, Florinda Di Piazza, Nadia Barraco, Antonina Cangemi, Maria Teresa Catarella, Lavinia Insalaco, Angela Listì, Rossella Maragliano, Daniela Massihnia, Alessandro Perez, Francesca Toia, Giuseppe Cicero, and Viviana Bazan. Stabilizing versus destabilizing the microtubules: A double-edge sword for an effective cancer treatment option. *Analytical Cellular Pathology (Amsterdam)*, 2015(PMC4592889):690916, September 2015.

[2] Sebastian Baumann, Thomas Pohlmann, Marc Jungbluth, Andreas Brachmann, and Michael Feldbrügge. Kinesin-3 and dynein mediate microtubule-dependent co-transport of mrnps and endosomes. *Journal of Cell Science*, 125(11):2740–2752, 2012.

[3] Johanna Block, Viktor Schroeder, Paul Pawelzyk, Norbert Willenbacher, and Sarah Köster. Physical properties of cytoplasmic intermediate filaments. *Biochimica et Biophysica Acta (BBA) - Molecular Cell Research*, 1853(11):3053–3064, nov 2015.

[4] Martin McCullagh, Marissa Saunders, and Gregory A. Voth. Unraveling the mystery of atp hydrolysis in actin filaments. *Journal of the American Chemical Society*, 136(PMC4183606):13053–13058, July 2014.

[5] Akhshi Tara Kafiyeh, Wernike Denise, and Piekny Alisa. Microtubules and actin crosstalk in cell migration and division. *Cytoskeleton*, 71(1):1–23, 2013.

[6] E Reichstein and E D Korn. Acanthamoeba profilin. a protein of low molecular weight from acanpthamoeba castellanii that inhibits actin nucleation. *Journal of Biological Chemistry*, 254(13):6174–6179, 1979.

[7] Colleen T. Skau and Clare M. Waterman. Specification of architecture and function of actin structures by actin nucleation factors. *Annual Review of Biophysics*, 44(1):285–310, jun 2015.

[8] Suk Namgoong, Malgorzata Boczkowska, Michael J. Glista, Jonathan D. Winkelman, Grzegorz Rebowski, David R. Kovar, and Roberto Dominguez. Mechanism of actin filament nucleation by vibrio vopl and implications for tandem w domain nucleation. *Nature Structural &Amp; Molecular Biology*, 18:1060, August 2011.

[9] Tatyana M. Svitkina and Gary G. Borisy. Arp2/3 complex and actin depolymerizing factor/cofilin in dendritic organization and treadmilling of actin filament array in lamellipodia. *The Journal of Cell Biology*, 145(PMC2133125):1009–1026, April 1999.

[10] Robert C. Robinson, Kirsi Turbedsky, Donald A. Kaiser, Jean-Baptiste Marchand, Henry N. Higgs, Senyon Choe, and Thomas D. Pollard. Crystal structure of arp2/3 complex. *Science*, 294(5547):1679–1684, 2001.

[11] Theresia EB Stradal and Giorgio Scita. Protein complexes regulating arp2/3-mediated actin assembly. *Current Opinion in Cell Biology*, 18(1):4 – 10, 2006. Cell structure and dynamics.

[12] Jaime Fernández-Barrera and Miguel A. Alonso. Coordination of microtubule acetylation and the actin cytoskeleton by formins. *Cellular and Molecular Life Sciences*, Jun 2018.

[13] Sonja Kühn and Matthias Geyer. Formins as effector proteins of rho gtpases. *Small GTPases*, 5(PMC4111664):e29513, June 2014.

[14] Naoki Watanabe, Takayuki Kato, Akiko Fujita, Toshimasa Ishizaki, and Shuh Narumiya. Cooperation between mdia1 and rock in rho-induced actin reorganization. *Nature Cell Biology*, 1:136, June 1999.

[15] Stéphanie Pellegrin and Harry Mellor. The rho family gtpase rif induces filopodia through mdia2. *Current Biology*, 15(2):129–133, January 2005.

[16] Tamás Matusek, Rita Gombos, Anita Szécsényi, Natalia Sánchez-Soriano, Ágnes Czibula, Csilla Pataki, Anita Gedai, Andreas Prokop, István Raskó, and József Mihály. Formin proteins of the daam subfamily play a role during axon growth. *J. Neurosci.*, 28(49):13310, December 2008.

[17] Shinri Yayoshi-Yamamoto, Ichiro Taniuchi, and Takeshi Watanabe. Frl, a novel formin-related protein, binds to rac and regulates cell motility and survival of macrophages. *Molecular and Cellular Biology*, 20(PMC86228):6872–6881, June 2000.

[18] Jennifer Block, Dennis Breitsprecher, Sonja Kühn, Moritz Winterhoff, Frieda Kage, Robert Geffers, Patrick Duwe, Jennifer L. Rohn, Buzz Baum, Cord Brakebusch, Matthias Geyer, Theresia E. B. Stradal, Jan Faix, and Klemens Rottner. Fmnl2 drives actin-based protrusion and migration downstream of cdc42. *Current Biology*, 22(PMC3765947):1005–1012, March 2012.

[19] Judith E. Gasteier, Ricardo Madrid, Ellen Krautkrämer, Sebastian Schröder, Walter Muranyi, Serge Benichou, and Oliver T. Fackler. Activation of the rac-binding partner fhod1 induces actin stress fibers via a rock-dependent mechanism. *Journal of Biological Chemistry*, 278(40):38902–38912, 2003.

[20] André Schönichen, Hans Georg Mannherz, Elmar Behrmann, Antonina J. Mazur, Sonja Kühn, Unai Silván, Cora-Ann Schoenenberger, Oliver T. Fackler, Stefan Raunser, Leif Dehmelt, and Matthias Geyer. Fhod1 is a combined actin filament capping and bundling factor that selectively associates with actin arcs and stress fibers. *J. Cell Sci.*, 126(8):1891, April 2013.

[21] Grzegorz Rebowski, Malgorzata Boczkowska, David B. Hayes, Liang Guo, Thomas C. Irving, and Roberto Dominguez. X-ray scattering study of actin polymerization nuclei assembled by tandem w domains. *Proceedings of the National Academy of Sciences*, 105(31):10785–10790, 2008.

[22] Praveen Suraneni, Boris Rubinstein, Jay R. Unruh, Michael Durnin, Dorit Hanein, and Rong Li. The arp2/3 complex is required for lamellipodia extension and directional fibroblast cell migration. *The Journal of Cell Biology*, 197(2):239–251, 2012.

[23] Congying Wu, Sreeja B. Asokan, Matthew E. Berginski, Elizabeth M. Haynes, Norman E. Sharpless, Jack D. Griffith, Shawn M. Gomez, and James E. Bear. Arp2/3 is critical for lamellipodia and response to extracellular matrix cues but is dispensable for chemotaxis. *Cell*, 148(5):973–987, mar 2012.

[24] Janet H. Iwasa and R. Dyche Mullins. Spatial and temporal relationships between actin-filament nucleation, capping, and disassembly. *Current biology : CB*, 17(PMC3077992):395–406, March 2007.

[25] Guillaume Jacquemet, Hellyeh Hamidi, and Johanna Ivaska. Filopodia in cell adhesion, 3d migration and cancer cell invasion. *Current Opinion in Cell Biology*, 36:23 – 31, 2015. Cell adhesion and migration.

[26] Valeri Vasioukhin, Christoph Bauer, Mei Yin, and Elaine Fuchs. Directed actin polymerization is the driving force for epithelial cell-cell adhesion. *Cell*, 100(2):209 – 219, 2000.

[27] Matthew P. Taylor, Orkide O. Koyuncu, and Lynn W. Enquist. Subversion of the actin cytoskeleton during viral infection. *Nature Reviews Microbiology*, 9:427, April 2011.

[28] Elias Lazarides and Keith Burridge. α-actinin: Immunofluorescent localization of a muscle structural protein in nonmuscle cells. *Cell*, 6(3):289 – 298, 1975.

[29] Klaus Weber and Ute Groeschel-Stewart. Antibody to myosin: The specific visualization of myosin-containing filaments in nonmuscle cells. *Proceedings of the National Academy of Sciences of the United States of America*, 71(PMC433927):4561–4564, November 1974.

[30] G. Isenberg, P. C. Rathke, N. Hülsmann, W. W. Franke, and K. E. Wohlfarth-Bottermann. Cytoplasmic actomyosin fibrils in tissue culture cells. *Cell and Tissue Research*, 166(4):427–443, Feb 1976.

[31] Kazuo Katoh, Yumiko Kano, Michitaka Masuda, Hirofumi Onishi, and Keigi Fujiwara. Isolation and contraction of the stress fiber. *Molecular Biology of the Cell*, 9(PMC25437):1919–1938, April 1998.

[32] J. Victor Small, K. Rottner, I. Kaverina, and K. I. Anderson. Assembling an actin cytoskeleton for cell attachment and movement. *Biochimica et Biophysica Acta (BBA) - Molecular Cell Research*, 1404(3):271–281, September 1998.

[33] Pirta Hotulainen and Pekka Lappalainen. Stress fibers are generated by two distinct actin assembly mechanisms in motile cells. *The Journal of Cell Biology*, 173(3):383–394, may 2006.

[34] Eli Zamir and Benjamin Geiger. Molecular complexity and dynamics of cell-matrix adhesions. *Journal of Cell Science*, 114(20):3583–3590, 2001.

[35] Dylan T. Burnette, Lin Shao, Carolyn Ott, Ana M. Pasapera, Robert S. Fischer, Michelle A. Baird, Christelle Der Loughian, Helene Delanoe-Ayari, Matthew J. Paszek, Michael W. Davidson, Eric Betzig, and Jennifer Lippincott-Schwartz. A contractile and counterbalancing adhesion system controls the 3d shape of crawling cells. *The Journal of Cell Biology*, 205(PMC3987145):83–96, March 2014.

[36] Catherine D Nobes and Alan Hall. Rho, rac, and cdc42 gtpases regulate the assembly of multimolecular focal complexes associated with actin stress fibers, lamellipodia, and filopodia. *Cell*, 81(1):53 – 62, 1995.

[37] Anne J. Ridley, Hugh F. Paterson, Caroline L. Johnston, Dagmar Diekmann, and Alan Hall. The small gtp-binding protein rac regulates growth factor-induced membrane ruffling. *Cell*, 70(3):401 – 410, 1992.

[38] A. Steffen, M. Ladwein, G. A. Dimchev, A. Hein, L. Schwenkmezger, S. Arens, K. I. Ladwein, J. M. Holleboom, F. Schur, J. V. Small, J. Schwarz, R. Gerhard, J. Faix, T. E. B. Stradal, C. Brakebusch, and K. Rottner. Rac function is crucial for cell migration but is not required for spreading and focal adhesion formation. *Journal of Cell Science*, 126(20):4572–4588, July 2013.

[39] B. Brett Finlay and Stanley Falkow. Salmonella interactions with polarized human intestinal caco-2 epithelial cells. *The Journal of Infectious Diseases*, 162(5):1096–1106, 1990.

[40] S. Pellegrin and H. Mellor. Actin stress fibres. *Journal of Cell Science*, 120(20):3491–3499, oct 2007.

[41] Campbell D. Lawson and Anne J. Ridley. Rho GTPase signaling complexes in cell migration and invasion. *The Journal of Cell Biology*, 217(2):447–457, dec 2017.

[42] Sandrine Etienne-Manneville and Alan Hall. Rho gtpases in cell biology. *Nature*, 420:629–35, 01 2003.

[43] Kent L. Rossman, Channing J. Der, and John Sondek. GEF means go: turning on RHO GTPases with guanine nucleotide-exchange factors. *Nature Reviews Molecular Cell Biology*, 6(2):167–180, feb 2005.

[44] Jason T. Snyder, David K. Worthylake, Kent L. Rossman, Laurie Betts, Wendy M. Pruitt, David P. Siderovski, Channing J. Der, and John Sondek. Structural basis for the selective activation of rho gtpases by dbl exchange factors. *Nature Structural Biology*, 9:468, May 2002.

[45] Björn U. Klink, Stephan Barden, Thomas V. Heidler, Christina Borchers, Markus Ladwein, Theresia E. B. Stradal, Klemens Rottner, and Dirk W. Heinz. Structure of shigellaipgb2 in complex with human rhoa. *Journal of Biological Chemistry*, 285(22):17197–17208, apr 2010.

[46] Jing Yang, Ziguo Zhang, S. Mark Roe, Christopher J. Marshall, and David Barford. Activation of rho gtpases by dock exchange factors is mediated by a nucleotide sensor. *Science*, 325(5946):1398–1402, 2009.

[47] Natasha K. Hussain, Sarah Jenna, Michael Glogauer, Christopher C. Quinn, Sylwia Wasiak, Michel Guipponi, Stylianos E. Antonarakis, Brian K. Kay, Thomas P. Stossel, Nathalie Lamarche-Vane, and Peter S. McPherson. Endocytic protein intersectin-l regulates actin assembly via cdc42 and n-wasp. *Nature Cell Biology*, 3:927, September 2001.

[48] Csépányi-Kömi Roland, Pásztor Máté, Bartos Balázs, and Ligeti Erzsébet. The neglected terminators: Rho family gaps in neutrophils. *European Journal of Clinical Investigation*, 0(ja):e12993, 2018.

[49] Etienne Boulter, Rafael Garcia-Mata, Christophe Guilluy, Adi Dubash, Guendalina Rossi, Patrick J. Brennwald, and Keith Burridge. Regulation of rho GTPase crosstalk, degradation and activity by RhoGDI1. *Nature Cell Biology*, 12(5):477–483, apr 2010.

[50] Patrick J. Roberts, Natalia Mitin, Patricia J. Keller, Emily J. Chenette, James P. Madigan, Rachel O. Currin, Adrienne D. Cox, Oswald Wilson, Paul Kirschmeier, and Channing J. Der. Rho family GTPase modification and dependence on CAAXMotif-signaled posttranslational modification. *Journal of Biological Chemistry*, 283(37):25150–25163, jul 2008.

[51] Yoshihiro Fukumoto, Kozo Kaibuchi, Yasuhiro Hori, Hisashi Fujioka, Shin Araki, Takashi Ueda, Akira Kikuchi, and Yoshimi Takai. Molecular cloning and characterization of a novel type of regulatory protein (gdi) for the rho proteins, ras p21-like small gtp-binding proteins. *Oncogene*, 5 9:1321–8, 1990.

[52] J. V. Platko, D. A. Leonard, C. N. Adra, R. J. Shaw, R. A. Cerione, and B. Lim. A single residue can modify target-binding affinity and activity of the functional domain of the rho-subfamily gdp dissociation inhibitors. *Proceedings of the National Academy of Sciences of the United States of America*, 92(PMC42341):2974–2978, March 1995.

[53] Rafael Garcia-Mata, Etienne Boulter, and Keith Burridge. The invisible hand: regulation of rho gtpases by rhogdis. *Nature Reviews. Molecular Cell Biology*, 12(PMC3260518):493–504, July 2011.

[54] Brunet Nicolas, Morin Annie, and Olofsson Birgitta. Rhogdi-3 regulates rhog and targets this protein to the golgi complex through its unique n-terminal domain. *Traffic*, 3(5):342–358, 2002.

[55] Linda A. Cannizzaro, Pascal Madaule, Frederick Hecht, Richard Axel, Carlo M. Croce, and Kay Huebner. Chromosome localization of human arh genes, a ras-related gene family. *Genomics*, 6(2):197 – 203, 1990.

[56] Ann P. Wheeler and Anne J. Ridley. Why three rho proteins? rhoa, rhob, rhoc, and cell motility. *Experimental Cell Research*, 301(1):43 – 49, 2004. Cytoskeleton Special Review Issue.

[57] Gerhard Fritz, Bernd Kaina, and Klaus Aktories. The ras-related small gtp-binding protein rhob is immediate-early inducible by dna damaging treatments. *Journal of Biological Chemistry*, 270(42):25172–25177, 1995.

[58] G. Zalcman, V. Closson, G. Linares-Cruz, F. Lerebours, N. Honore, A. Tavitian, and B. Olofsson. Regulation of ras-related rhob protein expression during the cell cycle. *Oncogene*, 10:1935–45, May 1995.

[59] Alexandra Gampel and Harry Mellor. Small interfering rnas as a tool to assign rho gtpase exchange-factor function in vivo. *Biochem.*, pages 393–398, 2002.

[60] Harry Mellor, Peter Flynn, Catherine D. Nobes, Alan Hall, and Peter J. Parker. Prk1 is targeted to endosomes by the small gtpase, rhob. *The Journal of Biological Chemistry*, 273(9):4811–4814, 1998.

[61] M. Fernandez-Borja. RhoB regulates endosome transport by promoting actin assembly on endosomal membranes through dia1. *Journal of Cell Science*, 118(12):2661–2670, jun 2005.

[62] Francesc Miralles, Guido Posern, Alexia-Ileana Zaromytidou, and Richard Treisman. Actin dynamics control srf activity by regulation of its coactivator mal. *Cell*, 113(3):329–342, May 2003.

[63] Hongpeng He, Zhaoqiang Wei, Fu Du, Chao Meng, Deliang Zheng, Yongwei Lai, Hailin Yao, Hao Zhou, Nan Wang, Xue-Gang Luo, Wenjian Ma, and Tong-Cun Zhang. Transcription of hotair is regulated by rhoc-mrtf-a-srf signaling pathway in human breast cancer cells. *Cellular Signalling*, 31:87 – 95, 2017.

[64] Mei Wu, Zhi-Fen Wu, Chandan Kumar-Sinha, Arul Chinnaiyan, and Sofia D. Merajver. Rhoc induces differential expression of genes involved in invasion and metastasis in mcf10a breast cells. *Breast Cancer Research and Treatment 84(1): 3-12*, 2004.

[65] Malvyne Rolli-Derkinderen, Vincent Sauzeau, Laurent Boyer, Emmanuel Lemichez, Céline Baron, Daniel Henrion, Gervaise Loirand, and Pierre Pacaud. Phosphorylation of serine 188 protects rhoa from

ubiquitin/proteasome-mediated degradation in vascular smooth muscle cells. *Circulation Research*, 96(11):1152–1160, 2005.

[66] P. Lang, F. Gesbert, M. Delespine-Carmagnat, R. Stancou, M. Pouchelet, and J. Bertoglio. Protein kinase a phosphorylation of rhoa mediates the morphological and functional effects of cyclic amp in cytotoxic lymphocytes. *The EMBO Journal*, 15(3):510–519, February 1996.

[67] Vanessa Tillement, Isabelle Lajoie-Mazenc, Anne Casanova, Carine Froment, Marie Penary, Daniel Tovar, Rudolfo Marquez, Bernard Monsarrat, Gilles Favre, and Anne Pradines. Phosphorylation of rhob by ck1 impedes actin stress fiber organization and epidermal growth factor receptor stabilization. *Experimental Cell Research*, 314(15):2811 – 2821, 2008.

[68] Quintin Pan, Li Wei Bao, Theodoros N. Teknos, and Sofia D. Merajver. Targeted disruption of protein kinase cε reduces cell invasion and motility through inactivation of rhoa and rhoc gtpases in head and neck squamous cell carcinoma. *Cancer research*, 66(PMC4383316):9379–9384, October 2006.

[69] T. Ishizaki, M. Maekawa, K. Fujisawa, K. Okawa, A. Iwamatsu, A. Fujita, N. Watanabe, Y. Saito, A. Kakizuka, N. Morii, and S. Narumiya. The small gtp-binding protein rho binds to and activates a 160 kda ser/thr protein kinase homologous to myotonic dystrophy kinase. *The EMBO Journal*, 15(8):1885–1893, April 1996.

[70] Linda Truebestein, Daniel J. Elsner, and Thomas A. Leonard. Made to measure - keeping rho kinase at a distance. *Small GTPases*, 7(2):82–92, March 2016.

[71] Mutsuki Amano, Kazuyasu Chihara, Kazushi Kimura, Yuko Fukata, Nao Nakamura, Yoshiharu Matsuura, and Kozo Kaibuchi. Formation of actin stress fibers and focal adhesions enhanced by rho-kinase. *Science*, 275(5304):1308–1311, 1997.

[72] Takekazu Kubo, Atsushi Yamaguchi, Nobuyoshi Iwata, and Toshihide Yamashita. The therapeutic effects of rho-rock inhibitors on cns disorders. *Therapeutics and Clinical Risk Management*, 4(PMC2500253):605–615, June 2008.

[73] Mutsuki Amano, Masanori Nakayama, and Kozo Kaibuchi. Rho-kinase/rock: A key regulator of the cytoskeleton and cell polarity. *Cytoskeleton (Hoboken, N.j.)*, 67(PMC3038199):545–554, July 2010.

[74] Miguel Vicente-Manzanares, Xuefei Ma, Robert S. Adelstein, and Alan Rick Horwitz. Non-muscle myosin ii takes centre stage in cell adhesion and migration. *Nature reviews. Molecular cell biology*, 10(11):778–790, November 2009.

[75] Mihály Kovács, Fei Wang, Aihua Hu, Yue Zhang, and James R. Sellers. Functional divergence of human cytoplasmic myosin II. *Journal of Biological Chemistry*, 278(40):38132–38140, jul 2003.

[76] Fei Wang, Mihály Kovács, Aihua Hu, John Limouze, Estelle V. Harvey, and James R. Sellers. Kinetic mechanism of non-muscle myosin IIB. *Journal of Biological Chemistry*, 278(30):27439–27448, apr 2003.

[77] Miguel Vicente-Manzanares, Margaret A. Koach, Leanna Whitmore, Marcelo L. Lamers, and Alan F. Horwitz. Segregation and activation of myosin iib creates a rear in migrating cells. *The Journal of Cell Biology*, 183(3):543–554, October 2008.

[78] Neil Billington, Aibing Wang, Jian Mao, Robert S. Adelstein, and James R. Sellers. Characterization of three full-length human nonmuscle myosin II paralogs. *Journal of Biological Chemistry*, 288(46):33398–33410, sep 2013.

[79] S Lee and S Kumar. Actomyosin stress fiber mechanosensing in 2d and 3d [version 1; referees: 3 approved]. *F1000Research*, 5(2261), 2016.

[80] J R Sellers, E Eisenberg, and R S Adelstein. The binding of smooth muscle heavy meromyosin to actin in the presence of atp. effect of phosphorylation. *Journal of Biological Chemistry*, 257(23):13880–3, 1982.

[81] M. Chrzanowska-Wodnicka. Rho-stimulated contractility drives the formation of stress fibers and focal adhesions. *The Journal of Cell Biology*, 133(6):1403–1415, jun 1996.

[82] S. Tojkander, G. Gateva, and P. Lappalainen. Actin stress fibers - assembly, dynamics and biological roles. *Journal of Cell Science*, 125(8):1855–1864, apr 2012.

[83] Takako Kaneko-Kawano, Fugo Takasu, Honda Naoki, Yuichi Sakumura, Shin Ishii, Takahiro Ueba, Akinori Eiyama, Aiko Okada, Yoji Kawano, and Kenji Suzuki. Dynamic regulation of myosin light chain phosphorylation by rho-kinase. *PLoS ONE*, 7(6):e39269, jun 2012.

[84] Simon Wilkinson, Hugh F. Paterson, and Christopher J. Marshall. Cdc42–MRCK and rho–ROCK signalling cooperate in myosin phosphorylation and cell invasion. *Nature Cell Biology*, 7(3):255–261, feb 2005.

[85] Fumio Matsumura. Regulation of myosin ii during cytokinesis in higher eukaryotes. *Trends in Cell Biology*, 15(7):371–377, July 2005.

[86] Jose Javier Bravo-Cordero, Marco A. O. Magalhaes, Robert J. Eddy, Louis Hodgson, and John Condeelis. Functions of cofilin in cell locomotion and invasion. *Nature reviews. Molecular cell biology*, 14(7):10.1038/nrm3609, June 2013.

[87] O'Neil Wiggan, Alisa E. Shaw, Jennifer G. DeLuca, and James R. Bamburg. Adf/cofilin regulates actomyosin assembly through competitive inhibition of myosin ii binding to f-actin. *Developmental Cell*, 22(3):530–543, March 2012.

[88] Cristian Suarez, Jérémy Roland, Rajaa Boujemaa-Paterski, Hyeran Kang, Brannon R. McCullough, Anne-Cécile Reymann, Christophe Guérin, Jean-Louis Martiel, Enrique M. De La Cruz, and Laurent Blanchoin. Cofilin modulates the nucleotide state of actin filaments and severs at boundaries of bare and decorated segments. *Current biology : CB*, 21(10):862–868, April 2011.

[89] Shoichiro Ono. Functions of actin-interacting protein 1 (AIP1)/WD repeat protein 1 (WDR1) in actin filament dynamics and cytoskeletal regulation. *Biochemical and Biophysical Research Communications*, oct 2017.

[90] Hugo Wioland, Berengere Guichard, Yosuke Senju, Sarah Myram, Pekka Lappalainen, Antoine Jégou, and Guillaume Romet-Lemonne. Adf/cofilin accelerates actin dynamics by severing filaments and promoting their depolymerization at both ends. *Current Biology*, 27(13):1956–1967.e7, May 2017.

[91] Samantha M. Chin, Silvia Jansen, and Bruce L. Goode. Tirf microscopy analysis of human cof1, cof2, and adf effects on actin filament severing and turnover. *Journal of Molecular Biology*, 428(8):1604 – 1616, 2016.

[92] Kyoko Okada, Laurent Blanchoin, Hiroshi Abe, Hui Chen, Thomas D. Pollard, and James R. Bamburg. XenopusActin-interacting protein 1 (XAip1) enhances cofilin fragmentation of filaments by capping filament ends. *Journal of Biological Chemistry*, 277(45):43011–43016, jun 2002.

[93] Silvia Jansen, Agnieszka Collins, Samantha M. Chin, Casey A. Ydenberg, Jeff Gelles, and Bruce L. Goode. Single-molecule imaging of a three-component ordered actin disassembly mechanism. *Nature Communications*, 6:7202, May 2015.

[94] W. Austin Elam, Hyeran Kang, and Enrique M. De La Cruz. Competitive displacement of cofilin can promote actin filament severing. *Biochemical and Biophysical Research Communications*, 438(4):728 – 731, 2013.

[95] Aggeli Dimitra, Kish-Trier Erik, Lin Meng Chi, Haarer Brian, Cingolani Gino, Cooper John A., Wilkens Stephan, and Amberg David C. Coordination of the filament stabilizing versus destabilizing activities of cofilin through its secondary binding site on actin. *Cytoskeleton*, 71(6):361–379, 2014.

[96] Xiaoyan Song, Xiaoming Chen, Hideki Yamaguchi, Ghassan Mouneimne, John S. Condeelis, and Robert J. Eddy. Initiation of cofilin activity in response to egf is uncoupled from cofilin phosphorylation and dephosphorylation in carcinoma cells. *Journal of Cell Science*, 119(14):2871–2881, 2006.

[97] Midori Maekawa, Toshimasa Ishizaki, Shuken Boku, Naoki Watanabe, Akiko Fujita, Akihiro Iwamatsu, Takashi Obinata, Kazumasa Ohashi, Kensaku Mizuno, and Shuh Narumiya. Signaling from rho to the actin cytoskeleton through protein kinases rock and lim-kinase. *Science*, 285(5429):895–898, 1999.

[98] Tomoyuki Sumi, Kunio Matsumoto, Akihiro Shibuya, and Toshikazu Nakamura. Activation of LIM kinases by myotonic dystrophy kinase-related cdc42-binding kinase α. *Journal of Biological Chemistry*, 276(25):23092–23096, may 2001.

[99] Jose Javier Bravo-Cordero, Ved P. Sharma, Minna Roh-Johnson, Xiaoming Chen, Robert Eddy, John Condeelis, and Louis Hodgson. Spatial regulation of rhoc activity defines protrusion formation in migrating cells. *Journal of Cell Science*, 126(15):3356–3369, April 2013.

[100] Yi Xiao, Haixia Ma, Ping Wan, Dandan Qin, Xiaoxiao Wang, Xiaoxin Zhang, Yunlong Xiang, Wenbo Liu, Jiong Chen, Zhaohong Yi, and Lei Li. Trp-asp (WD) repeat domain 1 is essential for mouse peri-implantation development and regulates cofilin phosphorylation. *Journal of Biological Chemistry*, 292(4):1438–1448, dec 2016.

[101] Vitaliy Y. Gorbatyuk, Neil J. Nosworthy, Scott A. Robson, Naresh P. S. Bains, Mark W. Maciejewski, Cris G. dos Remedios, and Glenn F. King. Mapping the phosphoinositide-binding site on chick cofilin explains how pip2 regulates the cofilin-actin interaction. *Molecular Cell*, 24(4):511–522, November 2006.

[102] Megan Chircop. Rho gtpases as regulators of mitosis and cytokinesis in mammalian cells. *Small GTPases*, 5(PMC4160341):e29770, June 2014.

[103] Helen K. Matthews, Ulysse Delabre, Jennifer L. Rohn, Jochen Guck, Patricia Kunda, and Buzz Baum. Changes in ect2 localization couple actomyosin-dependent cell shape changes to mitotic progression. *Developmental Cell*, 23(PMC3763371):371–383, June 2012.

[104] Arkadi Manukyan, Kirsten Ludwig, Sergio Sanchez-Manchinelly, Sarah J. Parsons, and P. Todd Stukenberg. A complex of p190rhogap-a and anillin modulates rhoa-gtp and the cytokinetic furrow in human cells. *Journal of Cell Science*, 128(PMC4282047):50–60, October 2014.

[105] Sadanori Watanabe, Tihana De Zan, Toshimasa Ishizaki, and Shuh Narumiya. Citron kinase mediates transition from constriction to abscission through its coiled-coil domain. *Journal of Cell Science*, 126(8):1773–1784, 2013.

[106] Marta Gai, Paola Camera, Alessandro Dema, Federico Bianchi, Gaia Berto, Elena Scarpa, Giulia Germena, and Ferdinando Di Cunto. Citron kinase controls abscission through rhoa and anillin. *Molecular Biology of the Cell*, 22(20):3768–3778, August 2011.

[107] Masakazu Yamazaki, Yue Zhang, Hiroshi Watanabe, Takeaki Yokozeki, Sigeo Ohno, Kozo Kaibuchi, Hideki Shibata, Hideyuki Mukai, Yoshitaka Ono, Michael A. Frohman, and Yasunori Kanaho. Interaction of the small g protein rhoa with the c terminus of human phospholipase d1. *Journal of Biological Chemistry*, 274(10):6035–6038, 1999.

[108] Kumiko Oishi, Mikiko Takahashi, Hideyuki Mukai, Yoshiko Banno, Shigeru Nakashima, Yasunori Kanaho, Yoshinori Nozawa, and Yoshitaka Ono. Pkn regulates phospholipase d1 through direct interaction. *Journal of Biological Chemistry*, 276(21):18096–18101, 2001.

[109] G. M. Jenkins and M. A. Frohman. Phospholipase d: a lipid centric review. *Cellular and Molecular Life Sciences*, 62(19-20):2305–2316, sep 2005.

[110] Lee Sang Do, Lee Byoung Dae, Han Jung Min, Kim Jae Ho, Kim Yong, Suh Pann-Ghill, and Ryu Sung Ho. Phospholipase d2 activity suppresses hydrogen peroxide-induced apoptosis in pc12 cells. *Journal of Neurochemistry*, 75(3):1053–1059, 2002.

[111] Alexandra Gampel, Peter J. Parker, and Harry Mellor. Regulation of epidermal growth factor receptor traffic by the small gtpase rhob. *Current Biology*, 9(17):955 – 958, 1999.

[112] Mei Ann Lim, Linda Yang, Yi Zheng, Hong Wu, Lily Q Dong, and Feng Liu. Roles of PDK-1 and PKN in regulating cell migration and cortical actin formation of PTEN-knockout cells. *Oncogene*, 23(58):9348–9358, nov 2004.

[113] Neal M. Alto, Feng Shao, Cheri S. Lazar, Renee L. Brost, Gordon Chua, Seema Mattoo, Stephen A. McMahon, Partho Ghosh, Timothy R. Hughes, Charles Boone, and Jack E. Dixon. Identification of a bacterial type III effector family with g protein mimicry functions. *Cell*, 124(1):133–145, jan 2006.

[114] Janet E. Deane, Patrizia Abrusci, Steven Johnson, and Susan M. Lea. Timing is everything: the regulation of type iii secretion. *Cellular and Molecular Life Sciences*, 67(PMC2835726):1065–1075, December 2009.

[115] Theresia E. B. Stradal and Mario Schelhaas. Actin dynamics in host-pathogen interaction. *FEBS Letters*, jul 2018.

[116] L H Su and Cheng-Hsun Chiu. Salmonella: clinical importance and evolution of nomenclature. *Chang Gung medical journal*, 30 3:210–9, 2007.

[117] Anamaria M. P. dos Santos, Rafaela G. Ferrari, and Carlos A. Conte-Junior. Virulence factors in salmonella typhimurium: The sagacity of a bacterium. *Current Microbiology*, may 2018.

[118] Shannon E. Majowicz, Jennie Musto, Elaine Scallan, Frederick J. Angulo, Martyn Kirk, Sarah J. O'Brien, Timothy F. Jones, Aamir Fazil, and

Robert M. Hoekstra. The global burden of nontyphoidal salmonella gastroenteritis. *Clinical Infectious Diseases*, 50(6):882–889, 2010.

[119] Hiroyuki Hata, Tatsuya Natori, Takuya Mizuno, Izumi Kanazawa, Ibrahim Eldesouky, Masahiro Hayashi, Machiko Miyata, Hajime Fukunaga, Shoko Ohji, Akira Hosoyama, Eiji Aono, Atsushi Yamazoe, Keiko Tsuchikane, Nobuyuki Fujita, and Takayuki Ezaki. Phylogenetics of family enterobacteriaceae and proposal to reclassify escherichia hermannii and salmonella subterranea as atlantibacter hermannii and atlantibacter subterranea gen. nov., comb. nov. *Microbiology and Immunology*, 60(5):303–311, 2016.

[120] Hui Zeng, Adam Q. Carlson, Yanwen Guo, Yimin Yu, Lauren S. Collier-Hyams, James L. Madara, Andrew T. Gewirtz, and Andrew S. Neish. Flagellin is the major proinflammatory determinant of enteropathogenic salmonella. *The Journal of Immunology*, 171(7):3668–3674, 2003.

[121] Emma J McGhie, Lyndsey C Brawn, Peter J Hume, Daniel Humphreys, and Vassilis Koronakis. Salmonella takes control: effector-driven manipulation of the host. *Current Opinion in Microbiology*, 12(1):117 – 124, 2009. Host-Microbe Interactions: Bacteria.

[122] Waterman Scott R. and Holden David W. Functions and effectors of the salmonella pathogenicity island 2 type iii secretion system. *Cellular Microbiology*, 5(8):501–511, 2003.

[123] Susanne Mirold, Wolfgang Rabsch, Manfred Rohde, Silke Stender, Helmut Tschäpe, Holger Rüssmann, Emeka Igwe, and Wolf-Dietrich Hardt. Isolation of a temperate bacteriophage encoding the type iii effector protein sope from an epidemic salmonella typhimurium strain. *Proceedings of the National Academy of Sciences of the United States of America*, 96(17):9845–9850, April 1999.

[124] Wolf-Dietrich Hardt, Li-Mei Chen, Kornel E. Schuebel, Xosé R. Bustelo, and Jorge E. Galán. S. typhimurium encodes an activator of rho gtpases that induces membrane ruffling and nuclear responses in host cells. *Cell*, 93(5):815–826, May 1998.

[125] Gretel Buchwald, Andrea Friebel, Jorge E. Galán, Wolf-Dietrich Hardt, Alfred Wittinghofer, and Klaus Scheffzek. Structural basis for the reversible activation of a rho protein by the bacterial toxin sope. *The EMBO Journal*, 21(13):3286–3295, May 2002.

[126] Konark Mukherjee, Seetharaman Parashuraman, Manoj Raje, and Amitabha Mukhopadhyay. Sope acts as an rab5-specific nucleotide exchange factor and recruits non-prenylated rab5 on salmonella-containing phagosomes to promote fusion with early endosomes. *Journal of Biological Chemistry*, 276(26):23607–23615, apr 2001.

[127] Shehla Hashim, Konark Mukherjee, Manoj Raje, Sandip K. Basu, and Amitabha Mukhopadhyay. Live salmonella modulate expression of rab proteins to persist in a specialized compartment and escape transport to lysosomes. *Journal of Biological Chemistry*, 275(21):16281–16288, 2000.

[128] C. S. Bakshi, V. P. Singh, M. W. Wood, P. W. Jones, T. S. Wallis, and E. E. Galyov. Identification of sope2, a salmonella secreted protein which is highly homologous to sope and involved in bacterial invasion of epithelial cells. *Journal of Bacteriology*, 182(8):2341–2344, January 2000.

[129] Stender Silke, Friebel Andrea, Linder Stefan, Rohde Manfred, Mirold Susanne, and Hardt Wolf-Dietrich. Identification of sope2 from salmonella typhimurium, a conserved guanine nucleotide exchange factor for cdc42 of the host cell. *Molecular Microbiology*, 36(6):1206–1221, 2000.

[130] A.S. Sechi and J. Wehland. The actin cytoskeleton and plasma membrane connection: Ptdins(4,5)p(2) influences cytoskeletal protein activity at the plasma membrane. *Journal of Cell Science*, 113(21):3685–3695, 2000.

[131] Carolyn A. Worby and Jack E. Dixon. Sorting out the cellular functions of sorting nexins. *Nature Reviews Molecular Cell Biology*, 3:919, December 2002.

[132] David Liebl, Xiaying Qi, Yang Zhe, Timothy C. Barnett, and Rohan D. Teasdale. Sopb-mediated recruitment of snx18 facilitates salmonella typhimurium internalization by the host cell. *Frontiers in Cellular and Infection Microbiology*, 7:257, May 2017.

[133] Piscatelli Heather L., Li Menghan, and Zhou Daoguo. Dual 4- and 5-phosphatase activities regulate sopb-dependent phosphoinositide dynamics to promote bacterial entry. *Cellular Microbiology*, 18(5):705–719, 2016.

[134] Defne Yarar, Clare M. Waterman-Storer, and Sandra L. Schmid. Snx9 couples actin assembly to phosphoinositide signals and is required for membrane remodeling during endocytosis. *Developmental Cell*, 13(1):43–56, July 2007.

[135] Hänisch Jan, Ehinger Julia, Ladwein Markus, Rohde Manfred, Derivery Emmanuel, Bosse Tanja, Steffen Anika, Bumann Dirk, Misselwitz Benjamin, Hardt Wolf-Dietrich, Gautreau Alexis, Stradal Theresia E. B., and Rottner Klemens. Molecular dissection of salmonella-induced membrane ruffling versus invasion. *Cellular Microbiology*, 12(1):84–98, 2010.

[136] Jan Hänisch, Robert Kölm, Milena Wozniczka, Dirk Bumann, Klemens Rottner, and Theresia E.B. Stradal. Activation of a RhoA/myosin II-dependent but arp2/3 complex-independent pathway facilitates salmonella invasion. *Cell Host & Microbe*, 9(4):273–285, apr 2011.

[137] Leann Clark, Charlotte A. Perrett, Layla Malt, Caryn Harward, Suzanne Humphrey, Katy A. Jepson, Isabel Martinez-Argudo, Laura J. Carney,

Roberto M. La Ragione, Tom J. Humphrey, and Mark A. Jepson. Differences in salmonella enterica serovar typhimurium strain invasiveness are associated with heterogeneity in spi-1 gene expression. *Microbiology*, 157(PMC3167892):2072–2083, April 2011.

[138] Jan Hänisch, Theresia E.B. Stradal, and Klemens Rottner. A novel contractility pathway operating in salmonella invasion. *Virulence*, 3(1):81–86, 2012. PMID: 22286705.

[139] Ila F.N. Lima, Alexandre Havt, and Aldo A.M. Lima. Update on molecular epidemiology of shigella infection. *Current Opinion in Gastroenterology*, 31(1):30–37, jan 2015.

[140] P. J. Sansonetti, D. J. Kopecko, and S. B. Formal. Involvement of a plasmid in the invasive ability of shigella flexneri. *Infection and Immunity*, 35(PMC351125):852–860, March 1982.

[141] Michinaga Ogawa, Yutaka Handa, Hiroshi Ashida, Masato Suzuki, and Chihiro Sasakawa. The versatility of shigella effectors. *Nature Reviews Microbiology*, 6:11, January 2008.

[142] N. High, J. Mounier, M. C. Prévost, and P. J. Sansonetti. Ipab of shigella flexneri causes entry into epithelial cells and escape from the phagocytic vacuole. *The EMBO Journal*, 11(5):1991–1999, May 1992.

[143] M. L. Bernardini, J. Mounier, H. d'Hauteville, M. Coquis-Rondon, and P. J. Sansonetti. Identification of icsa, a plasmid locus of shigella flexneri that governs bacterial intra- and intercellular spread through interaction with f-actin. *Proceedings of the National Academy of Sciences of the United States of America*, 86(10):3867–3871, May 1989.

[144] Hervé Agaisse. Molecular and cellular mechanisms of shigella flexneri dissemination. *Frontiers in Cellular and Infection Microbiology*, 6:29, February 2016.

[145] Gunnar N. Schroeder and Hubert Hilbi. Molecular pathogenesis of shigella spp.: Controlling host cell signaling, invasion, and death by type iii secretion. *Clinical Microbiology Reviews*, 21(1):134–156, January 2008.

[146] R. Bulgin, B. Raymond, J. A. Garnett, G. Frankel, V. F. Crepin, C. N. Berger, and A. Arbeloa. Bacterial guanine nucleotide exchange factors SopE-like and WxxxE effectors. *Infection and Immunity*, 78(4):1417–1425, feb 2010.

[147] Kenji Ohya, Yutaka Handa, Michinaga Ogawa, Masato Suzuki, and Chihiro Sasakawa. IpgB1 is a novel shigella effector protein involved in bacterial invasion of host cells. *Journal of Biological Chemistry*, 280(25):24022–24034, apr 2005.

[148] Yutaka Handa, Masato Suzuki, Kenji Ohya, Hiroki Iwai, Nozomi Ishijima, Anthony J. Koleske, Yoshinori Fukui, and Chihiro Sasakawa. Shigella

ipgb1 promotes bacterial entry through the elmo-dock180 machinery. *Nature Cell Biology*, 9:121, December 2006.

[149] Hironori Katoh and Manabu Negishi. Rhog activates rac1 by direct interaction with the dock180-binding protein elmo. *Nature*, 424:461, July 2003.

[150] Abderrahman Hachani, Latefa Biskri, Giacomo Rossi, Allison Marty, Robert Ménard, Philippe Sansonetti, Claude Parsot, Guy Tran Van Nhieu, Maria Lina Bernardini, and Abdelmounaaïm Allaoui. IpgB1 and IpgB2, two homologous effectors secreted via the mxi-spa type III secretion apparatus, cooperate to mediate polarized cell invasion and inflammatory potential of shigella flexenri. *Microbes and Infection*, 10(3):260–268, mar 2008.

[151] K. Heran Hong and Virginia L. Miller. Identification of a novel and salmonella invasion and locus and homologous to shigella and ipgde. *Journal of Bacteriology, Apr. 1998, p. 1793-1802*, 1998.

[152] Kirsten Niebuhr, Sylvie Giuriato, Thierry Pedron, Dana J. Philpott, Frédérique Gaits, Julia Sable, Michael P. Sheetz, Claude Parsot, Philippe J. Sansonetti, and Bernard Payrastre. Conversion of ptdins(4,5)p(2) into ptdins(5)p by the s.flexneri effector ipgd reorganizes host cell morphology. *The EMBO Journal*, 21(19):5069–5078, August 2002.

[153] Chun Hui Sun, Benjamin Wacquier, Daniel I Aguilar, Nathalie Carayol, Kevin Denis, Sylviane Boucherie, Cesar Valencia-Gallardo, Ceren Simsek, Christophe Erneux, Alexandre Lehman, Jost Enninga, Laurence Arbibe, Philippe Sansonetti, Geneviève Dupont, Laurent Combettes, and Guy Tran Van Nhieu. The shigella type iii effector ipgd recodes ca2+ signals during invasion of epithelial cells. *The EMBO Journal*, 36(17):2567–2580, 2017.

[154] Porfirio Nava, Ryuta Kamekura, and Asma Nusrat. Cleavage of transmembrane junction proteins and their role in regulating epithelial homeostasis. *Tissue Barriers*, 1(PMC3879235):e24783, April 2013.

[155] Janina Schweer, Devesha Kulkarni, Annika Kochut, Joern Pezoldt, Fabio Pisano, Marina C. Pils, Harald Genth, Jochen Huehn, and Petra Dersch. The cytotoxic necrotizing factor of yersinia pseudotuberculosis (cnf(y)) enhances inflammation and yop delivery during infection by activation of rho gtpases. *PLoS Pathogens*, 9(11):e1003746, September 2013.

[156] Alexander R. C. Wong, Benoit Raymond, James W. Collins, Valerie F. Crepin, and Gad Frankel. The enteropathogenic e. coli effector esph promotes actin pedestal formation and elongation via wasp-interacting protein. *Cellular microbiology*, 14(7):1051–1070, March 2012.

[157] Shadi Shahriari, James Gordon, and Reena Ghildyal. Host cytoskeleton in respiratory syncytial virus assembly and budding. *Virology Journal*, 13:161, September 2016.

[158] Tara L. Gower, Mark E. Peeples, Peter L. Collins, and Barney S. Graham. Rhoa is activated during respiratory syncytial virus infection. *Virology*, 283(2):188 – 196, 2001.

[159] Manoj K. Pastey, James E. Crowe, and Barney S. Graham. Rhoa interacts with the fusion glycoprotein of respiratory syncytial virus and facilitates virus-induced syncytium formation. *Journal of Virology*, 73(PMC104251):7262–7270, June 1999.

[160] Tara L. Gower, Manoj K. Pastey, Mark E. Peeples, Peter L. Collins, Lewis H. McCurdy, Timothy K. Hart, Alex Guth, Teresa R. Johnson, and Barney S. Graham. Rhoa signaling is required for respiratory syncytial virus-induced syncytium formation and filamentous virion morphology. *Journal of Virology*, 79(9):5326–5336, 2005.

[161] Masfique Mehedi, Thomas McCarty, Scott E. Martin, Cyril Le Nouën, Eugen Buehler, Yu-Chi Chen, Margery Smelkinson, Sundar Ganesan, Elizabeth R. Fischer, Linda G. Brock, Bo Liang, Shirin Munir, Peter L. Collins, and Ursula J. Buchholz. Actin-related protein 2 (ARP2) and virus-induced filopodia facilitate human respiratory syncytial virus spread. *PLOS Pathogens*, 12(12):e1006062, dec 2016.

[162] Hinsch Klaus-Dieter, Habermann Barbara, Just Ingo, Hinsch Elvira, Pfisterer Susanne, Schill Wolf-Bernhard, and Aktories Klaus. Adp-ribosylation of rho proteins inhibits sperm motility. *FEBS Letters*, 334(1):32–36, 1993.

[163] Yutaka Handa, Charlotte H. Durkin, Mark P. Dodding, and Michael Way. Vaccinia virus f11 promotes viral spread by acting as a pdz-containing scaffolding protein to bind myosin-9a and inhibit rhoa signaling. *Cell Host & Microbe*, 14(1):51–62, July 2013.

[164] Thary Jacob, Céline Van den Broeke, Cliff Van Waesberghe, Leen Van Troys, and Herman W. Favoreel. Pseudorabies virus us3 triggers rhoa phosphorylation to reorganize the actin cytoskeleton. *Journal of General Virology*, 96(8):2328–2335, 2015.

[165] Sibylle Haid, Christina Grethe, Dorothea Bankwitz, Thomas Grunwald, and Thomas Pietschmann. Identification of a human respiratory syncytial virus cell entry inhibitor by using a novel lentiviral pseudotype system. *Journal of Virology*, 90(6):3065–3073, 2016.

[166] Melody Redman, Andrew King, Caroline Watson, and David King. What is crispr/cas9? *Archives of Disease in Childhood - Education and Practice*, 2016.

[167] David L. Jaye, Robert A. Bray, Howard M. Gebel, Wayne A. C. Harris, and Edmund K. Waller. Translational applications of flow cytometry in clinical practice. *The Journal of Immunology*, 188(10):4715–4719, 2012.

[168] Anneliese M. Lengsfeld, Irmentraut Löw, Theodor Wieland, Peter Dancker, and Wilhelm Hasselbach. Interaction of phalloidin with actin. *Proceedings of the National Academy of Sciences of the United States of America*, 71(PMC388560):2803–2807, July 1974.

[169] J. Mounier, V. Laurent, A. Hall, P. Fort, M.F. Carlier, P.J. Sansonetti, and C. Egile. Rho family gtpases control entry of shigella flexneri into epithelial cells but not intracellular motility. *Journal of Cell Science*, 112(13):2069–2080, 1999.

[170] M. F. Santos, S. A. McCormack, Z. Guo, J. Okolicany, Y. Zheng, L. R. Johnson, and G. Tigyi. Rho proteins play a critical role in cell migration during the early phase of mucosal restitution. *Journal of Clinical Investigation*, 100(PMC508182):216–225, July 1997.

[171] Guolin Chen, Lu Lu, Chang Liu, Lei Shan, and Di Yuan. MicroRNA-377 suppresses cell proliferation and invasion by inhibiting TIAM1 expression in hepatocellular carcinoma. *PLOS ONE*, 10(3):e0117714, mar 2015.

[172] Séverine Steuve, Thalie Devosse, Elsa Lauwers, Jean-Marie Vanderwinden, Bruno André, Pierre J. Courtoy, and Isabelle Pirson. Rhophilin-2 is targeted to late-endosomal structures of the vesicular machinery in the presence of activated rhob. *Experimental Cell Research*, 312(20):3981 – 3989, 2006.

[173] Sari Tojkander, Gergana Gateva, Galina Schevzov, Pirta Hotulainen, Perttu Naumanen, Claire Martin, Peter W. Gunning, and Pekka Lappalainen. A molecular pathway for myosin ii recruitment to stress fibers. *Current Biology*, 21(7):539 – 550, 2011.

[174] Yunpeng Bai, Yong Luo, Sijiu Liu, Lujuan Zhang, Kui Shen, Yuanshu Dong, Chad D. Walls, Lawrence A. Quilliam, Clark D. Wells, Youjia Cao, and Zhong-Yin Zhang. Prl-1 protein promotes erk1/2 and rhoa protein activation through a non-canonical interaction with the src homology 3 domain of p115 rho gtpase-activating protein. *The Journal of Biological Chemistry*, 286(49):42316–42324, October 2011.

[175] K. Rottner, A. Hall, and J.V. Small. Interplay between rac and rho in the control of substrate contact dynamics. *Current Biology*, 9(12):640 – S1, 1999.

[176] Anne J. Ridley and Alan Hall. The small gtp-binding protein rho regulates the assembly of focal adhesions and actin stress fibers in response to growth factors. *Cell*, 70(3):389 – 399, 1992.

[177] Katsutoshi Nakano, Kenji Takaishi, Atsuko Kodama, Akiko Mammoto, Hitoshi Shiozaki, Morito Monden, and Yoshimi Takai. Distinct actions and cooperative roles of rock and mdia in rho small g protein-induced reorganization of the actin cytoskeleton in madin-darby canine kidney cells. *Molecular Biology of the Cell*, 10(PMC25478):2481–2491, May 1999.

[178] K. A. Giuliano, J. Kolega, R. L. DeBiasio, and D. L. Taylor. Myosin ii phosphorylation and the dynamics of stress fibers in serum-deprived and stimulated fibroblasts. *Molecular Biology of the Cell*, 3(PMC275664):1037–1048, September 1992.

[179] Avital A. Rodal, Jonathan W. Tetreault, Pekka Lappalainen, David G. Drubin, and David C. Amberg. Aip1p interacts with cofilin to disassemble actin filaments. *The Journal of Cell Biology*, 145(PMC2133144):1251–1264, May 1999.

[180] Georgios Kanellos, Jing Zhou, Hitesh Patel, Rachel A. Ridgway, David Huels, Christine B. Gurniak, Emma Sandilands, Neil O. Carragher, Owen J. Sansom, Walter Witke, Valerie G. Brunton, and Margaret C. Frame. ADF and cofilin1 control actin stress fibers, nuclear integrity, and cell survival. *Cell Reports*, 13(9):1949–1964, dec 2015.

[181] Olivia Steele-Mortimer, Leigh A. Knodler, Sandra L. Marcus, Michael P. Scheid, Benjamin Goh, Cheryl G. Pfeifer, Vincent Duronio, and B. Brett Finlay. Activation of akt/protein kinase b in epithelial cells by the-salmonella typhimurium effector sigd. *Journal of Biological Chemistry*, 275(48):37718–37724, 2000.

[182] Alex Toker and Sandra Marmiroli. Signaling specificity in the akt pathway in biology and disease. *Advances in biological regulation*, 0(PMC4062840):28–38, April 2014.

[183] Marie-Anne Rameix-Welti, Ronan Le Goffic, Pierre-Louis Hervé, Julien Sourimant, Aude Rémot, Sabine Riffault, Qin Yu, Marie Galloux, Elyanne Gault, and Jean-François Eléouët. Visualizing the replication of respiratory syncytial virus in cells and in living mice. *Nature Communications*, 5(1), oct 2014.

[184] Angika Basant and Michael Glotzer. Spatiotemporal regulation of rhoa during cytokinesis. *Current Biology*, 28(9):R570 – R580, 2018.

[185] Volker Königs, Richard Jennings, Thomas Vogl, Markus Horsthemke, Anne C. Bachg, Yan Xu, Kay Grobe, Cord Brakebusch, Albrecht Schwab, Martin Bähler, Ulla G. Knaus, and Peter J. Hanley. Mouse macrophages completely lacking rho subfamily GTPases (RhoA, RhoB, and RhoC) have severe lamellipodial retraction defects, but robust chemotactic navigation and altered motility. *Journal of Biological Chemistry*, 289(44):30772–30784, sep 2014.

[186] Robert J. Tushinski, Ivan T. Oliver, Larry J. Guilbert, P. Wendy Tynan, Jonathan R. Warner, and E. Richard Stanley. Survival of mononuclear phagocytes depends on a lineage-specific growth factor that the differentiated cells selectively destroy. *Cell*, 28(1):71–81, January 1982.

[187] Jaime Melendez, Kristy Stengel, Xuan Zhou, Bharesh K. Chauhan, Marcella Debidda, Paul Andreassen, Richard A. Lang, and Yi Zheng. Rhoa gtpase is dispensable for actomyosin regulation but is essential for mitosis in primary mouse embryonic fibroblasts. *The Journal of Biological Chemistry*, 286(PMC3083211):15132–15137, March 2011.

[188] Henry C. Orr, James Baker, and Judy O. Cheesman. Survival of animal tissue cells in primary culture in the absence of serum. *Applied Microbiology*, 25(PMC380734):49–54, January 1973.

[189] Aaron D. DeWard, Kellie Leali, Richard A. West, George C. Prendergast, and Arthur S. Alberts. Loss of rhob expression enhances the myelodysplastic phenotype of mammalian diaphanous-related formin mdia1 knockout mice. *PLoS ONE*, 4(PMC2740832):e7102, August 2009.

[190] Anne Hakem, Otto Sanchez-Sweatman, Annick You-Ten, Gordon Duncan, Andrew Wakeham, Rama Khokha, and Tak W. Mak. Rhoc is dispensable for embryogenesis and tumor initiation but essential for metastasis. *Genes & Development*, 19(PMC1199568):1974–1979, June 2005.

[191] Ben Jackson, Karine Peyrollier, Esben Pedersen, Astrid Basse, Richard Karlsson, Zhipeng Wang, Tine Lefever, Alexandra M. Ochsenbein, Gudula Schmidt, Klaus Aktories, Alanna Stanley, Fabio Quondamatteo, Markus Ladwein, Klemens Rottner, Jolanda van Hengel, and Cord Brakebusch. Rhoa is dispensable for skin development, but crucial for contraction and directed migration of keratinocytes. *Molecular Biology of the Cell*, 22(PMC3046057):593–605, December 2010.

[192] Kenan Xie, Yuehua Yang, and Hongyuan Jiang. Controlling cellular volume via mechanical and physical properties of substrate. *Biophysical Journal*, 114(3):675 – 687, 2018.

[193] Yongbo Yu, Junchao Duan, Weijia Geng, Qiuling Li, Lizhen Jiang, Yang Li, Yang Yu, and Zhiwei Sun. Aberrant cytokinesis and cell fusion result in multinucleation in hepg2 cells exposed to silica nanoparticles. *Chemical Research in Toxicology*, 28(3):490–500, 2015. PMID: 25625797.

[194] Mark Haynes, J. Jacob Strouse, Anna Waller, Andrei. Leitao, Ramona F. Curpan, Cristian Bologa, Tudori Oprea, Eric R. Prossnitz, Bruce S. Edwards, Larry A. Sklar, and Todda Thompson. Detection of intracellular granularity induction in prostate cancer cell lines by small molecules using the hypercyt high-throughput flow cytometry system. *Journal of biomolecular screening*, 14(PMC3666167):596–609, May 2009.

[195] Dina Dikovskaya, John J. Cole, Susan M. Mason, Colin Nixon, Saadia A. Karim, Lynn McGarry, William Clark, Rachael N. Hewitt, Morgan A. Sammons, Jiajun Zhu, Dimitris Athineos, Joshua D. G. Leach, Francesco Marchesi, John van Tuyn, Stephen W. Tait, Claire Brock, Jennifer P. Morton, Hong Wu, Shelley L. Berger, Karen Blyth, and Peter D. Adams. Mitotic

stress is an integral part of the oncogene-induced senescence program that promotes multinucleation and cell cycle arrest. *Cell Reports*, 12(9):1483–1496, September 2015.

[196] Judith Campisi. Aging, cellular senescence, and cancer. *Annual review of physiology*, 75(PMC4166529):685–705, November 2012.

[197] Kun Jiang, Jiazhi Sun, Jin Cheng, Julie Y. Djeu, Sheng Wei, and Saïd Sebti. Akt mediates ras downregulation of rhob, a suppressor of transformation, invasion, and metastasis. *Molecular and Cellular Biology*, 24(PMC419878):5565–5576, March 2004.

[198] Yuliya Zilberman, Naila O. Alieva, Stéphanie Miserey-Lenkei, Alexandra Lichtenstein, Zvi Kam, Helena Sabanay, and Alexander Bershadsky. Involvement of the rho-mdia1 pathway in the regulation of golgi complex architecture and dynamics. *Molecular Biology of the Cell*, 22(PMC3154885):2900–2911, June 2011.

[199] Hortensia Mircescu, Séverine Steuve, Valérie Savonet, Chantal Degraef, Harry Mellor, Jacques E. Dumont, Carine Maenhaut, and Isabelle Pirson. Identification and characterization of a novel activated RhoB binding protein containing a PDZ domain whose expression is specifically modulated in thyroid cells by cAMP. *European Journal of Biochemistry*, 269(24):6241–6249, dec 2002.

[200] Jeremy W. Peck, Michael Oberst, Kerrie B. Bouker, Emma Bowden, and Peter D. Burbelo. The RhoA-binding protein, rhophilin-2, regulates actin cytoskeleton organization. *Journal of Biological Chemistry*, 277(46):43924–43932, sep 2002.

[201] A.J. Ridley. RhoA, RhoB and RhoC have different roles in cancer cell migration. *Journal of Microscopy*, 251(3):242–249, mar 2013.

[202] Juan Wang and Ian C. Schneider. Myosin phosphorylation on stress fibers predicts contact guidance behavior across diverse breast cancer cells. *Biomaterials*, 120(PMC5291342):81–93, November 2016.

[203] Francisco M. Vega, Audrey Colomba, Nicolas Reymond, Mairian Thomas, and Anne J. Ridley. Rhob regulates cell migration through altered focal adhesion dynamics. *Open Biology*, 2(5):120076, May 2012.

[204] Ji Yun Zheng, Siew Ping Han, Yi-Jen Chiu, Ai Kia Yip, Nicolas Boichat, Shi Wen Zhu, Jun Zhong, and Paul Matsudaira. Epithelial monolayers coalesce on a viscoelastic substrate through redistribution of vinculin. *Biophysical Journal*, 113(7):1585 – 1598, 2017.

[205] Sejeong Shin, Laura Wolgamott, Yonghao Yu, John Blenis, and Sang-Oh Yoon. Glycogen synthase kinase (gsk)-3 promotes p70 ribosomal protein s6 kinase (p70s6k) activity and cell proliferation. *Proceedings of the National*

Academy of Sciences of the United States of America, 108(PMC3223461):E1204–E1213, November 2011.

[206] Jelena Jovanović, Sarah Iqbal, Sacha Jensen, Helen Mardon, and Penny Handford. Fibrillin-integrin interactions in health and disease. *Biochem Soc Trans*, 36(2):257, April 2008.

[207] W. Tony Parks, David B. Frank, Carla Huff, Carol Renfrew Haft, Jennifer Martin, Xianwang Meng, Mark P. de Caestecker, James G. McNally, Amit Reddi, Simeon I. Taylor, Anita B. Roberts, Tongwen Wang, and Robert J. Lechleider. Sorting nexin 6, a novel snx, interacts with the transforming growth factor-β family of receptor serine-threonine kinases. *Journal of Biological Chemistry*, 276(22):19332–19339, 2001.

[208] Christoph Schweingruber, Simone C. Rufener, David Zünd, Akio Yamashita, and Oliver Mühlemann. Nonsense-mediated mrna decay - mechanisms of substrate mrna recognition and degradation in mammalian cells. *Biochimica et Biophysica Acta (BBA) - Gene Regulatory Mechanisms*, 1829(6):612 – 623, 2013. RNA Decay Mechanisms.

[209] Eirini Nomikou, Melina Livitsanou, Christos Stournaras, and Dimitris Kardassis. Transcriptional and post-transcriptional regulation of the genes encoding the small gtpases rhoa, rhob, and rhoc: implications for the pathogenesis of human diseases. *Cellular and Molecular Life Sciences*, 75(12):2111–2124, Jun 2018.

[210] Eirini Nomikou, Christos Stournaras, and Dimitris Kardassis. Functional analysis of the promoters of the small gtpases rhoa and rhob in embryonic stem cells. *Biochemical and Biophysical Research Communications*, 491(3):754 – 759, 2017.

[211] Audrey Gérard, Rob A. van der Kammen, Hans Janssen, Saskia I. Ellenbroek, and John G. Collard. The rac activator tiam1 controls efficient t-cell trafficking and route of transendothelial migration. *Blood*, 113(24):6138, June 2009.

[212] T. T. Giang Ho, Sofia D. Merajver, Charles M. Lapière, Betty V. Nusgens, and Christophe F. Deroanne. RhoA-GDP regulates RhoB protein stability. *Journal of Biological Chemistry*, 283(31):21588–21598, jun 2008.

[213] Yan Wang and John S. Lazo. Metastasis-associated phosphatase prl-2 regulates tumor cell migration and invasion. *Oncogene*, 31(7):818–827, July 2011.

[214] James J. Fiordalisi, Patricia J. Keller, and Adrienne D. Cox. Prl tyrosine phosphatases regulate rho family gtpases to promote invasion and motility. *Cancer Research*, 66(6):3153–3161, 2006.

[215] Comunale Franck, Causeret Marie, Favard Cyril, Cau Julien, Taulet Nicolas, Charrasse Sophie, and Gauthier-Rouvière Cécile. Rac1 and rhoa gtpases have antagonistic functions during n-cadherin-dependent cell-cell contact formation in c2c12 myoblasts. *Biology of the Cell*, 99(9):503–517, 2012.

[216] Eric Ispanovic, Damiano Serio, and Tara L. Haas. Cdc42 and rhoa have opposing roles in regulating membrane type 1-matrix metalloproteinase localization and matrix metalloproteinase-2 activation. *American Journal of Physiology-Cell Physiology*, 295(3):C600–C610, 2008. PMID: 18562481.

[217] A. Hajdo-Milasinovic, S. I. J. Ellenbroek, S. van Es, B. van der Vaart, and J. G. Collard. Rac1 and rac3 have opposing functions in cell adhesion and differentiation of neuronal cells. *Journal of Cell Science*, 120(4):555–566, feb 2007.

[218] Pontus Aspenström, Asa Fransson, and Jan Saras. Rho gtpases and have diverse effects on the organization and of the actin filament system. In *Biochem. J. (2004) 377, 327-337 (Printed in Great Britain)*, 2004.

[219] Elena Kassianidou, Jasmine H. Hughes, and Sanjay Kumar. Activation of rock and mlck tunes regional stress fiber formation and mechanics via preferential myosin light chain phosphorylation. *Mol Biol Cell. 2017 Dec 15; 28(26): 3832-3843.*, 2017.

[220] S.Francesco Retta, Simon T. Barry, David R. Critchley, Paola Defilippi, Lorenzo Silengo, and Guido Tarone. Focal adhesion and stress fiber formation is regulated by tyrosine phosphatase activity. *Experimental Cell Research*, 229(2):307 – 317, 1996.

[221] Claudia Hoffmann, Marius Pop, Jost Leemhuis, Jörg Schirmer, Klaus Aktories, and Gudula Schmidt. The yersinia pseudotuberculosis cytotoxic necrotizing factor (cnfy) selectively activates rhoa. *Journal of Biological Chemistry*, 279(16):16026–16032, 2004.

[222] Manuel Wolters, Erin C. Boyle, Kerstin Lardong, Konrad Trülzsch, Anika Steffen, Klemens Rottner, Klaus Ruckdeschel, and Martin Aepfelbacher. Cytotoxic necrotizing factor-y BoostsYersiniaEffector translocation by activating rac protein. *Journal of Biological Chemistry*, 288(32):23543–23553, jun 2013.

[223] Gillian Groeger and Catherine D. Nobes. Co-operative cdc42 and rho signalling mediates ephrinb-triggered endothelial cell retraction. *Biochemical Journal*, 404(PMC1868826):23–29, February 2007.

[224] Jie Gao, Fu Shanmin, Zhaobin Zeng, Feifei Li, Qiannan Niu, Da Jing, and Xue Feng. Cyclic stretch promotes osteogenesis-related gene expression in osteoblast-like cells through a cofilin-associated mechanism. *Molecular Medicine Reports*, 14(PMC4918615):218–224, April 2016.

[225] Mouna A. Mikati, Dennis Breitsprecher, Silvia Jansen, Emil Reisler, and Bruce L. Goode. Coronin enhances actin filament severing by recruiting cofilin to filament sides and altering f-actin conformation. *Journal of molecular biology*, 427(PMC4579047):3137–3147, August 2015.

[226] Maria Meira, Régis Masson, Igor Stagljar, Susanne Lienhard, Francisca Maurer, Anne Boulay, and Nancy E. Hynes. Memo is a cofilin-interacting protein that influences plcγ1 and cofilin activities, and is essential for maintaining directionality during erbb2-induced tumor-cell migration. *Journal of Cell Science*, 122(6):787–797, 2009.

[227] Thomas Kuilman, Alessio Maiolica, Molly Godfrey, Noémie Scheidel, Ruedi Aebersold, and Frank Uhlmann. Identification of cdk targets that control cytokinesis. *The EMBO Journal*, 34(PMC4291482):81–96, October 2014.

[228] Pirta Hotulainen, Eija Paunola, Maria K. Vartiainen, and Pekka Lappalainen. Actin-depolymerizing factor and cofilin-1 play overlapping roles in promoting rapid f-actin depolymerization in mammalian nonmuscle cells. *Molecular Biology of the Cell*, 16(PMC545901):649–664, November 2004.

[229] Takashi Yugawa, Koichiro Nishino, Shin-ichi Ohno, Tomomi Nakahara, Masatoshi Fujita, Naoki Goshima, Akihiro Umezawa, and Tohru Kiyono. Noncanonical notch signaling limits self-renewal of human epithelial and induced pluripotent stem cells through rock activation. *Molecular and Cellular Biology*, 33(22):4434–4447, 2013.

[230] Xun Shang, Fillipo Marchioni, Nisha Sipes, Chris R. Evelyn, Moran Jerabek-Willemsen, Stefan Duhr, William Seibel, Matthew Wortman, and Yi Zheng. Rational design of small molecule inhibitors targeting RhoA subfamily rho GTPases. *Chemistry & Biology*, 19(6):699–710, jun 2012.

[231] Yoshiaki Yamaguchi, Hironori Katoh, Hidekazu Yasui, Kazutoshi Mori, and Manabu Negishi. Rhoa inhibits the nerve growth factor-induced rac1 activation through rho-associated kinase-dependent pathway. *Journal of Biological Chemistry*, 276(22):18977–18983, 2001.

[232] L. A. Knodler, B. B. Finlay, and O. Steele-Mortimer. The salmonella effector protein SopB protects epithelial cells from apoptosis by sustained activation of akt. *Journal of Biological Chemistry*, 280(10):9058–9064, jan 2005.

[233] Truong Dorothy, Boddy Kirsten C., Canadien Veronica, Brabant Danielle, Fairn Gregory D., D'Costa Vanessa M., Coyaud Etienne, Raught Brian, Perez-Sala Dolores, Park Wei Sun, Do Heo Won, Grinstein Sergio, and Brumell John H. Salmonella exploits host rho gtpase signalling pathways through the phosphatase activity of sopb. *Cellular Microbiology*, 0(ja):e12938, 2018. e12938 CMI-18-0067.R1.

[234] Malina A. Bakowski, Virginie Braun, Grace Y. Lam, Tony Yeung, Won Do Heo, Tobias Meyer, B. Brett Finlay, Sergio Grinstein, and John H. Brumell. The phosphoinositide phosphatase sopb manipulates membrane surface charge and trafficking of the salmonella-containing vacuole. *Cell Host & Microbe*, 7(6):453 – 462, 2010.

[235] Julie A. Wasylnka, Malina A. Bakowski, Jason Szeto, Maikke B. Ohlson, William S. Trimble, Samuel I. Miller, and John H. Brumell. Role for myosin ii in regulating positioning of salmonella-containing vacuoles and intracellular replication. *Infection and Immunity*, 76(PMC2423101):2722–2735, April 2008.

[236] Rui P. M. Mauricio, Cy M. Jeffries, Dmitri I. Svergun, and Janet E. Deane. The shigella virulence factor icsa relieves n-wasp autoinhibition by displacing the verprolin homology/cofilin/acidic (vca) domain. *The Journal of Biological Chemistry*, 292(1):134–145, November 2016.

[237] Michael B. Battles, Johannes P. Langedijk, Polina Furmanova-Hollenstein, Supranee Chaiwatpongsakorn, Heather M. Costello, Leen Kwanten, Luc Vranckx, Paul Vink, Steffen Jaensch, Tim H. M. Jonckers, Anil Koul, Eric Arnoult, Mark E. Peeples, Dirk Roymans, and Jason S. McLellan. Molecular mechanism of respiratory syncytial virus fusion inhibitors. *Nature chemical biology*, 12(PMC4731865):87–93, December 2015.

[238] Lewis H. McCurdy and Barney S. Graham. Role of plasma membrane lipid microdomains in respiratory syncytial virus filament formation. *Journal of Virology*, 77(PMC140864):1747–1756, October 2002.

[239] Block J., Stradal T.E.B., Hänisch J., Geffers R., Köstler S.A., Urban E., Small J.V., Rottner K., and Faix J. Filopodia formation induced by active mdia2/drf3. *Journal of Microscopy*, 231(3):506–517, 2008.

Danksagung

Zuerst möchte ich mich sehr herzlich bei Prof. Dr. Theresia Stradal für das tolle Projekt und die Unterstützung in allen Bereichen während der letzten Jahre bedanken. Ganz besonders dafür, dass sie immer eine offene Tür hatte und mir auch in schwierigen Zeiten den Rücken gestärkt hat.

Desweiteren danke ich Prof. Dr. Susanne Engelmann für die Übernahme des Zweigutachtens und für ihre Beiträge und Ratschläge während meiner Thesis Committee Meetings. PD Dr. Simone Bergmann danke ich für ihre Bereitschaft den Prüfungsvorsitz zu übernehmen. Außerdem danke ich Prof. Dr. Klemens Rottner für die konstruktiven Ideen und Vorschläge im Thesis Committee und auch außerhalb davon. Außerdem danke ich unseren Kooperationspartnern für die tollen Daten und Methoden: Dr. Lothar Gröbe, Petra Hagendorff, Dr. Robert Geffers, Lito Papaxenopoulou, Dr. Gang Zhao, Dr. Haralampos Hatzikirou, Prof. Dr. Michael Meyer-Hermann, Svenja Wiechert und Prof. Dr. Thomas Pietschmann. Vielen Dank an die HZI Grad School für die angebotenen Workshops und die Organisation von Symposien.

Ganz besonders danke ich der wundervollen Abteilung ZBIO für die tolle Zeit der vergangenen Jahre. Danke an Anika, Annette, Astrid, Frieda, Jan, Jana, Julia, Marco, Monique, Nadiia, Silvia, Steffi, Theresia und an all unsere Studenten, Azubis und HiWis für die gute Zusammenarbeit und den Spaß im Labor und auch außerhalb davon. Ein besonderer Dank geht an Jana für all die guten Gespräche und dafür, dass wir uns einfach perfekt ergänzen. Danke außerdem an Astrid für die Hilfe bei der Bürokratie und der Organisation der Dienstreisen. Danke an Anna, Frieda, Jana und Steffi für 2 unvergessliche Wochen in den USA. Ein riesiger Dank geht an Silvia für die Unterstützung bei den spontanen Experimenten in den letzten Monaten. Danke auch an Franzi für deine Hilfe und die tollen Daten. Auch ein besonderer Dank an Laura, es war wirklich schön mit dir. Ein riesiger Dank geht an Julia und Anika für die Korrektur meiner Arbeit und die vielen Ideen und Hilfestellungen zu jeder Zeit. Danke auch an Hinrich für die Hilfe bei spontanen LaTeX Schwierigkeiten.

Ein wirklich herzlicher Dank an die MIBI-Mittagessen-Fraktion: Carina, Maria, Vanessa und Ines. Es freut mich riesig, dass wir den Kontakt halten konnten und ich bin sehr froh euch zu haben. Danke für die vielen Gespräche und auch die schönen Treffen außerhalb der Arbeit. Ihr seid mir wirklich ans Herz gewachsen.

Der wichtigste Teil zum Schluss. Ich danke, und zwar unendlich und kaum in Worte zu fassen, meiner tollen Familie, meiner zweiten Familie Akablas und ganz besonders Lennart für die Unterstützung in all den Jahren, in guten und schlechten Momenten. Danke, dass ich mich auf euch verlassen kann und dass ihr mir ausnahmslos immer den Rücken stärkt.